DEACTIVATION AND REGENERATION KINETICS DURING BIOCONVERSIONS BY IMMOBILIZED *CLOSTRIDIUM ACETOBUTYLICUM*

Thesis by

Kenneth Frederick Reardon

in Partial Fulfillment of the Requirements

for the Degree of

Doctor of Philosophy

California Institute of Technology

Pasadena, California

1988

(submitted September 29, 1987)

To my parents

Acknowledgments

I would like to thank my advisor, Jay Bailey, for his advice and support during my work on this project. I have learned many things from him, not all of which are related to the details of this dissertation. I hope that I will be able to bring some of his enthusiasm and vision into my future work.

Many people have helped me in many ways during the past few years. I have particularly valued the friendship of Dave Dandy and Sonia Kreidenweis-Dandy, with whom I have shared many good times. My association with Ken Grace and the members of the Caltech Swim Club has been a source of great enjoyment to me. It will be very hard to leave so many friends.

The members of the Bailey research group deserve my thanks for sharing their expertise and camaraderie. Nancy DaSilva has earned special mention for being a great office mate who somehow put up with me. I am especially grateful to Thomas Scheper, whose help with fluorescence and fellowships was invaluable (and I still owe him a beer for it).

Several people offered key technical assistance at important points in this work: Pauline Doran shared many of her ideas and techniques with me as I learned my way around the lab, and Sheryl Bergstrom of JPL first taught me how to work with *C. acetobutylicum*. I also greatly appreciated Mike Hoffmann's offer to use an anaerobic hood in his laboratory for my final experiment.

I am grateful for the financial support of the National Science Foundation, Monsanto Company, and the President's Fund of the California Institute of Technology, and to Ingold Electrodes, Inc. for providing the fluorescence probe.

Most of all, I am thankful for the love and support of my family.

Abstract

The physiology and catabolic rates of calcium alginate-immobilized *Clostridium acetobutylicum* were studied under a variety of conditions, with an emphasis on the relationships between the activity and the environment of the immobilized cells during bioconversions of nitrogen-free glucose media and also during periods of activity regeneration under defined conditions. A number of experimental and analytical techniques were used to investigate these relationships, including measurements of product formation and substrate (glucose and nitrogen) consumption, quantification of immobilized cell concentrations by direct counts of several morphological types, and the *in situ* measurement of intracellular NAD(P)H-dependent fluorescence. In addition, a framework for the analysis of metabolic pathway rates from product and substrate concentration data was developed and applied to both suspended and immobilized cell cultivations of *C. acetobutylicum*.

Two *C. acetobutylicum* strains were used in this work; one was the type strain, the sporogenous ATCC 824, and the other was ATCC 39236, which was found to be oligosporogenous. When the immobilized cell bioreactor feed was a medium deficient in nitrogen and required vitamin sources (to maintain the immobilized cells in a non-growing but viable state), the major causes of product-forming activity loss were initial cell lysis and sporulation; the latter effect was minor in the ATCC 39236 experiment. The addition of ammonia or ammonia plus vitamins to the feed during a regeneration period increased the total activity of the immobilized cell preparation, and this increased activity was not always due to cell growth.

The patterns of product formation during repeated cycles of bioconversion (on nitrogen-free medium) and activity regeneration were discussed in terms of the

changes in the adenylate energy charge that occurred in the course of alternating periods of nitrogen starvation and surplus. Product formation during bioconversion periods was affected by environmental conditions such as pH and the presence of some intermediate metabolites in the feed; these effects were related to distinct features of the *C. acetobutylicum* metabolic pathways. This work shows that knowledge of the metabolism and the underlying physiological responses of the cell to environmental changes can be used to understand and predict cell behavior.

Table of Contents

List of Figures

List of Tables

CHAPTER 1

INTRODUCTION

Clostridium acetobutylicum is an anaerobic bacterium capable of converting a variety of pentoses and hexoses to acetone, butanol, ethanol, acetic and butyric acids, acetoin, carbon dioxide, and hydrogen gas. The particular products formed during any type of fermentation depend greatly on the cellular environment and state; the precise mechanisms of metabolic regulation are under investigation in many laboratories at this time. Since the rapid increase in crude oil prices during the early 1970's, there has been renewed interest in the fermentative production of butanol by *C. acetobutylicum*, with the goal of lowering production costs by improving the process technology over that used in the batch, suspended cell fermentations of the World War I era. A significant amount of progress has been made in understanding the basic metabolism of the organism and its regulation, although there have been relatively few cases in which this fundamental knowledge has been applied to process design.

The use of immobilized cells as biocatalysts is, by now, a well-known concept. Many studies of whole-cell immobilization have been reported, focusing on nonviable cells (sometimes permeabilized or ruptured), growing cells, and cells that are viable but not growing. Immobilized cell bioreactors possess a number of advantages over suspended cell fermentors, such as the decoupling of reactor biomass growth rate and process residence time, a relatively cell-free product stream, and the ability to control more carefully a cell's environment to affect product formation. The use of viable non-growing immobilized cells offers the additional potential for bioconversion without growth effects. For example, the formation of unwanted, exponential-phase metabolic products can be reduced or eliminated, and the conversion of a higher percentage of feed carbon to the desired products (and less to

biomass synthesis) has been reported with *C. acetobutylicum*.

However, preparations of non-growing viable cells usually have relatively short activity lifetimes. This observation is directly related to the non-growing condition and the means by which that condition is achieved. Typically, the immobilized cells are starved for a required nutrient; most often, the nitrogen source is withheld. A number of reports have been published in which the catabolic activity of low-activity immobilized cell preparations has been regenerated by exposing the cells to a full nutrient medium. Although this procedure appears to remove the most severe limitation on the use of this type of immobilized cell biocatalyst, there has not yet been enough learned about the fundamental effects of such starvation/regeneration conditions on the physiology of the immobilized cells to provide a basis for rational process design.

In this work, the physiology and catabolic rates of calcium alginate-immobilized *Clostridium acetobutylicum* were studied under a variety of conditions, with an emphasis on the relationship between the activity and the environment of immobilized cells during bioconversions of nitrogen-free glucose media and also during periods of activity regeneration under defined conditions. Several tools were used in this study: measurements of product formation and substrate consumption, quantification of immobilized cell concentrations during the cycles of bioconversion and activity regeneration phases, and *in situ* monitoring of intracellular NAD(P)H-dependent fluorescence all provided insights into the state of immobilized (and suspended) *C. acetobutylicum* cells. In addition, a framework for the analysis of metabolic pathway rates was developed and used to examine the changes in the rate of carbon flux through each branch of a fermentation. The combination of

these techniques and an understanding of the physiological effects of the different operating conditions led to new observations and conclusions on the operation of bioreactors utilizing this type of non-growing viable immobilized cells.

In Chapter 2, general information is presented on *Clostridium acetobutylicum*, the acetone-butanol fermentation, immobilized cells, and *in situ* NAD(P)H-dependent fluorescence monitoring. The information in these brief reviews will be used later in the analysis of experimental results. The materials and methods used in all of the experiments are described in Chapter 3.

The framework for pathway rate analysis is developed in Chapter 4 and is applied to two different batch, suspended cell *C. acetobutylicum* fermentations. The NAD(P)H-dependent fluorescence of these cultivations was also measured and integrated with the results of the pathway rate analysis calculations.

The next two chapters focus on the product-forming activity of immobilized *C. acetobutylicum*. In Chapter 5, the changing activity and selectivity of the immobilized cells is studied in a bioreactor system in which the feed medium contained no nitrogen or required-vitamin sources. Environmental effects on the bioconversion activity and product distribution were examined by varying the pH of the system and by supplementing the feed with three different weak acid metabolic intermediates. The effects of the sporulation process of the strain used in most of this work on the observed biocatalytic activity was studied by using a mutant strain that exhibited much lower rates of sporulation. Finally, the regeneration of activity by periodic exposure of the immobilized cells to feed streams consisting of ammonia- or ammonia and vitamin-supplemented media was investigated with both strains.

CHAPTER 2

BACKGROUND

INTRODUCTION

This chapter is intended to provide background information and discussion on a number of topics covered in this thesis, necessary for a better understanding of the work covered in Chapters 4, 5 and 6.

ORGANISM

Clostridium acetobutylicum is an anaerobic, nonpathogenic bacterium, with an optimal growth temperature of 37°C [1]. Like all members of the genus *Clostridium*, this species forms endospores, is incapable of dissimilatory sulfate reduction, and is usually Gram-positive, although older cells of this species can become Gram-negative [1]. The vegetative cells have the form of straight rods with rounded ends (0.6–0.72 μm by 2.6–4.7 μm), while the clostridial (pre-spore) forms (1.3–1.6 μm by 4.7–5.5 μm) are swollen at one end because of the presence of a subterminal ovoid endospore [2]. The mature spores are ovoid, measuring approximately 1.2 μm by 2.4 μm [2].

C. acetobutylicum is able to ferment a large variety of hexoses and pentoses [1,3]. Although some strains have weak nitrogen-fixing abilities, all require exogenous soluble nitrogen sources, either organic [4] or inorganic (nitrites, ammonia) [1,5], for growth. All strains require D-biotin for growth, and most have an additional growth factor requirement for the vitamin *p*-aminobenzoic acid [6].

Under certain conditions, such as low pH and high initial glucose concentration, batch fermentations of *C. acetobutylicum* display two different phases. In the first, glucose (or another suitable carbohydrate) is fermented to acetic and butyric acids,

accompanied by vigorous vegetative cell growth and the production of significant amounts of carbon dioxide and hydrogen gases. At some point in the cultivation, for reasons not yet entirely clear, new enzymes are induced or activated, and the acid products, together with glucose, are converted to "solvent" products (acetone, n-butanol, and ethanol). The metabolic pathways involved in each part of such a two-phase fermentation are discussed further in Chapter 4.

Several interesting morphological changes are often observed during the transition from the acidogenic phase to the solventogenic phase. Häggström and Förberg [7] reported the formation of an extracellular polymer during the growth and acid formation phase, which was reutilized at the start of the solvent production phase. The same research also investigated a polymer produced by mid-to-late solvent-phase cells. As this polymer was found to be highly acetylated, the suggestion has been made that polymer formation occurs when the organism requires more reducing power than is available by other means [7]. This solvent-phase polymer probably corresponds to the "slime layer" or extracellular capsule observed in a different strain (P262) [5,8].

Most strains of *C. acetobutylicum*, including ATCC 824 (the strain used in most of the work in this thesis), also produce granulose, a glycogen-like polysaccharide, beginning at the end of the acid phase [5,8,9]. Reysenbach *et al.* [9] found that maximum granulose accumulation occurred near the end of the solvent phase; it is consumed later as a source of carbon and energy for spore formation [9]. Granulose accumulation in *C. acetobutylicum* occurs when growth is inhibited in the presence of an excess source of carbon and the energy (ATP) charge of the cell is high; in addition, granulose formation did not occur under nitrogen limitation [9].

The motility and chemotactic behavior of *C. acetobutylicum* during a typical two-phase batch fermentation has been recently studied [10]. Motility during the early acidogenic phase consisted of "runs" (movement in smooth, straight lines), but motion during the solvent phase changed to "tumbles," a characteristic response to repellent compounds [10]. In this case, acetone, butanol, ethanol, and dissociated acetate and butyrate acted as repellents.

For most strains of *C. acetobutylicum*, sporulation is closely related to solvent production. Although the process of sporulation in *Bacillus subtilis* and other *Bacillus* species has been studied in detail, much less is known about sporulation and its regulation in clostridia [11]. In addition, because the genus *Clostridium* contains such a wide variety of species, care must be taken in generalizing the observations made on any single strain.

A few investigations have been published on the sporulation process in *C. acetobutylicum* [5,8,12,13,14] and in the closely related *C. butyricum* [15]. In general, the sequences of morphological stages in *C. acetobutylicum* sporulation (Figure 1A [16]) have been found to correspond closely with stages observed in *B. subtilis* (Figure 1B [17]) [13]. However, *C. acetobutylicum* strain P262 sporulation had a number of distinctive features. The two most prominent differences were the accumulation of granulose in the swollen, cigar-shaped "clostridial" forms (of *C. acetobutylicum*), and the initiation (in *C. acetobutylicum*) of spore coat formation before the start of spore cortex formation [13].

The use of asporogenous mutants has shown that spore formation is not required for solventogenesis [8,14]. Studies with various types of sporulation mutants [8,14] showed that mutants blocked in granulose formation, capsule production, and

endospore formation can still produce solvents, but that those mutants unable to produce a swollen clostridial stage were also not capable of solvent formation.

Although it has been established that sporulation in various *Bacillus* species is triggered by nutrient starvation, clostridia appear to require exogenous carbon, energy, and nitrogen sources [11,13,14]. In addition, catabolic repression of sporulation by glucose does not occur in *C. acetobutylicum* [14]. Rather than being affected by nutrient concentration, it appears that sporulation in *C. acetobutylicum* (and other saccharolytic clostridia) is regulated by end products and other metabolites that are generated during vegetative growth [11].

Studies involving the isolation and use of mutant strains of *C. acetobutylicum* for the investigation of metabolic and physiological phenomena have appeared only recently. Bowring and Morris [18] found that direct mutagens (*e.g.*, ethyl methane sulfonate (EMS)) were superior to indirect techniques (*e.g.*, UV radiation) for increasing the mutation frequency. They were able to isolate a number of strains, including auxotrophs for vitamins and amino acids [18]. The research group of Jones, Woods, *et al.* have used the EMS technique to isolate mutants for autolysin [19] and the sporulation mutants discussed above [8,14]. Other groups have isolated metabolic pathway mutants by other means, including the use of alkyl halogen analogues to act as suicide substrates [20], and the use of allyl alcohol to isolate a strain with no butyraldehyde dehydrogenase activity [21].

Systems and techniques for genetic studies on *C. acetobutylicum* are relatively few in number, but there have been some reports recently on plasmids (both naturally occurring and constructed) and gene cloning to and from *C. acetobutylicum.* These are discussed in a recent review [22].

Two strains were used in this work. One, American Type Culture Collection (ATCC) strain 824, is the type strain for the species and has been the strain most often utilized in *C. acetobutylicum* research. It is capable of producing granulose and forming mature spores. Although the clostridia are obligate anaerobes, some strains, including ATCC 824, can tolerate brief exposure to oxygen (4–6 hours) [23]. However, sufficiently high concentrations of oxygen can halt growth, decrease the rate of glucose consumption, stop net synthesis of nucleic acids and proteins, and lower the reducing power and ATP concentration of the organism [23]. All of these phenomena are rapidly reversed when anaerobic conditions are reestablished.

In one experiment, ATCC strain 39236 was used. This strain is a butanol-tolerant, asporogenic mutant of ATCC 4259 [24]. It was found to be a strict anaerobe; even brief exposure to oxygen appeared to result in cell death.

THE ACETONE-BUTANOL-ETHANOL FERMENTATION

Many reviews have been published on the history and process details of the acetone-butanol-ethanol (ABE) fermentation [*e.g.*, 25,26, 27,28,29,30,31]. The best such review, by D.T. Jones and D.R. Woods [22], covers all aspects of the fermentation, including its history, the industrial process, alternative fermentation substrates, and the biochemistry and physiology of the primary microorganism for the process, *C. acetobutylicum.*

Although butanol and acetone are currently produced synthetically with petrochemical feedstocks, the skyrocketing of crude oil prices in 1973 triggered an intense interest in the production of butanol (and, to a lesser extent, acetone) by microor-

ganisms. Several economic feasibility studies have appeared [*e.g.*, 32,33].

There are a number of problems with the traditional *C. acetobutylicum* fermentation; two of the most important are strain instability and end product toxicity. The use of continuous culture processes with *C. acetobutylicum* has often been hampered by a gradual loss of solvent-forming ability [22]. This metabolic degeneration has been the subject of several investigations [*e.g.*, 34,35,36]. Operation of the process under certain nutrient limitations (*e.g.*, phosphate), can result in the selection of an asporogenous mutant [34] capable of stable, continuous culture fermentation.

The economically preferred end product, n-butanol, is toxic to *C. acetobutylicum* [37,38]. The 50% levels of inhibition of maximum specific growth rate, nutrient uptake rate, and membrane-bound ATPase activity occur in the range of 0.10–0.15 M butanol [38]. Thus, the product streams from these fermentations are relatively dilute, and there is a high energy cost in the distillation to pure butanol. It may be possible to isolate mutant strains capable of withstanding higher butanol concentrations; some progress has been made in this direction [19].

IMMOBILIZED CELLS

The immobilization of whole microbial cells for heterogenous biocatalysis has been the subject of numerous investigations, although these studies have varied significantly in their depth. Many general reviews have been published on this subject [*e.g.*, 39–46], along with reviews of immobilization methods [46a,52] and those concerned with process engineering aspects, such as diffusion effects and reactor types [47,48,49].

Immobilized cell processes have a number of advantages over those involving suspended cells. First, the physical retention of the cells in the reactor provides a product stream free (in reality, *nearly* free) of cells. For this same reason, the dilution rate for the system is no longer bound by the maximum growth rate of the cells, and thus the washout constraint need not be a consideration in the optimization of productivity. Another advantage in immobilized cell systems is the high cell density achievable in a reactor, leading to higher volumetric productivities. Perhaps the most interesting feature in immobilized cell systems is the possibility of limiting cell growth (either by restricting the volume available for growth or by nutrient limitation) so that more feed carbon is directed to the formation of the desired product and less to biomass formation. There are, of course, some disadvantages to immobilized cell bioreactors, especially from a practical standpoint. Diffusional limitations may be severe in entrapped systems, and the cost of biocatalyst preparation may be high, especially if its operational lifetime is short.

It is helpful to view the types of reactions carried out in immobilized cell systems in terms of the complexity of the reaction network involved. A reaction involving one, or possibly two, enzyme(s) and requiring no cofactor regeneration is often best carried out by immobilized, non-viable cells, with permeabilization of the cell membrane to reduce diffusional resistance or crosslinking of the membrane for improved mechanical stability [50]. The next level of complexity is one in which a multistep pathway and cofactor regeneration are involved. This situation usually requires the use of viable cells, although they may be held in a non-growth state [51]. Finally, the process may require cell growth for product formation.

Cell immobilization may be achieved by a number of techniques; these can be

classed either as attachment or entrapment methods. Cellular aggregation can be viewed as an attachment method, although diffusion effects are as much a problem with this technique as with entrapment methods. The attachment of a cell to a solid surface can be accomplished via natural attractions (adsorption to ion exchange resins or spontaneous film formation) or by covalent binding. There are a large number of entrapment methods, often subdivided into those involving entrapment in a polymer network (*e.g.*, calcium alginate), those involving confinement in one phase of a liquid-liquid emulsion, and finally, methods in which cells are retained behind semipermeable membranes [52].

Since cellular physiology and metabolic activities are often quite sensitive to the environment of the cell, the substantial differences between the surroundings of a freely suspended cell and one that is immobilized (by any technique) indicate that some differences in cell behavior might be expected. A few studies have found evidence of such differences [*e.g.*, 53,54,55,56]; an investigation by Doran and Bailey on surface immobilized yeast reported increased ethanol production rates due to enhanced glucose uptake rates (as compared to suspended yeast cells), reduced immobilized cell specific growth rates, and increased quantities of polysaccharides (storage and structural) and DNA over the amounts found in suspended cells [55].

An obvious characteristic of immobilized cell systems is the large extension of reactor residence time of a cell over that found in a continuous suspended cell system. The stability of immobilized cell activity is a function of the number of enzymes utilized and their stability (in the microenvironment in question), the immobilization matrix or support, the particular microorganism being used, and also the state of the cell (viable or non-viable, growing or non-growing). Typically,

though, unless the immobilized cells are growing, a loss in desired catalytic activity will occur with time [*e.g.*, 57,58,59,60]. This activity decrease may be due to denatured, lost, or proteolyzed enzymes and cofactors; for viable non-growing cells, the complications and effects of starvation responses may be important. Biocatalyst deactivation has sometimes been reversed (in viable cells only) by the addition of an undefined nutrient complex such as yeast extract or peptone [51,60,61,62,63]. At least two studies have concluded that reactivation with these compounds is due to cell growth alone, and not to enzyme induction, renewal, or de-repression [61,63].

IMMOBILIZED SACCHAROLYTIC *CLOSTRIDIUM* SPP.

The first report of immobilized *C. acetobutylicum* was published in 1980 by Häggström and Molin [63a]. They demonstrated that, although immobilization of exponential or stationary phase vegetative cells yielded an active calcium alginate gel catalyst, the immobilization of spores followed by outgrowth in nutrient medium produced significantly higher volumetric activity. Two subsequent reports by Häggström [64,65] detailed additional calcium alginate immobilization experiments, all beginning with the immobilization and outgrowth of spores in nutrient medium. The gel preparations were then washed and incubated in a glucose-ammonium chloride-mineral salts medium, which also contained butyric acid. Although the initially high butanol-forming activity decreased soon after the start of a continuous experiment, butanol volumetric productivity after 1000 hours was still eight times that of the traditional batch fermentation [64]. More than half of the butanol produced was derived from the butyric acid in the feed.

A series of papers by Förberg and Häggström developed a nutrient dosing technique for *C. acetobutylicum* immobilized in calcium alginate [66] or adsorbed to beechwood shavings [67,68]. This feeding scheme involved constant feeding of a non-growth medium (glucose, inorganic salts, butyric acid (for the alginate experiment only), and no nitrogen source) and 15-minute periods in which a nutrient medium (containing NH_4Cl, peptone, and yeast extract) was fed, along with the non-growth medium, at intervals varying from 2 to 12 hours. An experiment in which the dosing interval was increased from 2 to 8 hours (over a four-day period) and then held at 8 hours resulted in a fairly high, steady productivity of butanol in the reactor [66]. Although the authors claimed that the typical biomass-to-butanol ratio found in traditional batch cultures (34%) was reduced to 2% with this dosing technique, they based their biomass calculations on the concentrations of suspended cells in the effluent from the immobilized cell experiments, ignoring the contribution of biomass production within the alginate matrix. The adsorption immobilization technique was successful in providing long-term butanol productivity when combined with the nutrient dosing scheme, though there were periods early in the experiments in which the majority of adsorbed cells deabsorbed from the shavings [68].

A different type of non-growth/growth feeding scheme was recently reported [69,70]; in this case the calcium alginate-immobilized cells were operated for 86 hours with a feed containing glucose and salts, but no nitrogen source. Ammonium chloride was then pulsed into the system and the feed switched to one containing this nitrogen source. The pattern of the loss of metabolic activity and the re-generation of product-forming activity during nitrogen feeding were followed with product concentration measurements and *in situ* NAD(P)H-dependent fluorescence

measurements on the immobilized cells.

Investigations involving growing, immobilized cells have also been carried out [71,72]. Although one study utilized the calcium alginate entrapment method [71], and the other focused on adsorption to coke [72], both featured continuous feed media containing undefined nitrogenous/vitamin mixtures (tryptone and/or yeast extract). While good productivities could be obtained, significant suspended cell production also occurred.

All of the aforementioned investigations have utilized *C. acetobutylicum* strain ATCC 824, but one report has been published on the immobilization of two sporulation-deficient *C. acetobutylicum* P262 mutants [73]. In an immobilized cell batch fermentation comparison, one strain, an early sporulation mutant unable to form a forespore septum or granulose, provided significantly higher solvent productivity than either the wild type or the other mutant strain. This high-productivity strain was then utilized in a continuous system, yielding very high butanol and total solvent productivities. However, because the feed was based on molasses (*i.e.*, was rich in nitrogen, vitamins, and complex organic compounds), significant immobilized and suspended cell growth took place.

Other clostridia closely related to *C. acetobutylicum* have also been immobilized. Kossen and coworkers entrapped *C. beijerinckii* in calcium alginate for use in packed-bed [74] and stirred-tank [75] systems with glucose feed, and also in a stirred-tank system with whey permeate (80% lactose) feed [76]. The catabolic pathways of this strain are identical to those of *C. acetobutylicum*, except that acetone is reduced to isopropanol in *C. beijerinckii*. Since cell growth caused fluid flow problems in the packed-bed experiments (and diverted glucose from product

formation), different media were tested for continuous fermentations. None were found to be satisfactory, and the packed-bed configuration was abandoned in favor of a stirred-tank apparatus. These experiments utilized growing immobilized cells and resulted in reactor solvent productivities (mass solvents formed·reactor liquid volume^{-1}·time^{-1}) 6–16 times greater than that found in comparable suspended cell batch cultivations.

Not all immobilized cell systems are operated for the purpose of chemical production; three reports on immobilized *C. butyricum* focus on NAD(P)H regeneration [77] and hydrogen production [78,79]. In the hydrogen-producing system, *C. butyricum* (producing acetic and butyric acids) was co-immobilized with either *Rhodopseudomonas* sp. RV [79] or spinach chloroplasts [78]; both systems were designed for photochemical energy production.

It is important to note that (with one exception) all of the above-mentioned studies discuss reactor parameters almost exclusively, paying virtually no attention to the metabolic, physiological, or morphological characteristics of the immobilized cells. A special note should be made of the lack of any report on cell concentrations in (or on) the immobilization support; absence of these measurements makes any real system-to-system comparison impossible. The "process" emphasis in these reports is representative of the rest of the immobilized cell literature (with a few notable exceptions). While immobilized cell systems can clearly outperform batch suspended cell fermentations in nearly all cases, the full potential of fixed cell bioreactors cannot be realized until the behavior of the immobilized cells themselves is better understood.

NAD(P)H-DEPENDENT CULTURE FLUORESCENCE

In situ NAD(P)H-dependent fluorescence measurements were first reported by Duysens and Amesz in 1957 [80], the technique was developed further by Chance and coworkers [*e.g.*, 81,82], and finally applied as an *in situ* measurement in cultivations of microorganisms by Harrison and Chance [83]. Since then, *in situ* fluorometry has been applied to batch and continuous suspended cell cultivations by several research groups [*e.g.*, 84,85,86,87]. Recently, on-line fluorescence monitoring was reported for immobilized *C. acetobutylicum* [69,70].

The *in vivo* fluorescence measurements described in these reports are based on the quantification of the 450 nm fluorescence of a cultivation excited by 360 nm light. Although other cell components may fluoresce in the same region under near-UV excitation, their contributions are small when compared with the fluorescence of NADH and NADPH. While the intracellular concentration of NADPH is nearly always much lower than that of NADH [88,89], the source of cellular fluorescence is usually referred to as "NAD(P)H" for generality.

One of the primary motivations behind the development of commercial fermentor fluorescence probes was the possibility for on-line biomass concentration estimation in suspended cell cultivations. Biomass concentration-fluorescence correlations have been developed in continuous and batch suspended cell cultivations of organisms with a single set of metabolic pathways (*i.e.*, **not** *C. acetobutylicum*) [*e.g.*, 85,86,90,91]. An important *caveat* in these correlations is the extreme sensitivity of the intracellular NAD(P)H content to process parameters such as aeration rate, pH, medium used, and reactor type [92]. It is necessary to derive the correlations under the same conditions as they are to be used.

A more interesting application for *in situ* NAD(P)H-fluorescence probes is the study of metabolic and physiological changes in microorganisms under cultivation conditions. Reports have been published describing NAD(P)H fluorescence changes due to glucose (or other carbon/energy substrate) or oxygen feeding after starvation [85,90,92,93,94,95], the change from batch to continuous-flow cultivation (*i.e.*, growth rate) [92], and the switch from the acid-producing phase to the solventogenic phase of batch fermentations of *C. acetobutylicum* [87,96]. Culture fluorescence measurements have also been combined with flow cytometric measurements of RNA, DNA, protein content and/or cell size during continuous steady-state and continuous but oscillating cultures of yeast [84,97].

Although the measured 360/450 nm fluorescence is due to the intracellular concentration of NAD(P)H of the organism under study, it is not possible to quantitatively convert fluorescence to NAD(P)H concentration *a priori*, if at all, because the measured fluorescence is attenuated by a number of factors [84,87]. However, it has been shown by enzymatic analysis of NADH content that culture fluorescence qualitatively describes intracellular NADH concentration [84]. While it is possible to make NADH-fluorescence correlations similar to the biomass-fluorescence relationships discussed previously, the extreme sensitivity of the level of intracellular NAD(P)H to environmental pertubations places very tight restrictions on the use of the correlation.

LITERATURE CITED

1. "Bergey's Manual of Determinative Bacteriology," 7^{th} Ed., R.S. Breed, E.G.D. Murray, and N.R. Smith (eds.), 1957, pp. 656–657.

2. M^{c}Coy, E., E.B. Fred, W.H. Peterson, and E.G. Hastings, "A Cultural Study of the Acetone Butyl Alcohol Organism," *J. Infect. Dis.*, **39**, 457–483 (1926).

3. Volesky, B. and T. Szczesny, "Bacterial Conversion of Pentose Sugars to Acetone and Butanol," *Adv. Biochem. Eng./Biotech.*, **27**, 101–120 (1983).

4. Welsh, F.W., R.E. Williams, and I.A. Veliky, "A Note on the Effect of Nitrogen Source on Growth of and Solvent Production by *Clostridium acetobutylicum*," *J. Appl. Bacteriol.*, **61**, 413–419 (1986).

5. Long, S., D.T. Jones, and D.R. Woods, "Initiation of Solvent Production, Clostridial Stage, and Endospore Formation in *Clostridium acetobutylicum* P262," *Appl. Microbiol. Biotechnol.*, **20**, 256–261 (1984).

6. Lampen, J.D. and W.H. Peterson, "Growth Factor Requirements of Clostridia," *Arch. Biochem.*, **2**, 443–449 (1943).

7. Häggström, L. and C. Förberg, "Significance of an Extracellular Polymer for the Energy Metabolism in *Clostridium acetobutylicum*: A Hypothesis," *Appl. Microbiol. Biotechnol.*, **23**, 234–239 (1986).

8. Jones, D.T., A. van der Westhuizen, S. Long, E.R. Allcock, S.J. Reid, and D.R. Woods, "Solvent Production and Morphological Changes in *Clostridium acetobutylicum*," *Appl. Env. Microbiol.*, **43**, 1434–1439 (1982).

9. Reysenbach, A.L., N. Ravenscroft, S. Long, D.T. Jones, and D.R. Woods, "Characterization, Biosynthesis, and Regulation of Granulose in *Clostridium acetobutylicum*," *Appl. Env. Microbiol.*, **52**, 185–190 (1986).

10. Gutierrez, N. and I.S. Maddox, "Role of Chemotaxis in Solvent Production by *Clostridium acetobutylicum*," *Appl. Env. Microbiol.*, **53**, 1924–1927 (1987).

11. Woods, D.R. and D.T. Jones, "Physiological Responses of *Bacteriodes* and *Clostridium* Strains to Environmental Stress Factors," *Adv. Microbiol. Physiol.*, **28**, 1–64 (1986).

12. Cho, K.Y. and C.H. Doy, "Ultrastructure of the Obligately Anaerobic Bacteria *Clostridium kluyveri* and *Clostridium acetobutylicum*," *Aust. J. Biol. Sci.*, **26**, 547–558 (1973).

13. Long, S., D.T. Jones, and D.R. Woods, "Sporulation of *Clostridium acetobutylicum* P262 in a Defined Medium," *Appl. Env. Microbiol.*, **45**, 1389–1393 (1983).

14. Long, S., D.T. Jones, and D.R. Woods, "The Relationship Between Sporulation and Solvent Production in *Clostridium acetobutylicum* P262," *Biotech. Lett.*, **6**, 529–534 (1984).

15. Takagi, A., T. Kawata, and S. Yamamoto, "Electron Microscope Studies on Ultrathin Sections of Spores of the Clostridium Group, with Special Reference to the Sporulation and Germination Process," *Jap. J. Microbiol.*, **4**, 37–55 (1960).

16. Fitz-James, P. and E. Young, "Morphology of Sporulation," in *The Bacterial Spore*, G.W. Gould and A. Hurst (eds.), Academic Press, London, 1969, pp. 39–72.

17. Young, M. and J. Mandelstam, "Early Events During Bacterial Endospore Formation," *Adv. Microb. Physiol.*, **20**, 102–162 (1979).

18. Bowring, S.N. and J.G. Morris, "Mutagenesis of *Clostridium acetobutylicum*,"

J. Appl. Bacteriol., **58**, 577–584 (1985).

19. Allcock, E.R., S.J. Reid, D.T. Jones, and D.R. Woods, "Autolytic Activity and an Autolysis-Deficient Mutant of *Clostridium acetobutylicum*," *Appl. Env. Microbiol.*, **42**, 929–935 (1981).

20. Junelles, A.M., R. Janati-Idrissi, A. El Kanouni, H. Petitdemange, and R. Gay, "Acetone-Butanol Fermentation by Mutants Selected for Resistance to Acetate and Butyrate Halogen Analogues," *Biotech. Lett.*, **9**, 175–178 (1987).

21. Dürre, P., A. Kuhn, and G. Gottschalk, "Treatment with Allyl Alcohol Selects Specifically for Mutants of *Clostridium acetobutylicum* Defective in Butanol Synthesis," *FEMS Microbiol. Lett.*, **36**, 77–81 (1986).

22. Jones, D.T. and D.R. Woods, "The Acetone-Butanol Fermentation Revisited," *Microbiol. Rev.*, **50**, 484–524 (1986).

23. O'Brien, R.W., and J.G. Morris, "Oxygen and the Growth and Metabolism of *Clostridium acetobutylicum*," *J. Gen. Microbiol.*, **68**, 307–318 (1971).

24. Lemme, C.J. and J.R. Frankiewicz, U.S. Patent 4,521,516, 1985.

25. M^{c}Cutchan, W.N. and R.J. Hickey, "The Butanol-Acetone Fermentation," in *Industrial Fermentations*, vol. 1, L.A. Underkofler and R.J. Hickey (eds.), Chemical Publishing Co., New York, 1954, pp, 347–388.

26. Prescott, S.C. and C.G. Dunn, *Industrial Microbiology*, M^{c}Graw-Hill, New York, 1959, pp. 250–284.

27. Ross, D., "The Acetone-Butanol Fermentation," *Prog. Ind. Microbiol.*, **3**, 73–90 (1961).

28. Walton, M.T. and J.L. Martin, "Production of Butanol-Acetone by Fermentation," in *Microbial Technology*, vol. 2, 2nd Ed., H.J. Peppler and D. Perlman

(eds.), Academic Press, New York, 1979, pp. 188–209.

29. Moreira, A.R., "Acetone-Butanol Fermentation," in *Organic Chemicals from Biomass*, D.L. Wise (ed.), The Benjamin/Cummings Publishing Co., London, 1983, pp. 385–406.

30. Ennis, B.M., N.A. Gutierrez, and I.S. Maddox, "The Acetone-Butanol-Ethanol Fermentation: A Current Assessment," *Proc. Biochem.*, **21**, 131–147 (1986).

31. M^{c}Neil, B. and B. Kristiansen, "The Acetone Butanol Fermentation," *Adv. Appl. Microbiol.*, **31**, 61–92 (1986).

32. Lenz, T.G. and A.R. Moreira, "Economic Evaluation of the Acetone-Butanol Fermentation," *Ind. Eng. Chem. Prod. Res. Dev.*, **19**, 478–483 (1980).

33. Schoutens, G.H. and W.J. Groot, "Economic Feasibility of the Production of *iso*-Propanol-Butanol-Ethanol Fuels from Whey Permeate," *Proc. Biochem.*, **20**, 117–121 (1985).

34. Meinecke, B., H. Bahl, and G. Gottschalk, "Selection of an Asporogenous Strain of *Clostridium acetobutylicum* in a Continuous Culture Under Phosphate Limitation," *Appl. Env. Microbiol.*, **48**, 1064–1065 (1984).

35. Stephens, G.M., R.A. Holt, J.C. Gottschal, and J.G. Morris, "Studies on the Stability of Solvent Production by *Clostridium acetobutylicum* in Continuous Culture," *J. Appl. Bacteriol.*, **59**, 597–605 (1985).

36. Hartmanis, M.G.N., H. Ahlman, and S. Gatenbeck, "Stability of Solvent Formation in *Clostridium acetobutylicum* During Repeated Subculturing," *Appl. Microbiol. Biotechnol.*, **23**, 369–371 (1986).

37. Moreira, A.R., D.C. Ulmer, and J.C. Linden, "Butanol Toxicity in the Butylic Fermentation," *Biotech. Bioeng. Symp. Ser.*, **11**, 567–579 (1981).

38. Costa, J.M., and A.R. Moreira, "Growth Inhibition Kinetics for the Acetone-Butanol Fermentation," *A. C. S. Symp. Ser.*, **207**, 501–512 (1983).

39. Klein, J. and F. Wagner, "Immobilized Whole Cells," in Proceedings of the First European Congress on Biotechnology, 1978, Part 3, Interlaken, Switzerland, 25 September 1978, DECHEMA Monograph, Band 82, New York, p. 152.

40. "Characterization of Immobilized Biocatalysts," K. Buchholz (ed.), DECHEMA Monograph No. 1724–1731, **84**, Verlag-Chemie, New York, 1979, pp. 265–335.

41. Kolot, F.B., "Microbial Carriers—Strategy for Selection," *Proc. Biochem.*, **16**, 2–9 (1981).

42. Kolot, F.B., "Microbial Carriers–Strategy for Selection. Part 2," *Proc. Biochem.*, **16**, 30–33 (1981).

43. Messing, R.A., "Support-Bound Microbial Cells," *Appl. Biochem. Biotech.*, **6**, 167–178 (1981).

44. Klein, J. and K.-D. Vorlop, "Immobilized Cells—Catalyst Preparation and Reaction Performance," *A. C. S. Symp. Ser.*, **207**, 377–392 (1982).

45. Cheetham, P.S.J., "The Application of Immobilized Enzymes and Cells and Biochemical Reactors in Biotechnology—Principles of Enzyme Engineering," in *Principles of Biotechnology*, A. Wiseman (ed.), Surrey Univ. Press, New York, 1983, pp. 172–208.

46. Linko, P. and Y.-Y. Linko, "Industrial Applications of Immobilized Cells," *CRC Crit. Rev. Biotech.*, **1**, 289–338 (1984).

46a. Jack, T.R. and J.E. Zajic, "The Immobilization of Whole Cells," *Adv. Biochem. Eng.*, **5**, 125–145 (1977).

47. Buchholz, K., "Reaction Engineering Parameters for Immobilized Biocatalysts,"

Adv. Biochem. Eng., **24**, 39–71 (1982).

48. Venkatasubramanian, K. and S.B. Karkare, "Process Engineering Considerations in the Development of Immobilized Living Cell Systems," in *Immobilized Cells and Organelles*, vol. II, B. Mattiasson (ed.), CRC Press, Boca Raton, 1983, pp. 134–144.

49. Karel, S.F., S.B. Libicki, and C.R. Robertson, "The Immobilization of Whole Cells: Engineering Principles," *Chem. Eng. Sci.*, **40**, 1321–1354 (1985).

50. Gestrelius, S., "Immobilized Nonviable Cells for Use of a Single or a Few Enzyme Steps," in *Immobilized Cells and Organelles*, vol. II, B. Mattiasson (ed.), CRC Press, Boca Raton, 1983, pp. 1–22.

51. Mattiasson, B., "Immobilized Viable Cells," in Immobilized Cells and Organelles, vol. II, B. Mattiasson (ed.), CRC Press, Boca Raton, 1983, p. 23–40.

52. Mattiasson, B., "Immobilization Methods," in *Immobilized Cells and Organelles*, vol. I, B. Mattiasson (ed.), CRC Press, Boca Raton, 1983, pp. 3–25.

53. Navarro, J.M. and G. Durand, "Modification of Yeast Metabolism by Immobilization onto Porous Glass," *Eur. J. Appl. Microbiol.*, **4**, 243–254 (1977).

54. Doran, P.M. and J.E. Bailey, "Enhanced Ethanol Production by Immobilized Yeast Cells," in Proceedings VIth Australian Biotech. Conf., Brisbane, 1984, p. 421.

55. Doran, P.M. and J.E. Bailey, "Effects of Immobilization on Growth, Fermentation Properties, and Macromolecular Composition of *Saccharomyces cerevisiae* Attached to Gelatin," *Biotech. Bioeng.*, **28**, 73–87 (1986).

56. Doran, P.M. and J.E. Bailey, "Effects of Immobilization on the Nature of Glycolytic Oscillations in Yeast," *Biotech. Bioeng.*, **29**, 892–897 (1987).

57. Scherer, P., M. Kluge, J. Klein, and H. Sahm, "Immobilization of the Methanogenic Bacterium *Methanosarcina barkeri*," **23**, 1057–1065 (1981).

58. M^{c}Ghee, J.E., G. St. Julian, R.W. Detroy, and R.J. Bothast, "Ethanol Production by Immobilized *Saccharomyces cerevisiae, Saccharomyces uvarum*, and *Zymomonas mobilis*," *Biotech. Bioeng.*, **24**, 1155–1163 (1982).

59. Inloes, D.S., A.S. Michaels, C.R. Robertson, and A. Matin, "Ethanol Production by Nitrogen-Deficient Yeast Cells Immobilized in a Hollow-Fiber Membrane Bioreactor," *Appl. Microbiol. Biotechnol.*, **23**, 85–91 (1985).

60. Klein, J. and F. Wagner, "Different Strategies to Optimize the Production Phase of Immobilized Cells," *Ann. N.Y. Acad. Sci.*, **501**, 306–316 (1987).

61. Ohlson, S., P.-O. Larsson, and K. Mosbach, "Steroid Transformation by Living Cells Immobilized in Calcium Alginate," *Eur. J. Appl. Microbiol. Biotechnol.*, **7**, 103–110 (1979).

62. Szwajcer, E., P. Brodelius, and K. Mosbach, "Production of α-Keto Acids: 2. Immobilized Whole Cells of *Providencia* sp. PCM 1298 Containing L-Amino Acid Oxidase," *Enz. Microb. Tech.*, **4**, 409–413 (1982).

63. Cheetham, P.S.J., C. Garrett, and J. Clark, "Isomaltulose Production Using Immobilized Cells," *Biotech. Bioeng.*, *bf 27*, 471–481 (1985).

63a. Häggström, L. and N. Molin, "Calcium Alginate Immobilized Cells of *Clostridium acetobutylicum* for Solvent Production," *Biotech. Lett.*, **2**, 241–246 (1980).

64. Häggström, L., "Immobilized Cells of *Clostridium acetobutylicum* for Butanol Production," in *Advances in Biotechnology*, vol. I, M. Moo-Young (ed.), Pergamon Press, New York, 1981, pp. 79–83.

65. Häggström, L. and S.-O. Enfors, "Continuous Production of Butanol with

Immobilized Cells of *Clostridium acetobutylicum*," *Appl. Biochem. Biotechnol.*, **7**, 35–37 (1982).

66. Förberg, C., S.-O. Enfors, and L. Häggström, "Control of Immobilized, Non-Growing Cells for Continuous Production of Metabolites," *Eur. J. Appl. Microbiol. Biotechnol.*, **17**, 143–147 (1983).

67. Förberg, C. and L. Häggström, *Adsorbed Cell Systems Controlled by the Nutrient Dosing Technique*, in 3rd European Congress on Biotechnology, vol. II, Munich, 10–14 September 1984, Verlag-Chemie, pp. II-115–II-120.

68. Förberg, C. and L. Häggström, "Control of Cell Adhesion and Activity During Continuous Production of Acetone and Butanol with Adsorbed Cells," *Enz. Microb. Tech.*, **7**, 230–234 (1985).

69. Reardon, K.F., T. Scheper, and J.E. Bailey, "*In Situ* Fluorescence Monitoring of Immobilized *Clostridium acetobutylicum*," *Biotech. Lett.*, **8**, 817–822 (1986).

70. Reardon, K.F., T.-H. Scheper, and J.E. Bailey, "Einsatz eines Fluoresczenzsensors zur Messung der NAD(P)H-abhängigen Kulturefluoreszenz Immobilisierter Zellsysteme," *Chem.-Ing.-Tech.*, **59**, 600–601 (1987).

71. Frick, C. and K. Schügerl, "Continuous Acetone-Butanol Production with Free and Immobilized *Clostridium acetobutylicum*," *Appl. Microbiol. Biotechnol.*, **25**, 186–193 (1986).

72. Welsh, F.W., R.E. Williams, and I.A. Veliky, "Solid Carriers for a *Clostridium acetobutylicum* That Produces Acetone and Butanol," *Enz. Microb. Tech.*, **9**, 500–502 (1987).

73. Largier, S.T., S. Long, J.D. Santangelo, D.T. Jones, and D.R. Woods, "Immobilized *Clostridium acetobutylicum* P262 Mutants for Solvent Production,"

Appl. Env. Microbiol., **50**, 477–481 (1985).

74. Krouwel, P.G., W.J. Groot, N.W.F. Kossen, and W.F.M. van der Laan, "Continuous Isopropanol-Butanol-Ethanol Fermentation by Immobilized *Clostridium beijerinckii* Cells in a Packed Bed Fermentor," *Enz. Microb. Tech.*, **5**, 46–54 (1983).

75. Krouwel, P.G., W.J. Groot, and N.W.F. Kossen, "Continuous IBE Fermentation by Immobilized Growing *Clostridium beijerinckii* Cells in a Stirred-Tank Fermentor," *Biotech. Bioeng.*, **25**, 281–299 (1983).

76. Schoutens, G.H., M.C.H. Nieuwenhuizen, and N.W.F. Kossen, "Continuous Butanol Production from Whey Permeate with Immobilized *Clostridium beijerinckii* LMD 276," *Appl. Microbiol. Biotechnol.*, **21**, 282–286 (1985).

77. Matsunaga, T., N. Matsunaga, and S. Nishimura, "Regeneration of NAD(P)H by Immobilized Whole Cells of *Clostridium butyricum* under Hydrogen High Pressure," *Biotech. Bioeng.*, **27**, 1277–1281 (1985).

78. Kayano, H., T. Matsunaga, I. Karube, and S. Suzuki, "Photochemical Energy Conversion System Using Immobilized Chloroplasts," *Biotech. Bioeng.*, **23**, 2283–2291 (1981).

79. Miyake, J., X.-Y. Mao, and S. Kawamura, "Photoproduction of Hydrogen from Glucose by a Co-Culture of a Photosynthetic Bacterium and *Clostridium butyricum*," *J. Ferment. Technol.*, **62**, 531–535 (1984).

80. Duysens, L.M.N. and J. Amesz, "Fluorescence Spectrophotometry of Reduced Phosphopyridine Nucleotide in Intact Cells in the Near-Ultraviolet and Visible Region," *Biochim. Biophys. Acta*, **24**, 19–26 (1957).

81. Chance, B. and V. Legallais, "Differential Microfluorimeter for the Localization

of Reduced Pyridine Nucleotide in Living Cells," *Rev. Sci. Instr.*, **30**, 732–735 (1959).

82. Chance, B., J.R. Williamson, D. Jamieson, and B. Schoener, "Properties and Kinetics of Reduced Pyridine Nucleotide Fluorescence of the Isolation and *in vivo* Rat Heart," *Biochem. Z.*, **341**, 357–377 (1965).

83. Harrison, D.E.F. and B. Chance, "Fluorimetric Technique for Monitoring Changes in the Level of Reduced Nicotinamide Nucleotides in Continuous Cultures of Microorganisms," *Appl. Microbiol.*, **19**, 446–450 (1970).

84. Scheper, T. and K. Schügerl, "Culture Fluorescence Studies on Aerobic Continuous Cultures of *Saccharomyces cerevisiae*, *Appl. Microbiol. Biotechnol.*, **23**, 440–444 (1986).

85. Zabriskie, D.W. and A.E. Humphrey, "Estimation of Fermentation Biomass Concentration by Measuring Culture Fluorescence," *Appl. Env. Microbiol.*, **35**, 337–343 (1978).

86. Luong, J.H.T. and D.J. Carrier, "On-line Measurement of Culture Fluorescence during Cultivation of *Methylomonas mucosa,*" *Appl. Microbiol. Biotechnol.*, **24**, *65–70 (1986).*

87. Reardon, K.F., T.-H. Scheper, and J.E. Bailey, "Metabolic Pathway Rates and Culture Fluorescence in Batch Fermetations of *Clostridium acetobutylicum*," *Biotech. Prog.*, **3**, 153–167 (1987).

88. Takebe, I. and K. Kitahara, "Levels of Nicotinamide Nucleotide Coenzymes in Lactic Acid Bacteria," *J. Gen. Appl. Microbiol.*, **9**, 31–40 (1963).

89. London, J. and M. Knight, " Concentrations of Nicotinamide Nucleotide Coenzymes in Micro-Organisms," *J. Gen. Microbiol.*, **44**, 241–254 (1966).

90. Beyeler, W., A. Einsele, and A. Fiechter, "On-Line Measurements of Culture Fluorescence: Method and Application," *Eur. J. Appl. Microbiol. Biotechnol.*, **13**, 10–14 (1981).

91. Meyer, H.-P., W. Beyeler, and A. Fiechter, "Experiences with the On-Line Measurement of Cuture Fluorescence during Cultivation of *Bacillus subtilis, Escheria coli*, and *Sporotrichum thermophile*," *J. Biotechnol.*, **1**, *341–349 (1984).*

92. Scheper, T., A. Gebauer, and K. Schügerl, "Monitoring of NADH-Dependent Culture Fluorescence during the Cultivation of *Escherichia coli*," *Chem. Eng. J.*, **34**, B7–B12 (1987).

93. Zabriskie, D.W., "Use of Culture Fluorescence for Monitoring of Fermentation Systems," *Biotechnol. Bioeng. Symp.*, **9**, 117–123 (1979).

94. Einsele, A., D.L. Ristroph, and A.E. Humphrey, "Substrate Uptake Mechanisms for Yeast Cells," *Eur. J. Appl. Microbiol. Biotechnol.*, **6**, 335–339 (1979).

95. Scheper, T., T. Lorenz, W. Schmidt, and K. Schügerl, "Measurement of Culture Fluorescence during the Cultivation of *Penicillium chrysogenum* and *Zymomonas mobilis*," *J. Biotechnol.*, **3** 231–238 (1986).

96. Srinivas, S.P., and R. Mutharason, "Culture Fluorescence Characteristics and Its Metabolic Significance in Batch Cultures of *Clostridium acetobutylicum*," *Biotech Lett.*, **9**, 139–142 (1987).

97. Scheper, T., H. Hoffmann, and K. Schügerl, "Flow Cytometric Studies during Culture of *Saccharomyces cerevisiae*," *Enz. Microb. Tech.*, **9**, (1987).

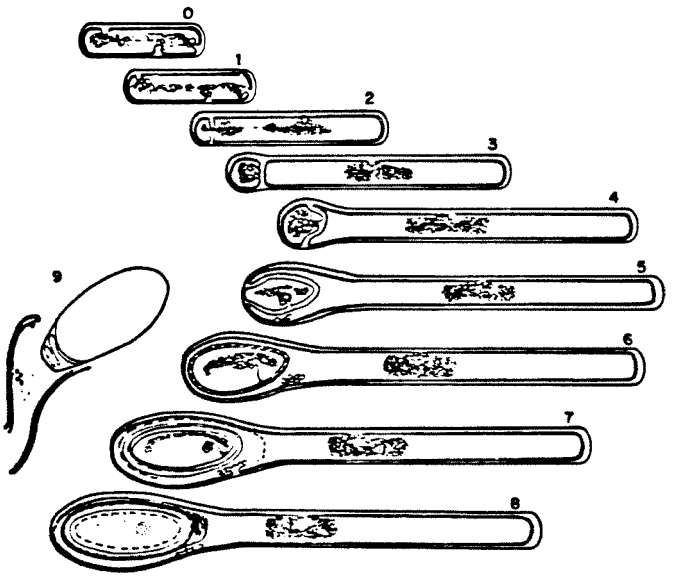

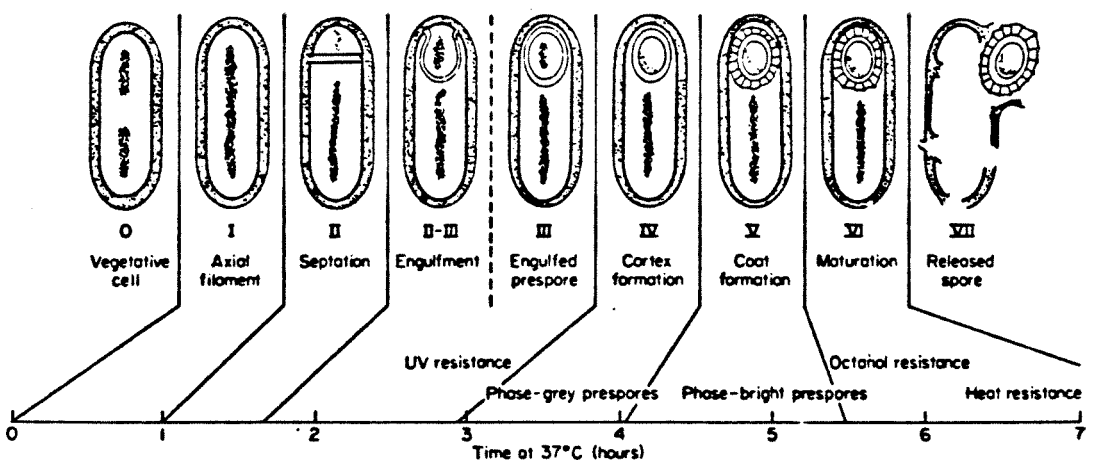

Figure 1. Sequence of sporulation events in
A (top): *Clostridium* spp. [16] and **B** (bottom): *Bacillus* spp. [17]

CHAPTER 3

MATERIALS AND METHODS

BACTERIAL STRAINS

The bacteria used in the majority of experiments in this thesis were of the American Type Culture Collection (ATCC) strain 824, the type strain for this species and the strain most often utilized in other research laboratories.

In experiment CI30, the ATCC strain 39236 was used. This strain, a butanol-tolerant, asporogenic mutant of ATCC 4259 [1,2], was developed at the Moffett Technical Center (Argo, IL).

STRAIN MAINTENANCE

Clostridium acetobutylicum ATCC 824 was maintained in corn mash medium [3]. This medium was prepared by boiling an aqueous mixture of 5% (w/v) corn meal ("Argo" brand) and 0.05% (w/v) cysteine for 1 hour before dispensing to screw cap culture tubes. The tubes were autoclaved for 15–20 minutes at 121°C. After inoculation, the tubes were incubated at 36°C in a GasPak anaerobic culture jar (Baltimore Biological Laboratories) [4] for 3–5 days. The culture tubes were then removed from the jar and stored at 4°C. This process was repeated every 2–4 months.

The asporogenic strain ATCC 39236 was typically maintained by more frequent transfers to screw cap tubes of fresh full growth medium (FGM) (see next section for composition). However, the corn mash medium was also used for culturing this strain. All transfers and operations involving ATCC 39236 were performed in an anaerobic glove box (Vacuum/Atmospheres Co., Model HE-63-P) because this strain was especially sensitive to oxygen.

CULTURE MEDIA

Two different media were used for routine culturing of the two strains (Table 1). Both were sterilized by autoclaving for 15–20 minutes at 121°C. FGM was autoclaved in three parts (glucose; yeast extract, peptone, and salts; and $FeCl_3$), then combined when cool.

Strain ATCC 824 was grown in starch medium for spore production (for the immobilized cell experiments and for short-term storage) and in FGM for vegetative cell growth. Cultures were inoculated with corn mash cultures (1–2% v/v) or with starch or FGM cultures (5–10% v/v). Inocula from corn mash or starch cultures were heat- shocked for 60 seconds in a 90–95°C water bath before addition to new medium in order to activate the spores.

The asporogenic strain ATCC 39236 was cultured only in FGM; it would not grow in the starch medium. New cultures were inoculated (typically 10% v/v) from older FGM cultures.

IMMOBILIZATION

All immobilized cell experiments in this project utilized the calcium alginate immobilization technique [6]. In the experiments involving *C. acetobutylicum* 824, 200 mL of a starch culture were centrifuged (Beckman Model J-21) for 10 minutes at 4°C and 8,000 RPM. The liquid was decanted and the pellet washed with 150 mL deionized water before being spun down for 8 minutes at 4°C and 6,000 RPM. After the rinse liquid was decanted, the cells were resuspended in 20 mL water (the final biomass concentration was approximately 8.5 mg dry cell weight/mL). Eight

milliliters of this suspension were mixed with a sterile (autoclaved) sodium alginate (Fisher) solution (3.15 g in 98 mL deionized water) to a final alginate concentration of 3% (w/v). Beads of about 2.5 mm diameter were formed by pumping the alginate-cell suspension dropwise through a Pasteur pipet and into 500 mL of 5% (w/v) $CaCl_2 \cdot 2H_2O$ (in a 1 L Erlenmeyer flask) on ice. The beads were refrigerated overnight in this solution, then rinsed before use in an experiment (for details, see Chapters 5 and 6). With this strain, the immobilization was done in air; *i.e.*, not in the anaerobic hood.

Immobilization of strain ATCC 39236 differed from that of strain 824 in that (1), 200 mL of FGM culture were used; (2), the beads were "cured" in the ice-cold $CaCl_2$ solution for only 2 hours after the last bead had been formed (bead dropping of 106 mL sodium alginate took about 1 hour); and (3), all aspects of the procedure were carried out anaerobically, either in a glove box or in sealed tubes.

REACTOR SYSTEM FOR SUSPENDED CELL EXPERIMENTS

Suspended cell batch fermentations (see Chapter 4) were performed in a system based on a New Brunswick MultiGen fermentor (Figures 2 and 3), which provided stirring as well as temperature (36°C) and pH control (Ingold pH probe 465-35 and Chemtrix pH Controller Type 45AR). Norprene tubing (Cole-Parmer Instrument Co.) was used exclusively for its low oxygen diffusivity (10^{-9} $cm^2 \cdot sec - 1 \cdot (cm\ Hg)^{-1}$ (personal communication, Norton Performance Plastics)) and long life in the peristaltic pumps (Masterflex) used in the system. Anaerobic conditions were maintained by sparging the fermentor liquid with the gases (H_2 and CO_2) from a

modified BBL GasPak (Baltimore Biological Laboratories) anaerobic culturing jar. With this technique, oxygen gas in the system is removed as water on a palladium catalyst contained in the GasPak jar [4] as the gas is continuously recirculated between the fermentor and the GasPak jar. Typically, the operating pressure in the system was 0 to 2 psig, controlled by a relief valve on the GasPak jar. Samples were taken with a syringe and needle through a septum-covered thick walled capillary tube.

Culture fluorescence was measured in a quartz column (40 mm ID and 157 mm height; the liquid volume was 135 mL), which was connected to the MultiGen vessel via a recirculation loop. Liquid from the fermentor jar flowed upwards through the column and back to the culture vessel at a rate of 255 mL/min. The total liquid in the system was 600 mL. An Ingold Fluorosensor probe (described further below) was attached to the column, using a plastic sleeve that had been glued (RTV Silicone Rubber Adhesive, General Electric Co.) to the column around a 3 cm diameter optical grade quartz window. The column and column-probe interface were covered with a plastic shield and aluminum foil to prevent stray light interference on the fluorescence measurements.

REACTOR SYSTEM FOR IMMOBILIZED CELL EXPERIMENTS

The immobilized cell experiments consisted of two major phases: a batch growth phase and a continuous phase (for bioconversion and regeneration). Different systems were used for each phase. In the batch growth phase of most experiments, a homemade fermentor was used to provide mixing, pH and temperature

control, but in runs CI28 and CI30 the batch vessel of the MultiGen unit was utilized. The batch fermentor vessel ports were the same as those of the continuous system vessel, except that there was no feed nor effluent line. With the homemade fermentor jar system, the liquid volume was 400 mL in the growth phase, whereas the liquid volume in the batch MultiGen jar system was 550 mL.

Oxygen was removed (in both experimental phases) with the modified GasPak jar described in the preceding section. Control of pH (with 2N NaOH for the growth phase and 1N NaOH for the continuous phase) and temperature control (36°C) took place in the fermentor jar, as described earlier. The feed medium (in 2 to 8 L jars) was kept anaerobic by bubbling oxygen-free nitrogen gas through the liquid.

A schematic of the system used for immobilized cell continuous packed column fermentations is shown in Figure 4. While most of the experiments employed the New Brunswick MultiGen fermentor described above as a control/mixing vessel, a homemade fermentor unit consisting of a Pyrex jar, rubber stopper, magnetic stirring plate, and controlled-temperature bath was used in the earlier experiments. In both cases, the fermentor vessel had the ports and connections shown in Figure 5, except that the homemade vessel required three conductivity probes for level control.

The feed medium was pumped (Masterflex peristaltic pump) into a break tube before entering the fermentor. Feed flow rates were measured with a 5 mL pipet (the tapered end had been adapted to fit tubing) that was attached to the feed line at a "T" connector and was located between the feed reservoir and pump. When the flow rate was to be measured, the measuring column was filled with medium by unclamping the short section of tubing leading to the feed line (the N_2 exit from

the feed bottle had been closed a few minutes prior to this, to provide pressure). Then, with the tubing leading from the feed bottle to the T clamped closed, the flow rate was measured by timing the removal of 1 or 2 mL from the pipet. Liquid level in the MultiGen system was controlled by overflow into a 500 mL Erlenmeyer flask. Liquid was pumped out of this flask, and the headspace of this flask was connected to the GasPak Jar in order to equilibrate the pressure in the system. In the system utilizing the homemade fermentor jar, level control was performed with a Dyna-Sense Electronic Liquid Level Controller and probes (Cole-Parmer Instrument Co.). Probes were sterilized in ethanol and rinsed with deionized water before use.

A packed-bed reactor design was utilized in all of the immobilized cell experiments. Two different columns were used; most experiments employed a Pyrex column (35 mm ID, 162 mm height), but a quartz column (40 mm ID, 157 mm height) was used for those runs in which immobilized cell fluorescence was measured. The interface with the fluorescence probe was described in the preceding section. Both columns tapered to a glass tube for connection to the Norprene tubing and were closed at the top with a rubber stopper fitted with an exit tube and a vent port, which was normally closed. The bead beds were supported on stainless steel screens (attached to short (1–2 cm) stainless steel annuli); these screens were in turn supported at the base of the columns by quartz projections (in the quartz column) or by a glass disc through which many small holes had been made (in the Pyrex column). The screen mesh openings were approximately 1.6 mm wide. An additional screen was placed at the top of the bead bed to prevent the escape of beads from the column. The column was connected to the fermentor vessel via a

recirculation loop; liquid from the vessel flowed upwards through the column and returned to the culture jar at a rate of 145 mL/min. The total liquid in the continuous phase was either 370 mL (Pyrex column and homemade fermentor), 460 mL (Pyrex column and MultiGen vessel), or 480 mL (quartz column and MultiGen vessel).

Three approaches were used to remove interstitial gas bubbles from the bead bed. First, a bubble trap was inserted in the tubing leading from the fermentor vessel to the base of the system (Figure 6). Second, the flow from the fermentor vessel to the column was occasionally pulsed by manually clamping the tubing closed momentarily (with the recirculation pump at normal speed) and then unclamping quickly. Finally, in runs CI28 and CI30, this flow pulsing was performed automatically with a solenoid pinch valve (Angar Scientific Co.) attached to an adjustable-period relay/timer (constructed at the Institut für Technische Chemie, Universität Hannover, FRG).

IN SITU FLUORESCENCE MEASUREMENTS

The NAD(P)H-dependent intracellular fluorescence of suspended and immobilized *C. acetobutylicum* was measured in several experiments (those described in Chapter 4, and runs CI23, CI28, and CI30 of Chapters 5 and 6). An Ingold Fluorosensor probe and signal processing unit were used to make this measurement; the interface of this probe with the quartz column has been discussed in the preceding sections. A schematic of the probe is shown in Figure 7 [7]. Light from a low-pressure mercury vapor lamp passes through a set of filters to produce a 360

nm light beam, which is then carried to the optical head by a short fiber optic cable. Fluorescent light from the culture (or immobilized cell bed) is collected at the optical head, passed through a 450 nm filter, and quantified with a photomultiplier tube. The photomultiplier signal was passed to a signal processing unit, which provided an output signal of -10V to +10V to a chart recorder. The relative fluorescence values were indicated on a $3\frac{1}{2}$-digit LED display. The processing unit also provided two measuring ranges (X1 and X10), three low-pass signal filters (0.1, 1, and 10 Hz), variable PMT amplifier gain (10 to 1000%), and a variable-interval "peak detector" (0.1 to 25 second interval). Typically, the unit was kept in the X10 range (*i.e.*, relative fluorescence values of 00.0 to +100.0); it was often necessary to change the signal offset to stay in this range. These offset changes were accounted for when the data were prepared for plotting.

In order to verify that the observed fluorescence signal changes were due to the cells and not to the liquid medium, background fluorescence measurements were made on cell-free liquid samples in a Shimadzu RF-540 spectrofluorometer (excitation wavelength 360 nm, emission 450 nm, low sensitivity, and excitation and emission slit widths 10 nm). The fluorescence values from the Shimadzu spectrofluorometer were compared to the Fluorosensor signal with the use of a calibration curve (*e.g.*, Figure 8). This calibration was performed before every second experiment to account for lamp aging. In this procedure, a 0.05N H_2SO_4 solution was circulated through the empty column (with the probe attached) to serve as the zero fluorescence mixture. Small volumes of a 0.1 mg/mL quinine sulfate (Sigma) solution were added periodically. When the Ingold signal had stabilized, a sample was taken and its fluorescence measured with the spectrofluorometer.

Another system, also suitable for *in situ* culture fluorescence measurements, was constructed with the assistance of Dr. Thomas Scheper (though not used in the experiments reported herein). This system (Figure 9) differed from the Ingold instrument in that it featured a 1 m bifurcated liquid/fiber optic cable. This cable was constructed by Volpi AG (Switzerland). The main section (0.4 m) of the cable consisted of a liquid core (for the conduction of UV light) surrounded by optical glass fibers (for the transmission of the 460 nm light). This main section branched into two "legs," one containing the liquid optical guide and the other containing the glass fibers. The entire cable was coated with plastic, and all ends were fitted with metal ferrules for attachment to filter holders. Light for this system was provided by a Pen-Ray Model 11-SC-1L mercury-argon low-pressure lamp (Ultra-Violet Products, Inc.); this lamp featured an integral tubular filter for the conversion of the 254 nm mercury line to 366 nm. The power was provided by a Model SCT-1 transformer (Ultra-Violet Products, Inc.). The lamp was mounted in an Oriel Model 77839 lamp mount and filter assembly, which had been bored slightly to accommodate the Pen-Ray lamp. After passing through a 365 nm interference filter (Oriel Corp.), the light entered the liquid fiber leg of the optical cable and was led to the emission/collection end of the "combination" section. Fluorescent light was also collected at this end and let through the glass fiber leg to a 460 nm interference filter (Oriel Corp.); the light was then measured with a photomultiplier tube (Oriel Corp. Model 77761) and the signal was processed and displayed on a Model 7070 Photometer Power Supply and Readout (Oriel Corp.).

A quinine sulfate calibration test (as described above for the background correlation) was performed on the Ingold Fluorosensor system and the system based on

the Volpi optic cable (Figure 10). As can be seen, the Volpi-based system actually has a slightly higher sensitivity at the instrument settings used for the calibration.

ASSAYS

A. Suspended Cells

The correlation curve shown in Figure 11 was obtained from a stationary culture of vegetative rods, grown in FGM. This correlation could not be used for suspended cell populations with significant numbers of spores or other non-vegetative forms, since these cell types absorb and scatter light differently.

Dry weight measurements on vegetative cell suspensions yielded a factor of 0.17 $mg/10^8$ cells.

B. Immobilized Cells

Calcium alginate bead samples were taken from the packed-bed column in experiments CI18, CI19, CI21, CI22, CI23, CI28, and CI30. The bead sampling procedure began by stopping the flow to the column, clamping off the column inlet and exit tubing, and venting the column to the atmosphere. The area around the top of the column and the rubber stopper was wiped with 95–100% ethanol and gently loosened, then lifted. The upper screen was lifted with a pair of forceps (sterilized in ethanol and rinsed in sterile water), the ends of which had been bent out to grip the screen mesh. With the column top and upper screen removed, a spoon-spatula (sterilized in ethanol and rinsed in sterile water), held in the same hand as the column top, was used to stir the bead bed and remove approximately

10 beads. The screen was then reinserted and the column top was wiped again with ethanol before being replaced in the column. A strip of tape was used to hold the stopper in place in case the pressure increased suddenly. The bead samples were stored in a buffer-salts solution (the bioconversion medium of Chapters 5 and 6, without glucose) at 4°C until analyzed.

The bead sampling procedure used in experiment CI30 was similar to that given above, with two exceptions. First, because of the high oxygen intolerance of the strain used in this experiment (ATCC 39236), a T connector was fitted to the tubing below the column; sterile, oxygen-free nitrogen gas was gently bubbled through this connection and up into the bead bed during the sampling. Secondly, because the number of cell micro-colonies in single alginate beads varied widely from bead to bead in this run, a larger number of beads (*ca.* 20) was taken per sample.

Two different methods were used to quantify the number of cells in the beads. For the samples of experiments CI18, CI19, CI21, and CI22, 5 beads from each sample were dissolved in 2.0 mL of a 50 g/L sodium tripolyphosphate (technical grade, 85% purity; Aldrich Chemical Co.) solution, at room temperature. The resulting liquid contained small colonies of cells from the beads; these clumps were gently broken apart by very low-power sonication (Heat Systems-Ultrasonics, Inc. Model W-375) for short (1–5 minutes, depending on the pulse interval) times. The optical density at 590 nm of these suspensions was measured in a Shimadzu Model UV-260 spectrophotometer (1 nm slit width, 1 cm path length, 25°C).

When it became apparent that immobilized cell morphology was changing because of sporulation and other processes, a new method, based on a microscope

counting chamber, was utilized. For these counts, two (CI22) or three (CI28) alginate beads were dissolved in 1.0 mL of 5 g/L technical-grade sodium tripolyphosphate. In order to average out the bead-to-bead variation in cell number per bead in run CI30, samples from this experiment were quantified by dissolving 15 beads in 3.0 mL of the tripolyphosphate solution. As in the other (A_{590}) method, the bead colonies were separated by gentle sonication. Cell counts were performed in a Petroff-Hausser bacteria-counting chamber, using an Olympus BHB microscope with a 40X phase contrast objective and 10X eyepieces. The different morphologies counted are described in the discussion of each experiment (Chapters 5 and 6).

C. Acetic Acid, Acetoin, Acetone, Butanol, Butyric Acid, and Ethanol

The concentrations of these fermentation products were measured by gas chromatography, utilizing a Shimadzu GC-9/CR-3A chromatograph (dual FID)/integrator system. The 2 m glass column (3 mm ID) was packed with Chromosorb 101 (80/100 mesh), the helium carrier gas flow rate was 50 mL/min, the detector temperature was 200°C, and the oven temperature was increased from 130°C to 160°C at 2°C/min. GC samples were prepared by mixing 900μL of fermentor sample (previously centrifuged and frozen) with 100μL of 10 g/L isbutanol (internal standard), and acidified with an additional 10μL of 6N HCl (50μL for the pH 6 fermentation samples of Chapter 4). A calibration mixture containing 2 g/L ethanol, 4 g/L acetone, 2 g/L acetic acid, 8 g/L butanol, 0.5 g/L acetoin, and 3 g/L butyric acid was used to convert the peak areas to concentration data; previous calibration experiments had shown that the concentration-area correlations were linear (for freshly prepared solutions) to at least twice the concentration levels used

in the calibration mixture. Each fermentor sample was analyzed twice, and the calibration mixture was injected after every 5–7 samples to check consistency. The glass wool pre-column was cleaned frequently to reduce acid component ghosting on carbon deposits.

D. Glucose

Glucose was determined with Sigma Kit 510, a glucose oxidase procedure, which yielded an orange-brown oxidized *o*-dianisidine complex, measured at 450 nm in either a Spectronic 21 (Bausch and Lomb) or a Shimadzu UV-160 spectrophotometer.

E. Ammonia

The concentration of ammonia in certain fermentor liquid samples of experiments CI23, CI28, and CI30 (Chapter 6) was measured with Sigma Kit 170. The decrease in 340 nm absorbance because of NADH consumption by the reductive amination of 2-oxoglutarate (by glutamate dehydrogenase) was measured with a Shimadzu UV-160 spectrophotometer.

F. Lactic Acid

L-(—)-lactic acid concentrations in fermentor samples were measured with a kit from Boehringer Mannheim, using a technique described by Noll [8]. D-(+)-lactic acid concentrations were determined by the method of Gawehn and Bergmeyer [9]. In both assays, the production of NADH in the lactate dehydrogenase reaction

was followed by the measurement of 340 nm absorbance on a Shimadzu UV-260 spectrophotometer (1 nm slit width, 1 cm path length, 25°C).

G. Riboflavin

The levels of total riboflavin (riboflavin, FMN, and FAD) in the fermentor medium of experiments CI28 and CI30 were determined by a direct fluorimetric assay. The level of 520 fluorescence resulting from 450 nm excitation was measured in a Shimadzu RF-540 spectrofluorometer (excitation and emission slit widths 10 nm, high sensitivity), and converted to concentrations using the calibration curve shown in Figure 12. Although no sample pretreatment procedures were used, the results should be quantitative and accurate, as none of the known interfering agents of riboflavin fluorescence were present in the samples [10].

H. Iron

Published assay methods [11,12] were adapted for the determination of iron in liquid samples from experiments CI28 and CI30. The methods are based on Ferrozine (3-(2-pyridyl)-5,6-bis(4-phenylsulfonic acid)-1,2,4-triazine, monosodium salt, monohydrate; Sigma), which forms a bright magenta complex with iron(II).

Three solutions were prepared for this assay: the reducing reagent (5 g hydroxylamine hydrochloride (Sigma), 10 g ammonium acetate, 10 mL glacial acetic acid, and 90 mL deionized water), the color reagent (75 mg Ferrozine, 100 μL 6N HCl, and 25 mL deionized water), and a concentrated iron standard solution (78.4 mg $Fe(NH_4)_2(SO_4)_2 \cdot 6H_2O$ and 50 μL concentrated sulfuric acid in 100 mL deionized

water, resulting in a 2mM iron solution). The reducing reagent was necessary to convert the iron(III) in the fermentation samples to iron(II) for the formation of the colored complex with Ferrozine.

Two similar procedures were followed for the iron assays. In one, 1.0 mL reducing reagent and 300 μL of sample were mixed in a small glass tube and the tube was placed in a boiling water bath for 5 minutes (no noticeable liquid loss occurred). Then, 100μL of color reagent was added, and the resulting color was measured as 562 nm absorbance (Shimadzu UV-260, 1 nm slit, 1 cm path length, 25°C). Deionized water was used as a blank. The absorbance values could be converted to concentration data with the use of the calibration curve shown in Figure 13.

For the determination of very low levels of iron, the above protocol was followed, except that 1.0 mL sample and 0.1 mL reducing reagent were used.

I. Lysis/Released Cell Material

Release of cytoplasmic constituents from the immobilized cells was measured as 260 nm absorbance (in experiments CI28 and CI30), using a Shimadzu UV-260 spectrophotometer (25°C, 1 nm slit width, 1 cm pathlength, deionized water zero). The primary compounds absorbing in this region are nucleic acids. This method has been used to monitor lysis [*e.g.*, 13] and to study the RNA degradation in starving cells [14,15].

Other compounds in the fermentation medium, such as acetone, acetoin, and riboflavin, also absorb at 260 nm. Their effects were accounted for with the calibration curves shown in Figure 14. Acetoin 260 nm absorbance was essentially

identical to that of acetone.

PHOTOGRAPHY

A. Light Microscope

Black-and-white photographs were taken of cell suspensions from the dissolved alginate bead samples of experiment CI28, using an Olympus BHB microscope, a Nikon F2 35 mm camera, and a special microscope-camera adapter. The samples for these photographs were prepared by centrifuging 200 μL of dissolved bead sample (from the microscope counting chamber procedure), removing 180 μL of the supernatant, and resuspending to yield a 10X concentrated mixture.

B. Scanning Electron Microscope

Alginate bead samples from experiments CI21 and CI22 (Chapter 5) were examined and photographed using an ETEC Autoscan scanning electron microscope with an accelerating voltage of 20 kV.

The following procedure was used to prepare the alginate bead samples for viewing: first, whole beads were immersed in 2% (v/v) glutaraldehyde solution for 12 hours. The beads were then washed in buffer and stored overnight at 4°C in bead storage buffer to remove excess glutaraldehyde. These rinsed beads were cut in half with a razor blade and covered with a 1% (w/v) buffered OsO_4 solution for 5 hours at 4°C. The stained bead halves were then drained, rinsed three times with buffer, and soaked in 30% ethanol for one hour. The dehydration process was continued by moving the bead samples to increasingly concentrated ethanol

solutions (50, 70, 90, 95, and 100%), each for approximately one hour. The samples were stored overnight in 100% ethanol before CO_2 critical-point drying (one hour). The samples were mounted on stubs drilled with pockets to accommodate the curved surface (*i.e.*, flat side up), using a silver cement. The mounted bead halves were shadowed with a 10 nm layer of 80:20 gold:palladium by vacuum deposition.

All SEM work was done with the assistance of Pat Koen.

LITERATURE CITED

1. Lemme, C.J., and J.R. Frankiewicz, U.S. Patent 4,521,516, 1985.

2. Datta, R. and J.G. Zeikus, "Modulation of Acetone-Butanol-Ethanol Fermentation by Carbon Monoxide and Organic Acids," *Appl. Env. Microbiol.*, **49**, 522–529 (1985).

3. Costa, J.M. and A.R. Moreira, "Growth Inhibition Kinetics for the Acetone-Butanol Fermentation," *A. C. S. Symp. Ser.*, **207**, 501–512 (1983).

4. Seip, W.F. and G.L. Evans, "Atmospheric Analysis and Redox Potentials of Culture Media in the GasPak System," *J. Clin. Microbiol.*, **11**, 226–233 (1980).

5. Förberg, C., S.-O. Enfors, and L. Häggström, "Control of Immobilized, Non-Growing Cells for Continuous Production of Metabolites," *Eur. J. Appl. Microbiol. Biotechnol.*, **17**, 143–147 (1983).

6. Mattiasson, B., "Immobilization Methods," in *Immobilized Cells and Organelles*, vol. I, B. Mattiasson (ed.), CRC Press, Boca Raton, 1983, pp. 3–25.

7. Reardon, K.F., T.-H. Scheper, and J.E. Bailey, "Einsatz eines Fluoreszenzsensors zur Messung der NAD(P)H-abhängigen Kulturfluoreszenz Immobilisierter Zellsysteme," *Chem.-Ing.-Tech.*, **59**, 600–601 (1987).

8. Noll, F., "L-(+)-Lactate. Determination with LDH, GPT, and NAD," in *Methods of Enzymatic Analysis*, vol. 3, H.U. Bergmeyer (ed.), Academic Press, New York, 1974, pp. 1475–1479.

9. Gawehn, K. and H.U. Bergmeyer, "D-(–)-Lactate," in *Methods of Enzymatic Analysis*, vol. 3, H.U. Bergmeyer (ed.), Academic Press, New York, 1974, pp. 1492–1495.

10. Pearson, W.N., "Riboflavin," in *The Vitamins*, 2^{nd} Ed., P. György and W.N.

Pearson (eds.), Academic Press, New York, 1967, pp. 99–136.

11. Gibbs, C.R., "Characterization and Application of FerroZine Iron Reagent as a Ferrous Iron Indicator," *Anal. Chem.*, **48**, 1197–1201 (1976).

12. Stookey, L.L., "Ferrozine—A New Spectrophotometric Reagent for Iron," *Anal. Chem.*, **42**, 779–781 (1970).

13. Mason, C.A. and G. Hamer, "Survival and Activity of *Klebsiella pneumoniae* at Super-Optimal Temperatures," *Bioproc. Eng.*, **2**, 121–127 (1987).

14. Boylen C.W. and J.C. Ensign, "Intracellular Substrates for Endogenous Metabolism during Long-Term Starvation of Rod and Spherical Cells of *Arthrobacter crystallopoietes*," *J. Bacteriol.*, **103**, 578–587 (1970).

15. Boyaval, P., E. Boyaval, and M.J. Desmazeaud, "Survival of *Brevibacterium linens* during Nutrient Starvation and Intracellular Changes," *Arch. Microbiol.*, **141**, 128–132 (1985).

POTATO STARCH MEDIUM (5)

Soluble potato starch (Sigma)	40 g/L
Yeast extract (Difco)	1 g/L
Peptone (Difco)	1 g/L
NH_4Cl	0.8g/L
Na_2HPO_4·	0.9 g/L
KH_2PO_4	0.4 g/L
$MgSO_4 \cdot 7H_2O$	0.2 g/L
Trace elements solution	10 mL/L

FULL GROWTH MEDIUM (5)

Glucose	40 g/L
Yeast extract (Difco)	10 g/L
Peptone (Difco)	10 g/L
$Na_2HPO_4 \cdot 7H_2O$	0.9 g/L
KH_2PO_4	0.4 g/L
$MgSO_4 \cdot 7H_2O$	0.2 g/L
NH_4Cl	0.8 g/L
$FeCl_3 \cdot 6H_2O$	0.01 g/L
Trace elements solution	0.5 mL/L

TRACE ELEMENTS SOLUTION (5)

$CaCl_2 \cdot 2H_20$	0.66 g/L
$ZnSO_4 \cdot 7H_2O$	0.18 g/L
$CuSO_4 \cdot 5H_2O$	0.16 g/L
$MnSO_4 \cdot 4H_2O$	0.16 g/L
$CoCl_2 \cdot 6H_2O$	0.18 g/L

Table 1. Composition of Media.

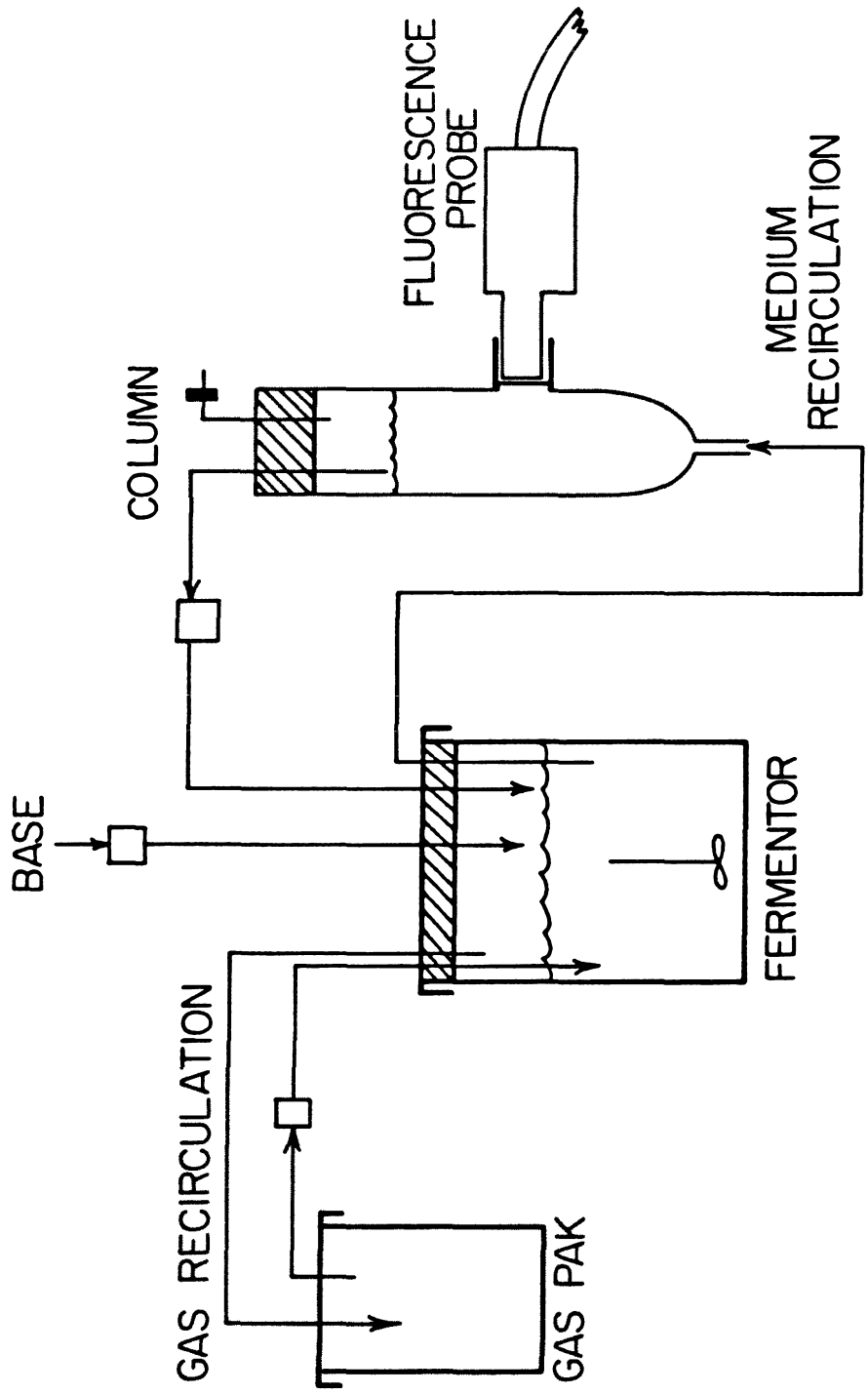

Figure 2. Apparatus for suspended cell experiments.

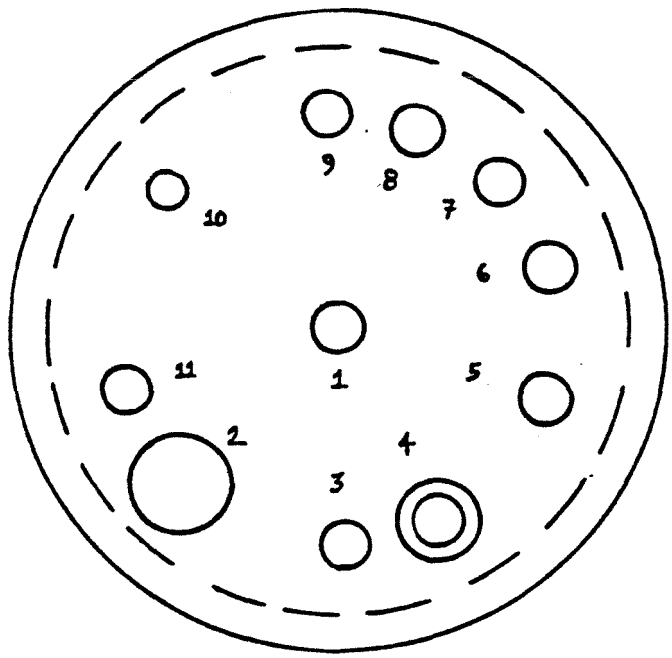

1. Gas return from GasPak
2. pH probe
3. Baffle
4. Sample tube
5. Heater well
6. Base addition
7. Thermometer
8. Baffle
9. Thermistor well
10. Gas to GasPak
11. Baffle

Figure 3. Schematic of fermentor vessel connections in suspended cell experiments.

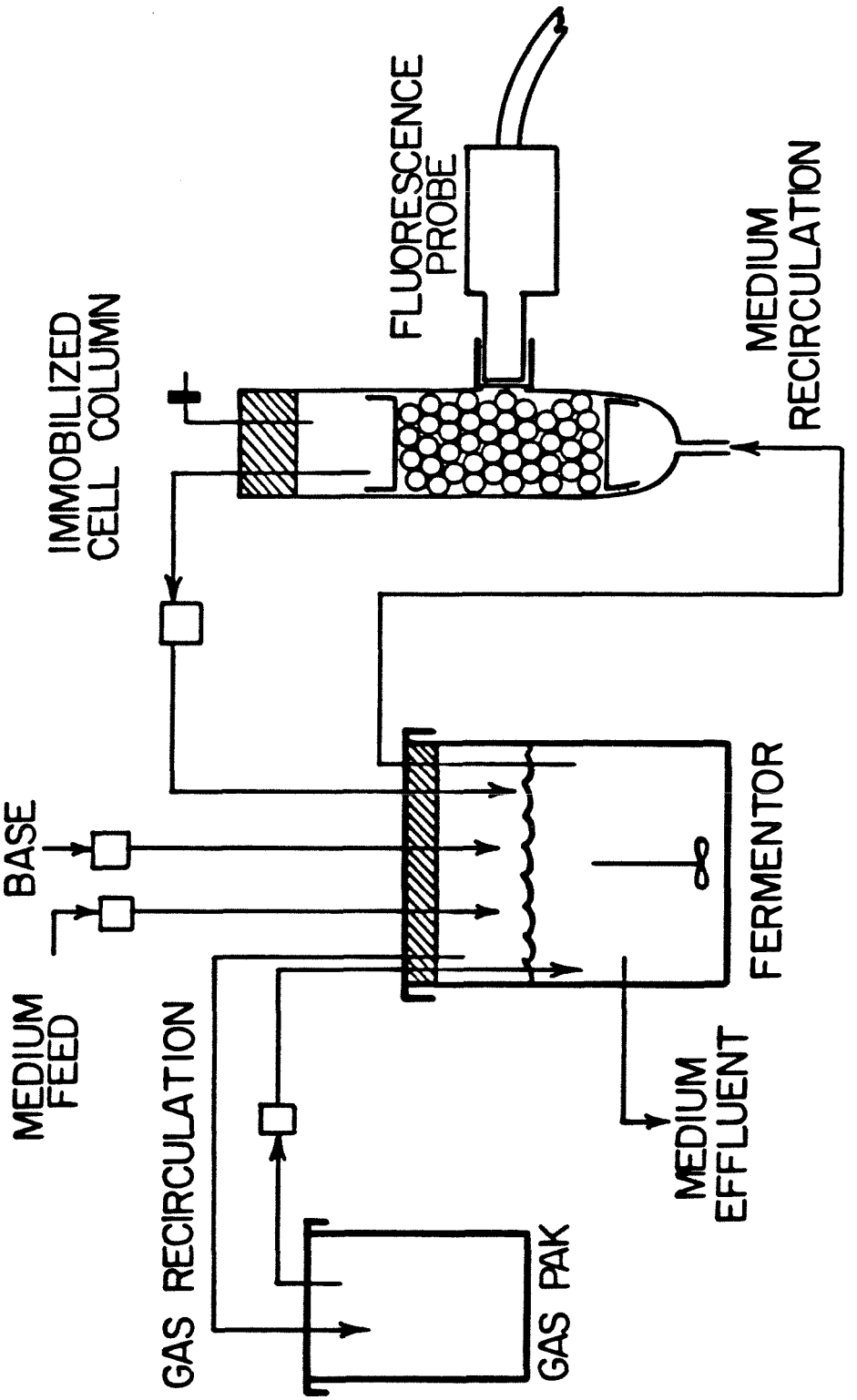

Figure 4. Apparatus for immobilized cell experiments.

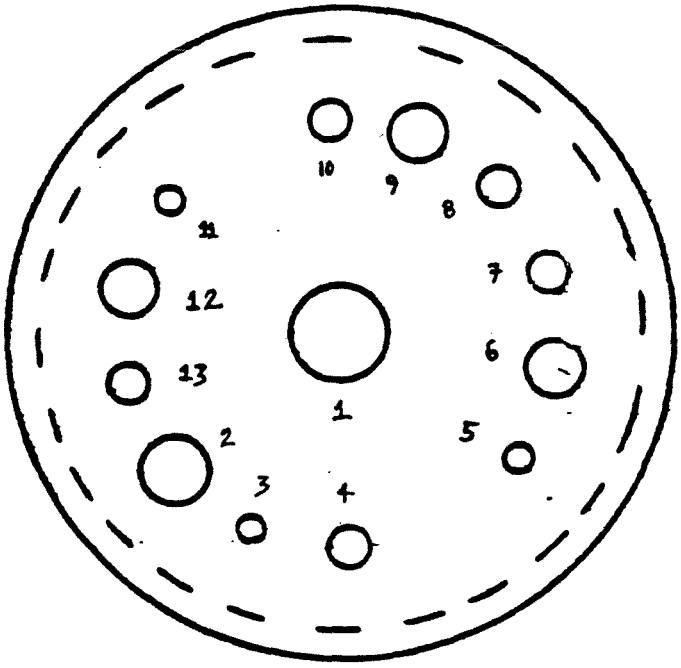

1. Gas from GasPak
2. pH probe
3. To column
4. Baffle
5. From column
6. Heater well
7. Thermometer
8. Thermistor well
9. Sample tube
10. Baffle
11. Base addition
12. Condenser and to GasPak
13. Baffle

Figure 5. Schematic of fermentor vessel connections in immobilized cell experiments.

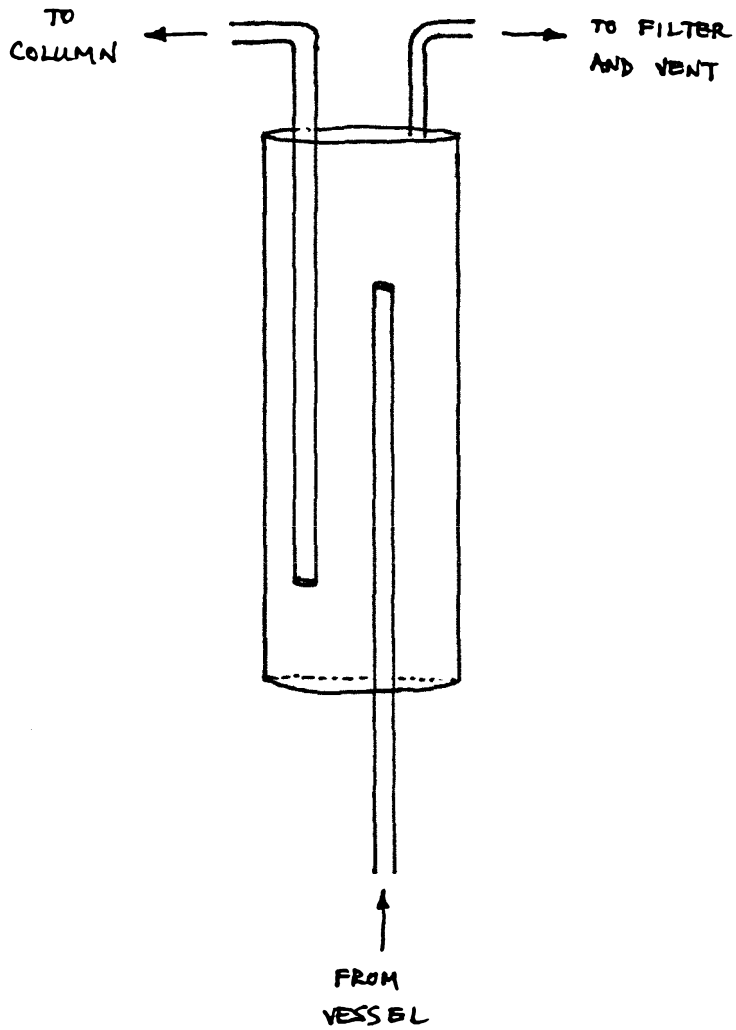

Figure 6. Bubble trap used in immobilized cell experiments.

Ingold Fluorosensor

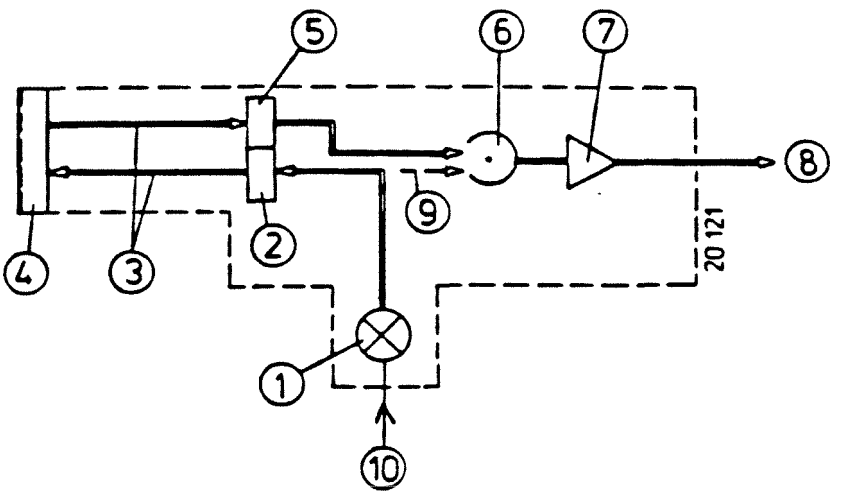

1. Lamp
2. Primary filter
3. Optical fibers
4. Optical head
5. Secondary filter
6. Photomultiplier tube
7. Amplifier
8. Cable
9. Calibration device
10. Power supply

Figure 7. Schematic of the Ingold Fluorosensor fluorescence probe [7].

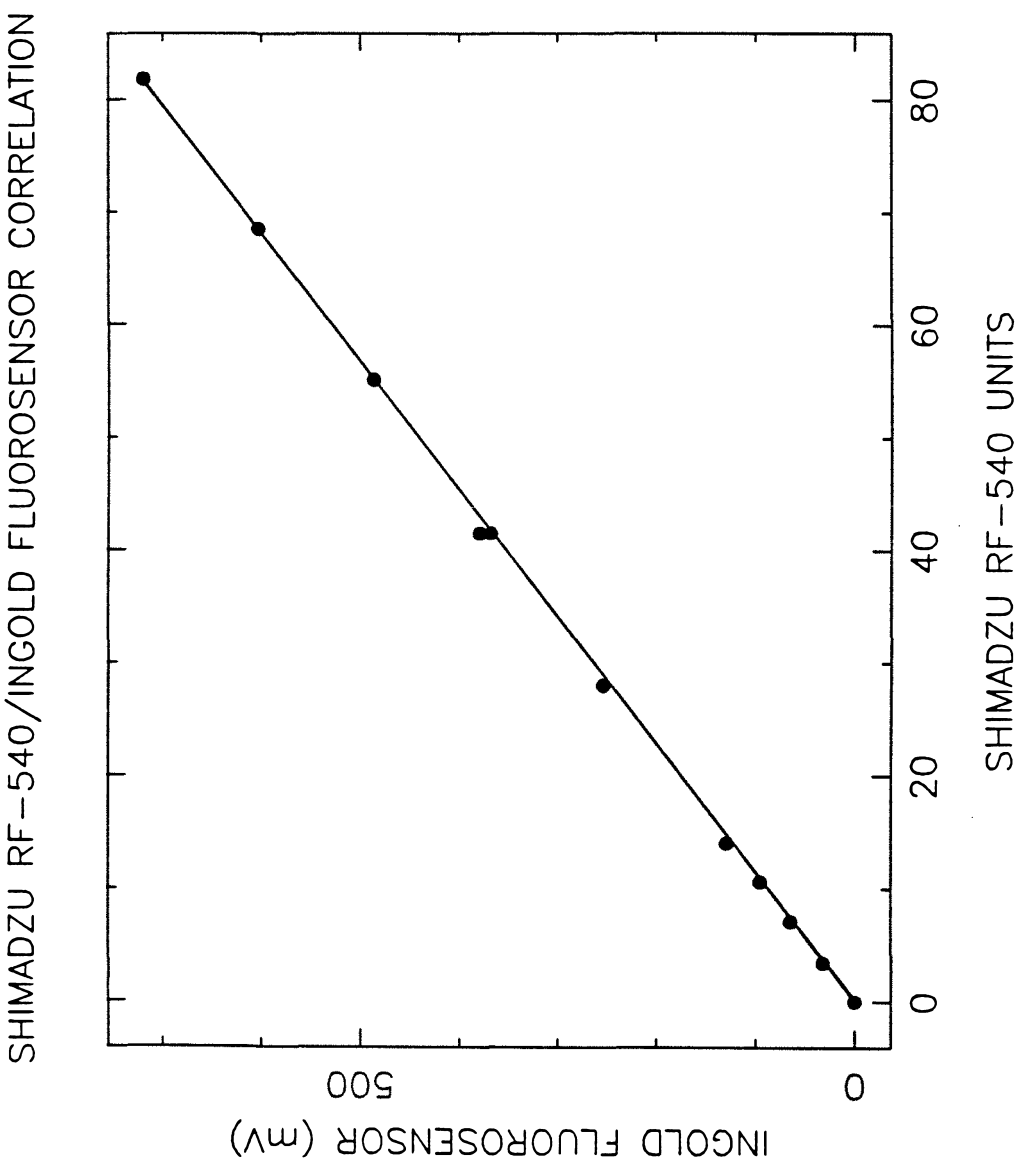

Figure 8. Correlation between fluorescence values of the Shimadzu RF-540 spectrofluorometer and the Ingold Fluorosensor probe. Data were obtained with quinine sulfate solutions.

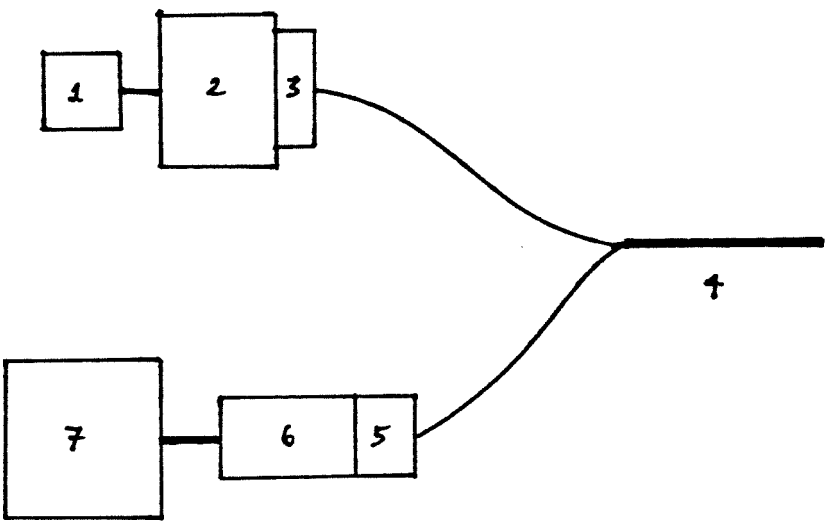

1. Power supply
2. Lamp and housing (water-cooled)
3. 365 nm filter and housing
4. Liquid/fiber optical light guide
5. 460 nm filter and housing
6. Photomultiplier tube and housing
7. Photometer power supply and readout

Figure 9. Schematic of the fluorometer apparatus based on a Volpi liquid-and-glass fiber optical light guide.

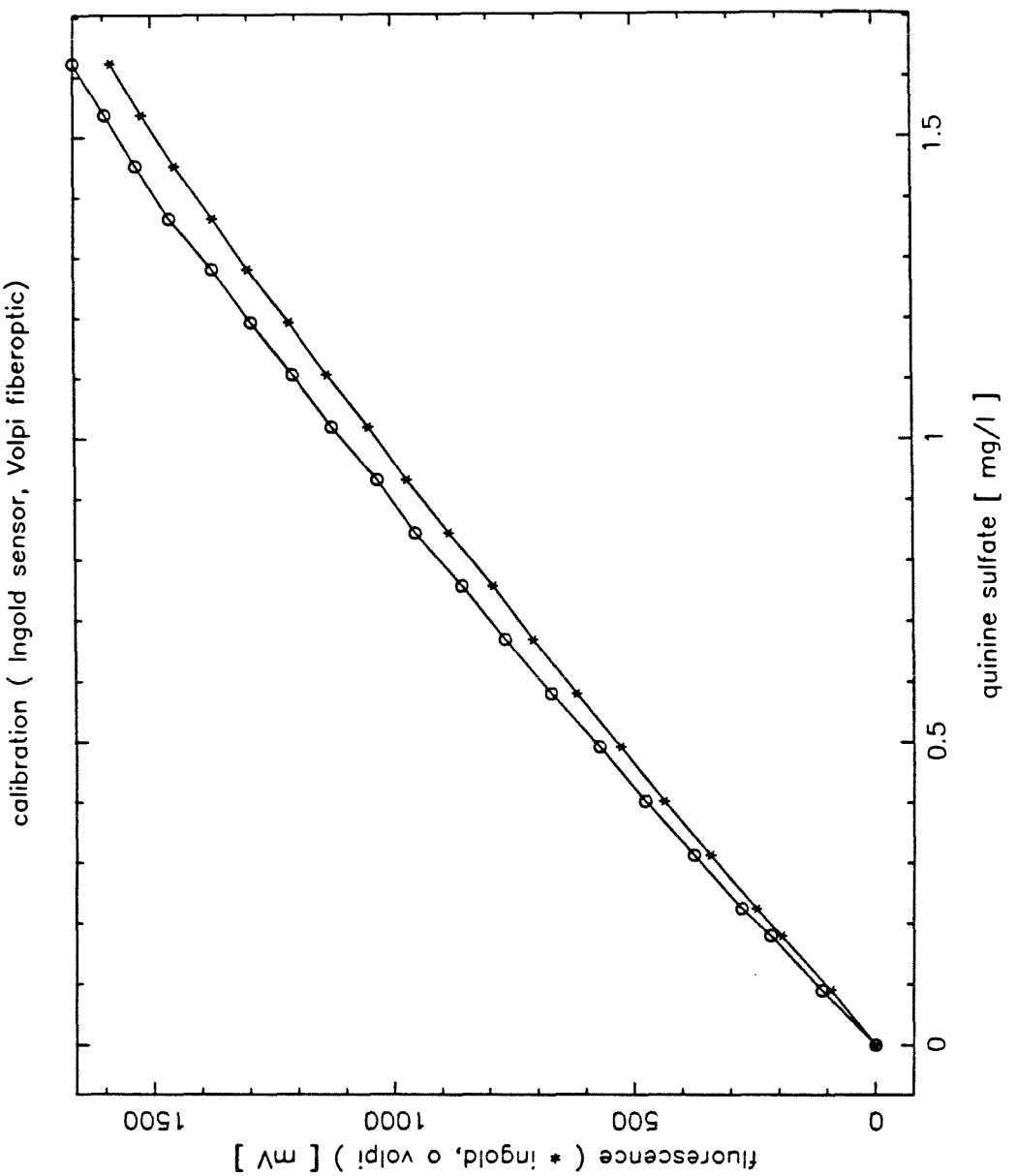

Figure 10. Fluorescence response curves for the Ingold Fluorosensor probe (circles) and the Volpi light guide system (stars).

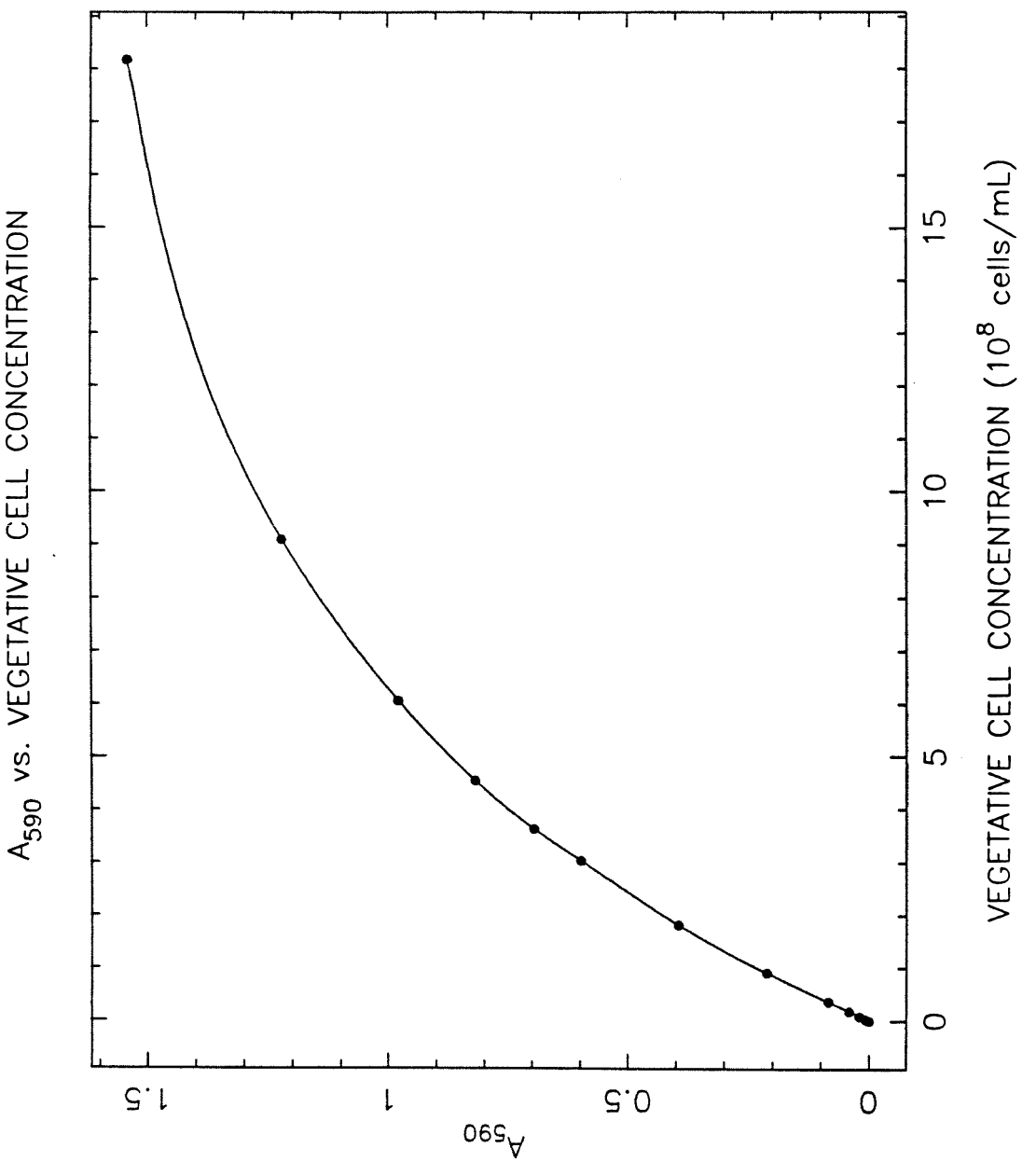

Figure 11. Absorbance of vegetative cell suspensions at 590 nm *vs.* cell concentration.

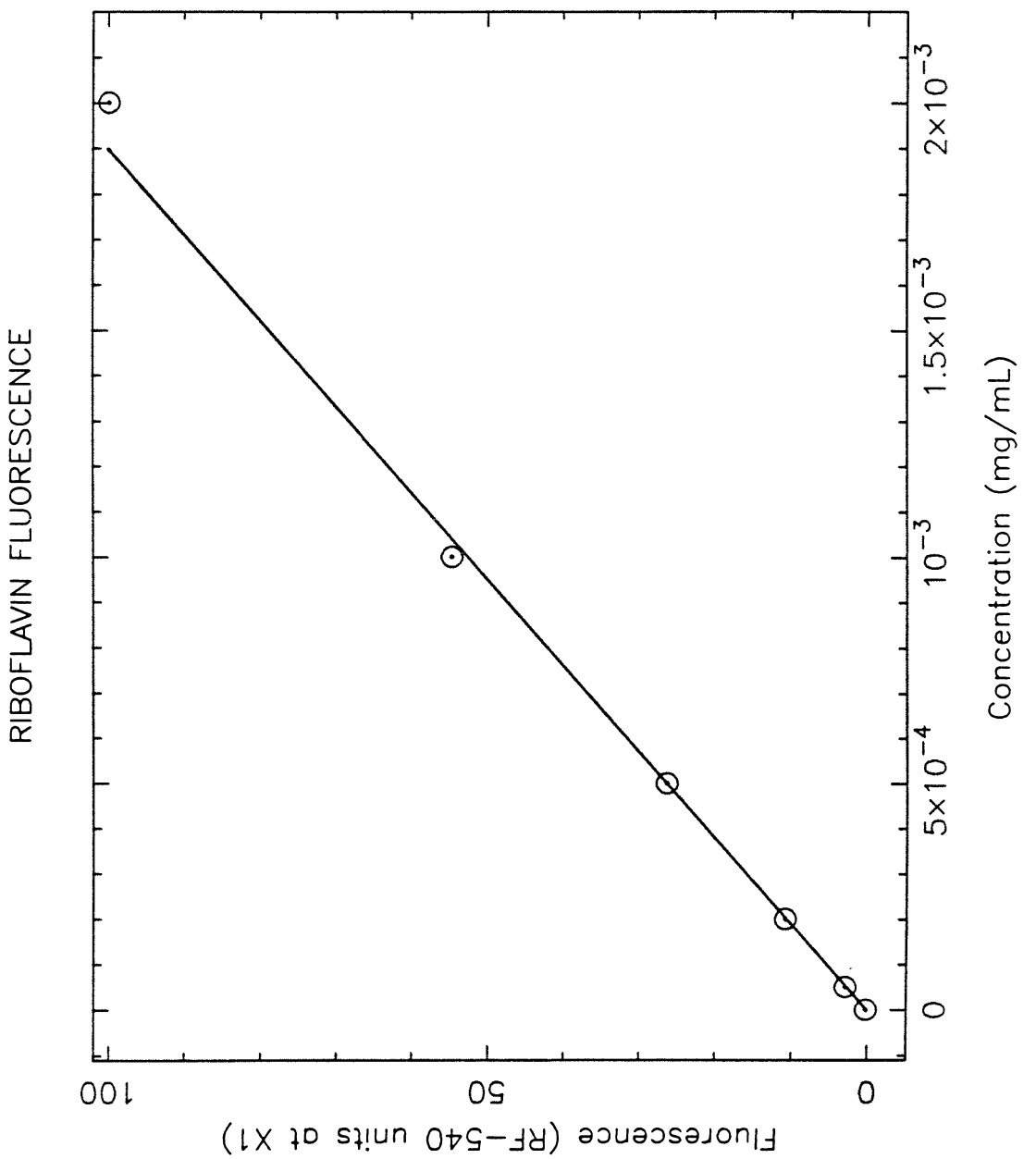

Figure 12. Riboflavin concentration vs. fluorescence (450 nm excitation, 520 nm emission).

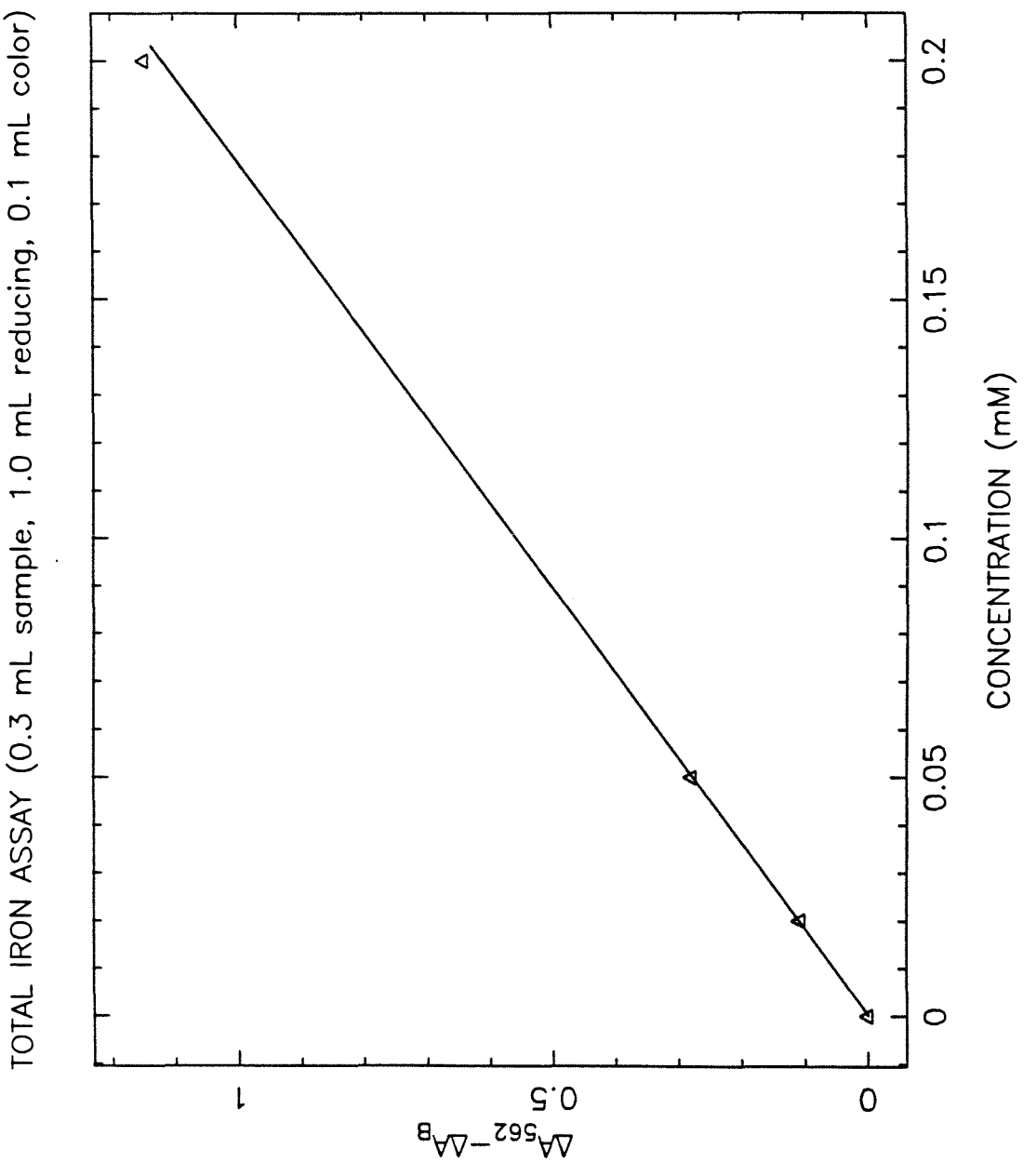

Figure 13. Calibration of total iron assay.

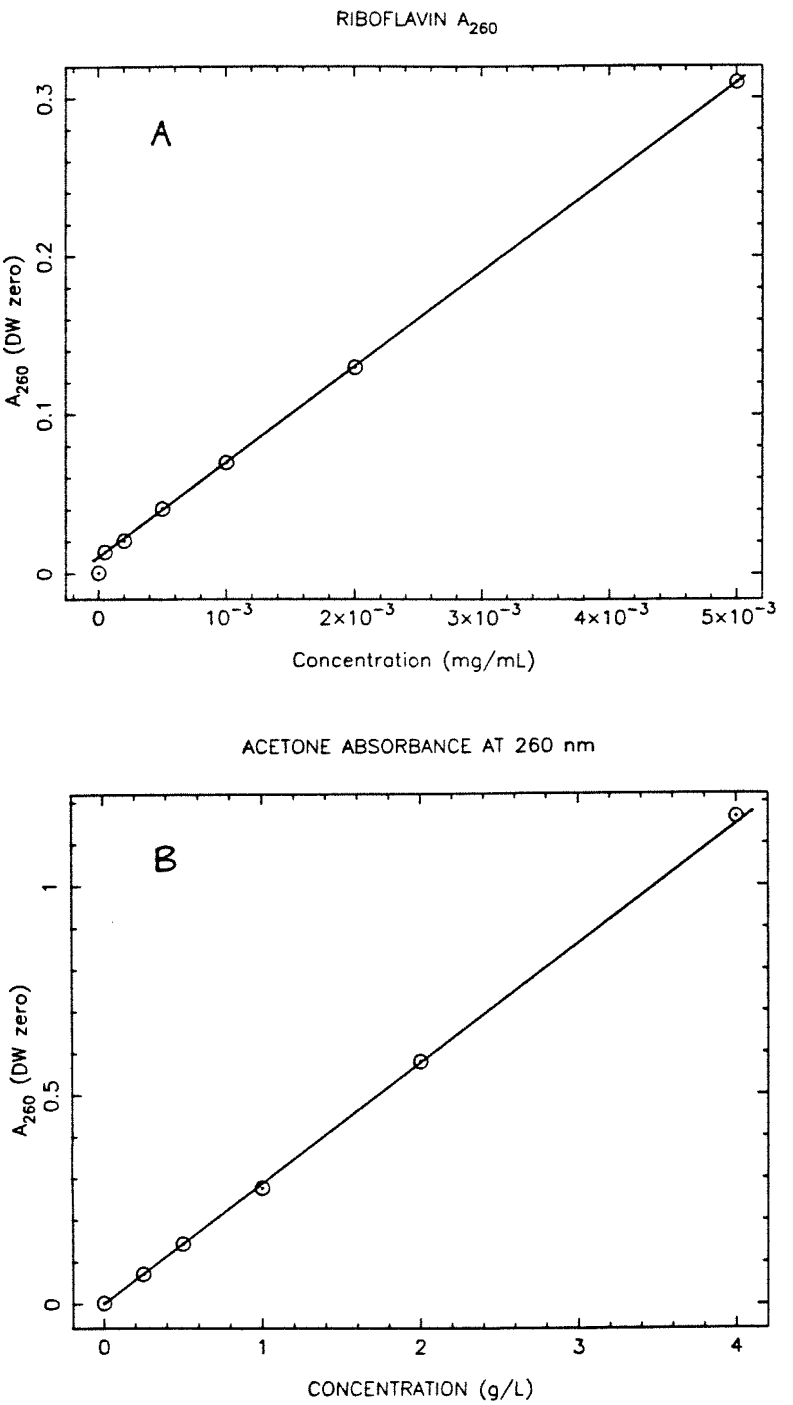

Figure 14. Correlations between 260 nm absorbance and the concentrations of TOP: Riboflavin and BOTTOM: Acetone.

CHAPTER 4

METABOLIC PATHWAY RATES AND CULTURE FLUORESCENCE IN BATCH FERMENTATIONS OF *CLOSTRIDIUM ACETOBUTYLICUM*

This chapter has been published as:

K.F. Reardon, T.-H. Scheper, and J.E. Bailey,

Biotechnology Progress, **3**, 153–167 (1987)

ABSTRACT

Stoichiometric relationships in the metabolic pathway of *Clostridium acetobutylicum* are used to formulate a framework for the analysis of pathway rates. This analytical tool, alone and in conjunction with intracellular NAD(P)H fluorescence measurements, is applied to two batch fermentations, one acidogenic and one solventogenic, to provide information on intracellular activities not readily obtainable by other methods.

INTRODUCTION

Clostridium acetobutylicum is an anaerobic bacterium capable of utilizing many different substrates for the production of organic acids and solvents. For several years, this microorganism and its complex fermentative properties have been the object of increasing research interest [*e.g.*, 1,2,3,4]. A branched and interconnected metabolic pathway allows *Cl. acetobutylicum* to produce acetic acid, butyric acid, acetone, butanol, and several other compounds in varying amounts, depending primarily on cultivation conditions. In order to further understand this metabolic response to environment, a method of metabolic pathway kinetic analysis was derived from metabolic stoichiometry and applied to two batch fermentations of *Cl. acetobutylicum*: one in which only acids were formed and another in which acetone and butanol were the major products. This methodology has its roots in the works of Humphrey [5], Aiba and Matsuoka [6], and Papoutsakis [7].

These cultures were also monitored *in situ* for intracellular NAD(P)H-dependent fluorescence. Since the first reported use of this technique by Duysens

and Amesz [8] and subsequent development by Chance *et al.* [9,10], *in situ* fluorometry has been applied to suspended cell fermentations by several research groups [11,12,13]. Recently, on-line fluorescence monitoring was reported for immobilized *Cl. acetobutylicum* [14]. When the fluorescence data are interpreted with the help of the pathway rate analysis, additional information on metabolic functioning is obtained.

Metabolic Pathway Description

It is clearly necessary to have some knowledge of the biochemical reactions of an organism's metabolic pathway before constructing a stoichiometric model for the analysis of metabolic network kinetics. Although industrially important for many years [15,16] and studied by many researchers [*e.g.*, 1,2,3,4,17], the complete enzyme system and regulatory mechanisms of the metabolism of *Cl. acetobutylicum* are not well known. Recent studies have contributed information on enzyme activities [1,4,18], and the effects of altered electron flows [19,20,21].

Under certain conditions (e.g., low pH), batch fermentations of *Cl. acetobutylicum* show two distinct phases. In the first phase, acetic and butyric acids are produced, causing a decrease in the pH of an uncontrolled fermentation. At some point, the fermentation moves into a solvent-producing phase, during which n-butanol, acetone, and ethanol are formed, butyrate and acetate are consumed, and the pH (if uncontrolled) rises. The factor(s) causing the shift from acid to solvent production are not currently understood; proposed influences include: the availability and demand of biosynthetic (ATP) and reduction energies [3,19], the amount of internal undissociated acids and the rate of glucose uptake [22,23], and the intracellular pH [24,25]. A comprehensive review of the acetone-butanol fermen-

tation has recently appeared [26], containing discussions on the metabolic reactions, their regulation, the factors involved in the transition to the solventogenic phase, and many other aspects of the fermentation.

While *Cl. acetobutylicum* has the ability to ferment numerous hexoses and pentoses [27,28], this work will focus exclusively on glucose as a substrate. Glucose is converted to pyruvate via the Embden-Meyerhoff-Parnas (EMP) pathway [29,30] (Figure 15). A small amount of pyruvate is converted to acetoin (acetomethylcarbinol) with the release of two molecules of CO_2 per molecule of acetoin formed. Most of the pyruvate is decarboxylated by pyruvate-ferredoxin oxidoreductase to form acetyl-coenzyme A and CO_2 [31]. Ferredoxin, a non-heme iron-sulfur protein with a low redox potential [32], acts as an electron acceptor in this reaction. There are two means of oxidizing the reduced form of ferredoxin: either by a reaction catalyzed by hydrogenase in which two hydrogen ions are reduced to H_2 [33,34], or by reduction of NAD^+ to NADH, catalyzed by NADH:ferredoxin oxidoreductase [35,36]. Another, analogous enzyme, NADPH:ferredoxin oxidoreductase [35,36], catalyzes the transfer of electrons to $NADP^+$. Studies have shown that NADH:ferredoxin oxidoreductase can either produce or oxidize NADH [36]. The fate of the reducing equivalents generated in the formation of acetyl-CoA from pyruvate seems to be different in the two phases of batch *Cl. acetobutylicum* fermentations [21]. A higher percentage of reducing equivalents are found in H_2 during the acid-forming phase than in the solvent phase. Perturbations in the pathways for ferredoxin reduction by CO-mediated hydrogenase inactivation [19,20,37] or by high H_2 partial pressures [21] have resulted in altered product distributions.

Some of the acetyl-CoA undergoes a transfer reaction by the action of phospho-

transacetylase to form acetyl phosphate [38], which is dephosphorylated by acetate kinase in the presence of ADP to form acetate and ATP [39].

The formation of butyrate begins with the condensation of two molecules of acetyl-CoA to form acetoacetyl-CoA; this intermediate is converted to butyryl-CoA by three enzymes, the activities of which appear to be coordinated [40]. From butyryl-CoA there are two paths to butyrate. One is analogous to the pathway used to form acetate from acetyl-CoA; phosphotransbutyrylase forms butyryl phosphate from butyryl-CoA [41,42], and butyrate kinase then catalyzes the formation of butyrate and ATP from butyryl phosphate and ADP [43]. The other possible route to butyrate from butyryl-CoA involves an acetate CoA-transferase -catalyzed reaction in which the CoA moeity is transferred from butyryl-CoA to acetate (forming acetyl-CoA and butyrate). While this type of transferase activity has been demonstrated in *Cl. aminobutyricum* [44] and *Cl. kluyveri* [45], Andersch *et al.* [4] were unable to detect acetate CoA-transferase activity in *Cl. acetobutylicum* DSM 1732 (*Cl. acetobutylicum* ATCC 824 (DSM 792) was used in this work). Another enzyme, acetoacetyl-CoA:acetate (butyrate) CoA-transferase [1,4], which transfers CoA from acetoacetyl-CoA to a number of substrates [1], has been demonstrated in *Cl. acetobutylicum* fermentations, although its activity in the acid phase was low [4].

As previously mentioned, the underlying cause(s) and mechanism(s) of the batch fermentation shift from acid to solvent formation are not understood. At some point in the fermentation a new set of enzymes are induced or activated (including butyraldehyde dehydrogenase, butanol dehydrogenase, and acetoacetate decarboxylase [4]) and the specific activity of others decreases (e.g., phosphotransacetylase,

acetate kinase, and phosphotransbutyrylase [4,40]).

One enzyme that seems to have an important role in the initiation of solvent formation is acetoacetate decarboxylase [46,47]. This enzyme irreversibly decarboxylates acetoacetate to form acetone and CO_2; acetoacetate is a product of a CoA exchange reaction between acetoacetyl-CoA and either acetate or butyrate, catalyzed by acetoacetyl-CoA:acetate (butyrate) CoA-transferase [1,4,29]. The activity of acetoacetate decarboxylase has a pH optimum of 5.0 [46] and was found to be present in solvent-forming cells only [4,18,46].

Butanol is formed from butyryl-CoA via two reduction steps: butyraldehyde dehydrogenase (acylating) reduces butyryl-CoA to butyraldehyde, which is then reduced to butanol by butanol dehydrogenase. Similarly, a small amount of ethanol is produced via the reduction of acetyl-CoA.

Butyryl-CoA for butanol formation is obtained in part from glucose through acetoacetyl-CoA and crotonyl-CoA. However, almost all solvent-producing batch fermentations of *Cl. acetobutylicum* consume butyrate from the medium; Wood *et al.* showed that nearly all of this butyrate was converted to butanol [48], and a similar result was obtained by Hartmanis *et al.* [1]. There are at least two possible paths from butyrate to butyryl-CoA. One involves a CoA-transferase, either the acetoacetyl-CoA:acetate (butyrate) CoA-transferase mentioned earlier [1,4] or perhaps an acetate CoA-transferase of the type found in *Cl. kluyveri* [45]. The other route would be through butyryl phosphate and would require the hydrolysis of ATP. Although one enzymatic study indicates that this second route cannot operate because phosphotransbutyrylase activity disappears in the solvent phase [1], other work has indicated that, under certain conditions, butyrate uptake via

the first path is unlikely [19].

Although acetate, butyrate, acetone, butanol, ethanol, acetoin, CO_2, and H_2 are typically the only products of *Cl. acetobutylicum* fermentations, other compounds may also be produced. Lactate, primarily in its L-(—) form, has been formed from pyruvate by lactate dehydrogenase with NADH under conditions of sulfate limitation [49], CO gassing [19,20,50], and iron deficiency [51]. Methylgloxal formation has been reported for cultures grown on fructose-1,6-diphosphate [50], presumably by methylgloxal synthase [30].

MATERIALS AND METHODS

The culture media, experimental apparatus for suspended cell fermentations, fluorescence measurement technique, and assay methods have been described in Chapter 3.

The medium used in these fermentations was a modified version of FGM (Chapter 3), which contained only 5 g/L each of yeast extract and peptone in order to reduce the background fluorescence.

At various times during the experiments, a few drops of liquid sample were placed on FGM-agar petri plates and incubated aerobically at 30°C to check for facultative anaerobic contamination.

DEVELOPMENT OF PATHWAY KINETICS ANALYSIS

As can be seen in Figure 15, *Cl. acetobutylicum* possesses a branched catabolic pathway, as do many anaerobic bacteria [52]. In contrast with a linear series of reactions (e.g., the homolactic acid fermentation), a branched network of metabolic reactions, each with different efficiencies for biosynthetic and reductive energy production, allows an organism to adjust the overall efficiency of its catabolism according to changing environmental conditions [52]. It follows, then, that knowledge of metabolic pathway fluxes under different conditions can provide insight into the response of a cell to its environment.

Humphrey [5] introduced the "gateway sensor" concept, in which measurements of product and substrate concentrations are used to infer cellular properties. This concept was extended to include metabolic pathway stoichiometry by Aiba and

Matsuoka [6], who applied the methodology to the problem of metabolic model discrimination in citrate production. Recently, Papoutsakis and coworkers have used similar principles to develop and apply "fermentation equations" for the acetone-butanol fermentation [3,7,19], butanediol and mixed-acid fermentations [53], and fermentations of propionic acid bacteria [54]. In this work, concepts such as these will be used to evaluate the carbon fluxes through the different branches of the metabolic pathway of *Cl. acetobutylicum* for the acid and solvent batch fermentations presented earlier.

As a first step in this procedure, the catabolic pathways shown in Figure 1 are simplified into a network of branches with connections at various common metabolic intermediate "nodes" (Figure 16). As can be seen in Figure 3, the CoA-exchange reaction catalyzed by acetate CoA-transferase has been included (path 10) for generality, but the butyryl-CoA synthetase reaction has not, as its activity has not been detected in any *Clostridium* strain. These pathway branch rates must now be related to the concentration changes of the external metabolites of the fermentation.

The material balance for an intracellular metabolite i is obtained by the method of Fredrickson [55], yielding

$$\frac{dc_i}{dt} = r_{f,i} - \mu c_i \ , \tag{1}$$

where c_i is the concentration of i (mol i·unit cell mass^{-1}), $r_{f,i}$ is the rate of formation of i (mol i·unit cell mass^{-1}·time^{-1}), and μ is the specific growth rate (time^{-1}).

The total rate of formation of compound i can be written as the sum of two contributions. Glucose consumed by the cells is allocated either to biomass synthesis (with rate r_G per unit mass of cells) or to the formation of end products. The rate v_i is defined as the rate of step i in Figure 16 for conversion of only that carbon

substrate which is used to produce end products. Then, the rate of formation of metabolite i may be written

$$r_{f,i} = \sum_j \nu_{ij} v_j + \alpha_i r_G \ . \tag{2}$$

Here, α_i is the fraction of i in biomass and the ν_{ij} are stoichiometric coefficients for each of the branch reactions (Figure 16). Substitution of Equation (2) into (1) leaves a material balance of:

$$\frac{dc_i}{dt} = \sum_j \nu_{ij} v_j + \alpha_i r_G - \mu c_i \ . \tag{3}$$

The last two terms in Equation (3) are alternative expressions for the same quantity, so that the material balance simplifies to:

$$\frac{dc_i}{dt} = \sum_j \nu_{ij} v_j \ . \tag{4}$$

The material balance for extracellular metabolic products in a batch reactor is:

$$\frac{d(V_R C_i)}{dt} = V_R R_{f,i} \ , \tag{5}$$

which can also be written as:

$$\frac{dC_i}{dt} = R_{f,i} - \frac{C_i}{V_R}\frac{dV_R}{dt} \ . \tag{6}$$

Here, V_R is the culture volume, and C_i and $R_{f,i}$ are the concentration and molar rate of formation on a per unit culture volume basis. The rate of formation of an extracellular compound i is the sum of the rates of the metabolic steps producing (or consuming) i, multiplied by the appropriate stoichiometric coefficient γ_{ij}:

$$R_{f,i} = x \cdot \sum_j \gamma_{ij} v_j \ , \tag{7}$$

where x is the biomass concentration in the reactor (cell mass per unit culture volume). The material balance on the fermentation products in a constant volume batch reactor can then be related to metabolic pathway rates by

$$\frac{dC_i}{dt} = x \cdot \sum_j \gamma_{ij} v_j \ . \tag{8}$$

As noted earlier, glucose carbon for biomass formation has been divided conceptually from that utilized for product formation as indicated by the biomass branch in the pathway schematic. While other compounds such as acetyl-CoA and pyruvate are certainly used directly in biosynthesis, their contributions will be represented as glucose carbon in this analysis. The growth equation here is based on a biomass formula of $CH_2O_{0.5}N_{0.25}$ [56]. This is an approximate description of elemental biomass composition which nonetheless falls within the normal ranges for weight fraction of carbon (σ_b = 0.462±0.023 [57]) and degree of reduction (γ_b = 4.291±0.172 [58]). The amount of ATP required to form one mole of biomass was calculated from an experimentally determined Y_{ATP} of 10.3 [59]. Finally, the reducing equivalents necessary for growth were calculated by a redox balance to yield the following overall growth equation:

$$C_6H_{12}O_6 + 1.5NH_3 + 0.75(NAD(P)H + H^+) + 14.9ATP \rightarrow$$

$$6CH_2O_{0.5}N_{0.25} + 0.75NAD(P)^+ + 14.9(ADP + P_i) + kH_2O \ .$$

This equation, then, will be used to represent the large number of reactions involved in cell growth.

It is now possible to write equations of the forms of Equations (4) or (8) for all of the compounds shown in Figure 16.

$$\text{glucose}: \quad \frac{dC_{glu}}{dt} = -xv_0 \tag{9a}$$

$$\text{biomass}: \frac{dC_{\text{bio}}}{dt} = xr_G \tag{9b}$$

$$\text{glucose 6} - \text{phosphate}: \frac{dc_{\text{G6P}}}{dt} = v_0 - 0.167r_G - 0.5v_1 \tag{9c}$$

$$\text{pyruvate}: \frac{dc_{\text{pyr}}}{dt} = v_1 - 2v_2 - v_3 - v_{12} \tag{9d}$$

$$\text{acetoin}: \frac{dC_{\text{AMC}}}{dt} = xv_2 \tag{9e}$$

$$\text{lactate}: \frac{dC_{\text{HLa}}}{dt} = xv_{12} \tag{9f}$$

$$\text{acetyl} - \text{CoA}: \frac{dc_{\text{AcCoA}}}{dt} = v_3 - v_4 - v_5 - 2v_6 + v_{7A} - v_{10} \tag{9g}$$

$$\text{ethanol}: \frac{dC_{\text{EtOH}}}{dt} = xv_4 \tag{9h}$$

$$\text{acetate}: \frac{dC_{\text{HAc}}}{dt} = xv_5 - xv_{7A} - xv_{10} \tag{9i}$$

$$\text{acetoacetyl} - \text{CoA}: \frac{dc_{\text{AcAcCoA}}}{dt} = v_6 - v_{7A} - v_{7B} - v_8 \tag{9j}$$

$$\text{acetone}: \frac{dC_{\text{AC=O}}}{dt} = xv_{7C} \tag{9k}$$

$$\text{butyryl} - \text{CoA}: \frac{dc_{\text{BuCoA}}}{dt} = v_8 - v_9 - v_{10} - v_{11} + v_{7B} \tag{9l}$$

$$\text{butyrate}: \frac{dC_{\text{HBu}}}{dt} = xv_9 + xv_{10} - xv_{7B} \tag{9m}$$

$$\text{butanol}: \frac{dC_{\text{BuOH}}}{dt} = xv_{11} \tag{9n}$$

$$CO_2: \frac{dC_{CO_2}}{dt} = xv_2 + xv_3 + xv_{7C} \tag{9o}$$

$$H_2: \frac{dC_{H_2}}{dt} = xv_{14} \tag{9p}$$

$$Fd_{red}: \frac{dc_{Fd_{red}}}{dt} = v_3 - v_{13} - v_{14} \tag{9q}$$

$$\text{NAD(P)H}: \frac{dc_{\text{NAD(P)H}}}{dt} = v_1 - 0.125r_G + v_{13} - 2v_4 - 2v_8 - 2v_{11} - v_{12} \tag{9r}$$

$$\text{CoA}: \frac{dc_{\text{CoA}}}{dt} = -v_3 + v_5 + v_6 + v_9 + v_{11} \tag{9s}$$

$$\text{ATP}: \frac{dc_{\text{ATP}}}{dt} = -2.5r_G + v_1 + v_5 + v_9 \tag{9t}$$

$$\text{acetoacetate}: \frac{dc_{\text{HAcAc}}}{dt} = v_{7A} + v_{7B} - v_{7C} \tag{9u}$$

In all cases, v_i is in units of mol·cell mass^{-1}·time^{-1} and the stoichiometry is normalized to the major product of the reaction. The subscripts i of the v_i correspond

to the numbered branches of the metabolic scheme of Figure 16. Pathway 7 has been further subdivided in Equations (9): 7A refers to the reaction transferring CoA from acetoacetyl-CoA to acetate, 7B denotes the analogous reaction involving butyrate, and path 7C is the step in which acetotacetate is decarboxylated to form acetone. The material balances of those compounds involved in the overall growth equation contain an additional term (of the form cr_G) to account for their consumption for cell growth.

A reasonable assumption for those metabolic intermediates at nodes in the pathway network is

$$\frac{dc_j}{dt} = 0 \, . \tag{10}$$

This situation, commonly described as "no accumulation of intermediates," can be more generally supported by use of the quasi-steady state hypothesis. The validity of this concept was demonstrated in an experiment by Hartmanis *et al.* [1], in which [1-^{13}C]butyrate uptake in solvent-producing cells was followed via NMR; the only peaks detected were those of [1-^{13}C]butyrate and [1-^{13}C]butanol. Use of Equation (10) gives:

$$v_0 = 0.167 r_G + 0.5 v_1 \tag{11a}$$

$$v_1 = 2v_2 + v_3 + v_{12} \tag{11b}$$

$$v_3 + v_{7A} + v_{10} = v_4 + v_5 + 2v_6 \tag{11c}$$

$$v_6 = v_{7A} + v_{7B} + v_8 \tag{11d}$$

$$v_8 + v_{7B} = v_9 + v_{10} + v_{11} \tag{11e}$$

$$v_{7C} = v_{7A} + v_{7B} \, . \tag{11f}$$

Note that this simplification has not been applied to the material balances for Fd and NAD(P)H, as they are not (glucose) carbon-containing metabolic intermediates. Since there are 18 unknown v_i's but only 11 measurable concentrations (glucose, butanol, *etc.*) and 6 QSSH equations, it is not possible to solve for all of the branch rates explicitly.

From Equations (9a), (9b), (9c), (9f), (9h), (9k), (9n), and (9p), the rates v_0, r_G, v_2, v_{12}, v_4, v_{7C}, v_{11}, and v_{14} are obtained, respectively. Use of Equation (11a) allows solution for v_1, and v_3 can be obtained either from Equation (11b) or (9o). Finally, v_6 and v_8 are obtained from Equations (9i) and (11c), and from (9m) and (11e) (or (11d) and (11f)). At this point, there are three available equations:

$$\frac{dC_{\mathrm{HAc}}}{dt} = xv_5 - xv_{7A} - xv_{10} \tag{9i}$$

$$\frac{dC_{\mathrm{HBu}}}{dt} = xv_9 + xv_{10} - xv_{7B} \tag{9m}$$

$$v_{7A} + v_{7B} = v_{7C} \ , \tag{11f}$$

and five unknowns: v_{7A}, v_{7B}, v_5, v_9, and v_{10}. In order to extract information from this situation, the unknown pathway branch rates will be lumped as

$$v_X = v_5 + v_9 \tag{12a}$$

$$v_Y = v_9 + v_{10} - v_{7B} \ . \tag{12b}$$

As defined, the rate v_X represents the total rate of acid production by phosphotransacylase-acyl kinase reactions (involving ATP production), and v_Y represents the total rate of butyrate production. The rate v_{7C} will serve as the lumped rate for v_{7A} and v_{7B} and indicates the rate of the reactions forming acetone from acetoacetyl-CoA. From Equations (9i), (9m), and (12), v_X and v_Y can be expressed as:

$$xv_X = \frac{dC_{\mathrm{HAc}}}{dt} + \frac{dC_{\mathrm{HBu}}}{dt} + xv_{7C} \tag{13a}$$

$$xv_Y = \frac{dC_{\mathrm{HBu}}}{dt} \ . \qquad (13b)$$

The rate v_{13} cannot be determined at this time, because no assumptions have been made about the time variations of the concentrations of the redox compounds ferredoxin and NAD(P)H. The fluorescence measurements will prove to be useful in the qualitative determination of v_{13}.

EXPERIMENTAL RESULTS

Two batch fermentations were performed, one at pH 6.0 and one at pH 4.5. In both cases, the pH was allowed to fall (through the effect of acetic and butyric acid formation) to the designated value before being controlled. The corresponding trajectories for product, glucose, and cell concentration are shown in Figure 17. As is typical in fermentations of *Cl. acetobutylicum* [22], acetic and butyric acids were the predominant products of the pH 6.0 cultivation, while in the pH 4.5 experiment these acids were consumed to form acetone and butanol. In both fermentations, the biomass concentration began to decrease at a point near glucose depletion. This decrease is apparently due to an autolysin produced by *Cl. acetobutylicum* [60].

The culture fluorescence was measured with an Ingold Fluorosensor, a commercially available fluorometric probe designed for on-line, *in situ* NAD(P)H monitoring. A low-pressure mercury lamp is used to provide 360 nm excitation light, and 450 nm fluorescence is quantified by a photomultiplier. At the signal processing conditions used, this unit provided a linear response over a reasonably wide range of quinine sulfate concentrations (Figure 18). Quinine sulfate is frequently used as a calibration compound for NAD(P)H fluorometers as it is strongly fluorescent

and has excitation and emission wavelengths similar to those of NADH [13,61]. As can be seen in Figure 18, the presence of the quartz window at the sensor-reactor interface results in a small loss (5–10%) in sensitivity relative to direct immersion in liquid; however, there is no change in the linear response range.

The culture fluorescence trajectories during the fermentations are presented in Figures 19A (pH 4.5) and 19B (pH 6.0). In both cases, the cell-free medium background fluorescence is relatively constant with respect to the changes observed in the total fluorescence. As can be seen, the NAD(P)H fluorescence intensity increases over the course of each experiment, and rises very rapidly in the last two hours before glucose depletion. The point at which all glucose is consumed appears as a maximum in the total fluorescence. The fluorescence trajectory of the pH 6.0 experiment differs noticeably from that of the pH 4.5 fermentation early in the experiment, when the fluorescence level decreases after the initiation of glucose consumption. The fluorescence trajectory of a third batch fermentation (at pH 6, data not shown) was very similar to that shown in Figure 19B, indicating the reproducibility of these results.

DISCUSSION

A. Pathway Rates

The time profiles for the various pathway branch rates are shown in Figures 20 and 21. The lumped rates v_X and v_Y are included, but not v_{13} and v_{14}; v_{14} was omitted because hydrogen gas production was not measured, and v_{13} cannot be calculated directly. The curves themselves were obtained from the data shown

in Figure 17, which were fitted with cubic splines to provide slopes for use in the equations of the previous section. Small fluctuations in the plots of Figures 20 and 21 are remnants of the spline-fitting procedure.

Differences in pathway carbon fluxes between the acidogenic pH 6.0 fermentation and the solventogenic pH 4.5 fermentation are readily apparent. For example, the plots for v_{7C} (acetone formation) and v_{11} (butanol formation) clearly show high activity along these branches during the latter part of the pH 4.5 experiment and only a very low rate for the entire pH 6.0 run. From the relatively high specific rates for v_6 and v_8, indicating significant availability of acetoacetyl-CoA and butyryl-CoA, it can be determined that absence of acetone and butanol production is a function of enzyme activity (or lack thereof) and not a matter of insufficient substrate.

Another notable feature is the consumption of butyric acid during the last 8–10 hours of the pH 4.5 fermentation, manifested as negative values for the lumped pathway rate v_Y. It is important to note that values of the other lumped rate involving butyric acid production, v_X, **never** become negative. Since v_X contains the rates of the two acyl kinase reactions, negative values of the v_X would indicate ATP consumption.

Although a lack of independent equations hinders the extraction of information about the relative carbon fluxes along pathways 5, 7A, 7B, 9, and 10, some trends may be discerned with further analysis. For example, to determine whether pathway 10 could be the sole route for acetic acid production and consumption, note first from Equation (9i) that this hypothesis implies

$$v_5 = v_{7A} \ . \tag{14}$$

Combining Equations (11f) and (12b) yields

$$v_Y = v_9 + v_{10} + v_{7A} - v_{7C} \ . \tag{15}$$

Finally, the use of Equations (12a) and (14) in Equation (15) gives

$$v_X - v_Y = v_{7C} - v_{10} \ . \tag{16}$$

The data in Figure 21 show that the left-hand side of Equation (16) is always positive. However, the right-hand side is the difference between the rate of acetone production and the rate of formation of acetate; this difference is not positive throughout the fermentation. Therefore, pathway 10 cannot be the only avenue for acetic acid production. Similar analysis provides the same conclusion for acetic acid formation by pathway 7A alone. In contrast, the production of acetic acid by pathway 9 alone, or by any combination of the three paths (7A, 9, and 10), is allowed by this analytical framework.

While this type of reasoning is unable to differentiate between the three proposed paths for butyrate production and consumption, the underlying knowledge of the metabolic network can be used to generate some additional insights. Although the primary usage of pathway 9 (through butyryl phosphate) for butyrate formation seems most likely because of the production of ATP, pathway carbon flux analysis does not require $v_9 \geq 0$. If $v_9 = 0$, then $v_{10} \geq 0$ and/or $v_{7B} \leq 0$. Butyrate production through pathway 7B would involve cocurrent use of path 7A to recycle acetoacetate and would seem an unlikely avenue. Significant fluxes along either branch 7B or 10 would require large values of v_5 to supply acetate. Analogous acetoacetate "recycling" or large v_9 values are required if paths 7A or 10 are used to form acetic acid. It should be recalled that while pathway 10 has been

included in this analysis for generality, this reaction has not been detected in *Cl. acetobutylicum* [4].

It was previously noted that the uptake of butyrate for the production of butanol occurs by one or more of the pathways lumped into v_Y (branches 7B, 9, and 10). Although this carbon flux analysis does not preclude $v_9 < 0$ (butyrate consumption), use of the data in Figures 20 and 21 does prove that pathway 9 cannot be the **only** reaction set used in butyrate uptake. This requirement and the existence of at least one non-ATP-consuming alternative make negative values of v_9 improbable under normal circumstances. An additional point is that as the pattern of carbon flux in branch 9 might be similar to that of the analogous pathway 5, and since v_X, the combined rate of these two paths, is always positive (Figure 21), then both v_5 and v_9 are probably also always positive.

A significant amount of acetate was consumed in the pH 4.5 fermentation (Figure 17), but often the acetate concentration remains nearly constant during solvent production. Equations (9k) and (13a) show that the relationship between acetate, butyrate, and acetone formation rates is:

$$\frac{dC_{\mathrm{AC=O}}}{dt} = xv_X - \frac{dC_{\mathrm{HAc}}}{dt} - \frac{dC_{\mathrm{HBu}}}{dt} \quad . \tag{17}$$

Figure 21 shows that v_X is slightly positive or zero during acetone production, so

$$\frac{dC_{\mathrm{AC=O}}}{dt} \approx -\frac{dC_{\mathrm{HAc}}}{dt} - \frac{dC_{\mathrm{HBu}}}{dt} \quad . \tag{18}$$

Thus, acetone formation occurs during butyrate uptake even if the acetate concentration remains constant. Hartmanis *et al.* [1] have presented evidence to support the contention that the amount of acetic and butyric acid consumed is equal to the amount of acetone produced (the integrated form of Equation (18)).

Their argument is based on the coupling of the acetoacete decarboxylation with the acetoacetyl-CoA:acetate (butyrate) CoA-transferase step used in acids uptake; this coupling is thought to be required to overcome the unfavorable equilibrium of the CoA-transferase reaction. However, Meyer *et al.* [19] recently reported butyrate uptake for butanol production, with no acetone formation, in cultures gassed with carbon monoxide. CO acts as an inhibitor of hydrogenase, the enzyme represented in pathway 14. Analysis of specific rate data for these cultivations shows that v_X is negative during the period of exposure to CO (see Equation (17)), and thus $v_5 < 0$ and/or $v_9 < 0$. Acid uptake by these energy-expensive pathways is possible in this situation because the ATP concentration in CO-gassed cells is very high [62].

B. Culture Fluorescence Analysis

The fluorescence profiles of the two fermentations were presented in Figure 15. These were obtained with an Ingold Fluorosensor, which measured 450 nm fluorescence resulting from 360 nm excitation. While other cell components may fluoresce slightly under these conditions, their contributions are small when compared with the fluorescence of NADH and NADPH. NADPH is used primarily in the synthesis of biomass and does not appear to be required as a cofactor in the catabolic pathways of *Cl. acetobutylicum* (Figure 15) [1,4,40]. It is usually present in much lower concentrations than NADH [68]. NADPH is apparently obtained by the oxidation of reduced ferredoxin (NADPH:ferredoxin oxidoreductase [35,36,64]) or by a transhydrogenation reaction with NADH. The source of cellular fluorescence is usually referred to as "NAD(P)H" for generality.

The measured NAD(P)H-dependent culture fluorescence is a function of the

actual cellular NAD(P)H concentration, which is the information of interest. Unfortunately, culture fluorescence data are obscured by factors attenuating both the exciting and fluorescent light. A common problem in solution fluorometry is the "inner filter effect" [65], in which the intensity of the exciting light decreases (because of solute absorption) as the light travels through the sample. The fluorescence is then a function of a distribution of exciting light intensities. In this case of culture fluorescence, there is a secondary inner filter effect due to the absorbance of fluorescent light by the cells. Both exciting and emitted light intensities are further decreased by scattering. The inner filter effect and scattering effects thus introduce a nonlinear influence of cell density on culture fluorescence. An advantage of the fiber optic system employed in the Ingold probe used in this work is the relatively short effective light penetration depth (small measuring volume); this depth becomes constant at relatively low culture optical densities. This was demonstrated in an experiment in which the fluorescence of a fluorophore solution was measured with the Fluorosensor as yeast cells were added. Although the measured tracer fluorescence decreased with increasing cell density at low biomass concentrations, the fluorescence signal was essentially independent of cell density above approximately 0.5 g/L of yeast. The fluorescence of cellular NAD(P)H may also be quenched (a process in which radiationless deactivation from the fluorophore excited state occurs instead of a fluorescent (radiational) deactivation process [65]) by compounds in the cytoplasm, cell membrane or wall. Additional measurement interference may arise from the fluorescence and quenching properties of the medium. Calibration measurements are used to verify the extent of some of these factors, which may change over the course of a cultivation [66]. Although these influences prevent

quantitative determination of cellular NAD(P)H concentration in nearly all cases, fluorescence data can still provide valuable information on culture metabolic activity on a qualitative scale. Culture fluorescence probes have been used successfully for biomass concentration estimation in several different cultivations (*e.g.*, *B. subtilis* [66], *S. cerevisiae* [12], and *Z. mobilis* [67]), and for metabolic studies (*e.g.*, with *S. cerevisiae* [11]).

The culture fluorescence measured in the two experiments was not affected by the pH changes that occurred early in the cultivations, before pH control was applied. Figure 9 shows that NADH fluorescence is independent of pH for pH values greater than 5.0. These data were obtained from anaerobic NADH solutions with the Fluorosensor probe. Measurements of intracellular pH values in batch cultivations of *Cl. acetobutylicum* have shown that the internal pH usually remains greater than 5.5 [24,68]; thus, the fluorescence measurements in these cultivations are not a function of pH.

It is important to note that the fluorescence, both total (Figure 19) and specific (Figure 23) shows significant variations in time for the two experiments, and that these changes occur before, during, and after detectable glucose consumption. In Figure 23, it is apparent that the fluorescence-time profiles of the two fermentations are similar, even though the end product distributions are quite different. In the beginning of each, the specific fluorescence level rises before beginning a rapid decrease. This local maximum in the specific fluorescence is a very sensitive indicator of the start of growth and glucose consumption; the change in glucose concentration is not measurable at this point but increases rapidly soon after. This decrease in specific fluorescence continues for several hours before a minimum is reached. For

both experiments, this minimum corresponds well with the onset of solvent formation. The latter parts of each fermentation were marked by increasing specific fluorescence levels. The time at which glucose is exhausted is marked by a rapid change of slope in the specific fluorescence trajectory.

The change in intracellular NAD(P)H concentration with time is given by:

$$\frac{dc_{\mathrm{NAD(P)H}}}{dt} = v_1 - 0.125v_G + v_{13} - 2v_4 - 2v_8 - 2v_{11} - v_{12} \ . \qquad (9r)$$

Interpretation of the profiles of Figure 23 can thus be accomplished in terms of the pathway branch rates. This interpretation must be qualitative, as it is not possible to equate a given fluorescence with a certain intracellular NAD(P)H concentration. Of the seven v_i branch carbon fluxes contributing to changes in the NAD(P)H concentration, all but v_{13} are known. This pathway rate corresponds to the NAD(P)H:ferredoxin oxidoreductase reaction(s) and could not be determined because neither ferredoxin nor NAD(P)H concentrations were considered to be constant with time. However, qualitative aspects of the variation of v_{13} with time may be discerned by comparing the specific fluorescence curves of Figure 23 with the following integrated form of Equation (9r), which assumes v_{13} to be zero:

$$NAD(P)H|_t - NAD(P)H|_0 = \int_0^t [v_1 - 0.125v_G - 2v_4 - 2v_8 - 2v_{11} - v_{12}]dt \ . \quad (19)$$

If these profiles, presented in Figure 24, could be compared directly with the specific fluorescence curves, then the difference between the ordinate values at a given time would be the amount of NAD(P)H produced (or consumed) by pathway 13 through that time in the batch fermentation. Alternatively, the slopes of the profiles in Figures 23 and 24 could be compared; the difference between the derivative of the specific fluorescence trajectory and the slope of the curve given by Equation (19) would indicate the sign and magnitude of v_{13}.

When this comparison is made for the pH 4.5 experiment, it becomes apparent that v_{13} must be negative for the early, acid-forming phase of the fermentation. Negative values of v_{13} mean that NAD(P)H is being oxidized by ferredoxin:

$$\mathrm{NAD(P)H} + \mathrm{Fd_{ox}} \rightarrow \mathrm{NAD(P)^+} + \mathrm{Fd_{red}} \ ;$$

reduced ferredoxin is undoubtedly oxidized in the hydrogenase reaction:

$$\mathrm{Fd_{red}} + 2\mathrm{H^+} \rightarrow \mathrm{Fd_{ox}} + \mathrm{H_2} \ .$$

However, a change occurs after about 13 hours; the specific fluorescence increases, and a comparison with Figure 24 shows that v_{13} must be positive (until all of the glucose is consumed). This change in sign of v_{13}, indicating that NAD(P)H is now being **produced** by the ferredoxin redox reaction, is clearly associated with the transition from acid to solvent production. Culture fluorescence measurements can thus be used to discern the onset of solvent formation.

Substantial evidence exists for the reversal of the NAD(P)H:ferredoxin oxidoreductase reaction during a solvent-producing batch fermentation. In a series of papers, Petitdemange *et al.* [35,36,64] found that one enzyme was responsible for both the reduction of NAD^+ and the oxidation of NADH; they hypothesized that two isoenzymes might exist. Consistent with the idea that reducing equivalents from the oxidation of NAD(P)H are released as H_2 in acid-producing cultures, several researchers have noted higher H_2 production during acid formation than in the solvent phase of a batch fermentation [3,21,69]. In an enzyme activity study, Andersch *et al.* [4] detected more than twice as much hydrogenase activity in the acid phase as in the solvent phase. In fact, solvent phase hydrogenase activity was evident only after a ten minute lag, possibly indicating that the hydrogenase was

present in an inactive form. Finally, in the detailed application of stoichiometry to *Cl. acetobutylicum* fermentations by Papoutsakis *et al.* [3,7,19,37], the parameter denoting moles of NADH formed from reduced ferredoxin was found to be positive for solvent-producing cultures and negative for those with acids as the primary end products.

Thus, the reactions catalyzed by NADH:ferredoxin oxidoreductase are vital to the cell for the control of intracellular NADH content. During acid production, the flux of carbon throughout the pathway results in a net production of NADH (Figure 24); these excess reducing equivalents are "vented" as H_2 via paths 13 and 14. Conversely, the reactions involved in solvent production indicate a net consumption of NADH . The necessary reducing equivalents are provided through the reduction of NAD^+ by FdH_2.

A comparision of the trajectories in Figures 23 and 24 for the pH 6.0 experiment shows a slightly different pattern. As in the pH 4.5 fermentation, v_{13} is initially negative, indicating the oxidation of NAD(P)H by ferredoxin. Although some reducing equivalents were used in the formation of lactic acid, the major route for NAD(P)H oxidation is clearly H_2 production via ferredoxin. However, at the 13 hour mark of the pH 6.0 cultivation, the specific fluorescence level begins to increase, signaling a significant change in the magnitude of v_{13}. It is not possible to determine the sign of v_{13} in this phase of the fermentation (since specific fluorescence changes cannot be converted to NAD(P)H concentration changes), but the rate of this redox reaction is clearly low. Apparently, even the initiation of low rates of solvent formation can stop the release of reducing equivalents to ferredoxin, either by providing alternative routes for NAD(P)H consumption or by requiring

higher intracellular NAD(P)H concentrations.

The specific fluorescence curves of Figure 23 imply that the NADH:ferredoxin oxidoreductase reaction does not operate to maintain a constant intracellular NADH concentration; rather, there seems to be a net consumption of NADH (production of NAD^+) during acid formation and a net production of NADH during the production of solvents. The reasons for this apparent "overproduction" are unclear.

The fluorescence plots of Figures 19 and 23 also indicate that a significant amount of metabolic activity occurs before measurable glucose consumption and after glucose depletion. The rapid increase in the fluorescence (NAD(P)H concentration) during the lag phase must be associated with events such as enzyme induction, which are required to prime a cell for growth in a new medium. The exhaustion of the glucose supply was signaled by a sudden change in the slope of the total fluorescence curve in both experiments. At this point, NAD(P)H consumption or production rates seem to be low, but nonzero. The rate of cell lysis was high at this time; reactions connected with this process, and with other events such as the consumption of storage compounds or the uptake and use of lysis products, may contribute to the changing NAD(P)H levels. Only a small percentage of cells sporulated in either fermentation.

CONCLUSIONS

Two techniques have been used to provide significant insights regarding the metabolic activities of *Clostridium acetobutylicum* in both acidogenic and solventogenic batch cultures. The application of metabolic pathway kinetic analysis fur-

nished information on the paths used for acid formation and uptake; the technique also proved useful in understanding the lack of acetone production in cultures gassed with carbon monoxide.

In situ fluorescence measurements during the fermentations clearly displayed the points of growth phase initiation, induction of solvent formation, and glucose depletion. When the fluorescence data were combined with the pathway branch kinetic analysis, it was shown that *Cl. acetobutylicum* uses a redox reaction catalyzed by NADH:ferredoxin oxidoreductase to control the intracellular NADH concentration. In fact, the reaction appears to operate in such a way as to provide a net consumption of NADH in the acid phase and a net production during high rates of solvent formation. Fluorescence measurements also proved to be an extremely sensitive indicator of intracellular metabolism; both pre- and post-glucose consumption NAD(P)H variations were noted.

LITERATURE CITED

1. Hartmanis, M.G.N., T. Klason, and S. Gatenbeck, "Uptake and Activation of Acetate and Butyrate in *Clostridium acetobutylicum*," *Appl. Microbiol. Biotechnol., 20, 66–71 (1984).*

2. Jones, D.T., A. van der Westhuizen, S. Long, E.R. Allcock, S.J. Reid, and D.R. Woods, "Solvent Production and Morphological Changes in *Clostridium acetobutylicum*," *Appl. Environ. Microbiol., 43, 1434–1439 (1982).*

3. Roos, J.W., J.K. McLaughlin, and E.T. Papoutsakis, "The Effect of pH on Nitrogen Supply, Cell Lysis, and Solvent Production in Fermentations of *Clostridium acetobutylicum*," *Biotechnol. Bioeng., 27, 681–694 (1985).*

4. Andersch, W., H. Bahl, and G. Gottschalk, "Level of Enzymes Involved in Acetate, Butyrate, Acetone and Butanol Formation by *Clostridium acetobutylicum*," *Eur. J. Appl. Microbiol. Biotechnol., 18, 327–332 (1983).*

5. Humphrey, A.E., "Present Limitations to the Control and Understanding of a Fermentation Process," in *Proc. LABEX Symp. Comput. Control Ferment. Processes*, 1 (1971).

6. Aiba, S. and M. Matsuoka, "Identification of Metabolic Model: Citrate Production from Glucose by *Candida lipolytica*," *Biotechnol. Bioeng., 21*, 1373–1386 (1979).

7. Papoutsakis, E.T., "Equations and Calculations for Fermentations of Butyric Acid Bacteria," *Biotechnol. Bioeng., 26*, 174–187 (1984).

8. Duysens, L.M.N. and J. Amesz, "Fluorescence Spectrophotometry and Reduced Phosphopyridine Nucleotide in Intact Cells in the Near-Ultraviolet and Visible Region," *Biochim. Biophys. Acta, 24*, 19–26 (1957).

9. Chance, B. and V. Legallais, "Differential Microfluorimeter for the Localization of Reduced Pyridine Nucleotide in Living Cells," *Rev. Sci. Instruments, 30*, 732–735 (1959).

10. Chance, B., J.R. Williamson, D. Jamieson, and B. Schoener, "Properties and Kinetics of Reduced Pyridine Nucleotide Fluorescence of the Isolation and *in vivo* Rat Heart," *Biochem. Zeit., 341*, 357–377 (1965).

11. Scheper, T. and K. Schügerl, "Culture Fluorescence Studies on Aerobic Continuous Cultures of *Saccharomyces cerevisiae*," *Appl. Microbiol. Biotechnol, 23*, 440–444 (1986).

12. Zabriskie, D. and A.E. Humphrey, "Estimation of Fermentation Biomass Concentration by Measuring Culture Fluorescence," *Appl. Environ. Microbiol., 35*, 337–343 (1978).

13. Luong, J.H.T. and D.J. Carrier, "On-line Measurement of Culture Fluorescence during Cultivation of *Methylomonas mucosa*," *Appl. Microbiol. Biotechnol., 24*, 65–70 (1986).

14. Reardon, K.F., T. Scheper, and J.E. Bailey, "*In situ* Fluorescence Monitoring of Immobilized *Clostridium acetobutylicum,*" *Biotech. Lett., 8, 817–822 (1986).*

15. Spivey, M.J., "The Acetone/Butanol/Ethanol Fermentation," *Proc. Biochem., 13*, 2–4,25 (1978).

16. Moreira, A.R., "Acetone–Butanol Fermentation," in *Organic Chemicals From Biomass*, D.L. Wise, Ed., The Benjamin/ Cummings Publishing Co., London (1983), pp. 385–406.

17. Davies, R., "Studies on the Acetone–Butyl Alcohol Fermentation," *Biochem. J., 36*, 582–599 (1942).

18. George, H.A. and J.-S. Chen, "Acidic Conditions Are Not Obligatory for Onset of Butanol Formation by *Clostridium acetobutylicum*," *Appl. Environ. Microbiol., 46, 321-327 (1983).*

19. Meyer, C.L., J.W. Roos, and E.T. Papoutsakis, "Carbon Monoxide Gasing Leads to Alcohol Production and Butyrate Uptake without Acetone Formation in Continuous Cultures of *Clostridium acetobutylicum*," *Appl. Microbiol. Biotechnol., 24, 159-167 (1986).*

20. Datta, R. and J.G. Zeikus, "Modulation of Acetone–Butanol–Ethanol Fermentation by Carbon Monoxide and Organic Acids," *Appl. Environ. Microbiol., 49*, 522–529 (1985).

21. Doremus, M.G., J.C. Linden, and A.R. Moreira, "Agitation and Pressure Effects on Acetone–Butanol Fermentation," *Biotechnol. Bioeng., 27*, 852–860 (1985).

22. Monot, F., J.-M. Engasser, and H. Petitdemange, "Influence of pH and Undissociated Butyric Acid on the Production of Acetone and Butanol in Batch Cultures of *Clostridium acetobutylicum*," *Appl. Microbiol. Biotechnol., 19, 422-426 (1984).*

23. Fond, O., J.-M. Engasser, G. Matta-El-Amouri, and H. Petitdemange, "The Acetone Butanol Fermentation on Glucose and Xylose. II. Regulation and Kinetics in Fed-Batch Cultures," *Biotechnol. Bioeng., 28*, 167–175 (1986).

24. Terracciano, J.S. and E.R Kashket, "Intracellular Conditions Required for Initiation of Solvent Production by *Clostridium acetobutylicum*," *Appl. Environ. Microbiol., 52, 86-91 (1986).*

25. Huesemann, M. and E.T. Papoutsakis, "Effect of Acetoacetate, Butyrate, and Uncoupling Ionophores on Growth and Product Formation of *Clostridium ace-*

tobutylicum," Biotech. Lett., 8, 37-42 (1986).

26. Jones, D.T. and D.R. Woods, "Acetone–Butanol Fermentation Revisited," *Microbiol. Rev., 50*, 484–524 (1986).

27. Volesky, B. and T. Szczesny, "Bacterial Conversion of Pentase Sugars to Acetone and Butanol," *Adv. in Biochem. Eng./Biotechnol., 27*, 101–118 (1983).

28. Maddox, I.S., "Production of EtOH and n-Butanol from Hexose/Pentase Mixtures using Consecutive Fermentation of *Saccharomyces cerevisiae* and *Clostridium acetobutylicum," Biotech. Lett., 4, 23-28 (1982).*

29. Doelle, H.W., "Fermentation," *Bacterial Metabolism*, 2nd Ed., Academic Press, New York, N.Y. (1975).

30. Gottschalk, G., "Bacterial Fermentations," *Bacterial Metabolism*, 2nd Ed., Springer-Verlag, New York, N.Y. (1986), pp. 208–282.

31. Uyeda, K. and J.C. Rabinowitz, "Pyruvate-Ferredoxin Oxidoreductase III. Purification and Properties of the Enzyme," *J. Biol. Chem., 246*, 3111–3119 (1971).

32. Yoch, D.C. and R.P. Carithers, "Bacterial Iron–Sulfur Proteins," *Microbiol. Rev., 43*, 384–421 (1979).

33. Chen, J.-S. and L.E. Mortenson, "Purification and Properties of Hydrogenase from *Clostridium pasteurianum* W5," *Biochim. Biophys. Acta, 371*, 283–298 (1974).

34. Mortenson, L.E., "Purification and Properties of Hydrogenase from *Clostridium pasteurianum*," *Methods in Enzymology, 53*, 286–296 (1978).

35. Petitdemange, H., M. Bellanger, D. Lambert, and R. Gay, "Activities of NAD and NAOP Ferredoxin Reductases in Cell-free Extracts of the Butyric Group

of *Clostridia*," *C.R. Acad. Sci. Paris Ser. D.*, *272*, 2840–2843 (1971).

36. Petitdemange, H., C. Cherrier, G. Raval, and R. Gay, "Regulation of the NADH and NADPH-Ferredoxin Oxidoreductases in *Clostridia* of the Butyric Group," *Biochim. Biophys. Acta*, *421*, 334–347 (1976).

37. M^{c}Laughlin, J.K., C.L. Meyer, and E.T. Papoutsakis, "Gas Chromatography and Gateway Sensors for On-line State Estimation of Complex Fermentations (Butanol–Acetone Fermentation)," *Biotechnol. Bioeng.*, *27*, 1246–1257 (1985).

38. Stadtman, E.R., G.D. Novelli, and F. Lipmann, "CoA Function in and Acetyl Transfer by the Phosphotransacetylase System," *J. Biol. Chem.*, *191*, 365–376 (1951).

39. Rose, I., "Acetate Kinase of Bacteria (Acetokinase)," *Methods in Enzymology*, *1*, 591–595 (1955).

40. Hartmanis, M.G.N. and S. Gatenbeck, "Intermediary Metabolism in *Clostridium acetobutylicum: Levels of Enzymes Involved in the Formation of Acetate and Butyrate," Appl. Environ. Microbiol., 47, 1277-1283 (1984).*

41. Gavard, R., B. Hautecoeur, and H. Descourtieux, "Phosphotransbutyrylase of *Clostridium acetobutylicum," C.H.R. Acad. Sci., 244, 2323-2326 (1957).*

42. Valentine, R.C. and R.S. Wolfe, "Purification and Role of Phosphotransbutyrylase," *J. Biol. Chem.*, *235*, 1948–1951 (1960).

43. Twarog, R. and R.S. Wolfe, "Role of Butyryl Phosphate in the Energy Metabolism of *Clostridium tetanomorphum*," *J. Bacteriol, 86*, 112–117 (1963).

44. Hardman, J.K. and T.C. Stadtman, "Metabolism of ω-Amino Acids. V. Energetics of the γ-Aminobutyrate Fermentation by *Clostridium aminobutyricum*," *J. Bacteriol, 85*, 1326–1333 (1963).

45. Stadtman, E.R., "The Coenzyme A Transphorase System in *Clostridium kluyveri*," *J. Biol. Chem., 203*, 501–512 (1953).

46. Davies, R., "Studies on the Acetone–Butanol Fermentation. 4. Acetoacetate Decarboxylase of *Clostridium acetobutylicum*," *Biochem. J., 37, 230–238 (1943).*

47. Zerner, B., S.M. Coutts, F. Lederer, H.H. Waters, and F.H. Westheimer, "Acetoacetate Decarboxylase. Preparation of the Enzyme," *Biochem., 5*, 813–816 (1966).

48. Wood, H.G., R.W. Brown, and C.H. Werkman, "Mechanism of the Butyl Alcohol Fermentation with Heavy Carbon Acetic and Butyric Acids and Acetone," *Arch. Biochem., 6*, 243–260 (1945).

49. Bahl, H. and G. Gottschalk, "Parameters Affecting Solvent Production by *Clostridium acetobutylicum in Continuous Culture*," *Biotechnol. Bioeng. Symp. Ser., 14, 215–223 (1984).*

50. Simon, E., "The Formation of Lactic Acid by *Clostridium acetobutylicum (Weizmann)*," *Arch. Biochem., 13, 237–243 (1947).*

51. Bahl, H., M. Gottwald, A. Kuhn, V. Rale, W. Andersch, and G. Gottschalk, "Nutritional Factors Affecting the Ratio of Solvents Produced by *Clostridium acetobutylicum*," *Appl. Environ. Microbiol, 52, 169–172 (1986).*

52. Thauer, R.K., K. Jungermann, and K. Decker, "Energy Conservation in Chemotrophic Anaerobic Bacteria," *Bact. Rev., 41*, 100–180 (1977).

53. Papoutsakis, E.T. and C.L. Meyer, "Equations and Calculations of Product Yields and Preferred Pathways for Butanediol and Mixed-Acid Fermentations," *Biotechnol. Bioeng., 27*, 50–66 (1985).

54. Papoutsakis, E.T. and C.L. Meyer, "Fermentation Equations for Propionic-Acid Bacteria and Production of Assorted Oxychemicals from Various Sugars," *Biotechnol. Bioeng., 27*, 67–80 (1985).

55. Fredrickson, A.G., "Formulation of Structured Growth Models," *Biotechnol. Bioeng., 18*, 1481–1486 (1976).

56. Van Dijken, J.P. and W. Harder, "Growth Yields of Microorganisms on Methanol and Methane. A Theoretical Study," *Biotechnol. Bioeng., 17*, 15–30 (1975).

57. Minkevich, J.G. and V.K. Eroshin, "Productivity and Heat Generation of Fermentation Under Oxygen Limitation," *Folia Microbiol., 18*, 376–385 (1973).

58. Erickson, L.E., "Biomass Elemental Composition and Energy Content," *Biotechnol. Bioeng., 22*, 451–456 (1980).

59. Daesch, G. and L.E. Mortenson, "Sucrose Catabolism in *Clostridium pasteurianum* and Its Relation to N_2 Fixation," *J. Bacteriology, 96*, 346–351 (1967).

60. van der Westhuizen, A., D.T. Jones, and D.R. Woods, "Autolytic Activity and Butanol Tolerance of *Clostridium acetobutylicum," Appl. Environ. Microbiol., 44, 1277-1281 (1982).*

61. Beyeler, W., A. Einsele, and A. Fiechter, "On-Line Measurements of Culture Fluorescence: Method and Application," *Eur. J. Appl. Microbiol. Biotechnol., 13*, 10–14 (1981).

62. Papoutsakis, E.T., M. Huesmann, C.L. Meyer, R.W. Welch, D.P. Wiesenborn, and F.B. Rudolph, paper no. 72d, AIChE Annual Meeting, Miami Beach, November 1986.

63. Takebe, I. and K. Kitahara, "Levels of Nicotinamide Nucleotide Coenzymes in

Lactic Acid Bacteria," *J. Gen. Appl. Microbiol., 9*, 31–40 (1963).

64. Petitdemange, H., C. Cherrier, J.M. Bengone, and R. Gay, "Etude des Activites NADH et NADPH-Ferredoxine Oxydoreductasiques chez *Clostridium acetobutylicum," Can. J. Microbiol., 23, 152–160 (1977).*

65. Udenfriend, S., *Fluorescence Assay in Biology and Medicine, II*, Academic Press, New York, N.Y. (1969).

66. Meyer, H.-P., W. Beyeler, and A. Fiechter, "Experiences with the On-Line Measurement of Culture Fluorescence during Cultivation of *Bacillus subtilis, Escherichia coli*, and *Sporotrichum thermophile*," *J. Biotech., 1*, 341–349 (1984).

67. Scheper, T., T. Lorenz, W. Schmidt, and K. Schügerl, "Measurement of Culture Fluorescence during the Cultivation of *Penicillium chrysogenum* and *Zymomonas mobilis*," *J. Biotech., 3*, 231–238 (1986).

68. Huang, L., L.N. Gibbins, and C.W. Forsberg, "Transmembrane pH Gradient and Membrane Potential in *Clostridium acetobutylicum during Growth under Acetogenic and Solventogenic Conditions," Appl. Environ. Microbiol., 50, 1043-1047 (1985).*

69. Moreira, A.R., B.E. Dale, and M.G. Doremus, "Utilization of the Fermentor Off-Gases from an Acetone-Butanol Fermentation," *Biotechnol. Bioeng. Sym Ser., 12*, 263–277 (1982).

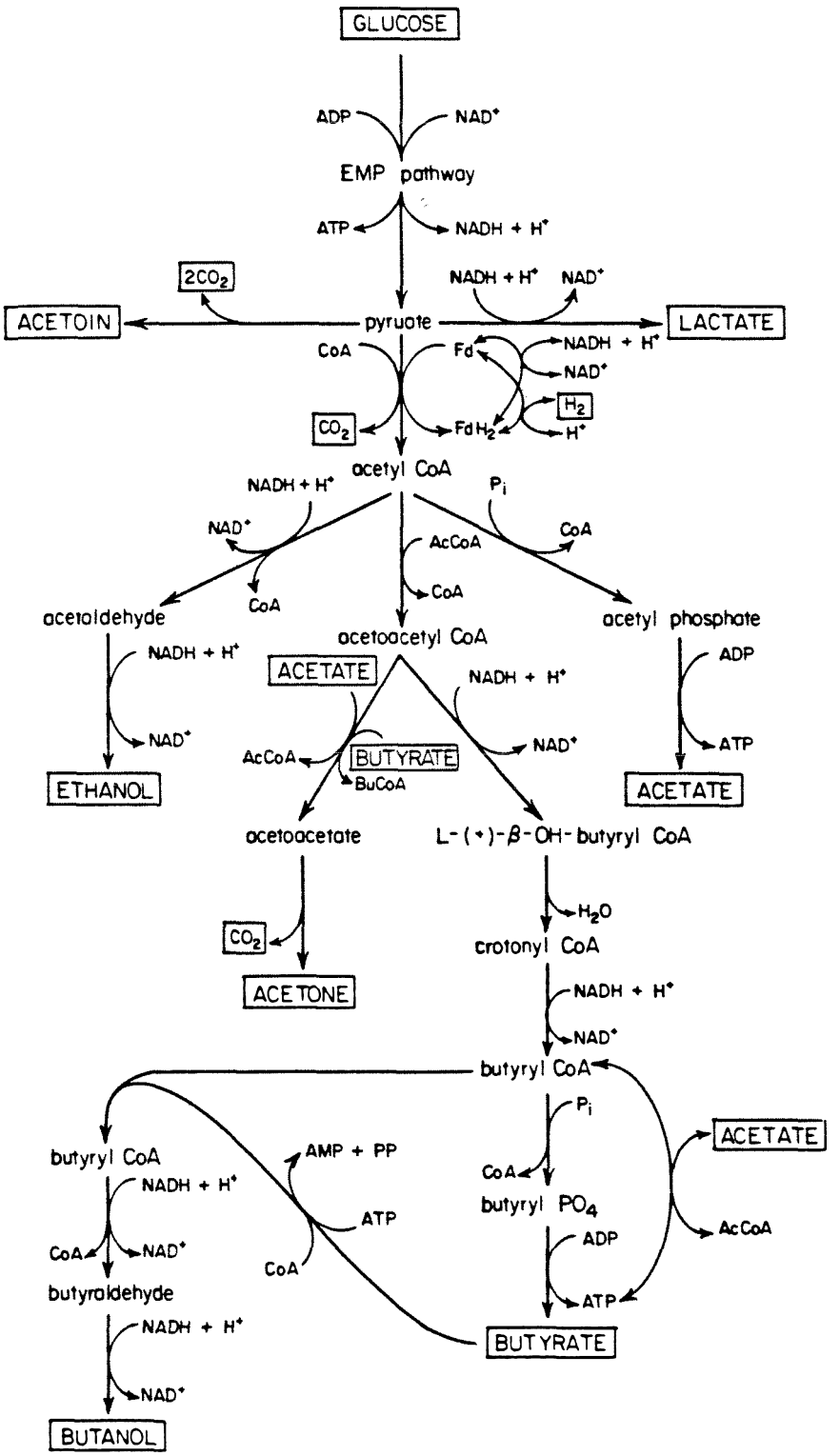

Figure 15. Metabolic pathways in *C. acetobutylicum*.

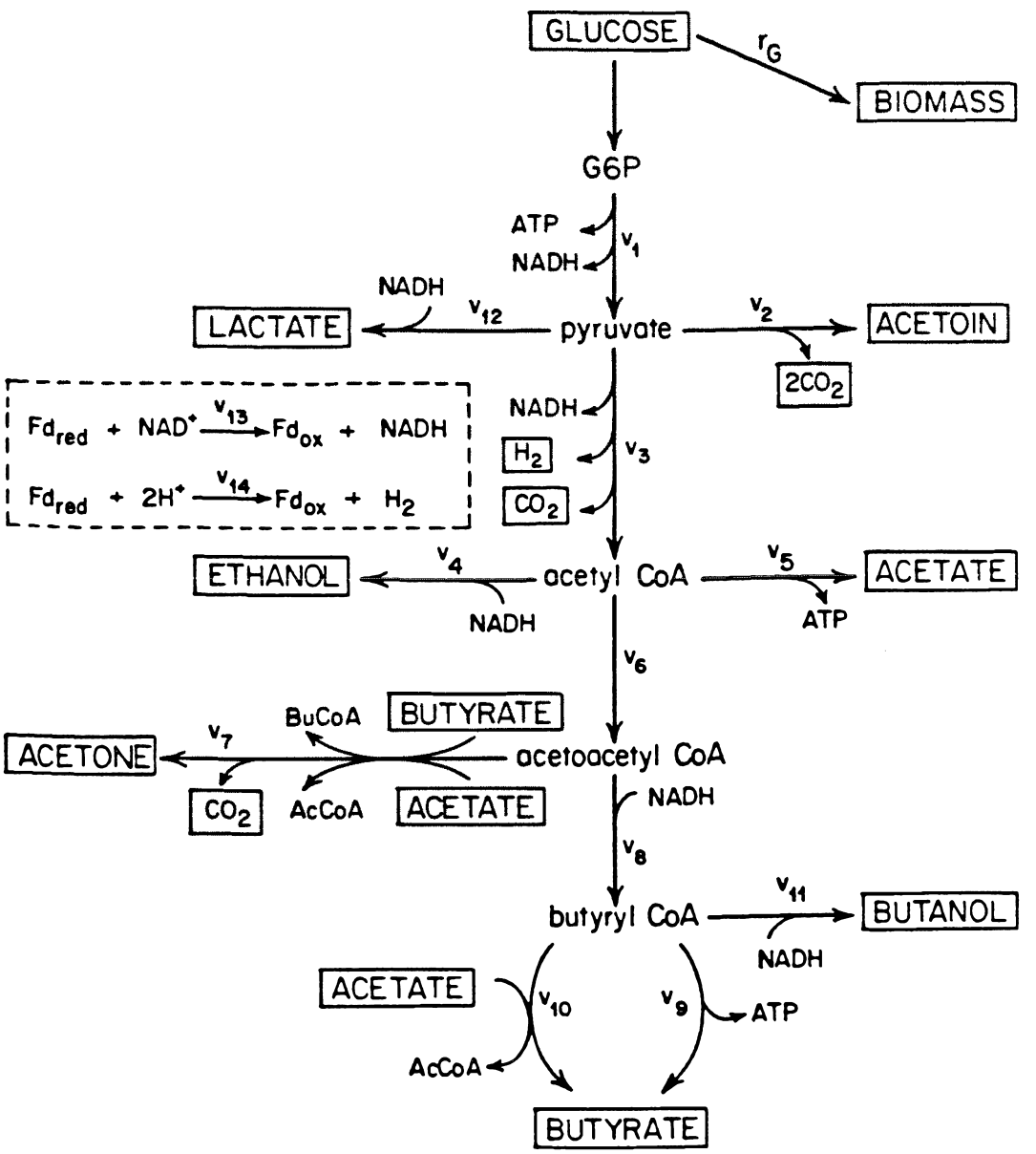

Figure 16. Simplified schematic of the *C. acetobutylicum* metabolic pathways.

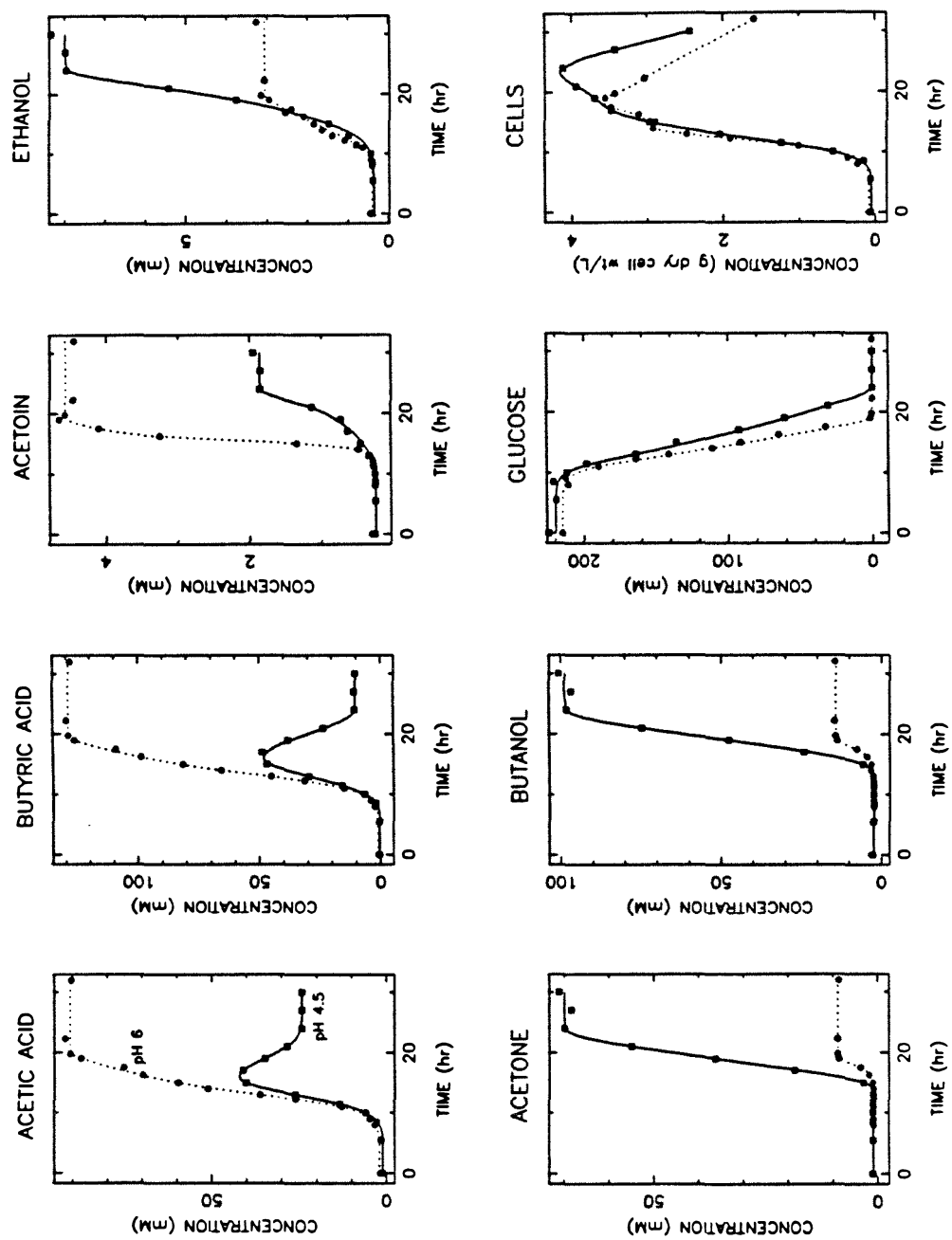

Figure 17. Concentration profiles for pH 4.5 and pH 6.0 batch suspended cell fermentations.

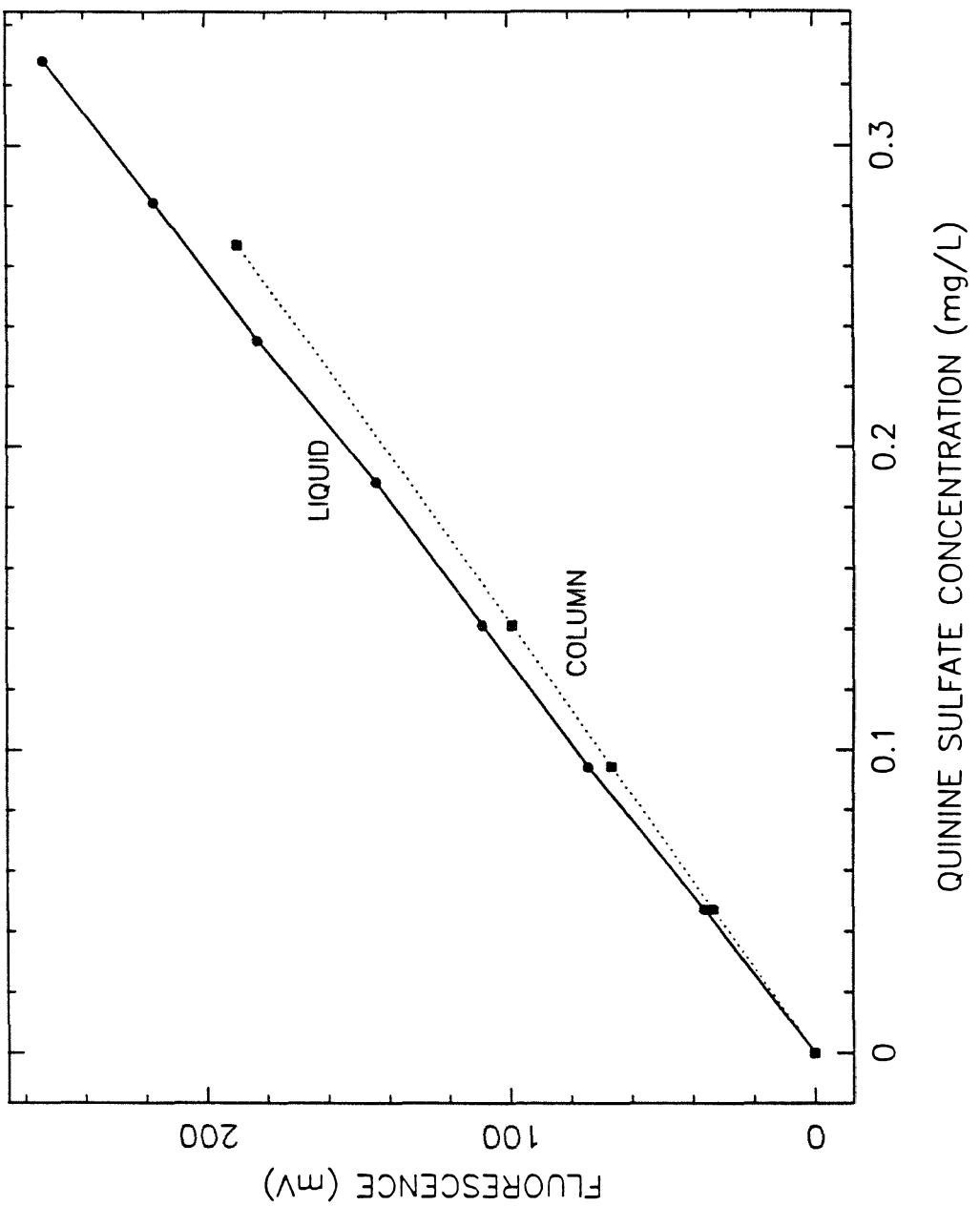

Figure 18. Quinine sulfate fluorescence calibration curve for the Ingold Fluorosensor probe.

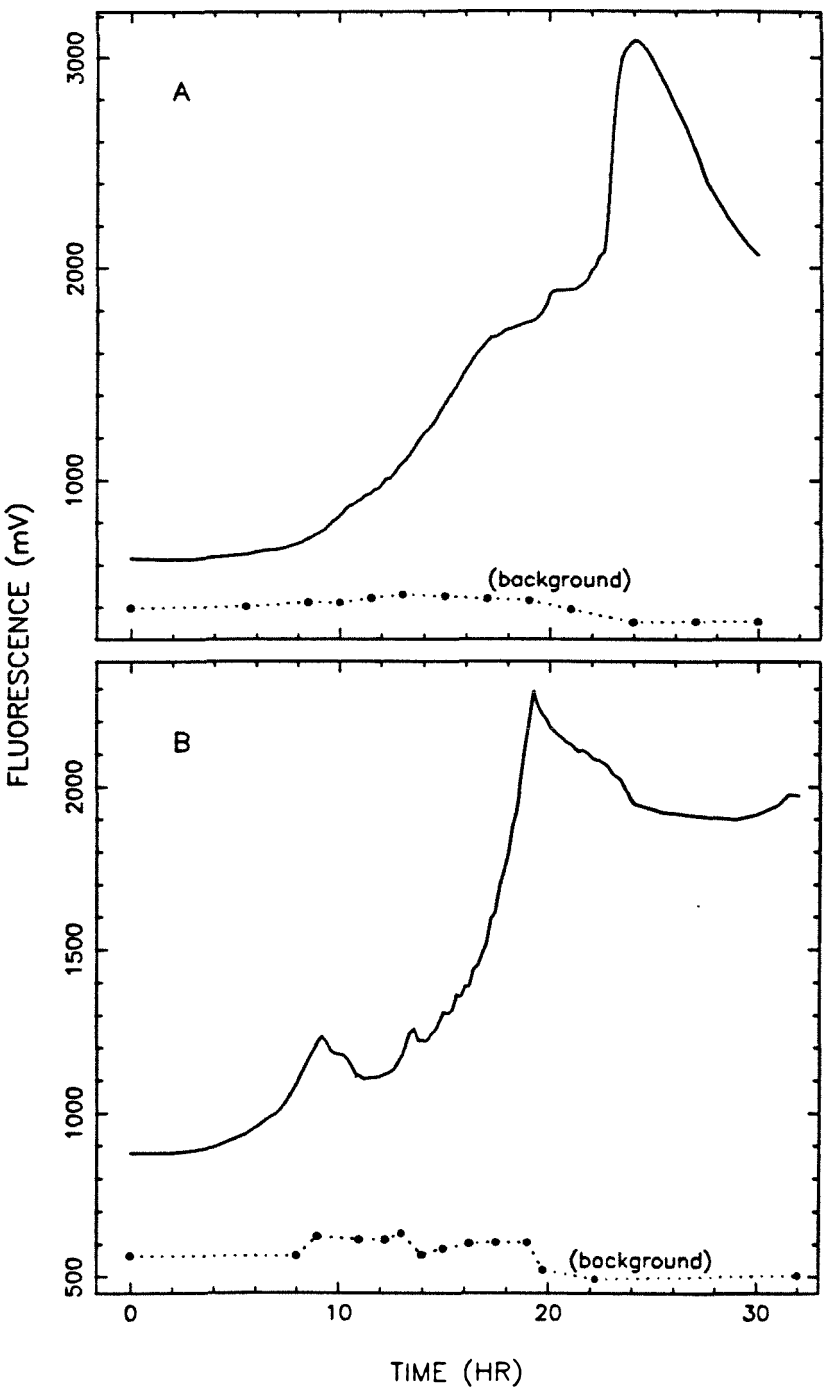

Figure 19. Total culture fluorescence trajectories. **A**: pH 4.5 and **B**: pH 6.

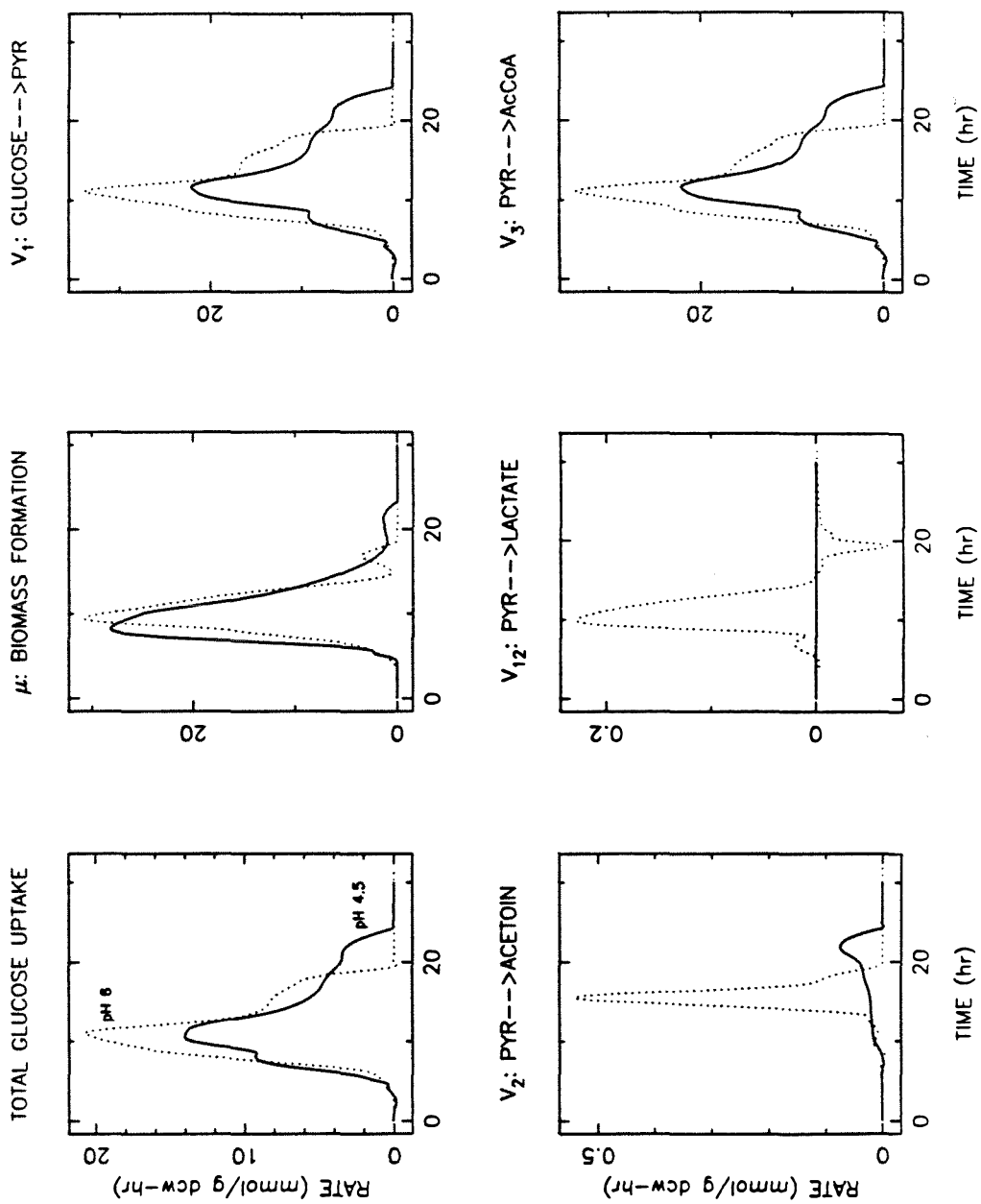

Figure 20. Metabolic pathway branch specific rate trajectories for pH 4.5 and pH 6 batch suspended cell fermentations.

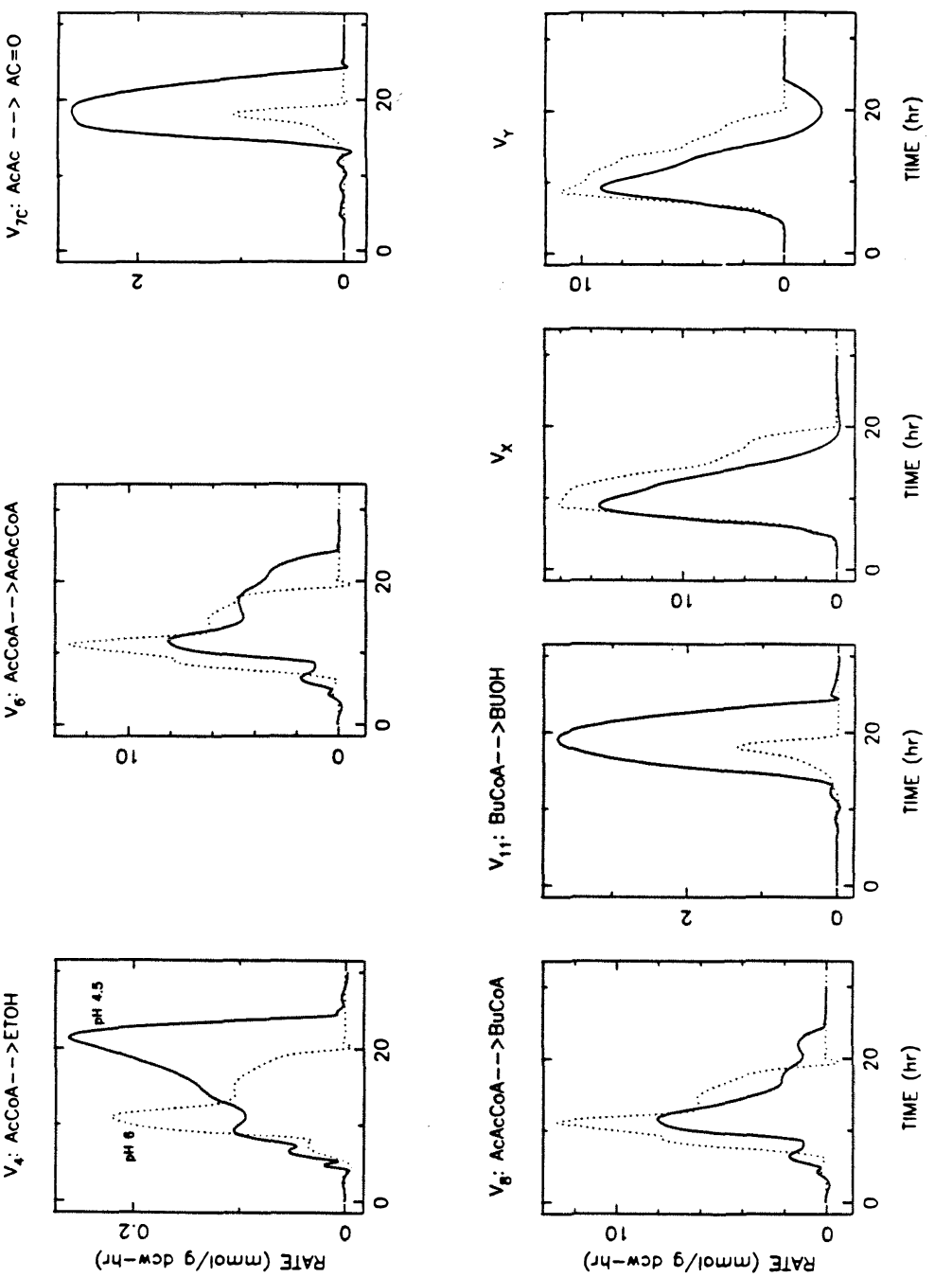

Figure 21. Metabolic pathway branch specific rate trajectories for pH 4.5 and pH 6 batch suspended cell fermentations.

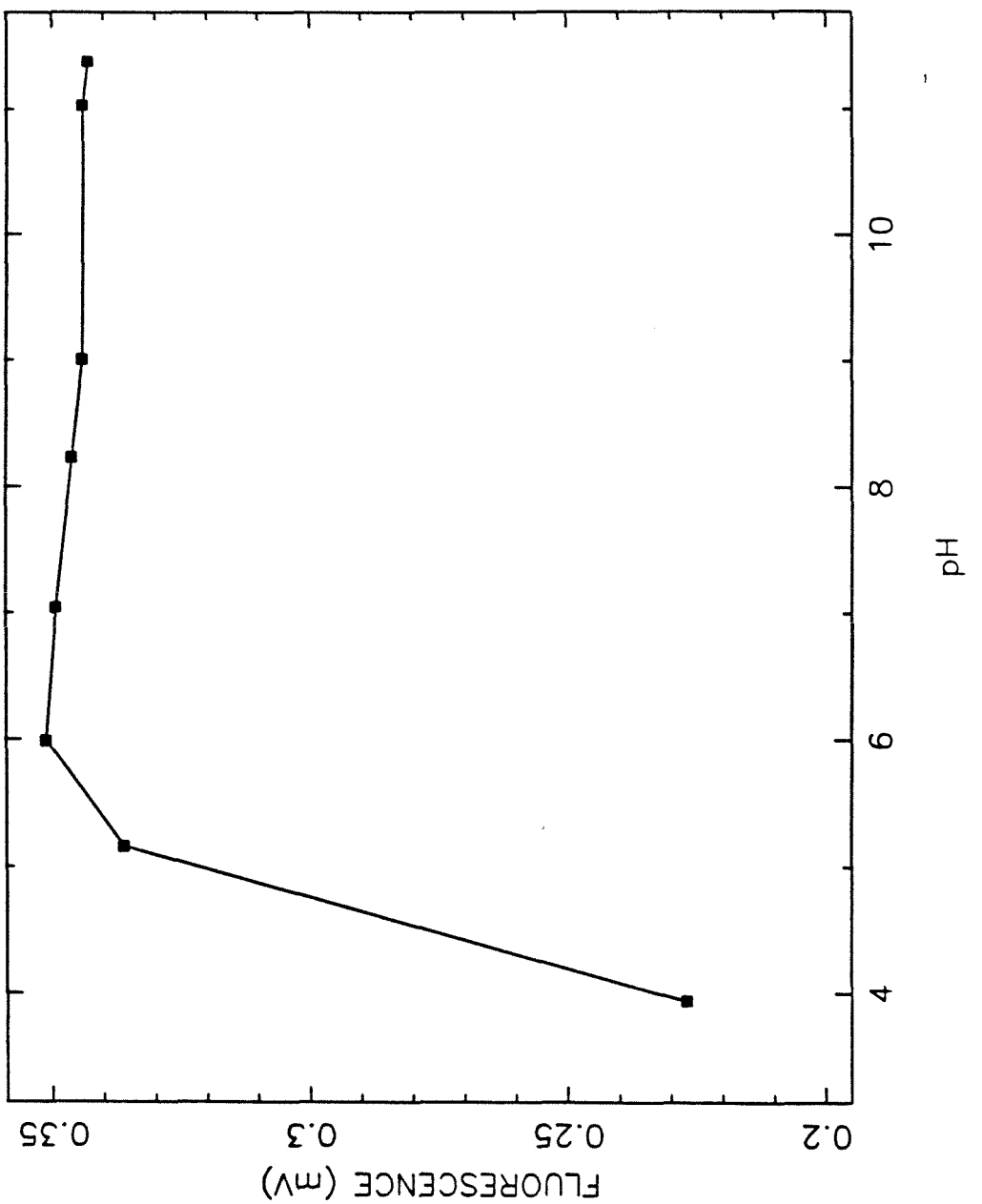

Figure 22. The pH dependence of the fluorescence of an anaerobic NADH solution, measured with an Ingold Fluorosensor.

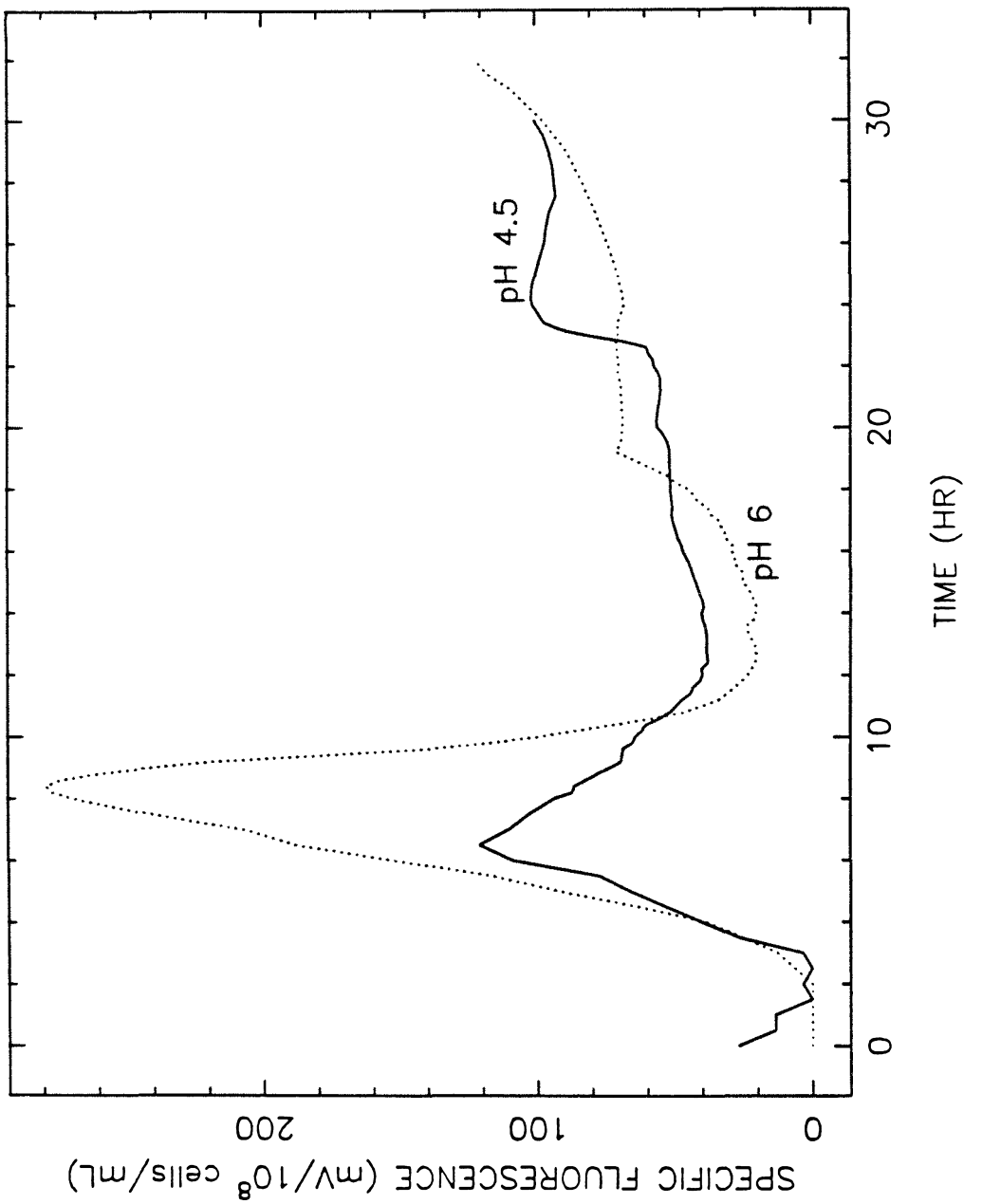

Figure 23. Specific fluorescence trajectories for the pH 4.5 and pH 6 fermentations.

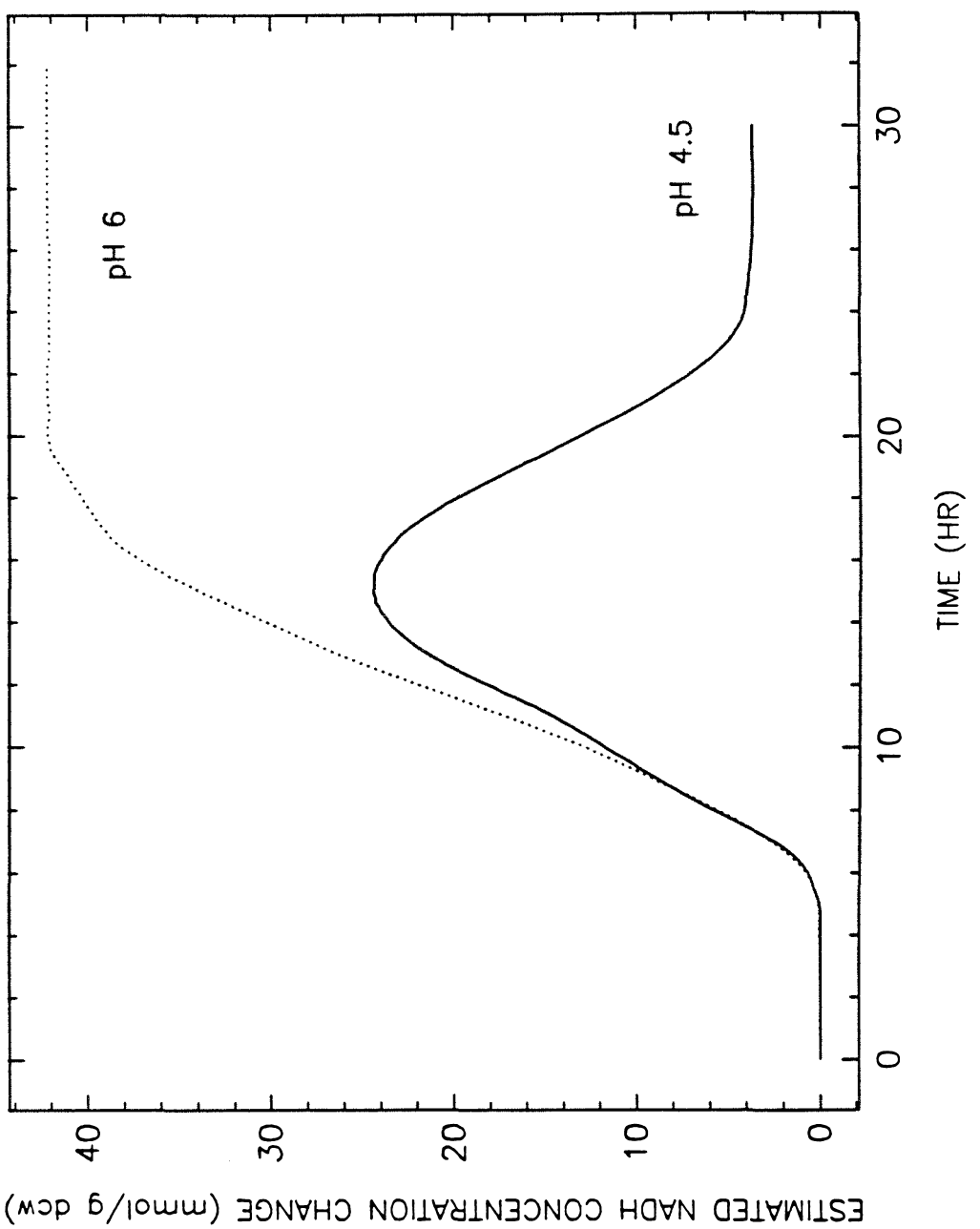

Figure 24. Estimated specific NAD(P)H concentration from Equation (19).

CHAPTER 5

CONTINUOUS BIOCONVERSIONS OF GLUCOSE BY NON-GROWING IMMOBILIZED *CLOSTRIDIUM ACETOBUTYLICUM*

INTRODUCTION

Immobilized cell fermentations may utilize microorganisms that are non-viable, viable but non-growing, or viable and growing. While the use of non-viable cells in immobilized biocatalysts may be the best choice (based on productivity and usable lifetime) for some processes, conversions requiring more than a few enzymes and/or cofactor regeneration dictate the use of viable cells. Growing, viable immobilized cells are able to carry out any chemical conversion characteristic of the organism, but immobilized growing cell systems often experience problems such as a high suspended cell concentration in the reactor effluent and, if entrapment techniques are utilized, physical damage to the immobilization matrix. At least in theory, viable non-growing cells offer multistep, cofactor regenerating bioconversions without the complications of cell growth (and suspended cell production). Also, the use of non-growing immobilized cells should allow a higher fraction of substrate carbon to appear as product, rather than as biomass.

In practice, systems in which immobilized, viable, non-growing cells are used often display relatively rapid declines in the desired catalytic activity [*e.g.*, 1,2,3,4,5]. Some reports on continuous immobilized fermentations involving significant cell growth have also indicated activity losses [2,6,7]; this behavior probably has different causes than that found in non-growth systems. The underlying causes for loss of productivity in non-growth immobilized cell systems undoubtedly depend on the method used to obtain such a condition—nutrient limitation or starvation, or exposure to an inhibitory agent and on the metabolic origin of the product, with differences expected between secondary metabolites or products typically associated with growth. The most common technique for growth limitation is nutrient

starvation—usually the omission of a nitrogen source [2,8,9,10], vitamins or minerals [4,11], or both nitrogen source and vitamins [2,3,5]. The use of hydroxyurea for the restriction of immobilized cell growth has also been reported [12]. Possible causes for biocatalyst activity losses include the inactivation or protease-dependent degradation of enzymes, loss of cofactor regenerative capacity, degradation or diffusive release of cofactors, or loss of membrane integrity or function (*i.e.*, the maintainance of various transmembrane gradients), among others.

In this study, the loss of catabolic activity of calcium alginate-immobilized *Clostridium acetobutylicum* was investigated in a continuous-feed, packed-bed bioreactor. With one exception, the feed to the system contained no source of nitrogen nor the necessary [13] growth factors *p*-aminobenzoic acid and D-biotin. In one experiment, only the vitamins were omitted. Factors affecting the decrease in biocatalytic activity were investigated by varying pH, by the addition of metabolites (acetate, butyrate, and acetoacetate) to the feed, and by the use of both spore-forming and asporogenous strains. Product formation rates, immobilized cell concentrations and morphological types, and intracellular NAD(P)H-dependent fluorescence trajectories were used to provide insights to the deactivation phenomena. In addition, a framework for metabolic pathway rate analysis [14] (Chapter 4) has been applied to examine the changing rates in each branch of the catabolic pathway network. A preliminary report on one of these experiments has been published [15,16].

MATERIALS AND METHODS

The culture media, immobilization procedure, experimental apparatus for the

growth and bioconversion phases, fluorescence measurement technique, and assay methods have been described in Chapter 3.

The medium used in the growth part of the experiments was a modified version of FGM (Chapter 3), containing an additional 0.55 g/L $CaCl_2$ (anhyd.) to maintain bead strength; in the runs in which immobilized cell fluorescence was measured, only 5 g/L yeast extract and 5 g/L peptone were used in order to reduce the background fluorescence. The growth medium was always autoclaved in four parts (glucose; yeast extract, peptone, and salts; $FeCl_3$; and $CaCl_2$), then cooled, combined, and added to the fermentor jar.

The bioconversion medium was based on the following nitrogen-free, vitamin-free solution: glucose, 10 g/L; $Na_2HPO_4 \cdot 7H_2O$, 0.9 g/L; KH_2PO_4, 0.4 g/L; $MgSO_4 \cdot 7H_2O$, 0.2 g/L; $FeCl_3 \cdot 6H_2O$, 0.01 g/L; $CaCl_2$, 0.55 g/L; and 0.5 mL/L of the trace elements solution (Chapter 3). The feed to experiments CI23, CI28, and CI30 contained 15 g/L glucose. In some experiments, additions were made to this medium (see Table 2). Two- to eight-liter volumes of the bioconversion feed were filter-sterilized (Gelman Mini Capsule Filter, 0.2 μm) after being acidified with 6N HCl to pH 3.5–4. Acidification prevented the formation of hydroxide precipitates and allowed the feed to assist in system pH control.

The feed to experiment CI22 contained acetoacetate, which spontaneously decomposes to acetone. The feed bottle was kept in an ice bath for the entire experiment, since the decomposition rate is a direct function of temperature.

EXPERIMENTAL PROCEDURE

These immobilized cell experiments consisted of two parts: a batch growth phase, in which the immobilized spore inoculum was allowed to germinate and grow, and a continuous-flow bioconversion phase, in which the cells were fed a growth-restricting medium, typically nitrogen- and vitamin-free.

After the alginate beads containing the spore inoculum had cured in the $CaCl_2$ solution for 8–12 hours (2 hours for run CI30), the liquid was drained away, and the beads rinsed with three 500 mL aliquots of deionized water. The immobilized spores were heat-shocked by the addition of 400 mL of 90–95°C water for 60 seconds, and then cooled quickly on ice. The alginate beads were then added asceptically to a Pyrex or quartz column.

To begin the growth phase, the bead-filled column was attached to the fermentor system as diagrammed in Figure 4 (Chapter 3), and the recirculating flow was begun. After solvent production had started, but before the glucose had been consumed, the column was detached from the growth fermentor and connected to a rinsing apparatus (a 1 L flask with a special stopper configuration). Three to four 500 mL deionized water washes and zero to two 500 mL bioconversion medium (minus glucose) washes were employed to remove nearly all extracellular growth phase nutrients and products. Each rinse solution was circulated for 3–4 minutes. This procedure was performed in an anaerobic hood for experiment CI30, but no special anaerobic techniques were used for rinsing the beads containing ATCC 824.

The column containing the rinsed alginate beads was connected to the continuous system (Figure 4, Chapter 3); as in the growth segments of the experiments, the vessel-column-vessel recirculation rate was 145 mL/min. The system was oper-

ated until the metabolic activity of the biocatalyst seemed to be very low (usually 80–100 hours after the start of continuous flow).

At various times during the experiments, a few drops of liquid sample were placed on FGM-agar petri plates and incubated aerobically at 30°C to check for facultative anaerobic contamination (*e.g.*, *Lactobacillus*).

Table 2 summarizes the experimental aspects of the runs discussed in this chapter.

RESULTS

The results of the growth/bioconversion experiments summarized in Table 2 are shown in Figures 25–60.

A. Immobilized Cell Growth

Figure 25 presents the time course of product formation, glucose consumption, and NAD(P)H-dependent culture fluorescence from the batch growth phase of experiment CI23 (pH 4.5, ATCC 39236). In Figure 26, the increase in the immobilized cell concentration during run CI30 (pH 4.5, ATCC 39236) is shown; these values were determined by the microscope-counting chamber method (Chapter 2). In each experiment, approximately 3,000 beads were present in the bioreactor system, and so the bioconversion phase usually began with about 1.4–1.8 $\times$ 10^{11} cells in the column, or an overall cell density of 3 to 4 $\times$ 10^{11} cells/L (based on the liquid volume in the system).

As can be seen, the cell growth and product formation qualitatively resemble

that observed in pH 4.5 suspended cell batch fermentations (Chapter 4). The fluorescence trajectory is also similar to the total fluorescence time course of a batch fermentation (Chapter 4, Figure 19), in that the most dominant feature is an overall fluorescence increase due to a large increase in cell number. The dip marked by the arrow indicates the response to a pulse addition of glucose solution. The patterns observed in Figures 25 and 26 are typical of the growth phases of all of the immobilized cell experiments.

B. Control Experiment (CI14)

This pH 4.5 run was performed to assess the effects of nutrients and metabolic products from the growth phase on the experimental results of the bioconversion segment of the immobilized cell experiments. The batch growth phase and rinsing procedure were the same in this experiment as in the other runs, but the feed during the bioconversion phase contained no glucose (or nitrogen). As can be seen in Figure 27, only very low amounts of the six products were released. However, a fairly significant amount of cells or cell material was released into the medium; in subsequent experiments, the bead-rinsing process was lengthened to lessen this effect.

When these concentration trajectories were compared with washout curves generated by the CSTR mass balance equation for an empty feed system

$$C = C_0 e^{-tD} \ , \tag{20}$$

where C_0 is the peak concentration of each component in Figure 27, an interesting pattern emerges. While the concentrations of acetic and butyric acid decreased more rapidly than predicted by feedstream dilution, acetone, butanol, and ethanol

remained in the system somewhat longer than predicted. Apparently, the acids were consumed for the production of the solvent compounds. The initial burst of 590 nm-absorbing cell material was washed out of the reactor as predicted by Equation (20).

C. Bioconversion At pH 4.5, pH 5, and pH 6

1. Product Concentration Profiles

In each of the experiments discussed in this section, the feed to the system lacked both nitrogen and vitamin sources, and the immobilized cells were of the type strain ATCC 824. The product concentration trajectories for the pH 4.5 (Figures 28, 29, and 30), pH 5.0 (Figure 31), and pH 6.0 (Figure 32) bioconversion experiments have a number of features in common. At all three pH values, the formation of solvents preceded that of the acid products, undoubtedly because the metabolism of the immobilized cells was in the solvent-producing mode at the time of the switch to nitrogen-free medium. The butanol concentration peaked soon after the medium switch in the pH 4.5 and pH 5 experiments, although a slight increase in the rate of solvent production can be noted about 10 hours after the initial concentration maximum. This secondary peak corresponded with the time of maximal acids concentration, and the two events were probably related. In each of the pH 4.5 experiments, the ethanol profile is more broad than that of butanol, and has two peaks which seem to coincide with the maxima in acids and butanol concentrations. Also, more acetoin was produced than ethanol (except in run CI23, which was also characterized by significantly lower total solvents production). In the pH 5 run, acetoin and ethanol were produced in similar amounts, and have sim-

ilar trajectories, although the acetoin concentration peaked a few hours later than the ethanol concentration. The glucose profiles of the pH 4.5 and 5.0 experiments all show minima near the time of maximum acids concentration, and, in the pH 4.5 experiments, shoulders related to the formation of the solvent products can be observed. The release of cells from the alginate beads into the medium, monitored as 590 nm absorbance, followed the same pattern in each experiment at the lower pHs: a single maximum near the time of the acid concentration maximum.

A comparison of the concentration profiles of the pH 6 bioconversion phase (Figure 32) with those at pH 4.5 and 5 shows some significant differences. Although acetone concentrations were lower at pH 6, higher concentrations of butanol were actually produced at pH 6 than at pH 4.5 (contrary to the situation in batch suspended cell cultures; see Chapter 4). In addition, butanol productivity did not decline rapidly, as was the case at lower pH values. Acetoin production was also much higher at this pH than at either pH 4.5 or 5, and more acetoin was formed than ethanol (although ethanol was produced at a constant rate throughout the experiment). The prolonged formation of the acids, butanol, and acetoin is reflected in a glucose concentration profile that is more broad than those found for the lower pH experiments. The release of suspended cells was also different at pH 6, as only a very low amount appeared during this run.

Lactic acid (L- or D- form) is typically not a significant product in *C. acetobutylicum* fermentations; *e.g.*, the highest concentration measured in run CI23 was 0.2 mM. For this reason, lactic acid concentrations were not measured in most of the experiments. The concentration profile for total lactic acid is presented in Figure 30. Other than an initial period of production, lactate concentrations were

essentially zero.

Overall activity loss was observed at all pH values, although decreases in individual product-forming activity and the rate of overall biocatalytic activity (represented by glucose consumption) differ as the pH values are varied.

2. Immobilized Cell Concentration Analysis

The two methods used for estimating the concentration of immobilized cells were presented in Chapter 2. Figures 33 and 34 present the results of the optical density method as applied to alginate bead samples from experiments CI18 (pH 4.5) and CI19 (pH 6), respectively. Each data point represents the 590 nm absorbance of two beads dissolved in 1 mL of tripolyphosphate solution. While the optical density declined similarly in both cases, the pH 4.5 bead samples became increasingly absorbant as the run progressed, in sharp contrast with the pH 6 samples.

The more accurate microscope-counting chamber method was applied to the immobilized cell bead samples of experiment CI28 (pH 4.5); cell-type concentration profiles for this run are presented in Figures 35–38. The different morphologies counted and the comparison with the A_{590} data will be discussed later.

3. NAD(P)H-Dependent Culture Fluorescence

The time course of immobilized cell culture fluorescence resulting from intracellular NAD(P)H was measured in experiments CI23 and CI28 (Figures 39 and 40); in both cases bioconversion was carried out at pH 4.5.

The two trajectories show some similarities: in both cases a brief, small decrease is followed by an increase to the first of two peaks. While the second peaks

occur at about the same time, the time of the initial peak and the amount of fluorescence decrease (on a relative basis) between the two peaks is different for the two experiments. In addition, the fluorescence in experiment CI28 increased towards the end of the experiment, while that of run CI23 remained almost constant.

Since the measured fluorescence is a function of the intracellular NAD(P)H concentration, and since this concentration is primarily changed in conjunction with metabolic changes, then the features in, and differences between, these two fluorescence profiles should be explainable in terms of the changing metabolic activities during the course of the runs. An obvious difference between these two experiments is the amount of solvents produced (Figures 29 and 30); this will be discussed further.

4. Other Measurements

Figures 41 and 42 show the concentration profiles of riboflavin and the amount of 260 nm-absorbing cell material in the effluent of experiment CI28 (pH 4.5). Riboflavin concentration peaked very early in the bioconversion phase, with another very small peak at about the 30 hour mark. The initial peak may be partially due to flavin compounds in the small amounts of yeast extract and peptone that may remain in the beads after rinsing. In contrast, the trajectory of effluent A_{260} shows a small initial peak and a much larger peak at about 25 hours. Riboflavin excretion by *C. acetobutylicum* is related to iron limitation, while 260 nm absorbance is a measure of nucleic acid release; both of these will be discussed shortly.

D. Bioconversion With An Asporogenous Mutant, pH 4.5

1. Product Concentration Profiles

Experiment CI30 utilized the asporogenic *C. acetobutylicum* strain ATCC 39236; the bioconversion phase was operated at pH 4.5. Concentration-time profiles for the products and glucose, as well as the trajectory for suspended cell release are shown in Figure 43. As in the experiments with the sporogenic strain ATCC 824, the solvent products acetone, butanol, and ethanol were formed during the first hours after the switch to nitrogen-free medium, but Figure 43 shows that acetic acid was also produced early. Although solvent-forming metabolic activity soon decreased in favor of the production of acetic and butyric acids, the maximum concentrations of the solvents were much higher than in an equivalent ATCC 824 pH 4.5 experiment (*e.g.*, Figure 30). This increase was not due to an increase in the amount of immobilized biomass alone, since the peak concentrations of both acetic and butyric acids were lower than in the ATCC 824 runs. As in other runs, the solvent profiles have shoulders (local maxima) near the time of the acid concentration peaks. In experiment CI30, the formation of acetoin occurred relatively soon after the medium switch; the peak concentration was higher than that of ethanol. Both of these maxima occurred at the same time as the maximum in the butanol concentration. Very little lactic acid was produced during this experiment.

The glucose concentration trajectory has a primary minimum corresponding to the peak butanol concentration, and two secondary minima, which seem to be related to peaks in the acid product profiles.

The release of suspended cells into the fermentor medium occurred at a lower rate than in the comparable ATCC 824 runs.

2. Immobilized Cell Concentration Analysis

The concentrations of each immobilized cell type as functions of time are plotted in Figures 44–46. These data were obtained with the microscope counting chamber. Clearly, this strain is not non-sporogenic: significant spore concentrations were observed late in the experiments. As in the ATCC 824 experiments, vegetative cell concentration decreased rapidly at the start of the bioconversion phase.

3. NAD(P)H-Dependent Culture Fluorescence

The fluorescence trajectory of the bioconversion phase of run CI30 is shown in Figure 47. After the initial, small fluorescence intensity decrease observed in the other fluorescence-monitored experiments, this profile increases rapidly to a single maximum before decreasing until the end of the experiment. This maximum occurs at about the same point after the medium switch as the second peaks in the ATCC 824 fluorescence profiles.

4. Other Measurements

Although the shape of the riboflavin concentration profile from this experiment (Figure 48) is similar to that of experiment CI28 (ATCC 824), the peak concentration is five times lower.

The amount of 260 nm-absorbing cell material (Figure 49) increases steadily from the start of the experiment until it peaks at about 20–25 hours after the medium switch. This profile lacks the early peak observed in run CI28, but the maximum A_{260} values are nearly the same in both cases.

E. Bioconversion With Metabolite-Containing Feed

1. Product Concentration Profiles

Three different experiments were performed in which a metabolite was added to the feed medium: CI17 (2 g/L butyric acid), CI21 (1 g/L acetic acid), and CI22 (10 mM lithium acetoacetate). All three runs utilized strain ATCC 824 and were operated at pH 4.5. The concentration *vs.* time profiles of the acid and solvent products, glucose, and 590 nm absorbance (suspended cell release) are presented in Figures 50, 51, and 52 for runs CI17, CI21, and CI22, respectively. In all cases, the concentration of component added to the feed has not been subtracted from the concentrations in these figures. Also, it is important to note that the acetone concentration profile for run CI22 (Figure 52) includes a contribution from the acetoacetate in the medium. Acetoacetate spontaneously decomposed to acetone in the injection region of the gas chromatograph (200°C). Although several other methods were tried, acetoacetate concentration (or true acetone concentration) could not be measured.

At the start of experiment CI17 (Figure 50), butyric acid in the feed was consumed to form butanol, resulting in a peak butanol concentration much higher than that observed in pH 4.5 runs without feed supplements (*e.g.*, CI28). Acetone concentrations were also much higher in this experiment. However, the duration of butanol production (and butyric acid consumption) was not longer than in comparable unsupplemented feed experiments, and, as usual, solvents production was replaced by acid product formation later in the experiment.

Suspended cell release, acetoin, and ethanol production, and glucose consumption followed patterns similar to those discussed earlier (*e.g.*, Figure 28).

The substrate, product and suspended cell concentrations during experiment CI21 are plotted in Figure 51. As was the case when butyric acid was included in the feed, acetic acid was clearly consumed from the feed medium, resulting in relatively high initial concentrations of acetone. In fact, early in the bioconversion phase the molar concentration of acetone was higher than that of butanol. Net acetic acid consumption did not last long, however, and both acetic and butyric acids were produced at significant rates until their concentrations peaked at about the 20 hour mark. It is interesting to note that, while butyric acid production in the butyrate-feed medium run occurred at a very low rate (Figure 50), acetic acid production with acetate feed took place at the high rates observed in other experiments and resulted in a peak acetate concentration about 6 mM higher than the feed level. More striking than this, however, is the observation that higher concentrations of acetone and butanol were formed after the maximal acids concentrations than at any other time during the bioconversion phase. Presumably, this is related to the elevated concentrations of acetic and butyric acids.

This delayed production of solvent products holds true for ethanol as well, and the acetoin concentration profile shows two peaks, one corresponding to the initial acetone concentration peak and the other to the late solvent peaks. The glucose and suspended cell trajectories are similar to those observed in previously discussed experiments.

In experiment CI22 (Figure 52), lithium acetoacetate was added to the nitrogen-free, vitamin-free medium at a concentration of about 10 mM. Although the feed bottle was kept in an ice bath during the bioconversion phase, some acetoacetate decomposition took place, and the concentration in the feed at the end

of the experiment was about 5% less than at the start of continuous feeding. Acetoacetate is the immediate precursor to acetone (only acetoacetate decarboxylase is required for the conversion), and so an increase in the acetone concentration would be expected. Unfortunately, the acetone concetration trajectory in Figure 52 represents the true concentration of acetone **plus** the concentration of acetoacetate, and this makes the interpretation of the data more difficult. It can be seen in Figure 52 that the sum of [acetone plus acetoacetate] decreased initially. Since acetone is never consumed by the cells, this decrease must be due to acetoacetate consumption. In addition, this consumption cannot be for the production of acetone only, or the measured acetone level would not change. A comparison with unsupplemented feed experiments also performed at pH 4.5 (*e.g.*, CI28 and Figure 30) shows that acetic acid formation was enhanced with acetoacetate feeding and was present in the medium in higher concentrations than butyric acid. Also, more acetoin was formed with acetoacetate in the feed medium. Shortly after the acid concentrations peak, the concentrations of butanol and ethanol rose to their second maxima, and the concentration of [acetone plus acetoacetate] increased to a maximum value higher than the feed concentration. Since acetoacetate is not excreted into the medium, this increase must have been due to acetone formation.

The concentration profiles of glucose and suspended cells are similar to those of other pH 4.5 bioconversion experiments.

2. Immobilized Cell Concentration Analysis

Figures 53 and 54 present the results of the dissolved-bead optical density method for immobilized cell concentration estimation for experiments CI21 (acetic

acid addition) and CI22 (acetoacetate addition). The time course of these two trajectories is very similar to that of run CI18 (plain feed, pH 4.5). In addition, the microscope-counting chamber technique was also applied to the bead samples of run CI22 for more detailed and accurate results. The concentrations of immobilized vegetative cells and spores are plotted as a function of bioconversion time in Figure 55. These profiles are comparable to the immobilized cell count results from run CI28 (Figures 35 and 38).

F. Bioconversion With Nitrogen-Containing, Vitamin-Free Feed

All of the bioconversion experiments discussed so far utilized a feed medium that contained neither a nitrogen source nor any vitamins (*e.g.*, biotin). In experiment CI12, 0.8 g/L of NH_4Cl was added to the standard feed to assess the effects of a nitrogen source; it is important that neither of the required vitamins was added, since they are necessary for cell growth.

The concentration profiles for glucose and the metabolic products are presented in Figure 56. The acid product concentration trajectories are similar to those in plain-feed pH 4.5 bioconversion experiments in their rise to a single major peak, the value of the peak, and the formation of more butyric than acetic acid. However, striking differences can be noted between the solvent product profiles this run and those of any plain-feed experiment. Instead of an initial production of butanol and acetone, which then decreased rapidly, bioconversion on nitrogen-containing feed resulted in relatively later, sustained solventogenesis, producing very high butanol concentrations. While rather large amounts of ethanol were also produced fairly late in the experiment, acetone and acetoin concentrations were not higher than in

the pH 4.5 plain-feed runs.

The glucose concentration-time profile has two minima, each corresponding to a peak in the butanol trajectory. Two peaks are observed in the A_{590} results, one occurring at nearly the same time as the maxima of acetic and butryic acid concentrations, and the other near the time of maximum butanol concentration.

Although riboflavin concentration was not assayed in this experiment, the appearance of a yellow color (riboflavin) in the fermentor vessel was noted from about 20 hours to 105 hours, when the color intensity lessened. This color (riboflavin) appearance seems to have occurred during the same interval that butanol was produced.

G. Scanning Electron Micrographs

Figures 57 through 60 are photographs obtained with an ETEC Autoscan scanning electron microscope. The bead samples were obtained at the start and midpoint of experiment CI22 (pH 4.5, ATCC 824, acetoacetate-supplemented feed) (Figures 57B through 60A) and the start and end of run CI21 (pH 4.5, ATCC 824, acetate-supplemented feed) (Figures 57A and 60B).

Figure 57A shows a cross section of an alginate bead near the start of the bioconversion phase. The distribution of microcolonies, each formed from an immobilized spore, is seen to be homogeneous, with no concentration of colonies near the bead surface. The large pocket in the photograph background is probably due to gas generation by rapidly growing cells.

Figures 57B and 58A are magnified views of an individual colony at the start of bioconversion in run CI22. The individual cells are virtually all rod-shaped

vegetative forms (Figure 58B). Many appear to be in the form of chains (septa between individual cells can be observed in Figure 58B), which might be expected in an environment in which the cells do not move and are not exposed to shear forces.

Figures 59A, 59B, and 60A were taken after 54 hours of bioconversion. The appearance of the microcolonies is quite different in these photographs than in Figures 57B–58B. The presence of cell debris indicates that significant cell lysis has occurred. Very few vegetative (rod) cell forms are apparent, but a number of clostridial (pre-spore) forms are present (Chapter 2), and some mature spores can also be observed.

The photograph in Figure 60B shows a group of mature spores in a bead sample from the end of run CI21, 79 hours after the switch to vitamin-free, nitrogen-free bioconversion medium.

ANALYSIS AND DISCUSSION

Immobilized cell biocatalyst systems can be classed, based on whether the immobilized cells are non-viable (*i.e.*, not capable of growth), viable but non-growing, or growing. Each type has its advantages for certain desired bioconversions. Since the use of immobilized *Clostridium acetobutylicum* for glucose conversion to solvent products involves many enzymes and significant requirements for cofactor regeneration, nonviable cells are not an option. In general, the use of non-growing immobilized cell offers several potential advantages over immobilized systems operated under growth conditions, including the potential for the conversion of a higher frac-

tion of substrate carbon to products (and less to biomass) than in other systems. However, the results obtained here and elsewhere [3,9] indicate that establishing non-growth conditions by nutrient starvation may decrease the productivity lifetime and product specificity of the immobilized cell biocatalyst. The best way to extend this operational stability and to control the specific product(s) formed is to understand the underlying causes and mechanisms for decreases in the desired activity by studying the metabolic and physiological responses of the immobilized cells to bioconversion under various environmental conditions. The experiments discussed in this chapter are an attempt to perform this type of an investigation.

A well-known aspect of entrapped immobilized cell systems is the possibility of diffusion-limited mass transfer of substrate and products through the support matrix [17,18]. While this phenomenon is not necessarily a negative feature (overloading with cells or enzymes can provide longer apparent operational lifetimes), diffusion effects mask the intrinsic kinetic behavior of the cells. In studies focusing on kinetic aspects, the most common approach to reduce mass-transfer considerations is to use very small particles. However, the use of very small beads in packed bed columns often results in liquid flow problems. In these immobilized cell bioconversion experiments, medium-sized alginate beads were used, but the cell loading was kept relatively low, so that the "reaction" rate (represented by glucose consumption) would be slower than the diffusion of glucose in the alginate gel.

The extent of mass-transfer limitation and its effect on reaction rate(s) is usually estimated by the calculation of the Thiele modulus ϕ. However, the evaluation of this quantity requires knowledge of the kinetic rate equation. Such a representation of the *C. acetobutylicum* metabolic reactions has not been formulated, and thus

the Weisz observable modulus Φ [19] has been used in this work. This modulus,

$$\Phi = \eta\phi^2 = \left(\frac{dC}{dt}\right)\frac{R^2}{C_e D_m}\ , \tag{21}$$

contains only the observed reaction rate and does not require kinetic rate constants for evaluation. In Equation (21), η is the effectiveness factor, $\left(\frac{dC}{dt}\right)$ is the actual, observable reaction rate per unit volume of catalyst particles, R is the (equivalent) particle radius, C_e is the external (bulk phase) reactant concentration, and D_m is the substrate diffusivity in the immobilized matrix [19].

Values of D_m for glucose in various calcium alginate gels have been evaluated in several studies [*e.g.*, 20,21] and have generally been found to be near the value in water. An effective diffusivity of 5.5×10^{-6} $cm^2 \cdot sec^{-1}$ was obtained from the report of Hannoun and Stephanopoulos [21] for the 3% alginate used in this work. The beads ranged from 2 to 2.5 mm in diameter. Values of Φ during the bioconversion phase of an experiment could be calculated by using the volumetric glucose consumption rate (corrected for total bead volume) and the fermentor glucose concentration. Figure 61 presents these values of Φ during run CI28. Except for time very early in the bioconversion phase, Φ is $\leq$ 0.6. Comparison with a plot of the effectiveness factor, η, *versus* Φ (based on known particle geometry and kinetic form), shows that η in experiment CI28 is $\geq$ 0.9 (at $\Phi \leq 0.3$, $\eta \approx 1$). Thus, the system is nearly free of glucose diffusion limitations. Evaluation of product diffusion requires the diffusivities of those compounds in alginate gels. While they have not been measured in alginate, Leung found that the diffusivites in κ-carrageenan gel of ethanol, butanol, and acetic acid were essentially the same as in water: 1.7×10^{-5}, 1.2×10^{-5}, and 1.6×10^{-5} $cm^2 \cdot sec^{-1}$, respectively [22]. These values are lower than the glucose diffusivity, but since their molar rates of production are less than

that of glucose, and since the product concentration levels are low (butanol toxicity begins at ~100 mM), product diffusion effects on the observed kinetic results are negligible.

A similar observable modulus can be defined for external diffusion:

$$\Omega = \eta Da = \left(\frac{dC}{dt}\right)\frac{R}{k_L C_e} , \tag{22}$$

where Da is a Damkholer number and k_L is the mass transfer coefficient in the liquid phase [18]. Values of Ω near 1 indicate external diffusion control, while kinetic effects dominate for $\Omega \ll 1$. For Reynolds numbers in the range

$$10 \leq Re \leq 10^4$$

(Re = 110 in these experiments), the Sherwood number ($\frac{k_L d_p}{D_L}$) in packed beds has been correlated as:

$$Sh = 0.95 Re^{\frac{1}{2}} Sc^{\frac{1}{3}} , \tag{23}$$

where Sc is the Schmidt number ($\frac{\mu_L}{\rho_L D_L}$), d_p is the bead diameter, μ_L is the liquid viscosity, ρ_L is the liquid density, and D_L is the diffusivity of the solute in the bulk phase [23]. This correlation provides a value for k_L of 2.8×10^{-3} cm·sec^{-1} under the conditions found in these experiments. Since both Φ and Ω are of the form [constant]·[rate]·[concentration]$^{-1}$, the two quantities have the same profile during an experiment. From Figure 61, it is clear that $\Omega \ll 1$ always, and thus external diffusion resistance is not significant in these experiments.

These conclusions regarding the extent of diffusion limitation have been derived for the bioconversion phases of the experiments discussed in this chapter. Evidence that internal diffusion was not limiting in the growth phase of the experiments is provided by the photograph of Figure 57A. This cross-sectional view of an alginate

bead shows that germination and outgrowth of the immobilized spores occurred uniformly throughout the bead.

The control experiment, run CI14, was performed to determine the amounts of metabolic products and complex nutrients from the growth phase which remain in the beads after the rinsing procedure. It is clear from Figure 27 that the amounts of products released into the medium are negligible.

One further comment should be made regarding the immobilized cell system used in these experiments before discussing more specific aspects of the results: the contribution of suspended cells to glucose consumption and product formation is negligible (if not zero), for two reasons. First, while the typical immobilized cell preparation contained 3–4 $\times$ 10^8 cells per milliliter of reactor liquid volume, an estimate of the maximum suspended cell concentration from the A_{590} data gives a value of 2 $\times$ 10^7 cells/mL. This latter value is probably an overestimate, since the 590 nm optical density at the time of the maximum appears to be due in part to cell lysis products and highly refractile cell types such as the pre-spore forms. Secondly, the released cells do not grow at all in this minimal, nitrogen-free medium (confirmed by experiment).

A. Bioconversion With Sporogenous *vs.* Asporogenous Strains

Since the sporulation of immobilized *C. acetobutylicum* occurs during extended bioconversion with nitrogen-and vitamin-free feed, it is important to compare the two experiments involving different strains, one spore-forming (ATCC 824, run CI28) and one that is asporogenic (ATCC 39236, run CI30). As the two runs were otherwise identical, such a comparison should illustrate the effects of the sporulation

process upon the product-forming activity of the immobilized cells.

Sporulation and its relationships with solventogenesis and environmental conditions were discussed briefly in Chapter 2. A generalized representation of the morphological stages during clostridial sporulation is shown in Figure 1A (Chapter 2). When environmental (or other) conditions trigger the start of sporulation, the relatively thin, short vegetative rods begin to accumulate the storage polysaccharide granulose, becoming swollen, phase-bright clostridial forms. Some time after the start of granulose accumulation, forespore septum formation occurs; the forespore is visible as a dark tip at one end of the phase-bright clostridial form. The dark forespore becomes phase-bright during spore maturation, resulting in the club-shaped cell forms shown in Figure 1A. Eventually, the mature, phase-bright spore is released from its sporangium. Details on these events can be found in the literature [24,25,26,27,28,29].

Figures 35–38 and 44–46 show the numbers of four different morphological types found in the alginate beads during the course of the bioconversion phase for runs CI28 and CI30, respectively. The cell types counted were: vegetative rods (phase dark), clostridial forms (larger, phase bright, swollen cigar shapes), forespore-containing cells (club-shaped, phase-bright forespore at one end), and mature spores (smaller, phase-bright ovoids). The changes in the immobilized cell population can also be observed in the scanning electron micrographs (Figures 57–60).

In experiment CI28, a rapid initial decline in the number of vegetative rods occurs, apparently due to cell lysis. After about 25 hours of bioconversion, a significant increase in the number of clostridial forms was observed (Figure 36), reaching

a peak at about 40 hours. The transition from the clostridial stage to the club-shaped forespore stage is apparent in Figure 37, which shows that the formation of semimature endospores follows clostridial stage formation by about 10 hours. Finally, a near step change in the number of mature spores occurred (Figure 38). Although the data points in Figure 35 indicate that the number of vegetative rod shapes that were counted increased during the 30–60 hour interval of the experiment, this was not due to an increase in vegetative cell number, but rather to the presence of sporangia that accumulated after the release of mature spores.

The initial immobilized vegetative cell lysis observed in the bead samples of experiment CI28 was also observed in run CI30 (Figure 44). While the initial cell loading was higher, the same rapid decline in cell number occurred. Figures 45 (clostridial forms) and 46 (mature spores) show that sporulation events in strain ATCC 39236 happened just as in strain ATCC 824 (*i.e.*, the formation of clostridial forms, which were then transformed to mature spores), although at a much lower frequency. Virtually no club-shaped pre-spore forms were observed. This mutant strain (ATCC 39236) is thus not asporogenous, but rather oligosporogenous [25,30]. In cultures of oligosporogenic strains, only a few cells (one in 10^5–10^6) are capable of producing mature spores; when these spores are recultured, the resultant population contains the same low fraction of spore-forming cells [30].

The level of 260 nm-absorbing cell material released into the culture medium has been used to study RNA degradation in starving cells [31,32] and as an indicator of cell lysis [33]. In these two experiments, the early increase to high 260 nm absorbance is evidence of the initial period of cell lysis; the cause of this lysis is not clear.

The excretion of fluorescent flavin compounds into the fermentation medium is a result of inadvertent iron limitation due to precipitation of iron(III) phosphate compounds before medium filtration for sterilization. This caused the feed iron(III) concentration to be lowered to *ca.* 1.6 μM. The oversynthesis of riboflavin by *C. acetobutylicum* in response to iron limitation has been utilized for commercial riboflavin production [34,35]. When *C. acetobutylicum* is exposed to media with iron contents lower than 1 μM, the iron-heme redox protein ferredoxin is degraded (to provide iron for other iron-containing proteins) [36], and replaced by a different redox protein, flavodoxin, which contains 1 mol of flavin mononucleotide (FMN) per mol of protein [37,38]. Flavodoxin is capable of participating in the same electron-transfer reactions as ferredoxin, and the catabolic activity of the cell seems not to be affected by the substitution [37]. The flavin fluorescence observed during the bioconversion phases of runs CI28 and CI30 fell rapidly from initial levels and was negligible for most of the experiments; this early peak may be due in part to the release of growth-phase flavin compounds from the gel matrix in addition to flavodoxin synthesis.

The aforementioned observations on sporulation frequency and lysis in each experiment can be combined with the concentration data (Figures 30 and 43) to provide more information on the variations in product-forming activity during bioconversion. As a first step, the concentration data are smoothed with a cubic spline; the slopes of these curves were used in the general CSTR mass-balance equation

$$\frac{dC_i}{dt} = D\,(C_{i,in} - C_i) + R_{f,i}\ , \tag{24}$$

to solve for the volumetric rate of formation of each compound (D is the reactor dilution rate, hr^{-1}). The time course of these rates of formation are plotted in

Figures 62 and 63 for experiments CI28 and CI30, respectively. Some small fluctuations in the curves are remnants of the spline-fitting process. Again, it is apparent from these figures that the initially high volumetric rates of acetone and butanol formation declined fairly rapidly and were replaced by increasing rates of acid production. Secondary peaks or shoulders in the solvent rate profiles occur near the time of maximum acid formation rates. The rate of glucose consumption declined from its initial high value in both runs, although in experiment CI28 the consumption rates peaked again because of rapid increases in the acid product formation rates. Butyric and acetic acid formation rates declined to zero much more slowly in the experiment utilizing the oligosporogenous strain.

Lactic acid production was significant only during the early hours of Experiment CI28; rates after the 10 hour mark of both Runs CI28 and CI30 were essentially zero, and thus neither the volumetric nor the specific rates of lactic acid formation are plotted.

The volumetric product formation rates and the immobilized cell concentration data (Figures 35, 36, 44, and 45) were used to produce the profiles for the specific rates of product formation during the bioconversion phase of experiments CI28 and CI30 (Figures 64–65 and 66–67, respectively). For each product (and glucose), two trajectories are presented: the solid curve was obtained by viewing product formation as a function of vegetative cells alone, and the dotted line assumes equal product-forming abilities in both clostridial forms and vegetative cells. Some catabolic activity resulting in acid and/or solvent formation was undoubtedly carried out by the swollen clostridial cells, since batch cultures producing butanol at high rates contain as much as 80% clostridial forms [25,39]. However, since these

cells also performed other sporulation-specific activities, such as granulose storage and forespore formation, the efficiency of glucose conversion to acid and solvent products in this cell type is likely to be different than in vegetative cells. Thus, the true specific rates of formation probably lie between the two curves. The immobilized cell concentrations used in the calculations are also plotted in Figures 65 and 67.

Although the highest molar rate of butanol production based on the reactor liquid volume occurred at the start of the bioconversion phase, the profiles in Figures 64–65 indicate that the highest specific rate of butanol formation occurred at the 30 hour mark of experiment CI28. In fact, the specific rates of formation of all of the products and the specific glucose uptake rate were at their maxima at this time. This is a result of the faster decline in cell number than in the volumetric rates during the run. The most likely explanation for this result on a biological level is the metabolic activation of the cells by the cytoplasmic constituents of the cells which lysed during the first 10–20 hours of the bioconversion phase. These materials are sufficient to fuel the cryptic metabolism of glucose to acid and solvent products at higher rates than those observed on the nitrogen- and vitamin-free minimal medium alone. The presence of nitrogenous lysis products also explains the ability of the ATCC 824 cells to sporulate in the absence of a medium-supplied nitrogen source, since *C. acetobutylicum* sporulation will not occur without exogenous carbon, energy and nitrogen sources [24,40,41]. In many species of *Clostridia*, the onset of sporulation is marked by the concomitant autolysis of a significant percentage of vegetative cells; researchers have concluded that the autolytically released cell components may provide the sporulating cells with important nutrients [41].

The time courses of the specific rates of product formation during bioconversion with the immobilized oligosporogenous strain also show this lysis-enhanced rate increase near the 20 hour mark, but the effect is not nearly as pronounced. In addition, peak butanol and acetone rates occurred before peak rates in acetic and butyric acids. It is interesting to note that, given the difficulty of obtaining accurate cell counts from the immobilized cell beads, the maximum specific rates of formation for each of the products were nearly the same between the two experiments. The major exceptions to this were the specific rates of formation of acetic and butyric acids, which had peak rates between 2.5 and 4 times higher in run CI28 than in run CI30.

The specific rate data of Figures 64–65 and 66–67 were used in the metabolic pathway rate analysis framework of Chapter 4 to obtain profiles of the variation of the specific pathway branch rates during the bioconversion phase of each experiment. These are presented in Figures 68–70 (CI28) and 71–73 (CI30). Since the calculation of the specific rates of product formation is subject to more error for the start of each run than for the remainder of an experiment, the pathway rates during the first 10 hours have been omitted from each plot. The results for both experiments illustrate further the overall enhancement of the metabolic rate due to consumption of lysis products. The sudden availability of amino acids, nucleic acids, and macromolecules to cells which had been nitrogen starved clearly enhanced the total glucose uptake rate in both experiments, and thus the carbon flow through all of the pathway branches increased during this period. Similarly, because the products of vegetative cell lysis were consumed or washed away in a relatively short time, the metabolic acitivity of the cells decreased accordingly. The difference be-

tween the extent of the increase in specific reaction rate enhancement between the two experiments is significant. It is possible that this disparity is due to the consumption of the same amount of lysis products by a smaller number of cells (in the case of run CI28). While the rates of carbon flow through the catabolic pathways decreased more rapidly during the first 50 hours of the ATCC 824 experiment than during the same period of the ATCC 39236 run, the metabolic activity plateaued during the second half of run CI28. In contrast, the specific pathway branch rates declined steadily during experiment CI30. In both cases, the rates of carbon flow through those pathway branches leading directly to acetone and butanol (v_7 and v_{11}) decline much more rapidly than the rates of the steps leading to acid formation (v_X and v_Y).

B. NAD(P)H-Dependent Fluorescence During Bioconversion

The immobilized cell NAD(P)H-dependent fluorescence levels during bioconversion were measured in experiments CI23, CI28, and CI30. All were conducted at pH 4.5 with nitrogen-free, vitamin-free medium; run CI30 used the oligosporogenous mutant discussed in the previous section, while the other two runs utilized strain ATCC 824. The three trajectories have been replotted in Figure 74 for comparison. Both similarities and differences can be observed, but the two ATCC 824 fluorescence profiles resemble one another more in their qualitative features than they do the ATCC 39236 (CI30) curve. The explanations of these features must involve the differences in catabolic rates among the three experiments. However, the explanation of the changing fluorescence levels given in Chapter 4 for batch suspended cell fermentations is not capable of describing these trajectories, in part

because both solvent and acid production is occurring at the same time for most of the bioconversion phase. In addition, it is not possible to interpret these results on a specific fluorescence basis, since the club-shaped forespore cells and mature spores do not contribute to acid and solvent formation but do undoubtedly contribute to the measured fluorescence.

Although an obvious difference between experiments CI28 and CI30 is the much higher degree of sporulation in run CI28, it does not appear that this can explain the fluorescence profile differences. The majority of sporulation events occurred between the 20 and 40 hour marks of experiment CI28; at this time the fluorescence levels in **both** run CI28 and CI30 increased, *i.e.*, they behaved similarly.

C. pH Effects on Bioconversion

The volumetric rates of product formation and glucose consumption are shown in Figures 75, 76, and 77 for bioconversion phases operated at pH 4.5 (CI18), pH 5.0 (CI15), and pH 6.0 (CI19), respectively.

In standard suspended cell batch fermentations, experiments performed at a low pH (4–4.5) display a highly productive solvent phase, while those conducted at pH values near 6 form solvents weakly or not at all (Figure 17, Chapter 4). This trend is not apparent in Figures 75 through 77 (see also Figures 28, 31, and 32). A comparison of the maximum butanol production rates (Table 3) shows that these values are approximately the same at the three different pH conditions (2.8–3.0 $mM \cdot hr^{-1}$), while the peak acetic and butyric acid formation rates actually declined as the pH was increased. Both ethanol and acetone production was highest at pH 5, and virtually no acetone was formed at pH 6. The rate of acetoin formation was

much higher at pH 6 than at either of the two lower pH conditions. While strict quantitative interpretations of these volumetric rates are not valid (specific rates should be used for this purpose), qualitative conclusions can be made, because the initial cell loadings were nearly the same in all three runs.

The production of solvent compounds at the start of the pH 6 bioconversion phase is not unexpected, since all three experiments began with a pH 4.5 batch growth phase which did not end until well after the enzymes for solvent formation were induced or activated. Rather, the notable feature of the pH 6 experiment is that significant amounts of some solvent-producing activity (namely, for butanol) were present even at the midpoint of the bioconversion segment. This indicates that the activities of the two enzymes leading to butanol formation from butyric acid, butyraldehyde dehydrogenase and butanol dehydrogenase, were not affected by pH changes in the range of 4.5 to 6. However, the relationship between pH and acetone formation (Table 3) implies that the enzyme(s) involved in acetone synthesis were strongly affected by pH. In fact, the activity of acetoacetate decarboxylase (catalyzing the irreversible decarboxylation of acetoacetate) was maximal at pH 5, 85% of the maximum at pH 4.5, and only 23% of the maximum at pH 6 [42,43]. It is possible that the pH dependence of at least one of the dehydrogenases leading to ethanol formation may show a similar behavior.

The large increase in acetoin synthesis rates at pH 6 over those found at pH 4.5 and 5 indicates that this process may also be pH dependent. Although the enzymes used in acetoin formation in *C. acetobutylicum* have not been studied, it is generally assumed that the reactions are identical to those found in bacilli and in the enterobacteria; that is, a decarboxylation of pyruvate to α-acetolactate by α-

acetolactate synthase followed by a second decarboxylation to acetoin, catalyzed by α-acetolactate decarboxylase [44]. Acetolactate synthase is also known as "the pH 6 enzyme" [44,45], and has been reported to show a sharp pH optimum at 5.8 [45]. Acetoin is often a minor product in suspended cell batch fermentations, and thus its formation kinetics are usually overlooked. These results show that the primary link between acetoin formation and acid product synthesis is that both occur in high pH batch fermentations. Acetoin production does not occur in high-dilution rate pH 4.5 suspended cell continuous fermentations, in which the dominant products are acetic and butyric acids (experimental results not shown).

The microscope-counting chamber method was not used on the bead samples from these pH-effect experiments, but some information on the relative number and makeup of the immobilized cell population can be gained from the results of the dissolved bead 590 nm absorbance assays. These were presented in Figure 33 for the pH 4.5 experiment (CI18) and in Figure 34 for the pH 6 experiment (CI19). Comparison of the actual cell count profiles from experiment CI28 (pH 4.5, strain ATCC 824) with the CI18 A_{590} results shows that while the initial decline in 590 nm absorbance corresponds to a rapid drop in vegetative cell concentration, the increase in A_{590} after about 20 hours is not due to the growth of vegetative cells but rather to the production of phase-bright spores and clostridial forms. This is confirmed by the results of the run CI22 alginate bead analysis, in which both microscope and A_{590} assays were used (Figures 54 and 55). With this information, it is apparent that the sustained biocatalytic activity in the pH 6 bioconversion was due to the very low sporulation frequency which occurred during that experiment. Microscopic examination of the cell suspension from end-of-experiment bead samples confirmed

the absence of spore formation at this pH. In runs CI18 and CI15 (by virtue of short productivity lifetimes similar to those of CI18), the high rates of sporulation, indicated by the large increase in A_{590} after 20 hours, reduced the concentration of vegetative cells to a very low level. This pH dependence of the sporulation process has been noted in *C. acetobutylicum* strain P262, which would sporulate only in a narrow pH range [46], and in other *Clostridium* species [47,48].

D. Bioconversion With Added Metabolites

The time-dependent volumetric rates of product formation and glucose consumption during experiments CI17 (butyric acid addition), CI21 (acetic acid addition), and CI22 (acetoacetate addition) are presented in Figures 78, 79, and 80, respectively. The addition of acetate and butyrate to the feed medium was taken into account in the calculation of the rates of formation of those compounds in Figures 78 and 79; in Figure 80, the addition of acetoacetate was represented as acetone in the calculations, since the acetone data shown for this experiment is actually the combination of acetone and added acetoacetate concentrations.

Before discussing the rate trajectories for each experiment, it should be noted that sporulation occurred in at least two of the runs (CI21 and CI22, Figures 53, 54, and 55) and probably all three, since the metabolic activity in run CI17 declines as rapidly as in the other two experiments. All three bioconversion phases took place at pH 4.5. The manifestation of sporulation as a rapid increase in the A_{590} of dissolved bead suspensions was confirmed by comparing the results of both immobilized cell analyses from experiment CI22 (Figures 54 and 55). By calculating extinction coefficients for vegetative cells and spores (based on the first and last bead samples),

the A_{590} *vs.* time profile (Figure 54) could be approximated closely.

The consumption of butyrate from the butyric acid-containing medium of experiment CI17 is shown in Figure 78 as a negative rate of formation. The consumption of butyrate resulted in a much higher butanol formation rate (7 $mM \cdot hr^{-1}$ as compared with 2.4–3 $mM \cdot hr^{-1}$ in plain feed experiments). Acetone formation rates were especially enhanced by butyrate addition, with a peak rate of about 1.8 $mM \cdot hr^{-1}$ as compared to 0.2–0.3 $mM \cdot hr^{-1}$ in pH 4.5 experiments using plain feed. This increase can be explained in terms of the catabolic reactions. Since the most likely means of butyrate uptake is via a CoA-exchange reaction with acetoacetyl-CoA, significant amounts of acetoacetate are available for decarboxylation to acetone. Peak rates of formation of ethanol and acetoin were slightly higher with butyrate in the feed than not. Acetate formation was not affected by butyrate addition, and it occurred with the same rate-time behavior observed in most other runs.

The negative rate of acetate formation at the start of run CI21 (Figure 79) indicates that acetic acid was consumed from the medium; this early consumption clearly resulted in high initial acetone formation rates. A decline in the rate of acetone production occurred as acetate consumption slowed, but both acetone and butanol rates increased as acid production increased. More visible evidence of the consumption of excreted acids is apparent in these curves than in the results of most other runs. The enhanced rate of acetone production at the start of the bioconversion phase of this experiment occurred because acetate uptake is effected by the same CoA-exhange mechanism used for butyrate uptake; again, the resulting acetoacetate was converted to acetone. The unusually high rate of acetone formation

later in the experiment, together with the lower peak rate of acetate synthesis implies that acetic acid was also consumed at this time. Other experiments with acetate addition to growing suspended cells have also reported increases in acetone, but not butanol, production [49].

Although the volumetric rate of production of measured acetone was negative during the first 20 hours of the run CI22 bioconversion experiment (Figure 80), this was due to the consumption of acetoacetate (acetone uptake does not occur). This consumption appears as an enhancement of the early acetic acid formation rate, which was greater than the rate of formation of butyric acid for most of the run. As in the acetate-feeding experiment, the consumption of excreted acetic and butyric acids was observed and resulted in increased acetone and butanol formation rates after 20–25 hours of bioconversion. The rates of ethanol and acetoin production also increased slightly during this time.

Huesemann and Papoutsakis found that the addition of acetoacetate to growing suspended cell batch cultures resulted in enhanced butanol formation; also, they reported that butyrate addition increased the amount of butanol formed by the end of growth [50]. These authors argued that these effects were caused by the uncoupling action of the weak acids on the membrane ΔpH, and were able to achieve similar increases by adding non-metabolizable uncoupling agents to growing cultures [50].

E. Bioconversion With Nitrogen-Containing But Vitamin-Free Feed

The addition of 0.8 g/L NH_4Cl to the bioconversion feed resulted in dramatically higher butanol productivities as compared to plain-feed experiments (Figure

56). Acetone and acetoin concentrations were only slightly increased over typical levels. Unfortunately, bead samples were not taken during this experiment, and thus no direct information is available regarding the immobilized cell population numbers and composition. However, microscopic examination of dissolved end-of-experiment bead samples showed that significant levels of sporulation had occurred. The second peak in 590 nm absorbance may be associated with this sporulation.

F. Bioconversion With *Clostridium acetobutylicum*

It is apparent that the major causes for the loss of immobilized *C. acetobutylicum* product-forming activity in most of these bioconversion experiments are (1), the early lysis of most of the immobilized cells and (2), the sporulation of the majority of the remaining cells (Figures 57–60). The obvious exceptions to the latter event were the experiment using the oligosporogenous strain ATCC 39236 (instead of ATCC 824) and the run in which bioconversion occurred at pH 6.

Sporulation in preparations of immobilized *C. acetobutylicum* has been reported previously; Förberg *et al.* observed evidence of sporulation in calcium alginate-immobilized cells which were pulse-fed nutrients at 2 to 12 hour intervals while being fed a non-nitrogen medium continuously [51].

The initial lysis episode occurred in all of the experiments, for reasons that are not clear. Although immobilized cell counts were not reported, Häggström reported a rapid initial loss in butanol-forming activity in an immobilized *C. acetobutylicum* reactor system [52]. Also, Wada *et al.* observed high rates of autolysis and cell death immediately after transfer of κ-carrageenan-entrapped yeast cells to nitrogen-deficient medium [53].

It should be noted that neither lysis nor sporulation seems to have been triggered by exposure of the immobilized ATCC 824 cells to air during the rinsing procedure between the growth and bioconversion phases. The effect of sufficient exposure to oxygen is to stop all processes in the cell; normal growth and product formation resume when anaerobic conditions are re-established [54,55]. Furthermore, sporulation began long after the start of anaerobic bioconversion phase. Finally, the same early lysis process was observed even in experiment CI30, in which the beads were rinsed anaerobically.

Sporulation in *C. acetobutylicum* differs from that in the bacilli because exogenous sources of carbon, energy, and nitrogen are required [24,41,46]. The ability of these immobilized *C. acetobutylicum* cells to sporulate in nitrogen-free medium seems to depend on the uptake of nitrogenous cell lysis products released during the first few hours of bioconversion. At the same time, the specific rates of product formation in the bioreactor increased due to cryptic metabolism on the lysis-released cellular nutrients.

While the sporulation of most of the immobilized cell population is the main cause of post-lysis activity loss in the ATCC 824 experiments, a different, slower mechanism is responsible for activity losses in the ATCC 39236 experiment, since only a few immobilized cells sporulated. Although the causes of this deactivation were not revealed directly by these experimental results, the most likely possibilities center around the missing nutrients: nitrogen and growth vitamins. Nitrogen is required for the synthesis of amino acids and nucleic acids. While starved cells may utilize such endogenous nitrogen sources as ribosomal RNA for the continued synthesis of required macromolecules [56], it is unlikely that these cells would con-

tinue to exhibit high rates of glucose catabolism. The lack of an exogenous supply of required growth vitamins such as biotin and *p*-aminobenzoic acid further inhibits some biosynthetic activities; however, this effect would not be evident during the early part of the bioconversion phase, as bacterial cells require only very small concentrations of vitamins. It may be that the shortage of these vitamins after 100 hours of bioconversion caused sporulation in the experiment in which nitrogen was supplied.

In nearly all of the experiments, early solvent product formation was replaced later by the production of acetic and butyric acids. Formation of these acids was observed even after 80 hours of bioconversion on the starvation medium, when most immobilized cells had lysed or sporulated. It is possible that the enzymes required only for solvent production (acetoacetate decarboxylase, butyraldehyde and butanol dehydrogenases, *etc.*) are less stable than the other catabolic enzymes, forcing the cell to the acidogenic state. However, this seems unlikely, if only for the reason that some similar enzymes (dehydrogenases), the half-lives of which should be similar, are required for the formation of butyric acid. A more reasonable hypothesis is that the starving cells require the highest possible ATP production rate; the phosphorylation of ADP in the kinase reactions leading to acetate and butyrate formation do not occur when solvent production predominates, and so acidogenesis produces more ATP per glucose molecule consumed.

The results of all of these experiments show variations in product selectivity, even beyond the general observation that solvent production was replaced by the formation of acids. As an illustration of the effects of variations in environmental conditions on selectivity during bioconversion, the molar ratios of butanol to acetone

concentrations for each experiment are presented in Table 4; concentration data were taken at the time of maxiumum butanol concentration. This ratio is often used in the *C. acetobutylicum* fermentation literature, since butanol is the economically desired product. Typical butanol:acetone ratios at the end of suspended cell batch fermentations are about 2:1. Of course, this ratio is only one indicator of the desirability of a certain set of operating conditions.

The highest butanol:acetone ratio in the right-hand column of Table 4 was found in run CI19, bioconversion at pH 6. This was apparently due to the different effects of pH on acetone- and butanol-forming enzymes. While the addition of acetate, and especially butyrate, to the feed medium resulted in increased butanol formation, the B:A ratios for these runs were low, because acetone production was also enhanced. The experiment in which a nitrogen source was supplied to the immobilized cells resulted in the highest overall butanol productivity (mol butanol per experiment), with a very high B:A ratio. It is worth noting that in virtually all of the experiments, this ratio was higher than that found in suspended cell fermentations.

CONCLUSIONS

The results of these experiments indicate that although immobilized *Clostridium acetobutylicum* are metabolically active in a non-growth state, the activity changes from solventogenesis to acid formation with 10–15 hours of continuous feeding with a nitrogen-free, vitamin-free medium. Furthermore, the loss of cells because of an initial period of lysis, and later, the sporulation of most of the cell

population, decreased the overall metabolic activity of the biocatalyst. Sporulation did not occur in two experiments: in one, an oligosporogenous mutant was utilized, and in the other sporulation was inhibited by an unfavorable pH. In both of these cases, activity losses were slower than in most of the experiments, and biocatalyst deactivation could be attributed to the effects of nitrogen starvation on macromolecular turnover and degradation.

Differences in the bioconversion phase environmental conditions, such as pH or metabolizable acid feed additions, resulted in different patterns of product-forming activity and product selectivity. Many of these differences could be explained in terms of the metabolic pathways of *C. acetobutylicum*. Some environmental operating conditions had more dramatic effects; bioconversion at pH 6 inhibited sporulation and overall activity levels (including butanol production) were maintained for significantly longer times than at lower pH values.

In situ monitoring of immobilized cell NAD(P)H-dependent fluorescence showed that the intracellular NAD(P)H levels in the cells changed during the course of bioconversion. Although these fluorescence trajectories are complex and could not be interpreted fully at this time, it is clear that *in vivo* fluorescence measurements are sensitive indicators of changes in cellular metabolism which are not obvious by other methods.

Finally, these experiments showed that many effects of environmental changes cannot be predicted from experiments performed with growing cultures of suspended cells. More studies on very slowly or non-growing immobilized cells are required to define further the kinetic and deactivation properties of this type of immobilized cell biocatalysis.

LITERATURE CITED

1. Häggström, L. and N. Molin, "Calcium Alginate Immobilized Cells of *Clostridium acetobutylicum* for Solvent Production," *Biotech. Lett.*, **2**, 241–246 (1980).

2. Krouwel, P.G., W.J. Groot, N.W.F. Kossen, and W.F.M. van der Laan, "Continuous Isopropanol-Butanol-Ethanol Fermentation by Immobilized *Clostridium beijerinckii* Cells in a Packed Bed Fermentor," *Enz. Microb. Tech.*, **5**, 46–54 (1983).

3. M^{c}Ghee, J.E., G. St. Julian, R.W. Detroy, and R.J. Bothast, "Ethanol Production by Immobilized *Saccharomyces cerevisiae, Saccharomyces uvarum*, and *Zymomonas mobilis*," *Biotech. Bioeng.*, **24**, 1155–1163 (1982).

4. Somerville, H.J., J.R. Mason, and R.N. Ruffell, "Benzene Degradation by Bacterial Cells Immobilized in Polyacrylamide Gel," *Eur. J. Appl. Microbiol.*, **4**, 75–85 (1977).

5. Scherer, P., M. Kluge, J. Klein, and H. Sahm, "Immobilization of the Methanogenic Bacterium *Methanosarcina barkeri*," *Biotech. Bioeng.*, **23**, 1057–1065 (1981).

6. Krouwel, P.G., W.J. Groot, and N.W.F. Kossen, "Continuous IBE Fermentation by Immobilized Growing *Clostridium beijerinckii* Cells in a Stirred-Tank Fermentor," *Biotech. Bioeng.*, **25**, 281–299 (1983).

7. Lee, T.H., J.C. Ahn, and D.D.Y. Ryu, "Performance of an Immobilized Yeast Reactor System for Ethanol Production," *Enz. Microb. Tech.*, **5**, 41–45 (1983).

8. Briffaud, J. and M. Engasser, "Citric Acid Production From Glucose. II. Growth and Excretion Kinetics in a Trickle-Flow Fermentor," *Biotech. Bioeng.*, **21**, 2093–2111 (1979).

9. Inloes, D.S., A.S. Michaels, C.R. Robertson, and A. Matin, "Ethanol Production by Nitrogen-Deficient Yeast Cells Immobilized in a Hollow-Fiber Membrane Bioreactor," *Appl. Microbiol. Biotechnol.*, **23**, 85–91 (1985).

10. Klein, J. and F. Wagner, "Different Strategies to Optimize the Production Phase of Immobilized Cells," *Ann. N.Y. Acad. Sci.*, **501**, 306–316 (1987).

11. Doran, P.M. and J.E. Bailey, "Fermentation Patterns and Macromolecular Composition of Immobilized and Suspended Yeast during Biotin Starvation," *Ann. N.Y. Acad. Sci.*, **501**, 330–334 (1987).

12. Doran, P.M. and J.E. Bailey, "Effects of Hydroxyurea on Immobilized and Suspended Yeast Fermentation Rates and Cell Cycle Operation," *Biotech. Bioeng.*, **28**, 1814–1831 (1986).

13. Lampen, J.D. and W.H. Peterson, "Growth Factor Requirements of Clostridia," *Arch. Biochem.*, **2**, 443–449 (1943).

14. Reardon, K.F., T.-H. Scheper, and J.E. Bailey, "Metabolic Pathway Rates and Culture Fluorescence in Batch Fermentations of *Clostridium acetobutylicum*," *Biotech. Prog.*, **3**, 153–167 (1987).

15. Reardon, K.F., T. Scheper, and J.E. Bailey, "*In situ* Fluorescence Monitoring of Immobilized *Clostridium acetobutylicum*," *Biotech. Lett.*, **8**, 817–822 (1986).

16. Reardon, K.F., T.-H. Scheper, and J.E. Bailey, "Einsatz eines Fluoreszenzsensors zur Messung der NAD(P)H-abhängigen Kulturfluoreszenz Immobilisierter Zellsysteme," *Chem.-Ing.-Tech.*, **59**, 600-601 (1987).

17. Characterization of Immobilized Biocatalysts, K. Buchholz (ed.), DECHEMA Monograph No. 1724–1731, **84**, Verlag-Chemie, New York, 1979, pp. 265–335.

18. Karel, S.F., S.B. Libicki, and C.R. Robertson, "The Immobilization of Whole

Cells: Engineering Principles" *Chem. Eng. Sci.*, **40**, 1321–1354 (1985).

19. Weisz, P., "Diffusion and Chemical Transformation," *Science*, **179**, 433–440 (1973).

20. Tanaka, H., Matsumura, M., and I.A. Veliky, "Diffusion Characteristics of Substrates in Calcium Alginate Gel Beads," *Biotech. Bioeng.*, **26**, 53–58 (1984).

21. Hannoun, B.J.M. and G. Stephanopoulos, "Diffusion Coefficients of Glucose and Ethanol in Cell-Free and Cell-Occupied Calcium Alginate Membranes," *Biotech. Bioeng.*, **28**, 829–835 (1986).

22. Leung, J.C.-Y., "Production of Acetone and Butanol by *Clostridium acetobutylicum* Using Free and Immobilized Cells," Ph.D. Thesis, Massachusetts Institute of Technology, Cambridge, MA, 1982.

23. Moo-Young, M. and H.W. Blanch, "Design of Biochemical Reactors. Mass Transfer Criteria for Simple and Complex Systems," *Adv. Biochem. Eng.*, **19**, 1–69 (1981).

24. Long, S., D.T. Jones, and D.R. Woods, "Sporulation of *Clostridium acetobutylicum* P262 in a Defined Medium," *Appl. Env. Microbiol.*, **45**, 1389–1393 (1983).

25. Jones, D.T., A. van der Westhuizen, S. Long, E.R. Allcock, S.J. Reid, and D.R. Woods, "Solvent Production and Morphological Changes in *Clostridium acetobutylicum*," *Appl. Env. Microbiol.*, **43**, 1434–1439 (1982).

26. Hanson, R.S., J.A. Peterson, and A.A. Yousten, "Unique Biochemical Events in Bacterial Sporulation," *Ann. Rev. Microbiol.*,**24**, 53–90 (1970).

27. *Biochemistry of Bacterial Growth*, 2nd Ed., J. Mandelstam and K. McQuillen (eds.), J. Wiley and Sons, New York, 1973, pp. 494–516.

28. Robinow, C.F., "Morphology of Bacterial Spores, Their Development and Germination," in *The Bacteria*, vol. 1, I.C. Gunsalus and R.Y. Stanier (eds.), Academic Press, New York, 1960, pp. 207–248.

29. Young, M. and J. Mandelstam, "Early Events During Bacterial Endospore Formation," *Adv. Microb. Phsiol.*, **20**, 102–162 (1979).

30. Fitz-James, P. and E. Young, "Morphology of Sporulation," in *The Bacterial Spore*, G.W. Gould and A. Hurst (eds.), Academic Press, London, 1969, pp. 39–72.

31. Boylen, C.W. Boylen and J.C. Ensign, "Intracellular Substrates for Endogenous Metabolism During Long-Term Starvation of Rod and Spherical Cells of *Arthrobacter crystallopoietes*," *J. Bacteriol.*, **103**, 578–587 (1970).

32. Boyaval, P. E. Boyaval, and M.J. Desmazeaud, "Survival of *Brevibacterium linens* During Nutrient Starvation and Intracellular Changes," *Arch. Microbiol.*, **141**, 128–132 (1985).

33. Mason, C.A. and G. Hamer, "Survival and Activity of *Klebsiella pneumoniae* at Super-Optimal Temperatures," *Bioproc. Eng.*, **2**, 121–127 (1982).

34. Demain, A.L., "Riboflavin Oversynthesis," *Ann. Rev. Microbiol.*, **26**, 369–388 (1972).

35. Perlman, D., "Microbial Process for Riboflavin Production," in *Microbial Technology*, 2^{nd} Ed., vol. 1, H.J. Peppler and D. Perlman (eds.), Academic Press, New York, 1979, pp. 521–527.

36. Schöneit, P. A. Brandis, and R.K. Thauer, "Ferredoxin Degradation in Growing *Clostridium pasteurianum* During Periods of Iron Deprivation," *Arch. Microbiol.*, **120**, 73–76 (1979).

37. Ragsdale, S.W. and L.G. Ljungdahl, "Characterization of Ferredoxin, Flavodoxin, and Rubredoxin from *Clostridium formicoaceticum* Grown in Media with High and Low Iron Contents," *J. Bacteriol.*, **157**, 1–6 (1984).

38. Knight, Jr., E. and R.W.F. Hardy, "Isolation and Characteristics of Flavodoxin from Nitrogen-Fixing *Clostridium pasteurianum*," *J. Biol. Chem.*, **241**, 2752–2756 (1966).

39. Largier, S.T., S. Long, J.D. Santangelo, D.T. Jones, and D.R. Woods, "Immobilized *Clostridium acetobutylicum* P262 Mutants for Solvent Production," *Appl. Env. Microbiol.*, **50**, 477–481 (1985).

40. S. Long, D.T. Jones, and D.R. Woods, "The Relationship Between Sporulation and Solvent Production in *Clostridium acetobutylicum* P262," *Biotech. Lett.*, **6**, 529–534 (1984).

41. Woods, D.R. and D.T. Jones, "Physiological Responses of *Bacteriodes* and *Clostridium* Strains to Environmental Stress Factors," *Adv. Microbial Physiol.*, **28**, 1–64 (1986).

42. Davies, R., "Studies on the Acetone-Butanol Fermentation. 4. Acetoacetate Decarboxylase of *Clostridium acetobutylicum*," *Biochem. J.*, **37**, 230–238 (1943).

43. Ballongue, J., J. Amine, E. Masion, H. Petitdemange, and R. Gay, "Induction of Acetoacetate Decarboxylase in *Clostridium acetobutylicum*," *FEMS Microbiol. Lett.*, **29** 273–277 (1985).

44. Gottschalk, G., "Bacterial Fermentations," in *Bacterial Metabolism*, 2nd Ed., G. Gottschalk (ed.), Springer-Verlag, New York, 1985, pp. 208–282.

45. Stormer, F.C., "2,3-Butanediol Biosynthetic System in *A. aerogenes*," in *Methods in Enzymology*, vol. 41, S.P. Colowick and N.O. Kaplan (eds.), Academic

Press, New York, 1975, pp. 518–533.

46. Long, S., D.T. Jones, D.R. Woods, "Initiation of Solvent Production, Clostridial Stage, and Endospore Formation in *Clostridium acetobutylicum* P262," *Appl. Microbiol. Biotechnol.*, **20**, 256–261 (1984).

47. Mackey, B.M. and J.G. Morris, "Sporulation in *Clostridium pasteurianum*," in *Spore Research 1971*, A.N. Barker, G.W. Gould, and J. Wolf (eds.), Academic Press, New York, 343 (1971).

48. Wiegel, J. and M. Dykstra, "*Clostridium thermocellum*: Adhesion and Sporulation While Adhered to Cellulose and Hemicellulose," *Appl. Microbiol. Biotechnol.*, **20**, 59–65 (1984).

49. Matta-el-Amouri, G., R. Janati-Idrissi, O. Assobhei, H. Petitdemange, and R. Gay, "Mechanism of the Acetone Formation by *Clostridium acetobutylicum*," *FEMS Microbiol. Lett.*, **30**, 11–16 (1985).

50. Huesmann, M. and E.T. Papoutsakis, "Effect of Acetoacetate, Butyrate, and Uncoupling Ionophores on Growth and Product Formation of *Clostridium acetobutylicum*," *Biotech. Lett.*, **8**, 37–42 (1986).

51. Fõrberg, C., S.-O. Enfors, and L. Häggströom, "Control of Immobilized, Non-Growing Cells for Continuous Production of Metabolites," *Eur. J. Appl. Microbiol, Biotechnol.*, **17**, 143–147 (1983).

52. Häggströom, L., "Immobilized Cells of *Clostridium acetobutylicum* for Butanol Production," in *Advances in Biotechnology*, vol. 1, M. Moo-Young (ed.), Pergamon, New York, 1981, pp. 79–83.

53. Wada, M., J. Kato, and I. Chibata, "Continuous Production of Ethanol Using Immobilized Growing Yeast Cells," *Eur. J. Appl. Microbiol. Biotechnol.*, **10**,

275–287 (1980).

54. Morris, J.G. and R.W. O'Brien, "Oxygen and Clostridia: A Review," in *Spore Research 1971*, A.N. Barker, G.W. Gould, and J. Wolf (eds.), Academic Press, New York, 1971, pp. 1–37.

55. O'Brien, R.W. and J.G. Morris, "Oxygen and the Growth and Metabolism of *Clostridium acetobutylicum*," *J. Gen. Microbiol.*, **68**, 307–318 (1971).

56. Dawes, E.A., "Endogenous Metabolism and the Survival of Starved Prokaryotes," *Symp. Soc. Gen. Microbiol.*, **26**, 19–53 (1976).

RUN	pH	D (hr-1)	LENGTH (hr)	FEED GLUCOSE (g/L)	SPECIAL CONDITIONS
CI14	4.5	0.21	24	0	control
CI18	4.5	0.21	76	10	-
CI23	4.5	0.20	86	15	-
CI28	4.5	0.20	101	15	-
CI30	4.5	0.20	85	15	ATCC 39236
CI15	5.0	0.21	75	10	-
CI19	6.0	0.21	75	10	-
CI17	4.5	0.20	116	10	2 g/L butyrate
CI21	4.5	0.21	79	10	1 g/L acetate
CI22	4.5	0.21	77	10	10 mM acetoacetate
CI12	4.5	0.23	157	10	0.8 g/L NH_4Cl

Table 2. Bioconversion Phase Experimental Conditions.

PRODUCT	Maximum Volumetric Rate of Formation ($mM \cdot hr^{-1}$) pH 4.5	pH 5	pH 6
Ethanol	0.2	0.5	0.3
Acetone*	0.3	0.8	0.1
Acetic acid	2.2	1.8	1.2
Butanol	3.0	2.8	2.8
Acetoin	0.5	0.4	0.9
Butyric acid	2.6	1.8	1.8

*The rate at the 3 hour mark was used

Table 3. Maximum Volumetric Rates of Formation.

RUN	TYPE	TIME OF MAX. BUTANOL CONC. (hr)	(mM) BUTANOL	(mM) ACETONE	B:A
CI18	pH 4.5	8	7.8	1.2	6.5
CI23	pH 4.5	7	1.5	0.4	3.8
CI28	pH 4.5	9	7.5	0.7	10.7
CI30	pH 4.5, 39236	8	12.8	2.5	5.1
CI15	pH 5	8	9.3	2.7	3.4
CI19	pH 6	18	10.5	0.2	52.5
CI17	+butyrate	10	26.0	6.2	4.2
CI21	+acetate	25	8.4	7.4	1.1
CI22	+acetoacetate	9	7.4	*	*
CI12	+NH_4Cl	96	19.7	0.8	24.6

*True acetone concentrations could not be measured in this experiment

Table 4. Comparison of Maximum Butanol and Acetone Concentrations.

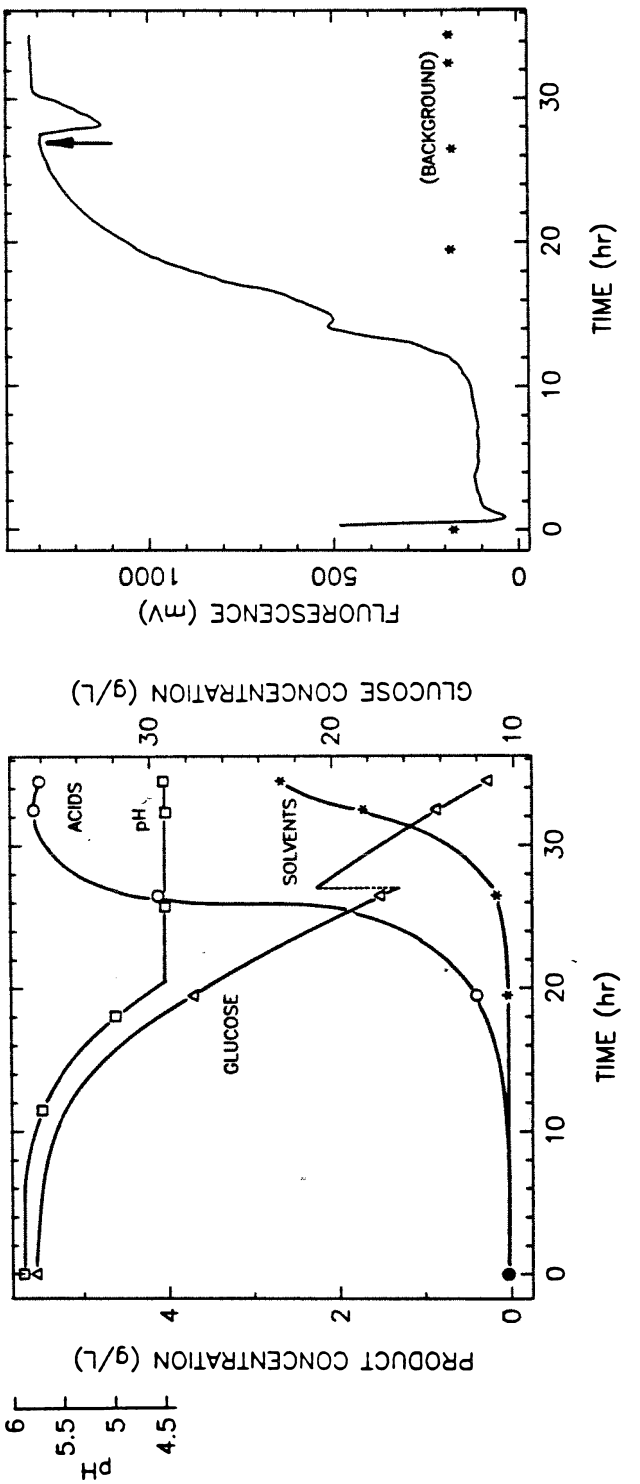

Figure 25. Results of experiment CI23 immobilized cell batch growth phase. **A**: Substrate and product concentrations, and pH. **B**: Immobilized cell NAD(P)H fluorescence.

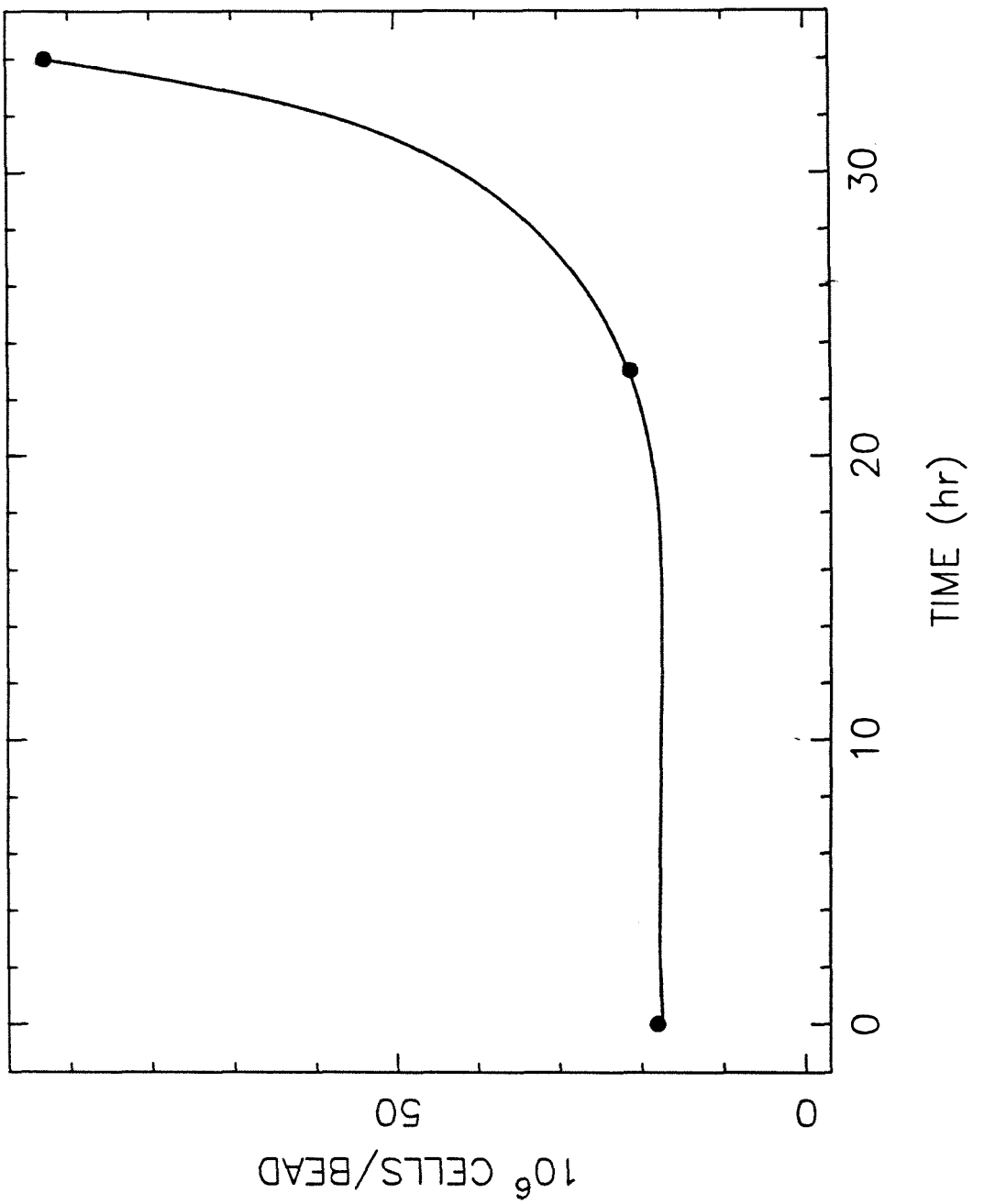

Figure 26. Immobilized vegetative cell concentration profile during the batch growth phase of experiment CI30.

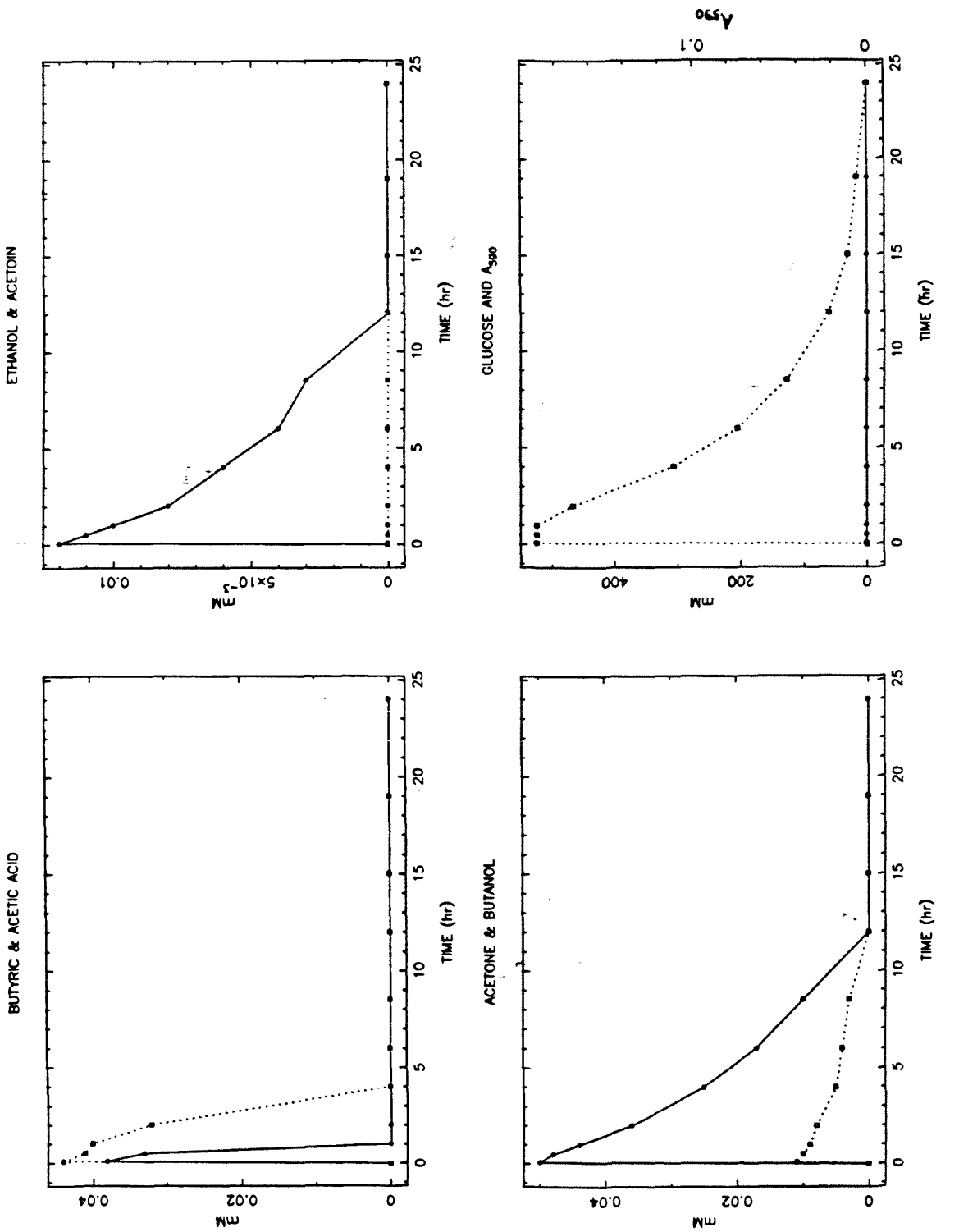

Figure 27. Concentration profiles for experiment CI14, control run. **Upper left**: Butyric acid (solid line) and acetic acid (dotted line). **Upper right**: Ethanol (solid line) and acetoin (dotted line). **Lower left**: Butanol (solid line) and acetone (dotted line). **Lower right**: Glucose (solid line) and A590 (dotted line, right-hand scale).

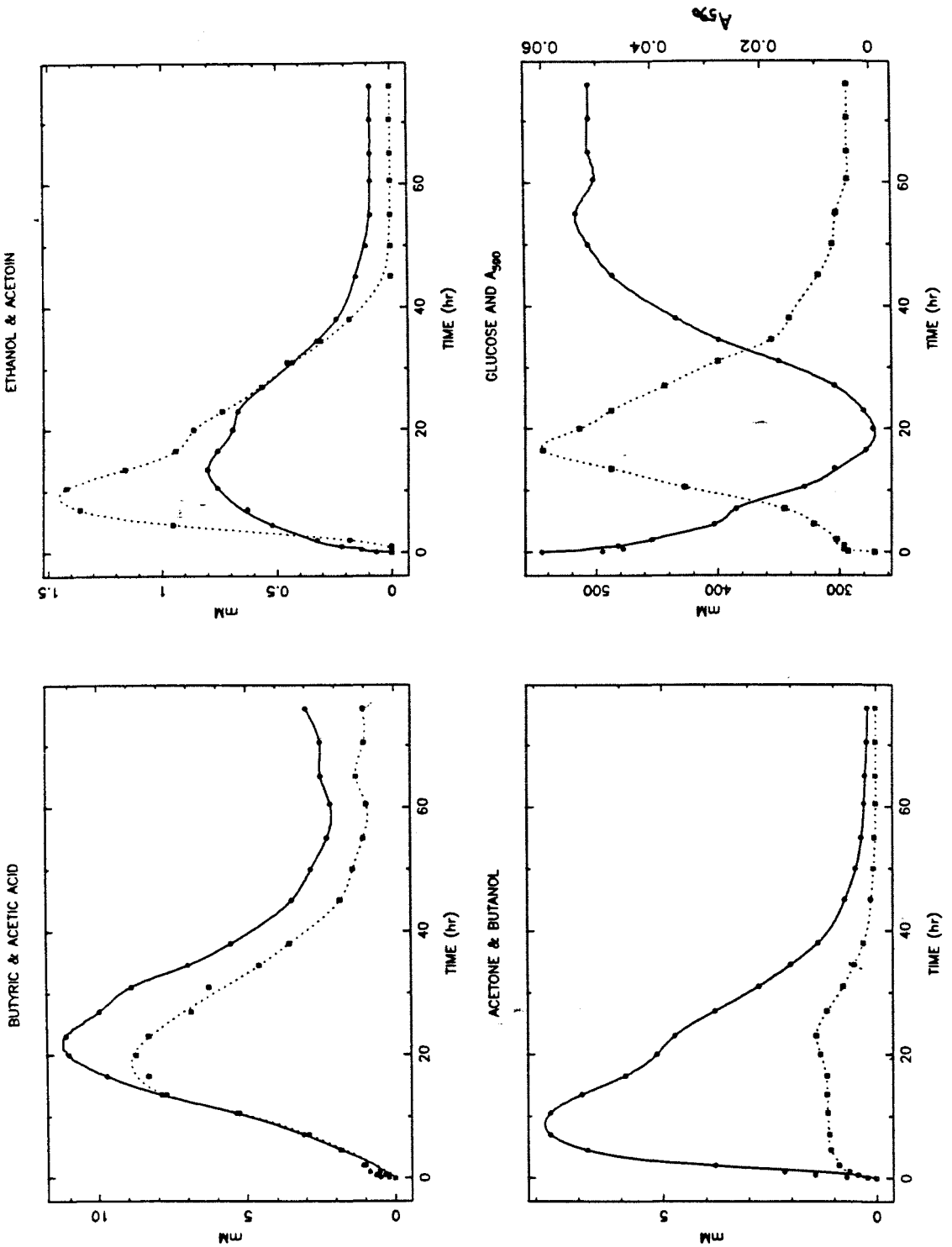

Figure 28. Concentration profiles for experiment CI18. **Upper left**: Butyric acid (solid line) and acetic acid (dotted line). **Upper right**: Ethanol (solid line) and acetoin (dotted line). **Lower left**: Butanol (solid line) and acetone (dotted line). **Lower right**: Glucose (solid line) and A590 (dotted line, right-hand scale).

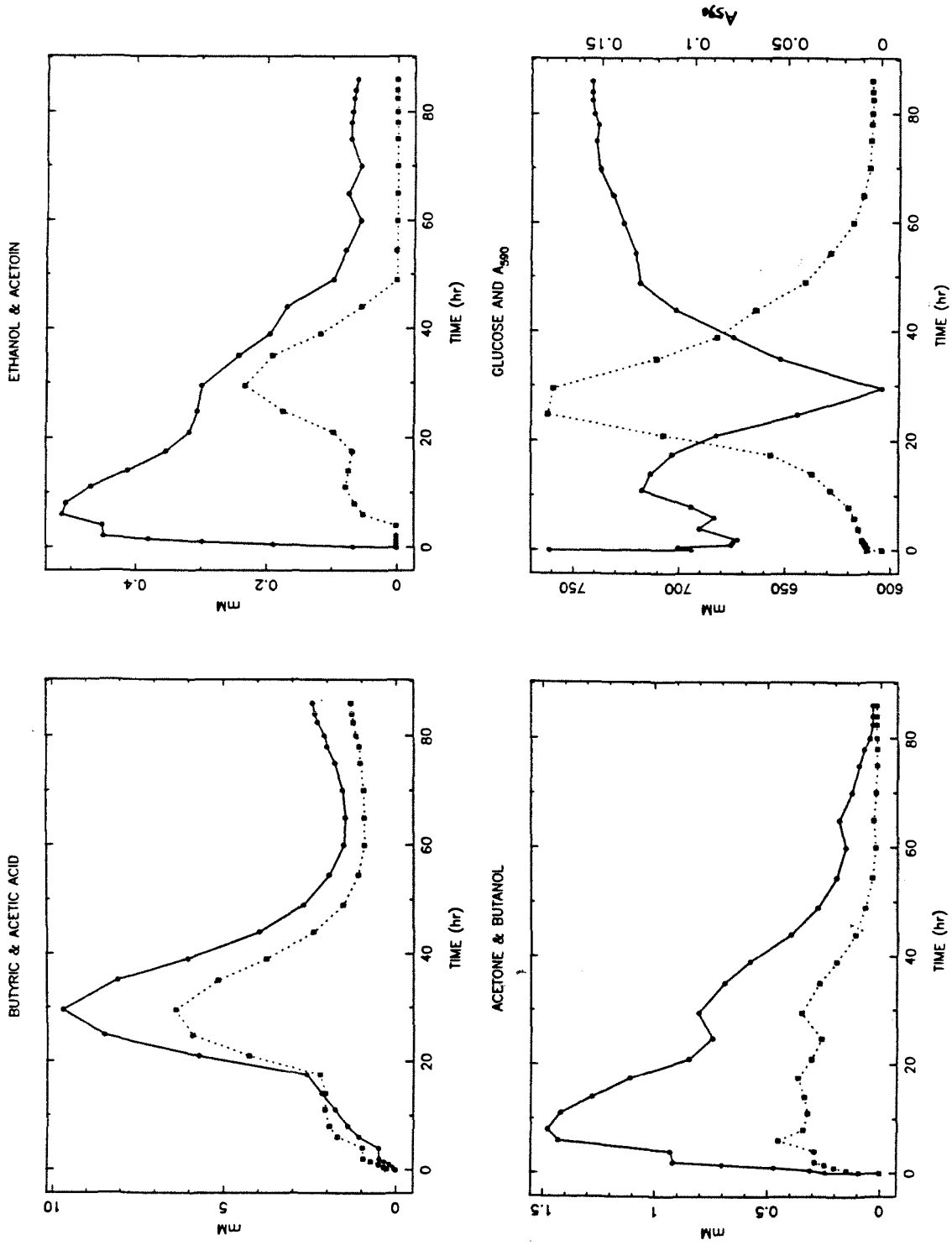

Figure 29. Concentration profiles for experiment CI23. **Upper left**: Butyric acid (solid line) and acetic acid (dotted line). **Upper right**: Ethanol (solid line) and acetoin (dotted line). **Lower left**: Butanol (solid line) and acetone (dotted line). **Lower right**: Glucose (solid line) and A590 (dotted line, right-hand scale).

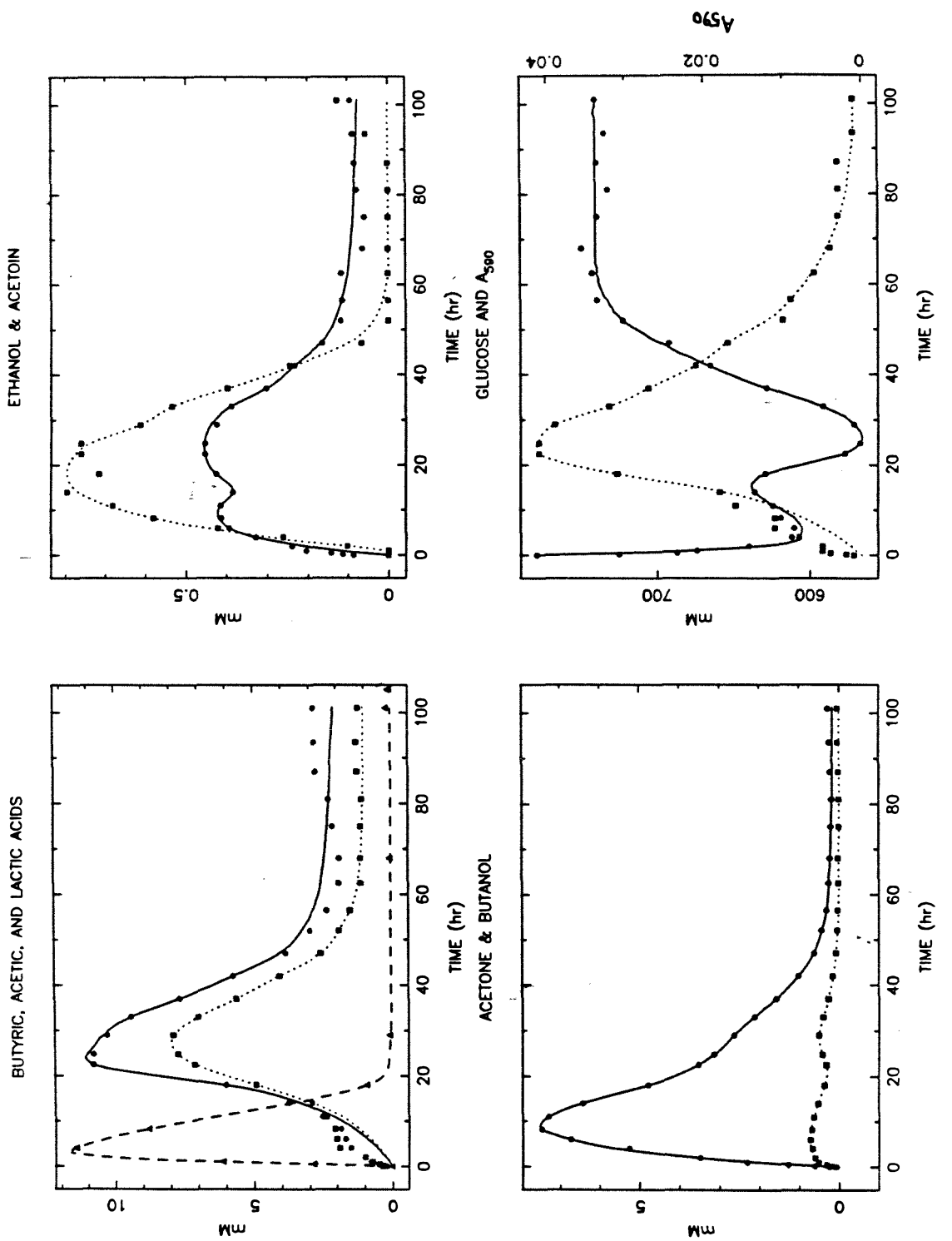

Figure 30. Concentration profiles for experiment CI28. **Upper left**: Butyric acid (solid line), acetic acid (dotted line), and total lactic acid (dashed line). **Upper right**: Ethanol (solid line) and acetoin (dotted line). **Lower left**: Butanol (solid line) and acetone (dotted line). **Lower right**: Glucose (solid line) and A590 (dotted line, right-hand scale).

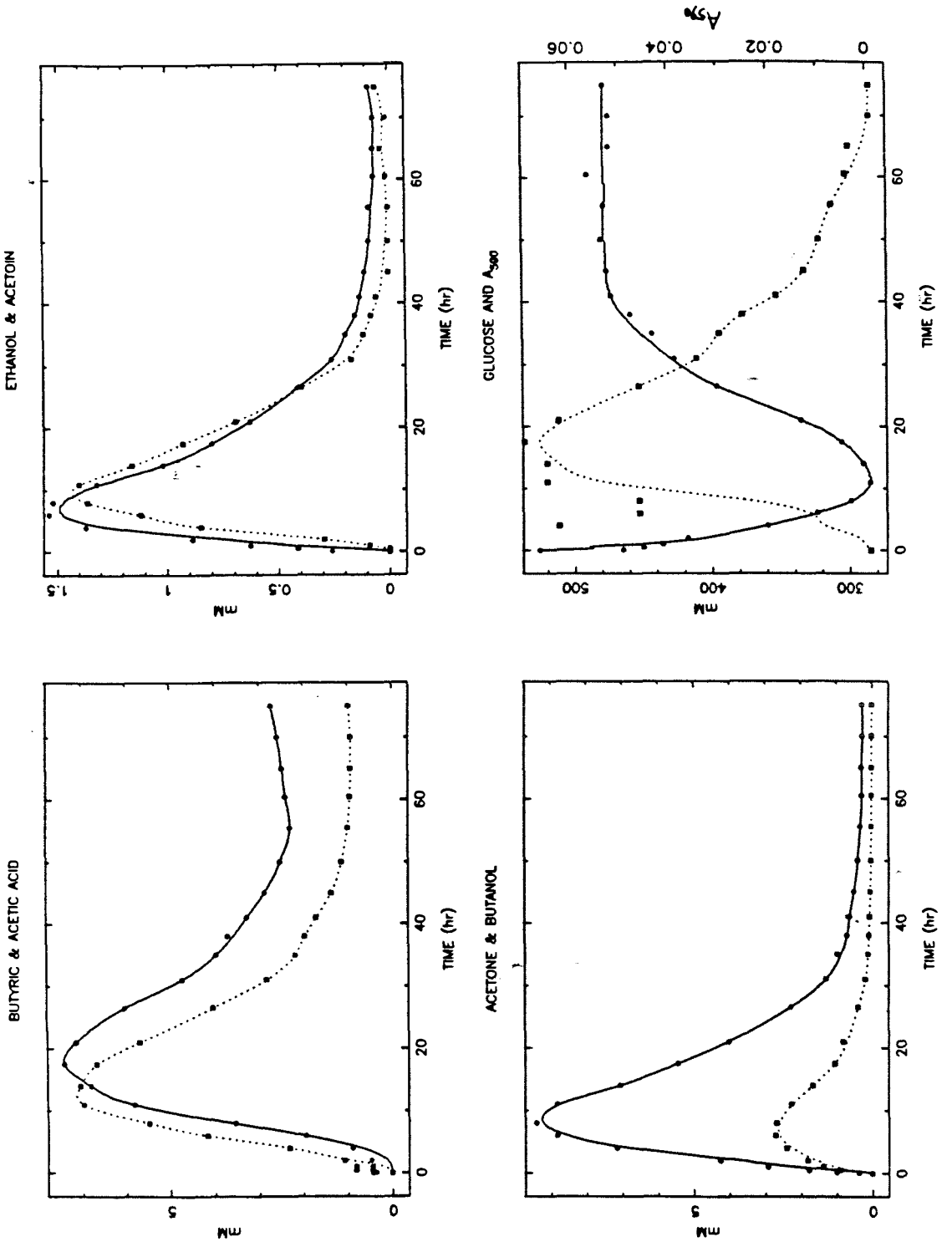

Figure 31. Concentration profiles for experiment CI15. **Upper left**: Butyric acid (solid line) and acetic acid (dotted line). **Upper right**: Ethanol (solid line) and acetoin (dotted line). **Lower left**: Butanol (solid line) and acetone (dotted line). **Lower right**: Glucose (solid line) and A590 (dotted line, right-hand scale).

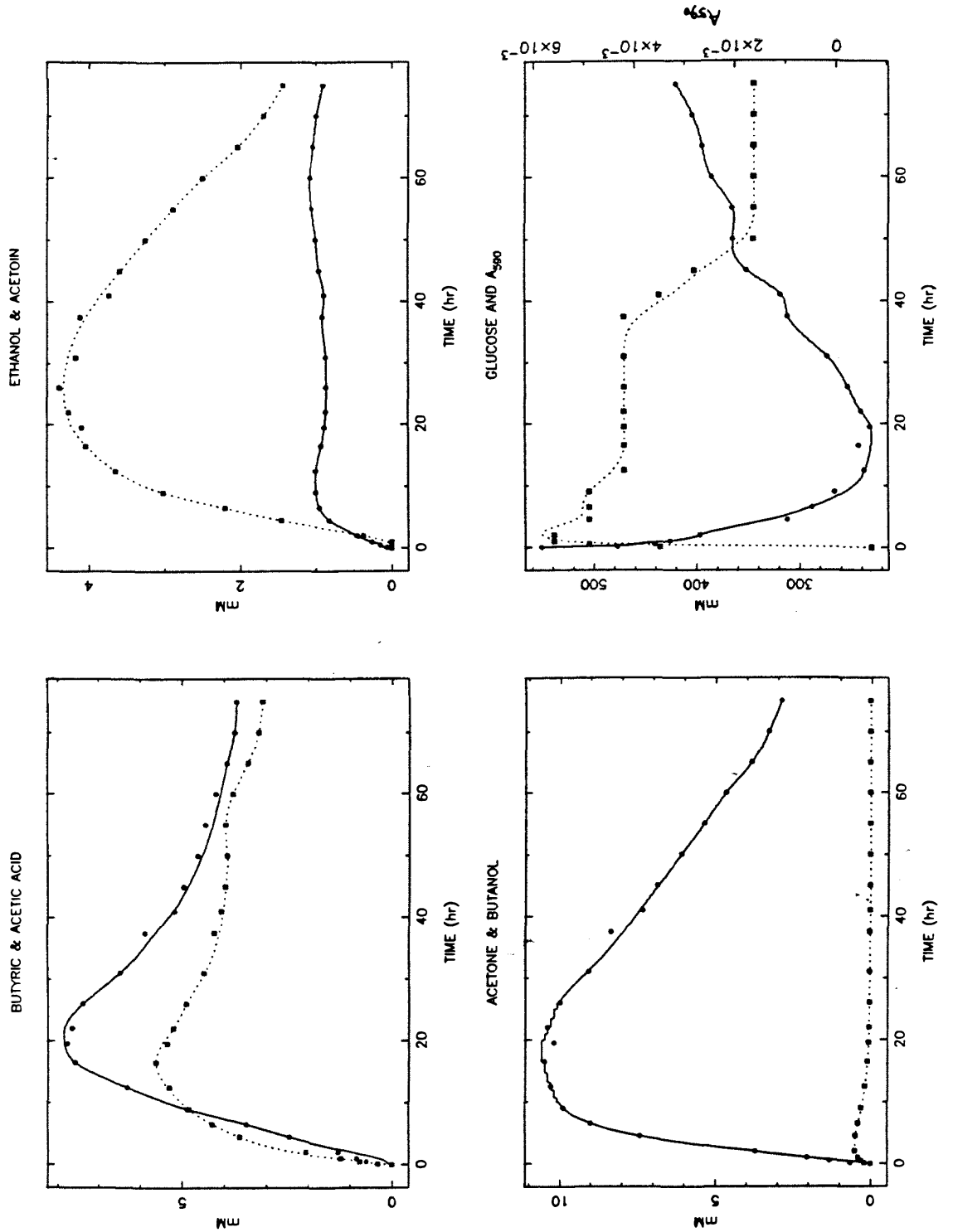

Figure 32. Concentration profiles for experiment CI19. **Upper left**: Butyric acid (solid line) and acetic acid (dotted line). **Upper right**: Ethanol (solid line) and acetoin (dotted line). **Lower left**: Butanol (solid line) and acetone (dotted line). **Lower right**: Glucose (solid line) and A590 (dotted line, right-hand scale).

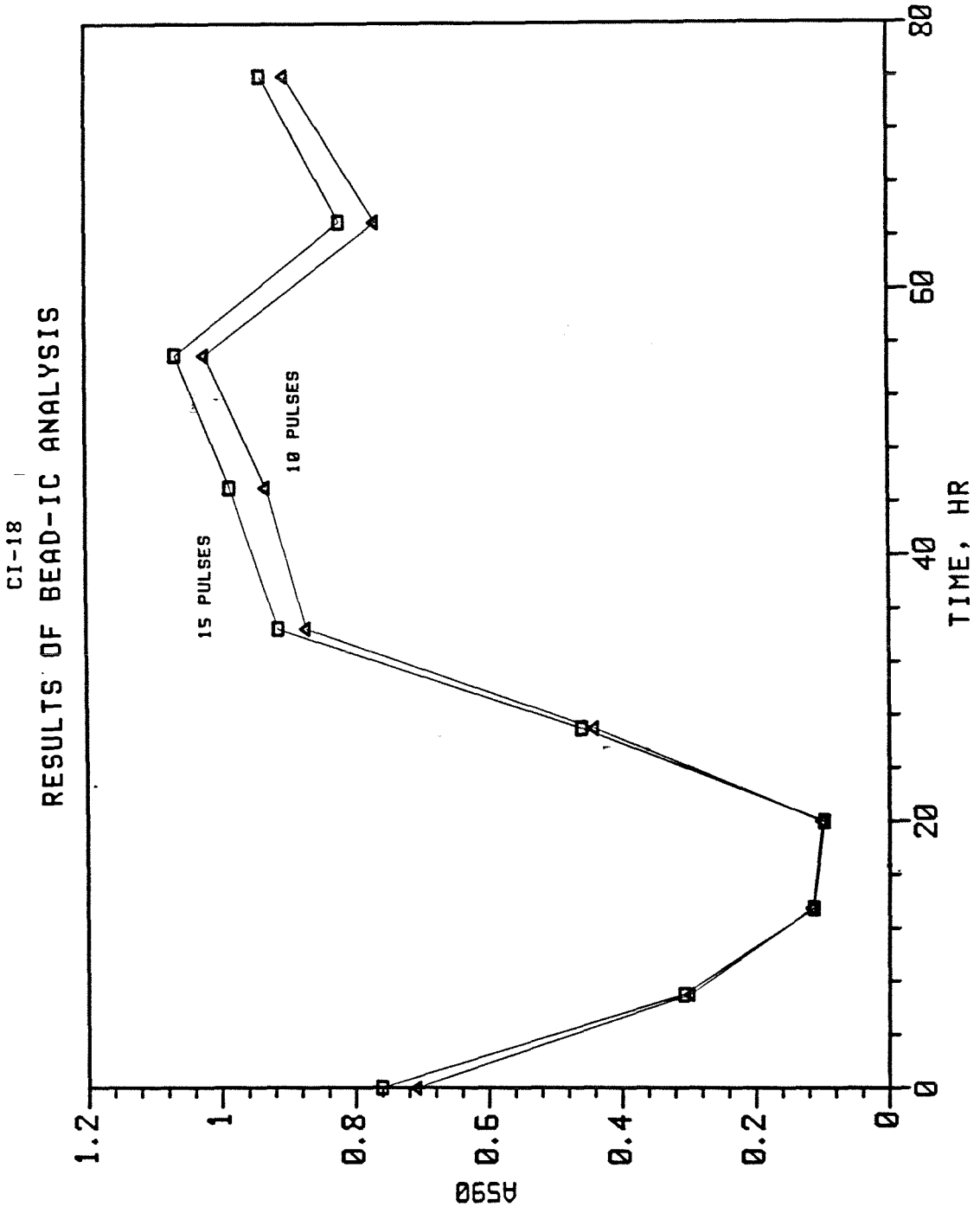

Figure 33. Results for run CI18 of immobilized cell concentration estimation by A590 method. The pulse count refers to the number of 10 second sonicator pulses used.

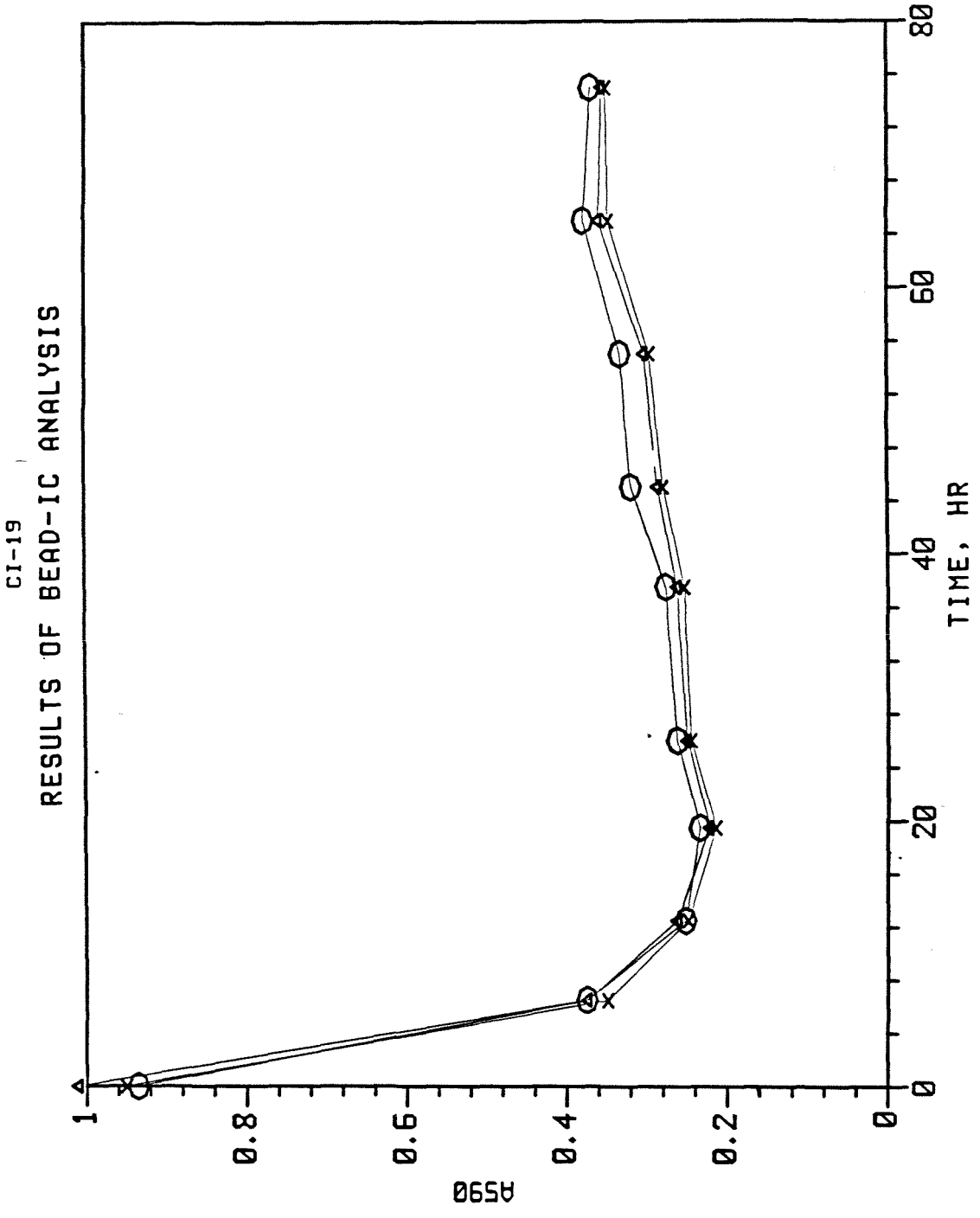

Figure 34. Results for run CI19 of immobilized cell concentration estimation by A590 method.

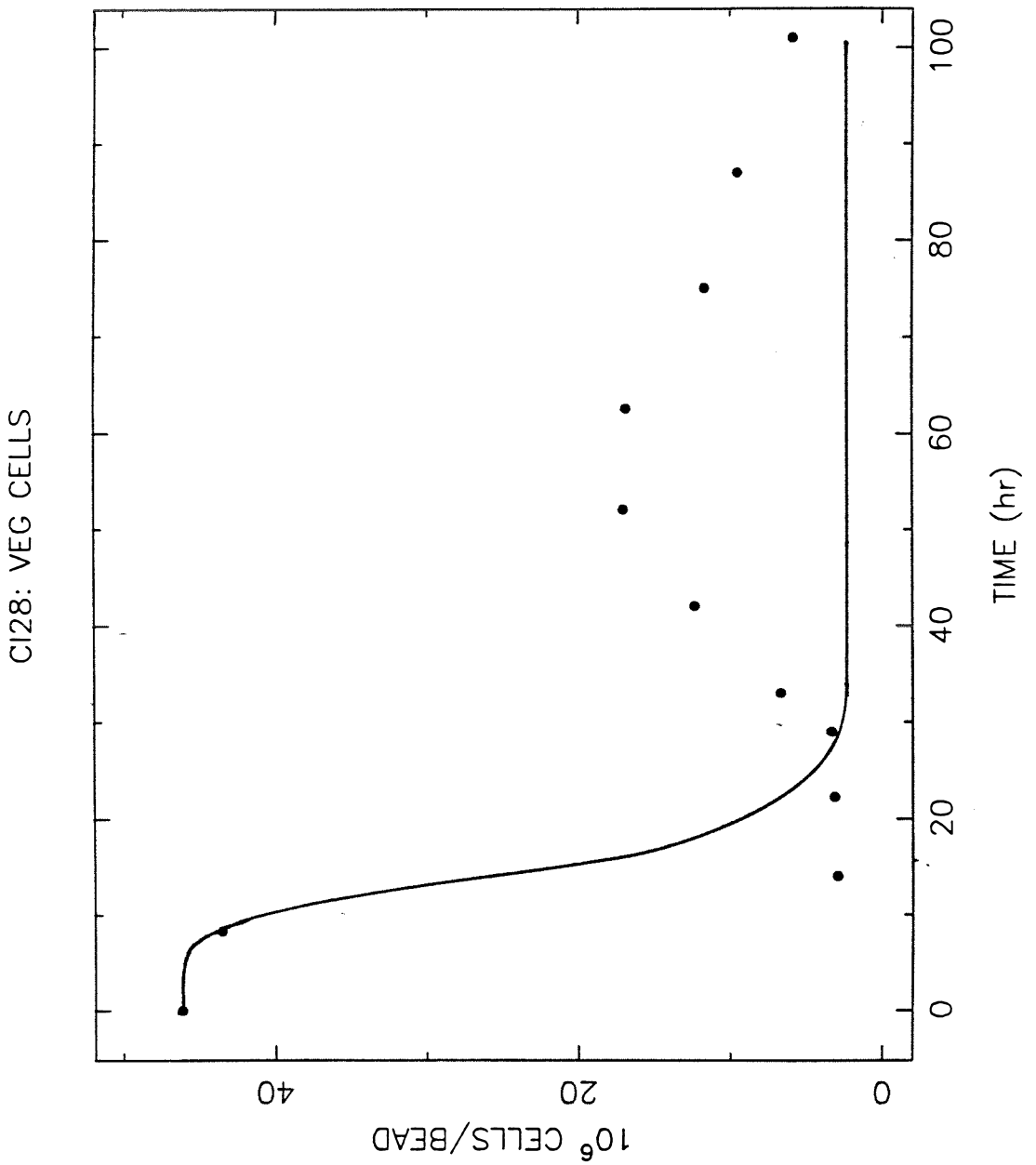

Figure 35. Run CI28 immobilized vegetative cell concentration.

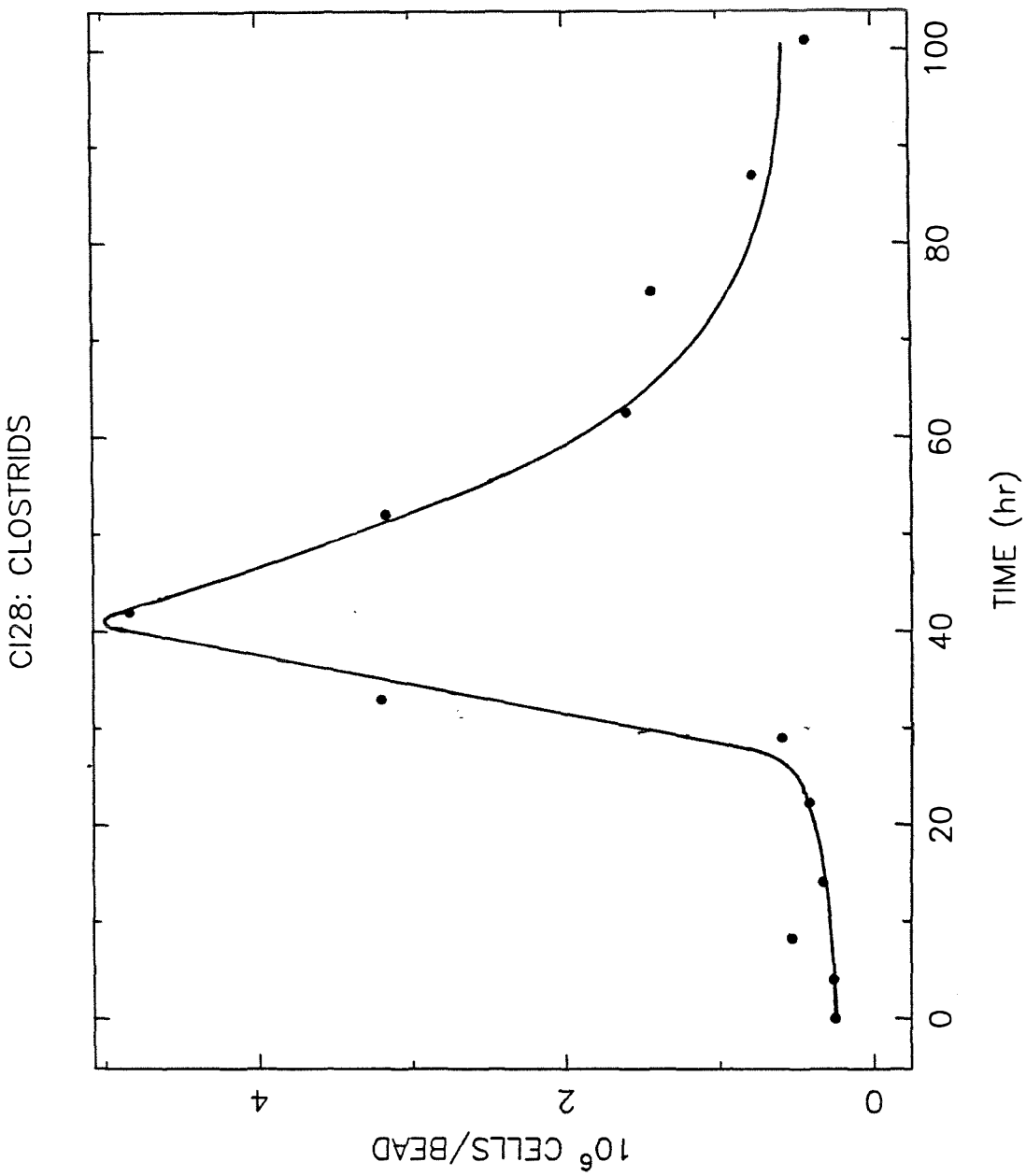

Figure 36. Run CI28 immobilized clostridial cell concentration.

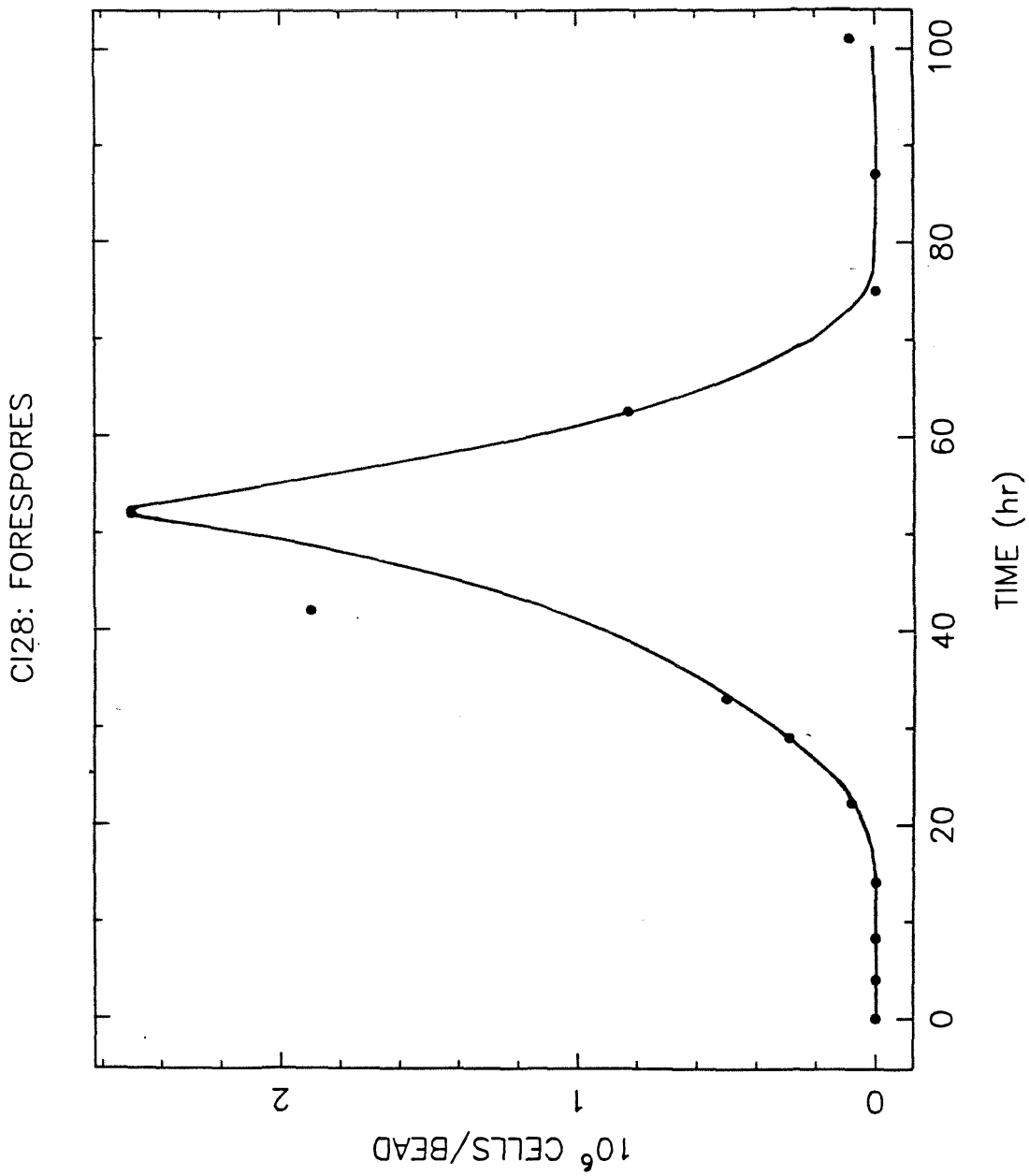

Figure 37. Run CI28 immobilized forespore-containing cell concentration.

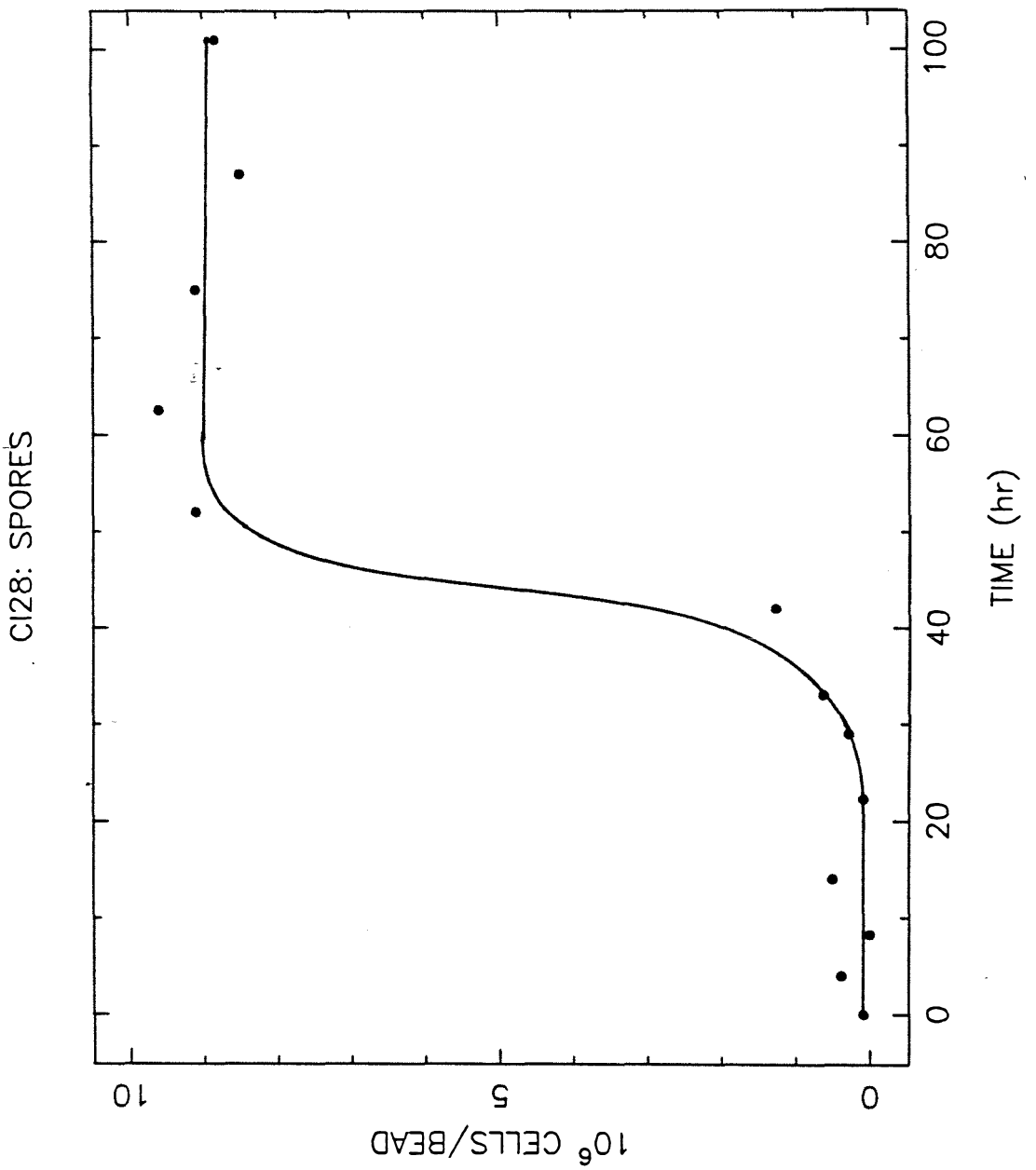

Figure 38. Run CI28 immobilized spore concentration.

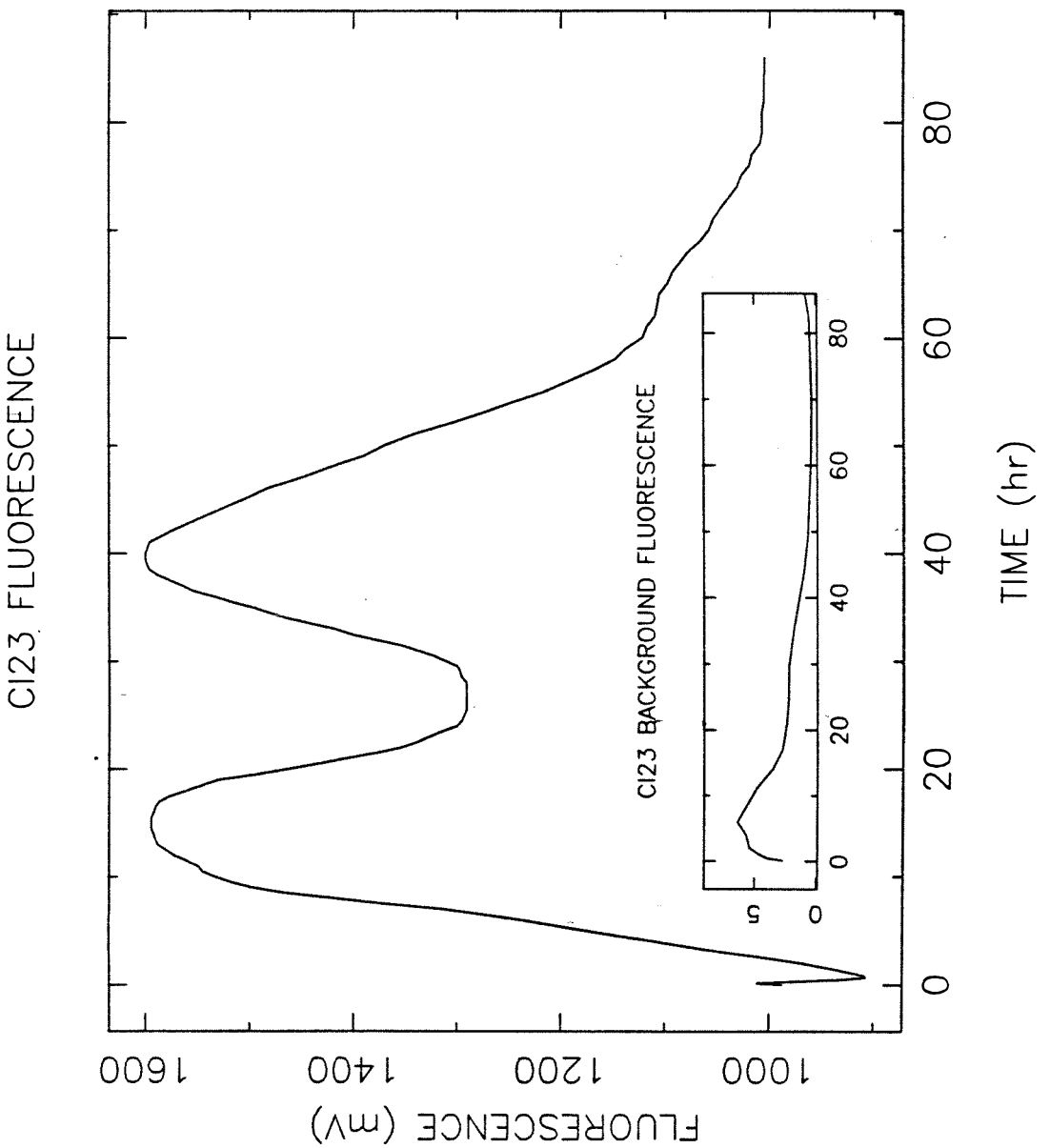

Figure 39. Run CI23 NAD(P)H-dependent fluorescence.

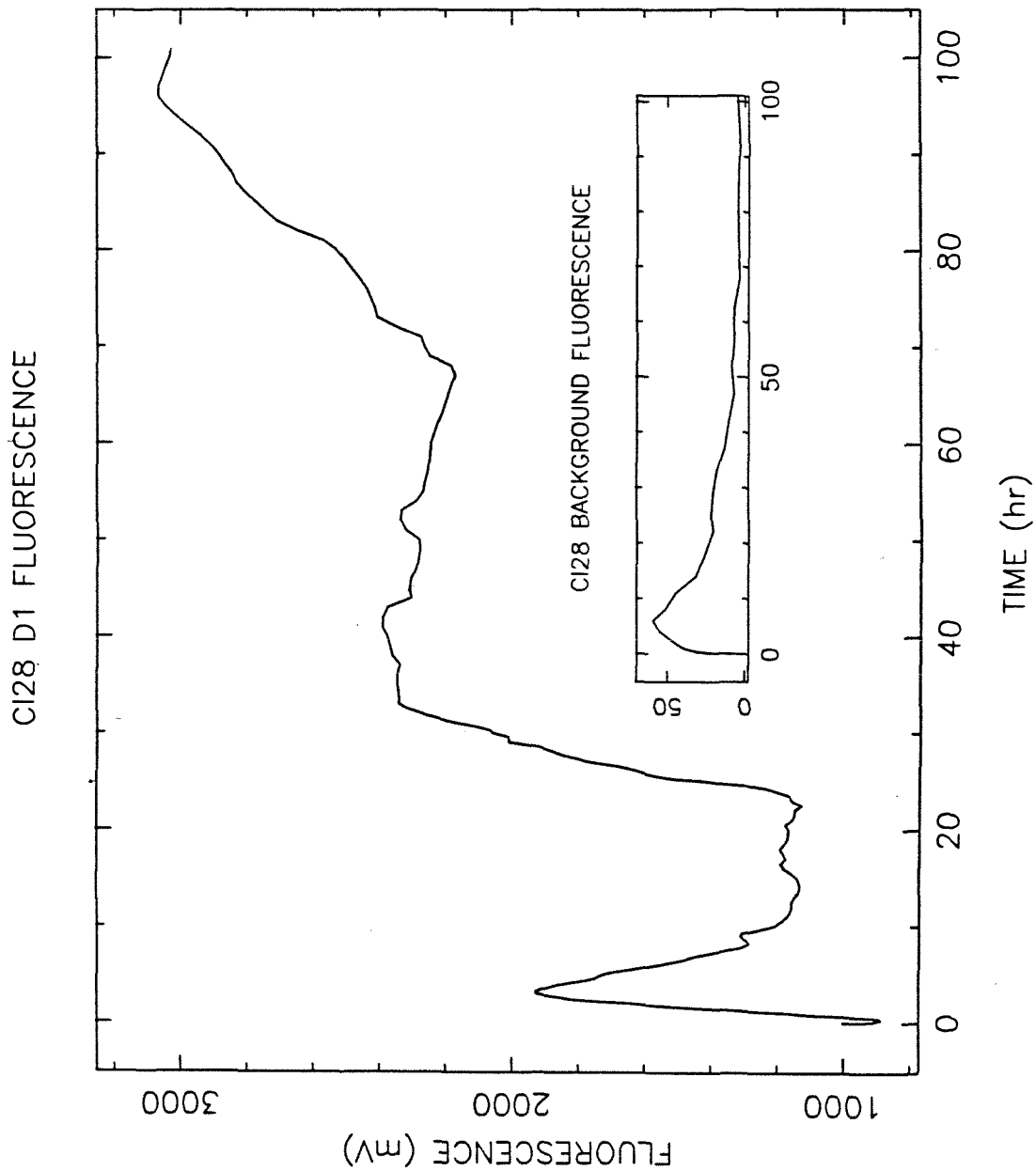

Figure 40. Run CI28 NAD(P)H-dependent fluorescence.

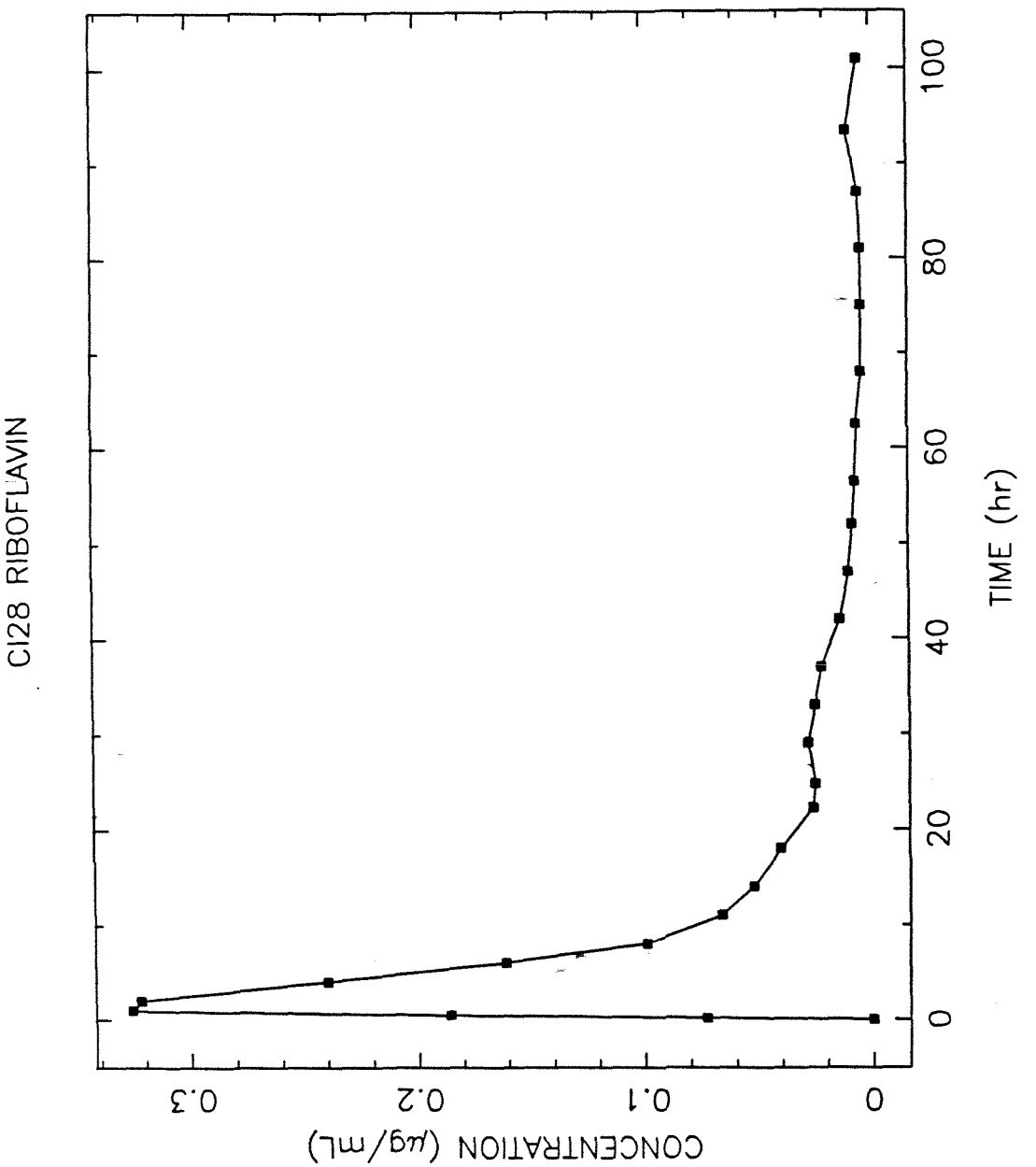

Figure 41. Run CI28 riboflavin concentration profile.

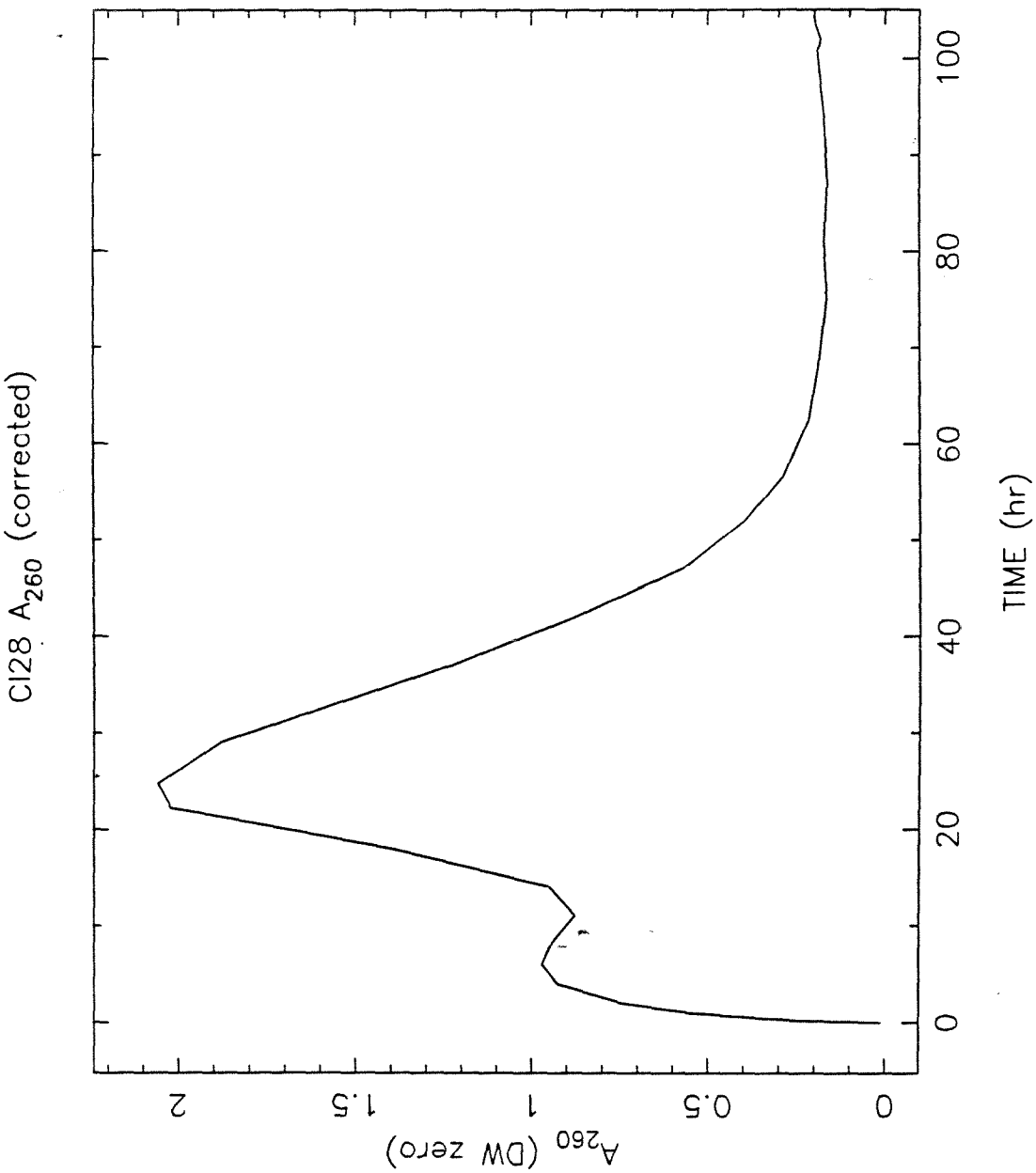

Figure 42. Run CI28 A260 profile.

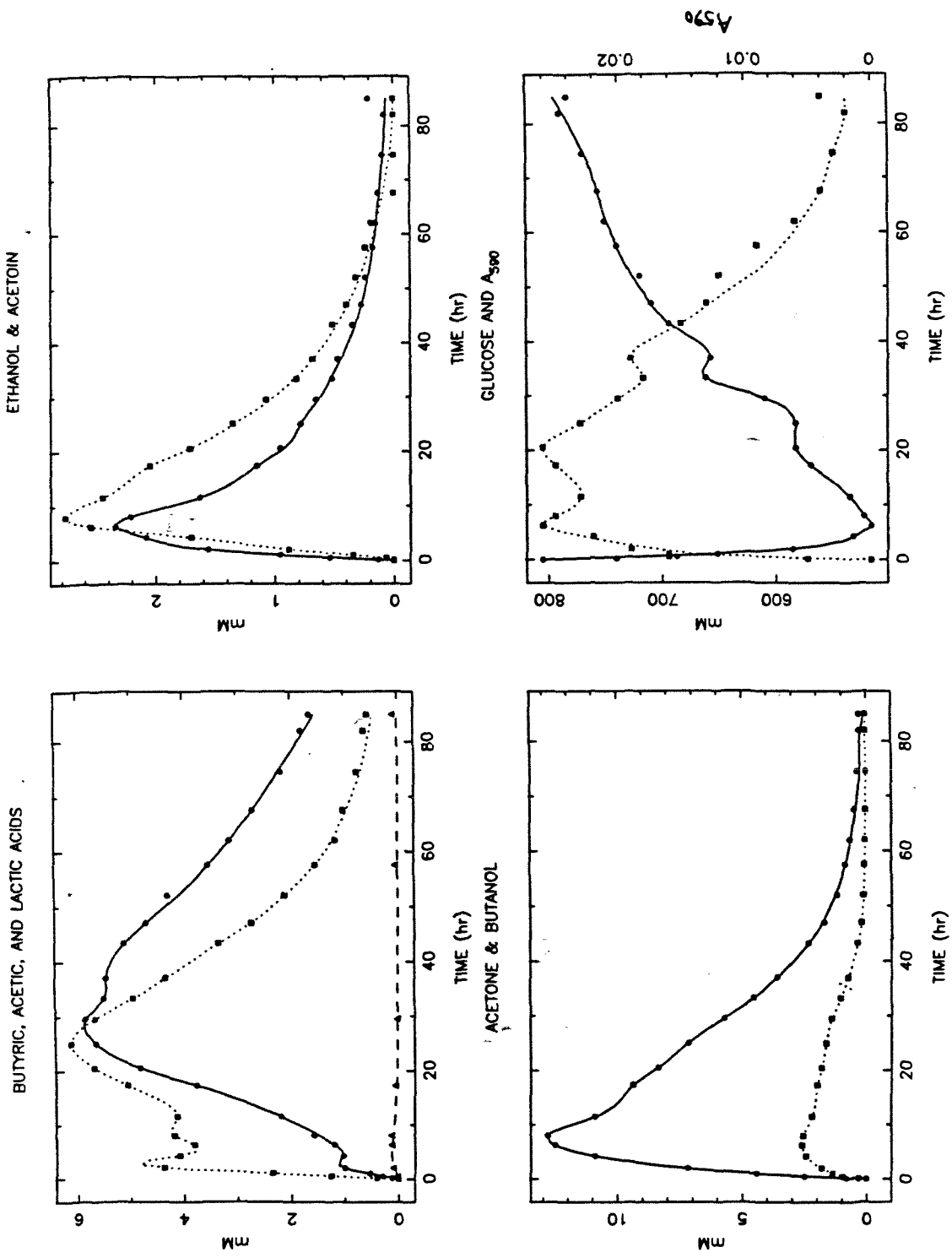

Figure 43. Concentration profiles for experiment CI30. **Upper left**: Butyric acid (solid line), acetic acid (dotted line), and total lactic acid (dashed line). **Upper right**: Ethanol (solid line) and acetoin (dotted line). **Lower left**: Butanol (solid line) and acetone (dotted line). **Lower right**: Glucose (solid line) and A590 (dotted line, right-hand scale).

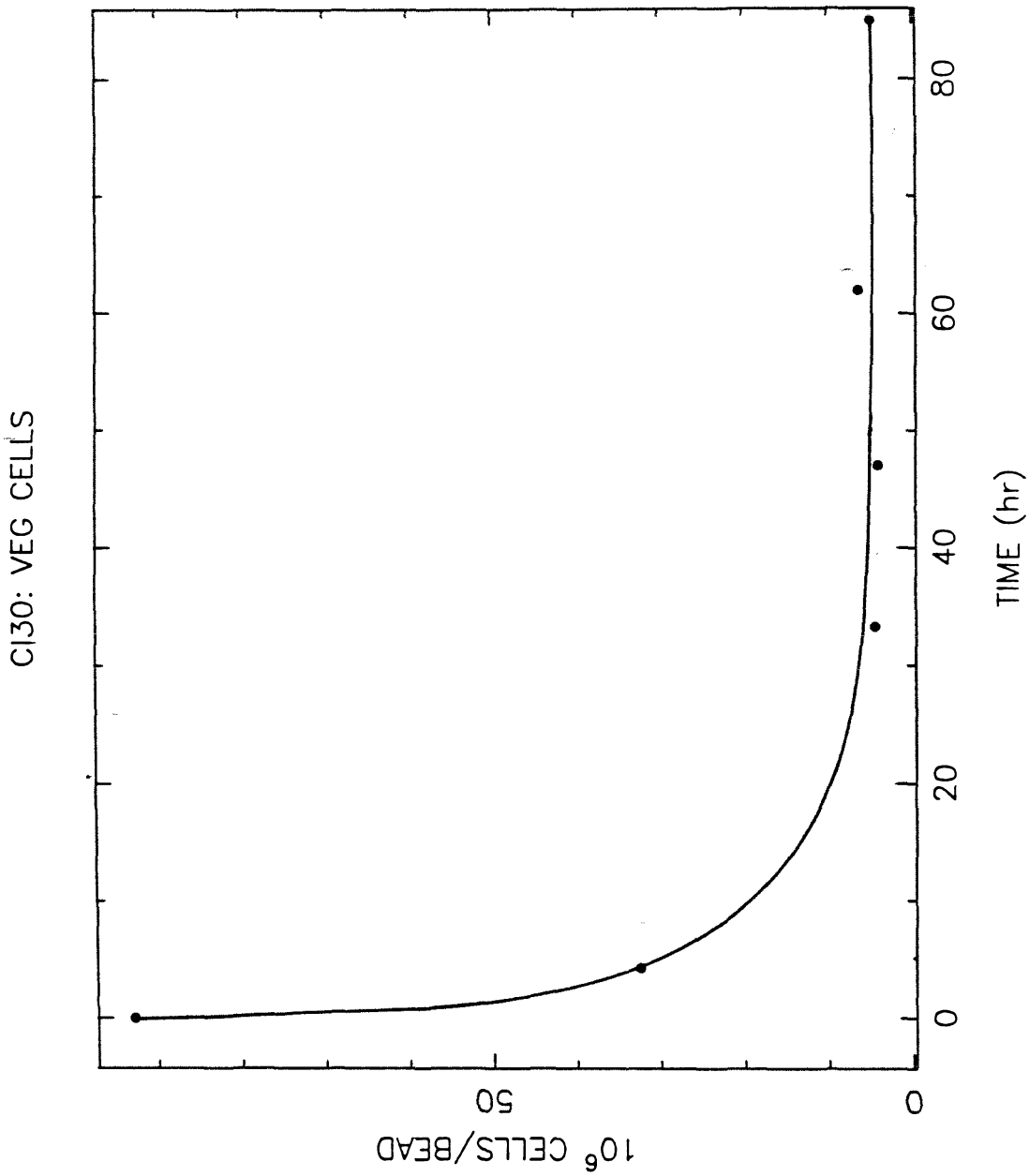

Figure 44. Run CI30 immobilized vegetative cell concentration.

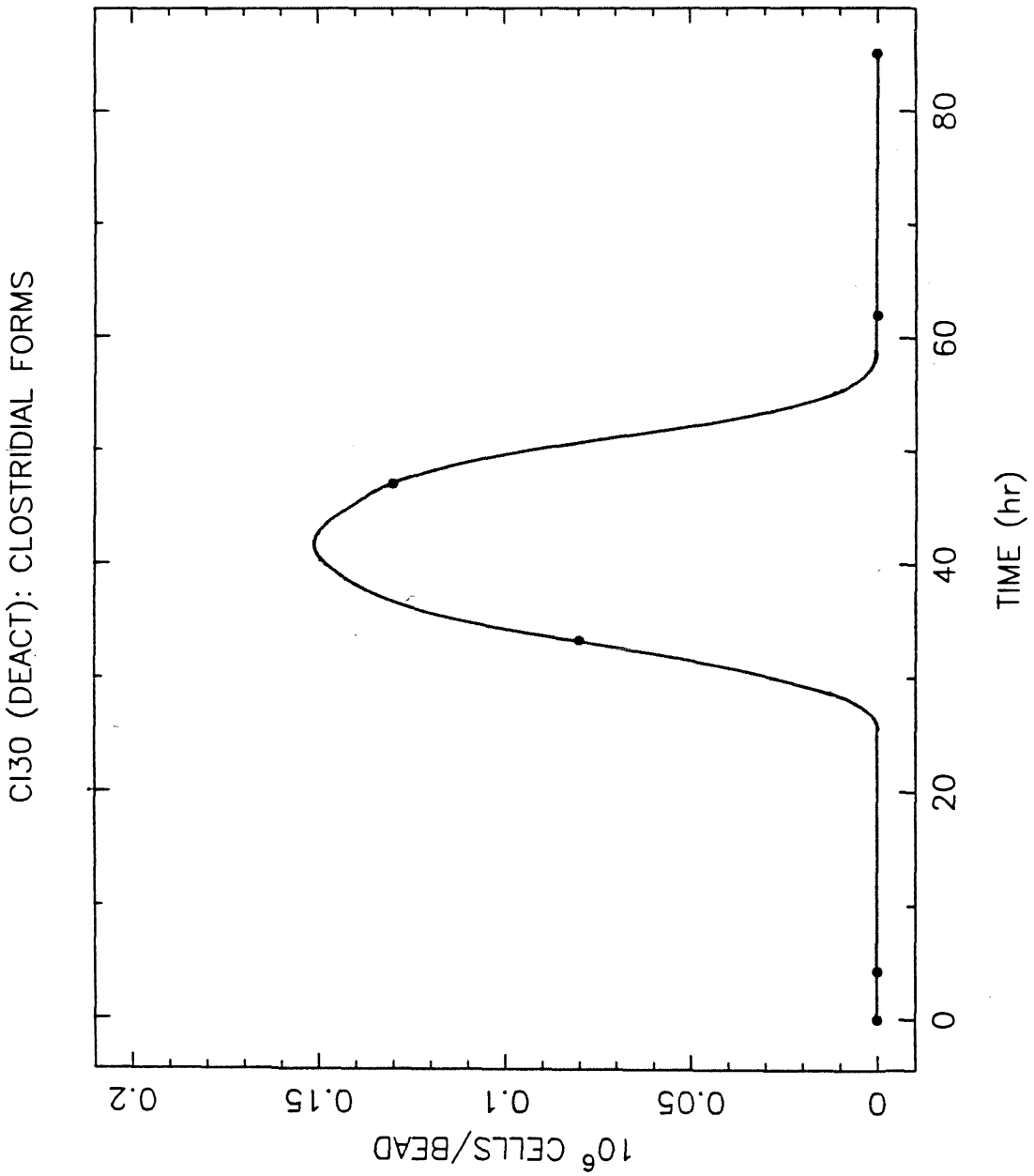

Figure 45. Run CI30 immobilized clostridial form concentrations.

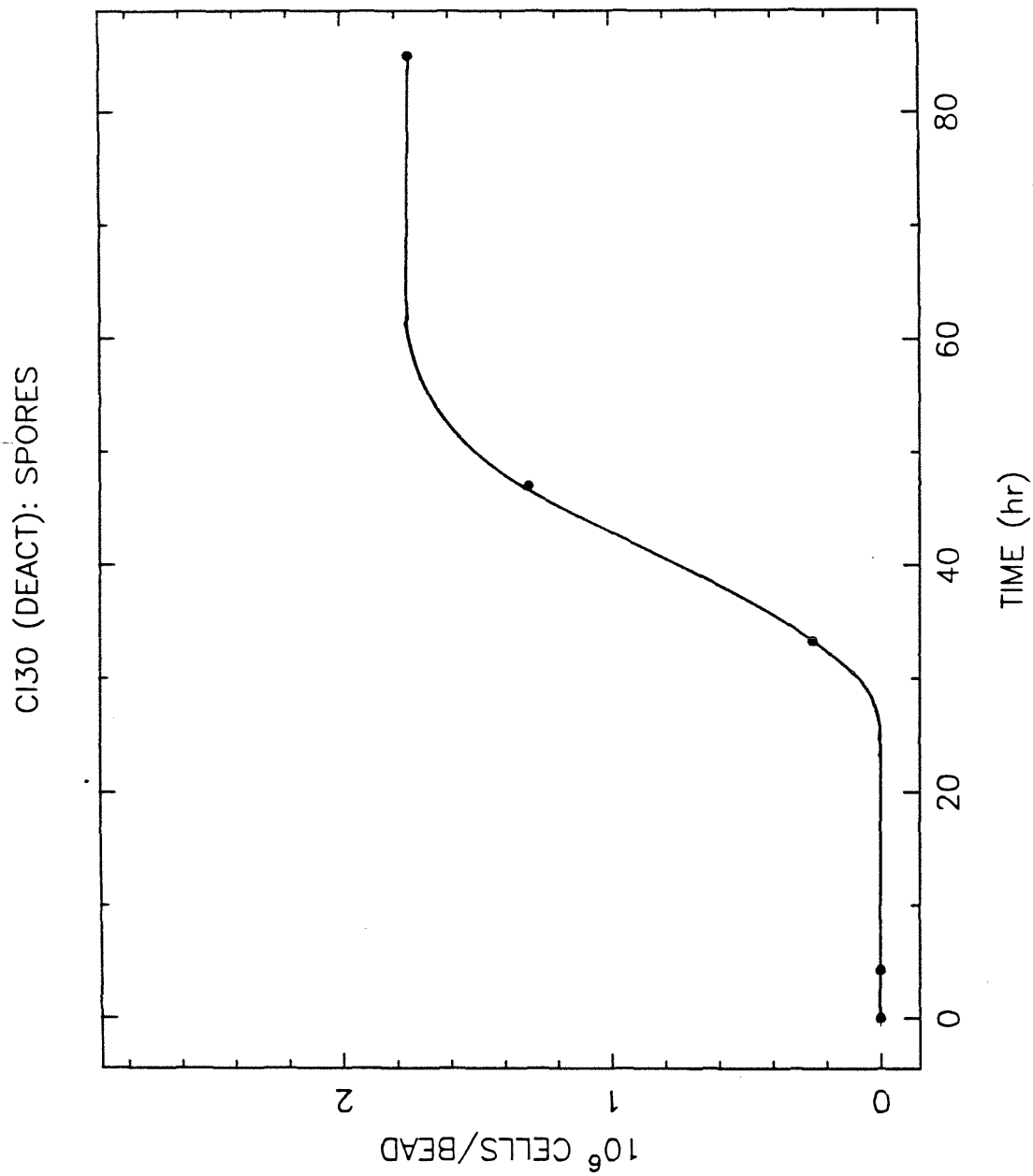

Figure 46. Run CI30 immobilized spore concentrations.

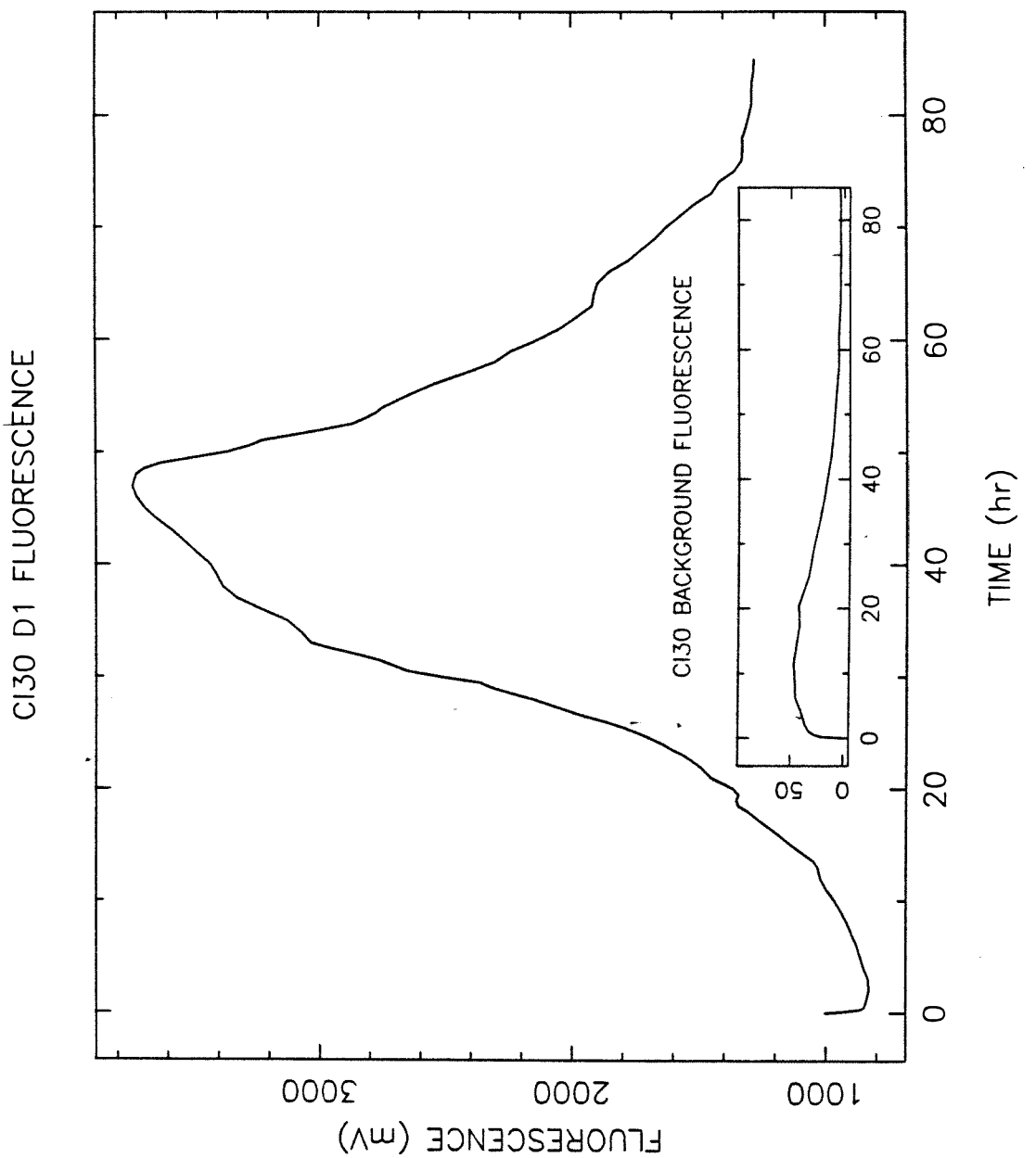

Figure 47. Run CI30 NAD(P)H-dependent fluorescence.

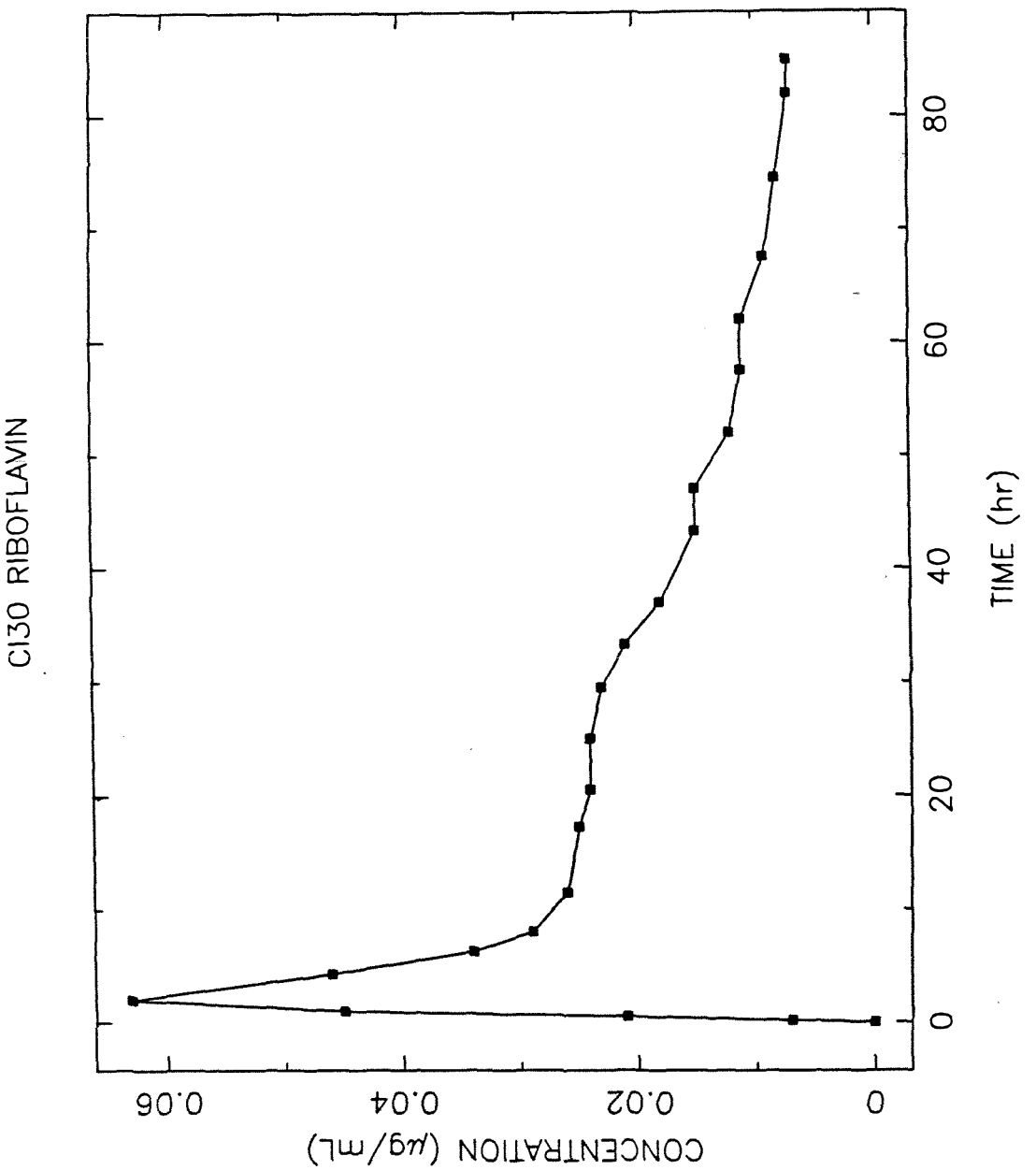

Figure 48. Run CI30 riboflavin concentration profile.

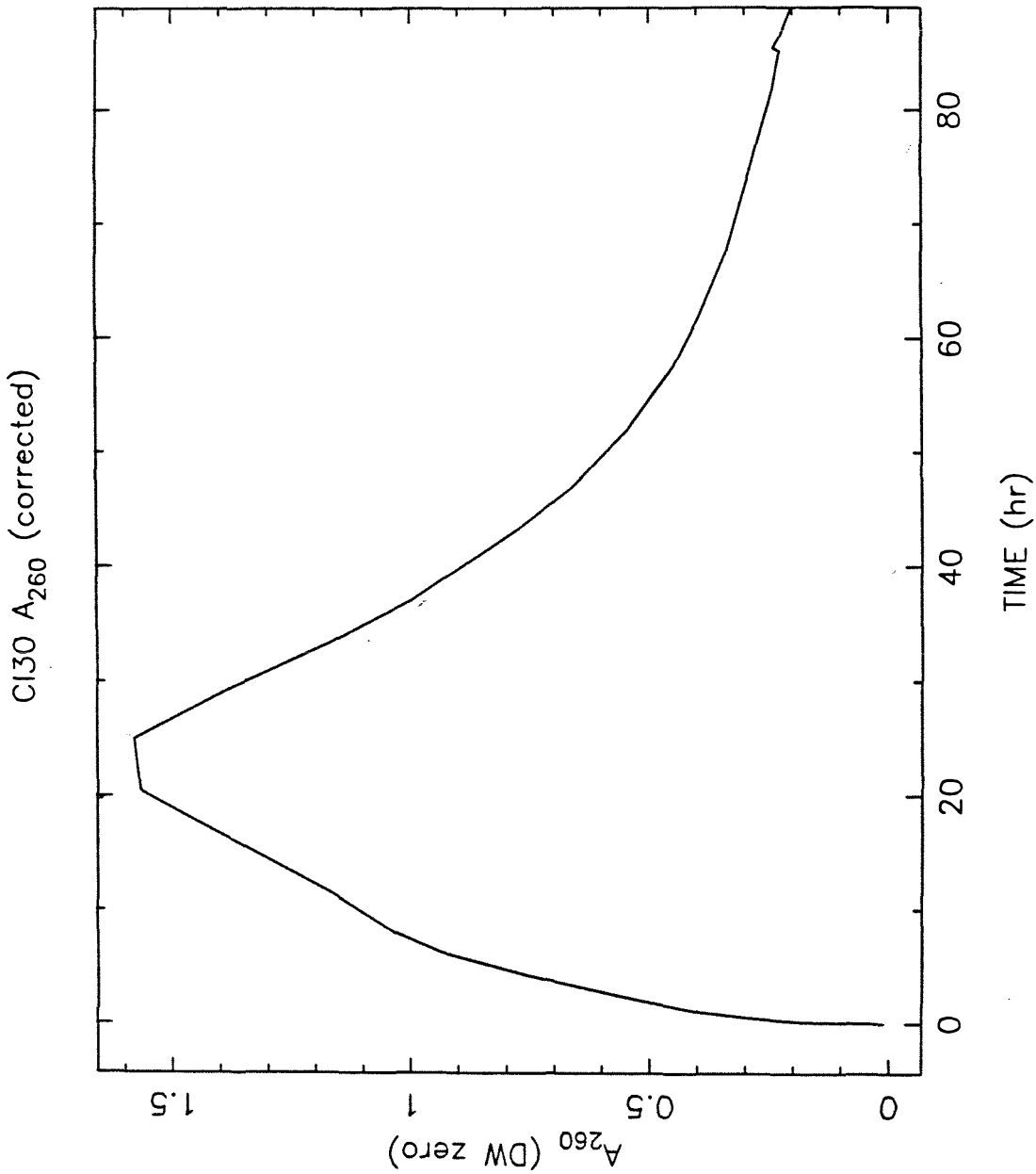

Figure 49. Run CI30 A_{260} profile.

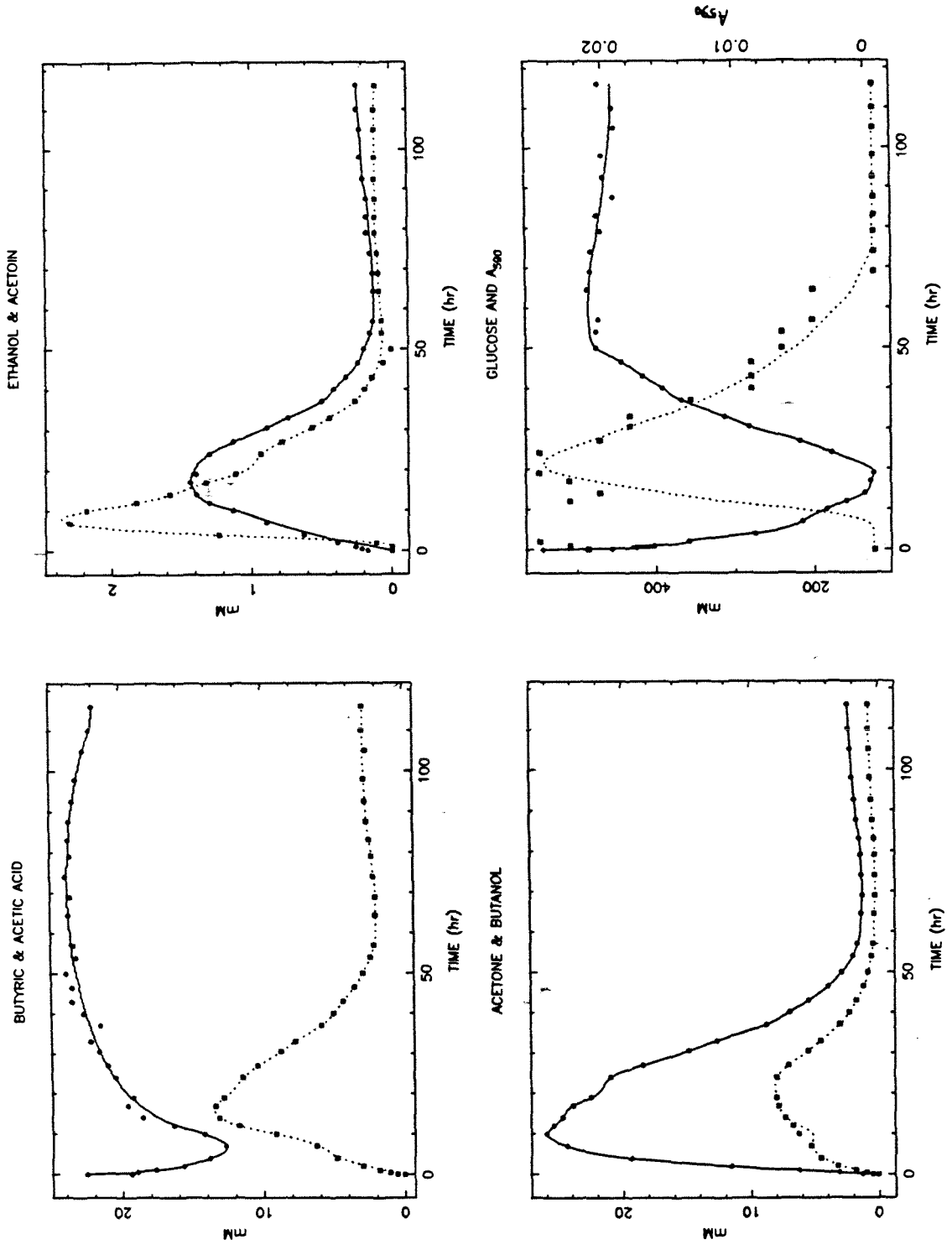

Figure 50. Concentration profiles for experiment CI17. **Upper left**: Butyric acid (solid line) and acetic acid (dotted line). **Upper right**: Ethanol (solid line) and acetoin (dotted line). **Lower left**: Butanol (solid line) and acetone (dotted line). **Lower right**: Glucose (solid line) and A590 (dotted line, right-hand scale).

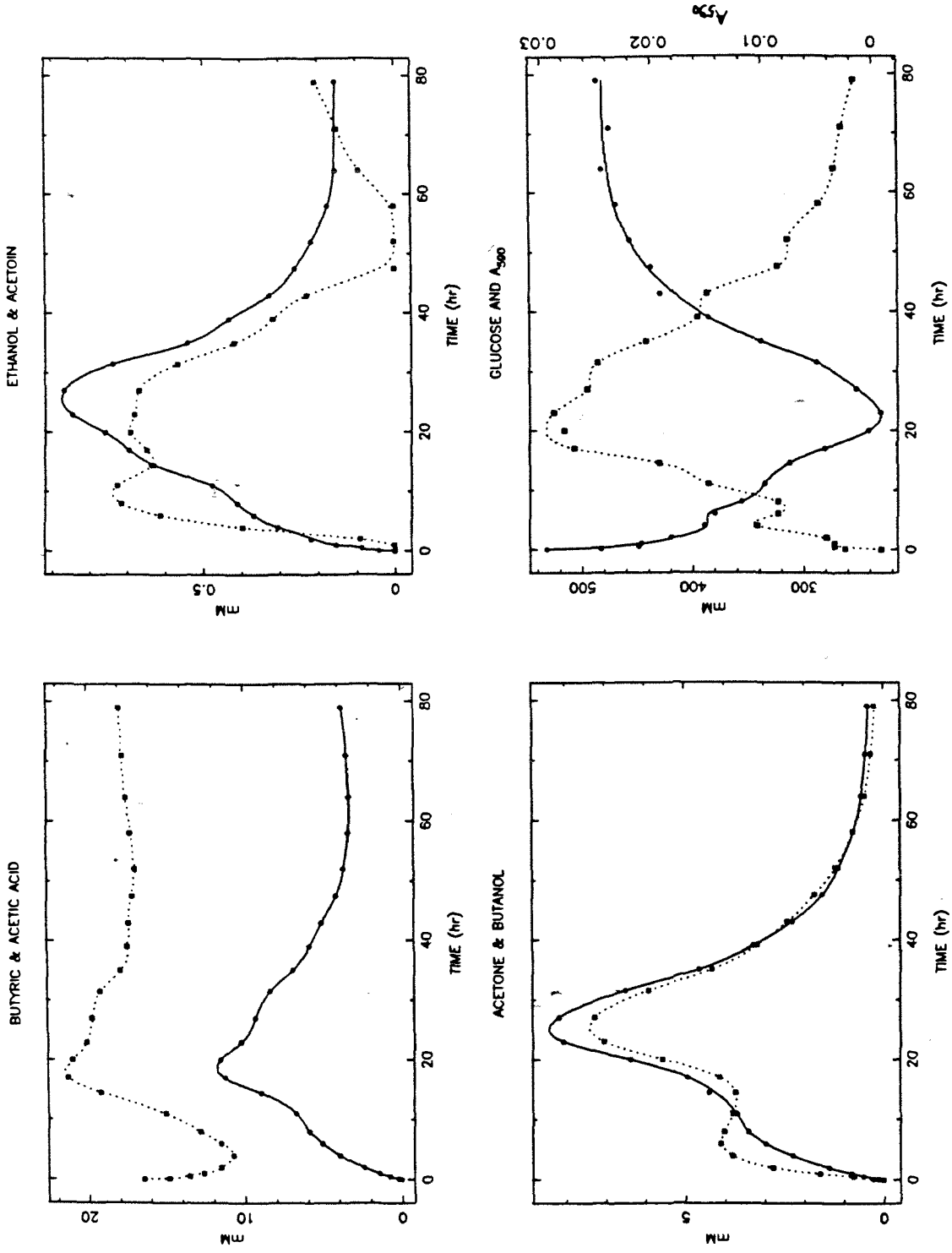

Figure 51. Concentration profiles for experiment CI21. **Upper left**: Butyric acid (solid line) and acetic acid (dotted line). **Upper right**: Ethanol (solid line) and acetoin (dotted line). **Lower left**: Butanol (solid line) and acetone (dotted line). **Lower right**: Glucose (solid line) and A590 (dotted line, right-hand scale).

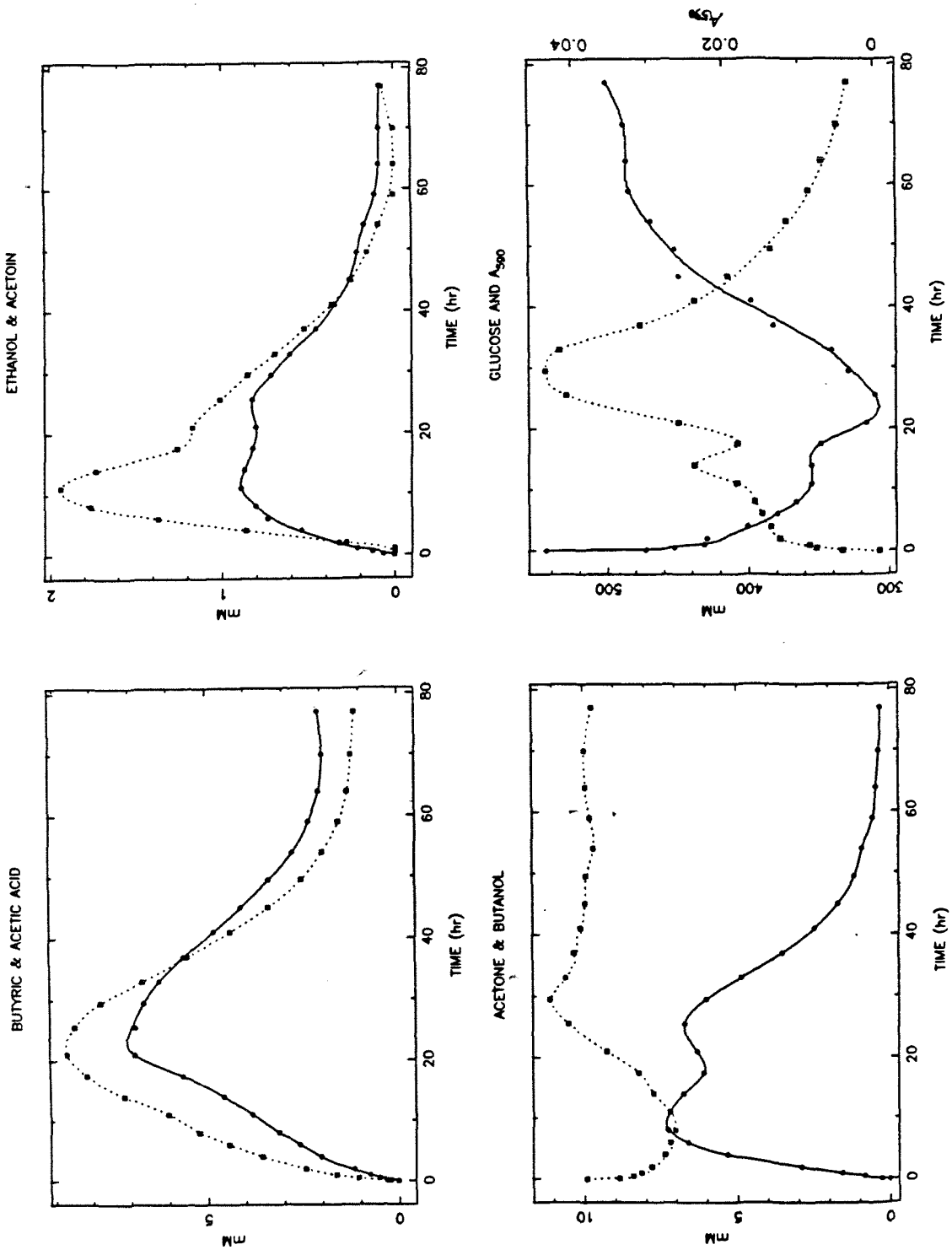

Figure 52. Concentration profiles for experiment CI22. **Upper left**: Butyric acid (solid line) and acetic acid (dotted line). **Upper right**: Ethanol (solid line) and acetoin (dotted line). **Lower left**: Butanol (solid line) and acetone (dotted line). **Lower right**: Glucose (solid line) and A590 (dotted line, right-hand scale).

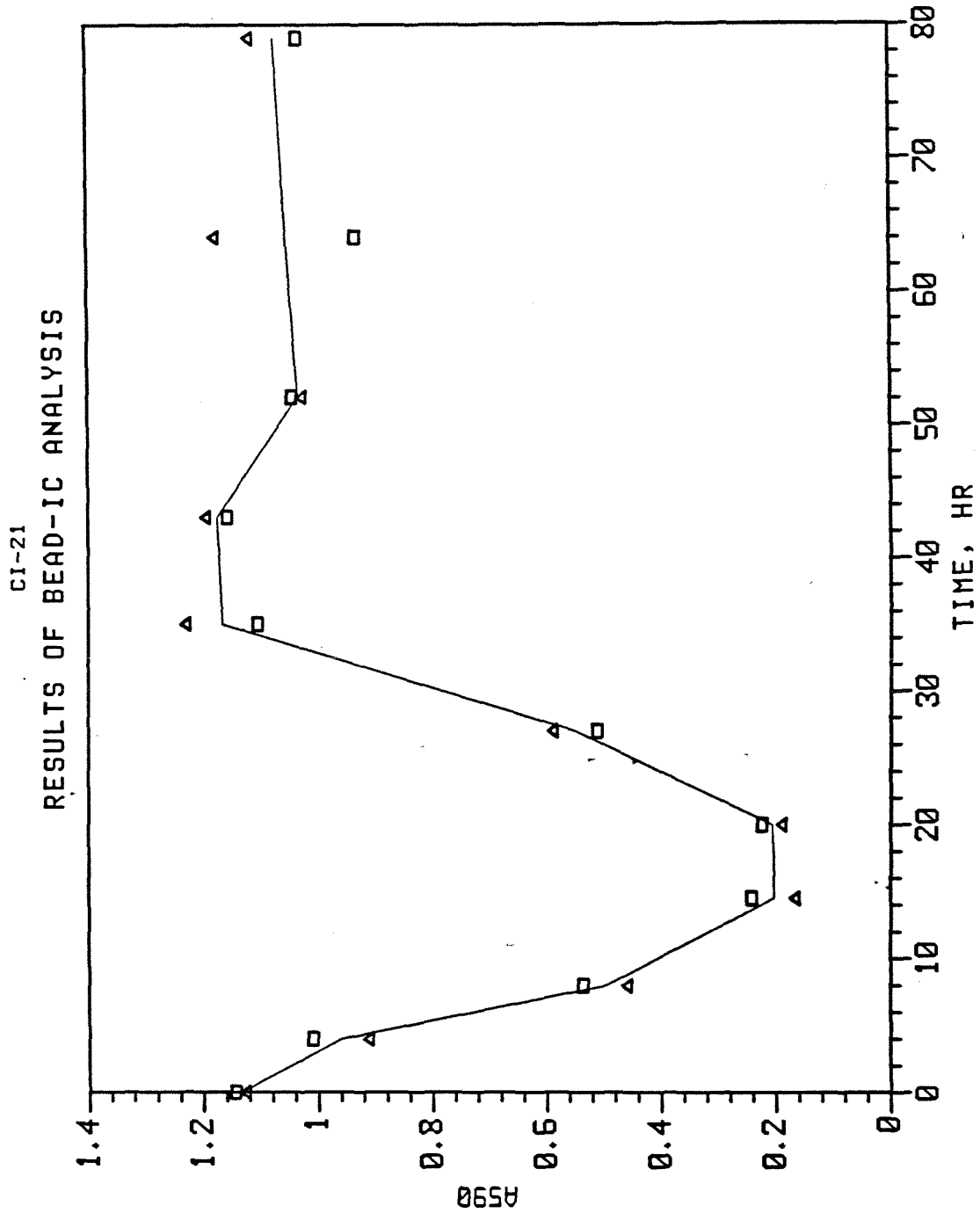

Figure 53. Results for run CI21 of immobilized cell concentration estimation by A_{590} method.

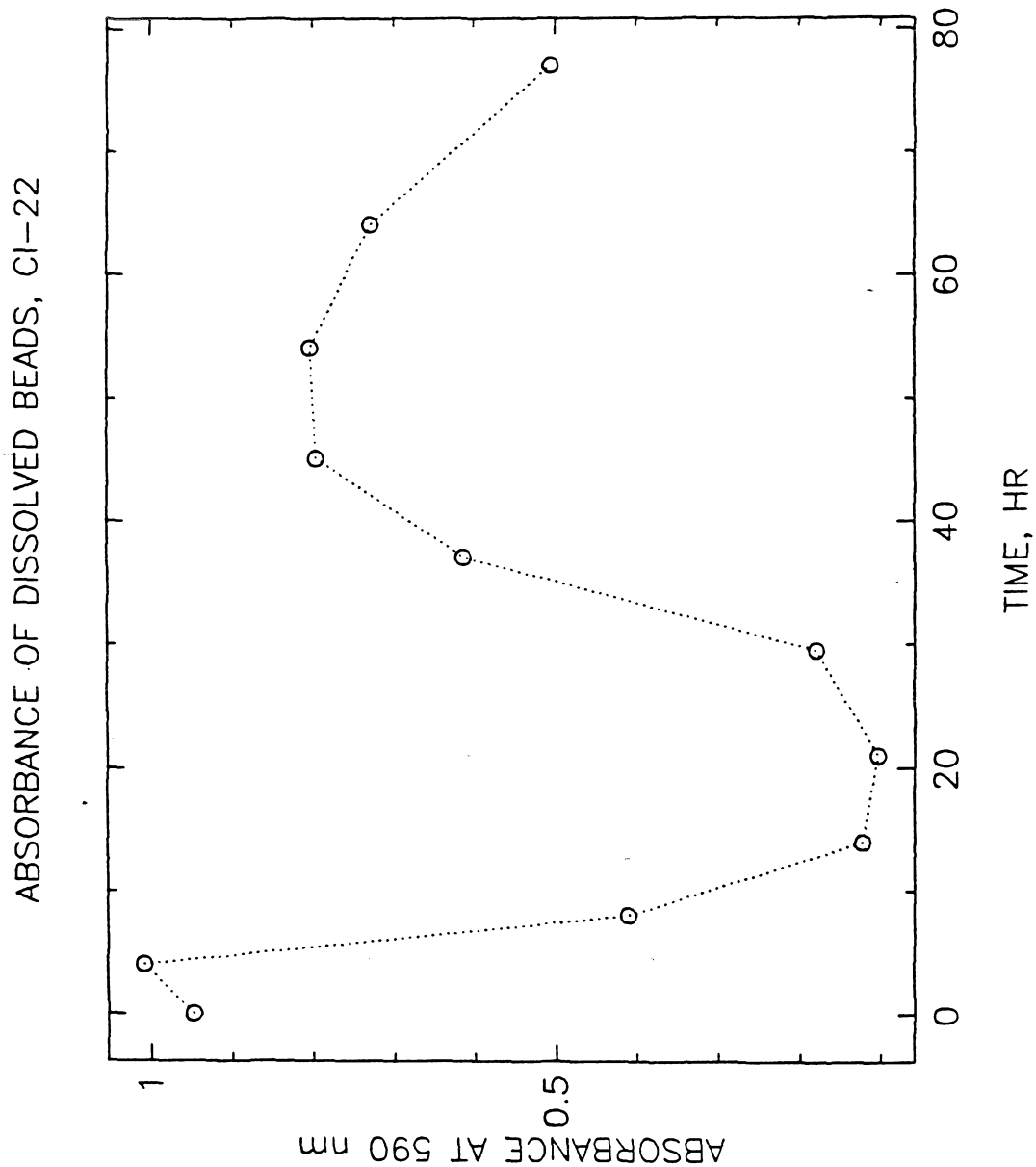

Figure 54. Results for run CI22 of immobilized cell concentration estimation by A_{590} method.

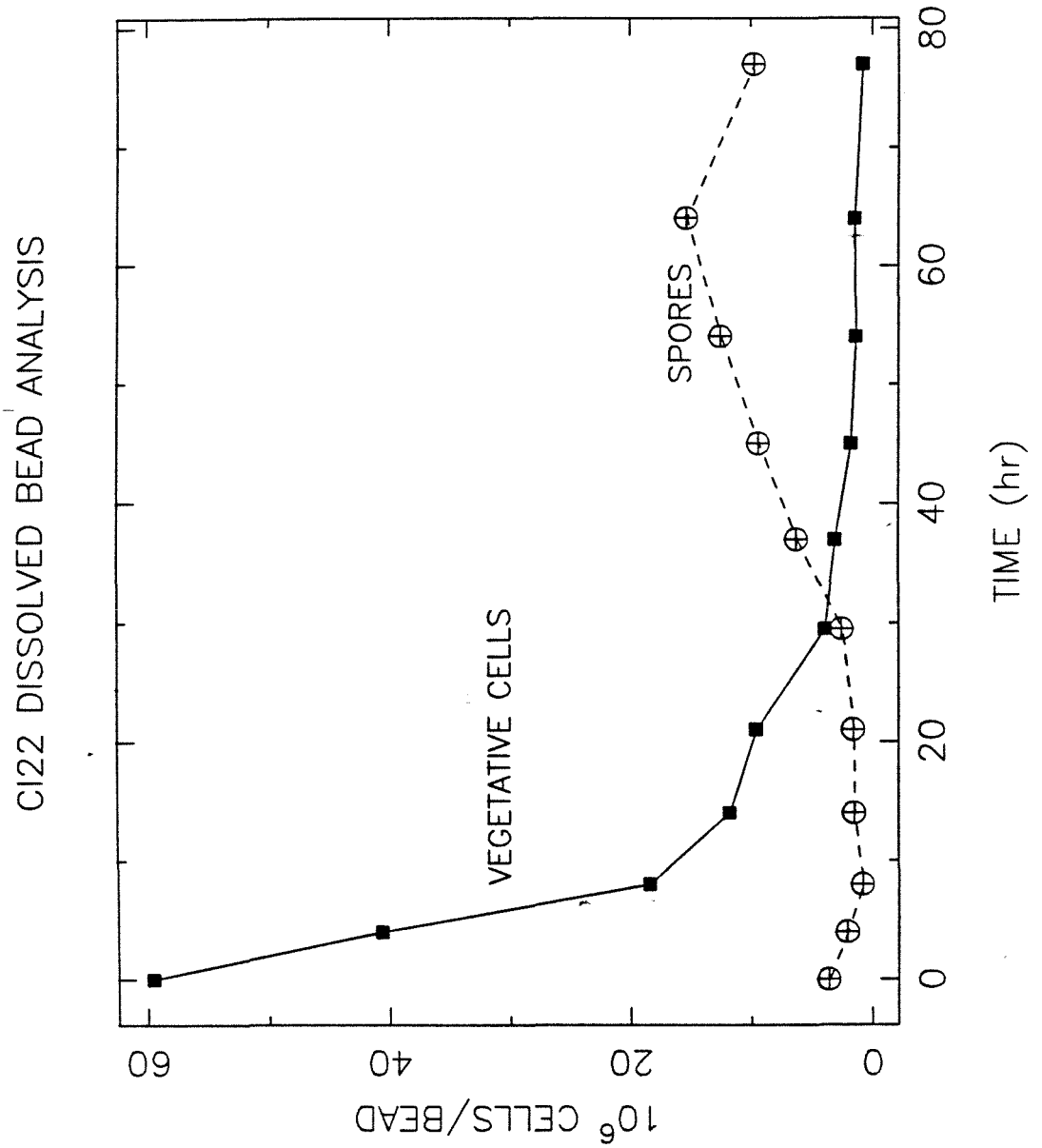

Figure 55. Run CI22 vegetative and spore concentrations determined by direct counting.

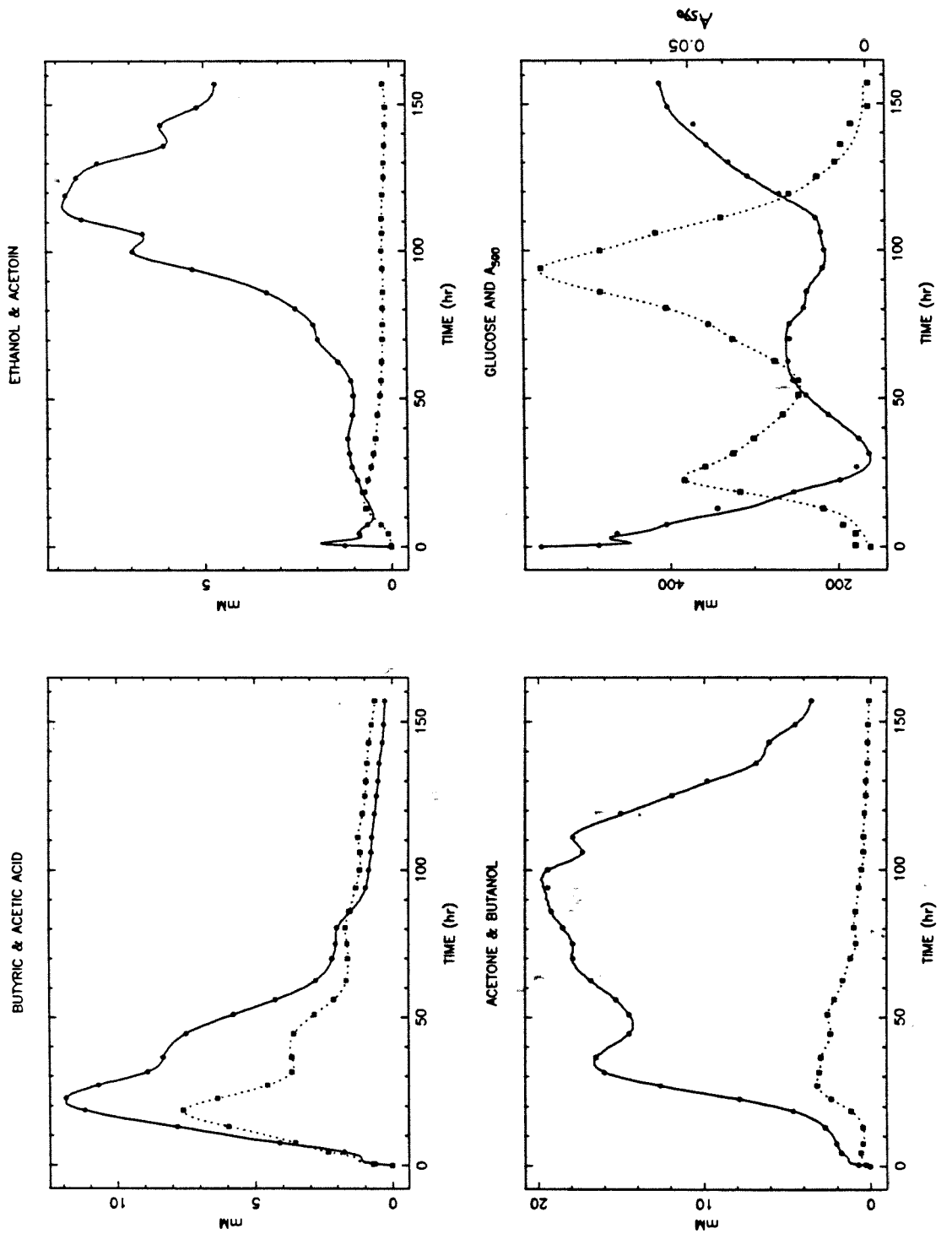

Figure 56. Concentration profiles for experiment CI12. **Upper left**: Butyric acid (solid line) and acetic acid (dotted line). **Upper right**: Ethanol (solid line) and acetoin (dotted line). **Lower left**: Butanol (solid line) and acetone (dotted line). **Lower right**: Glucose (solid line) and A590 (dotted line, right-hand scale).

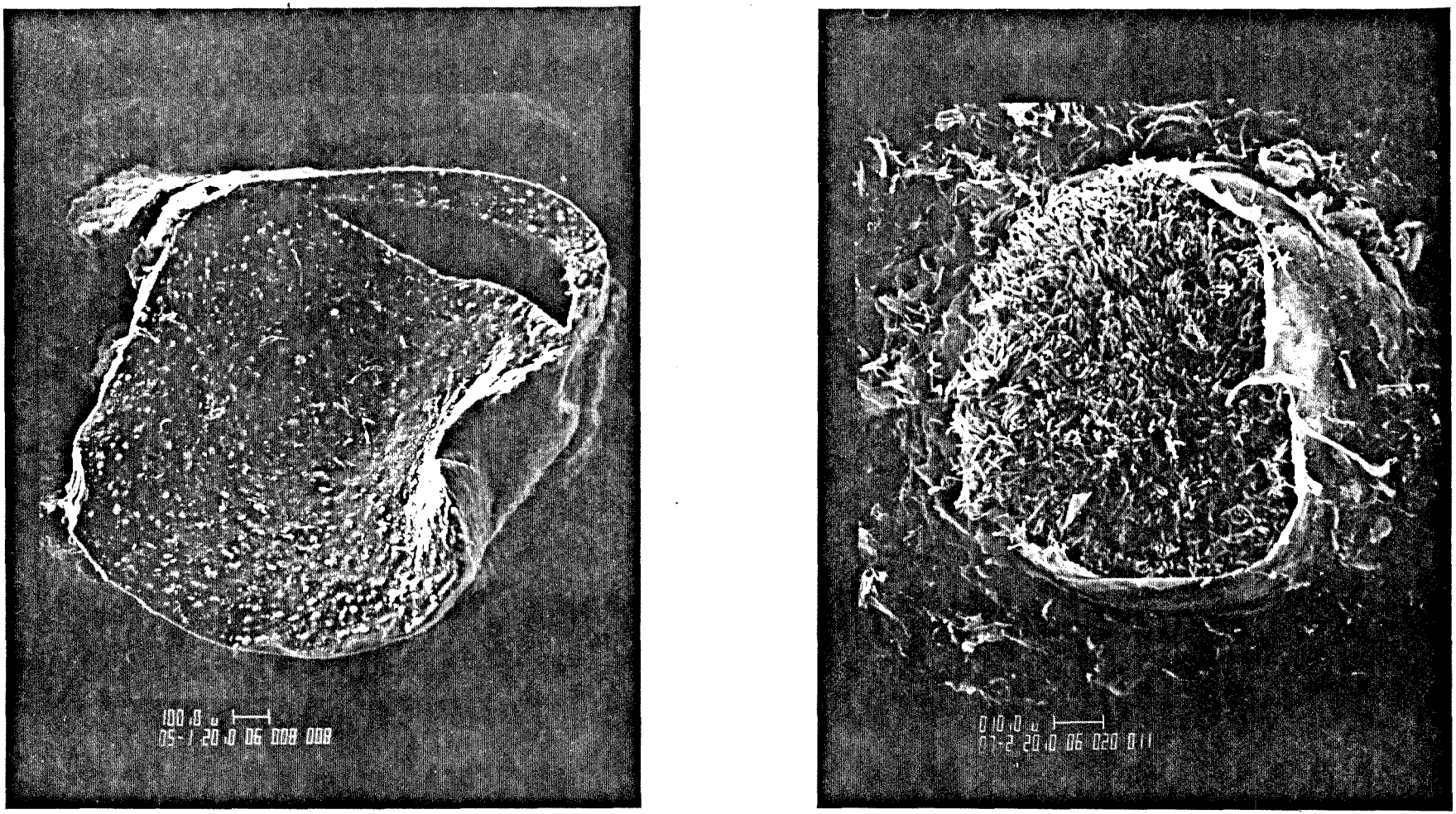

Figure 57. Scanning electron micrographs. The bar in the legend below each photograph shows the length scale in μm. **A (left)**: Bead sample from run CI21 showing homogeneous distribution of immobilized cell colonies. **B (right)**: Run CI22 sample, start of bioconversion.

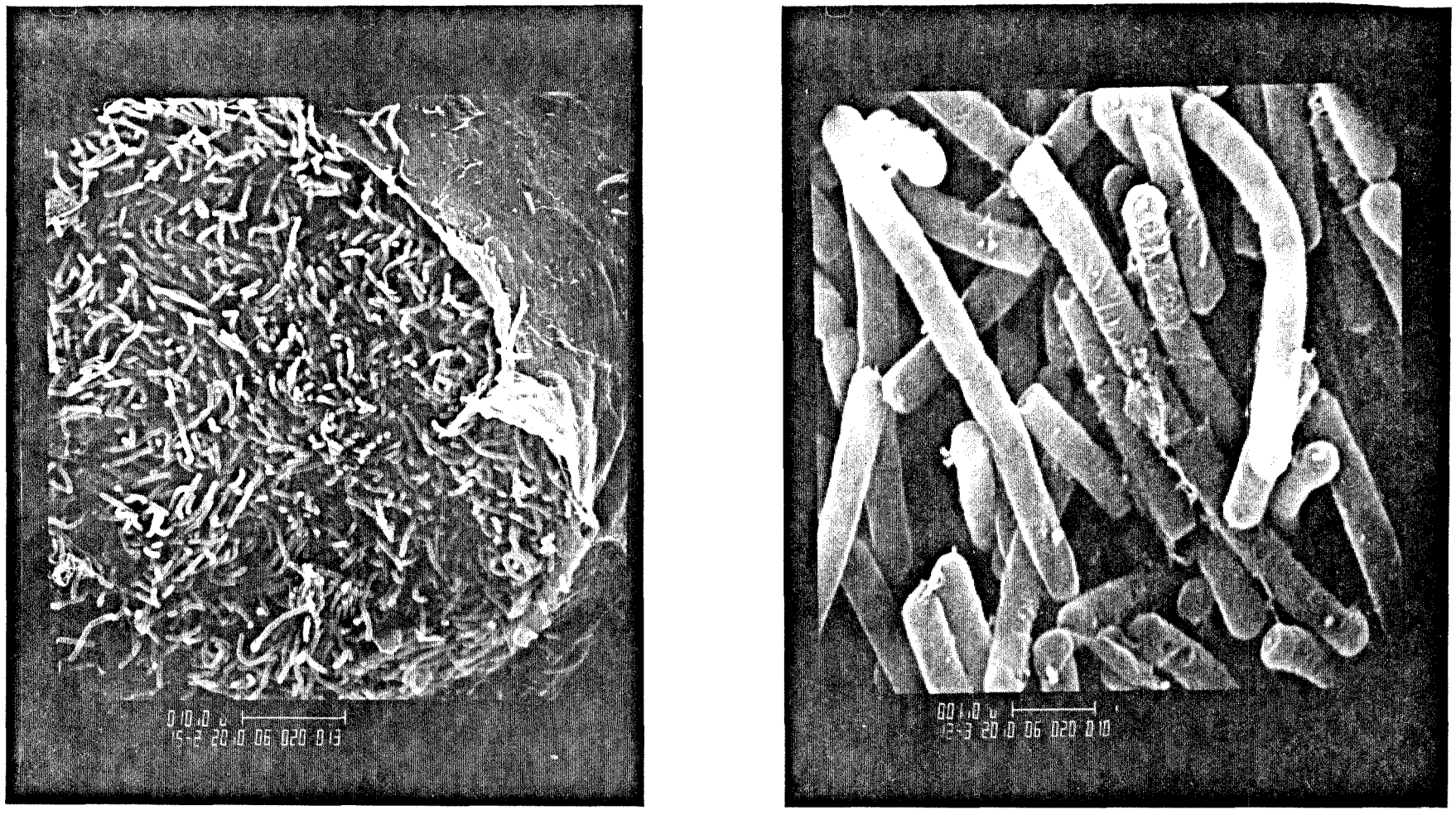

Figure 58. Scanning electron micrographs. The bar in the legend below each photograph shows the length scale in μm. **A (left)**: Run CI22 sample, start of bioconversion. **B (right)**: Vegetative cells at start of run CI22.

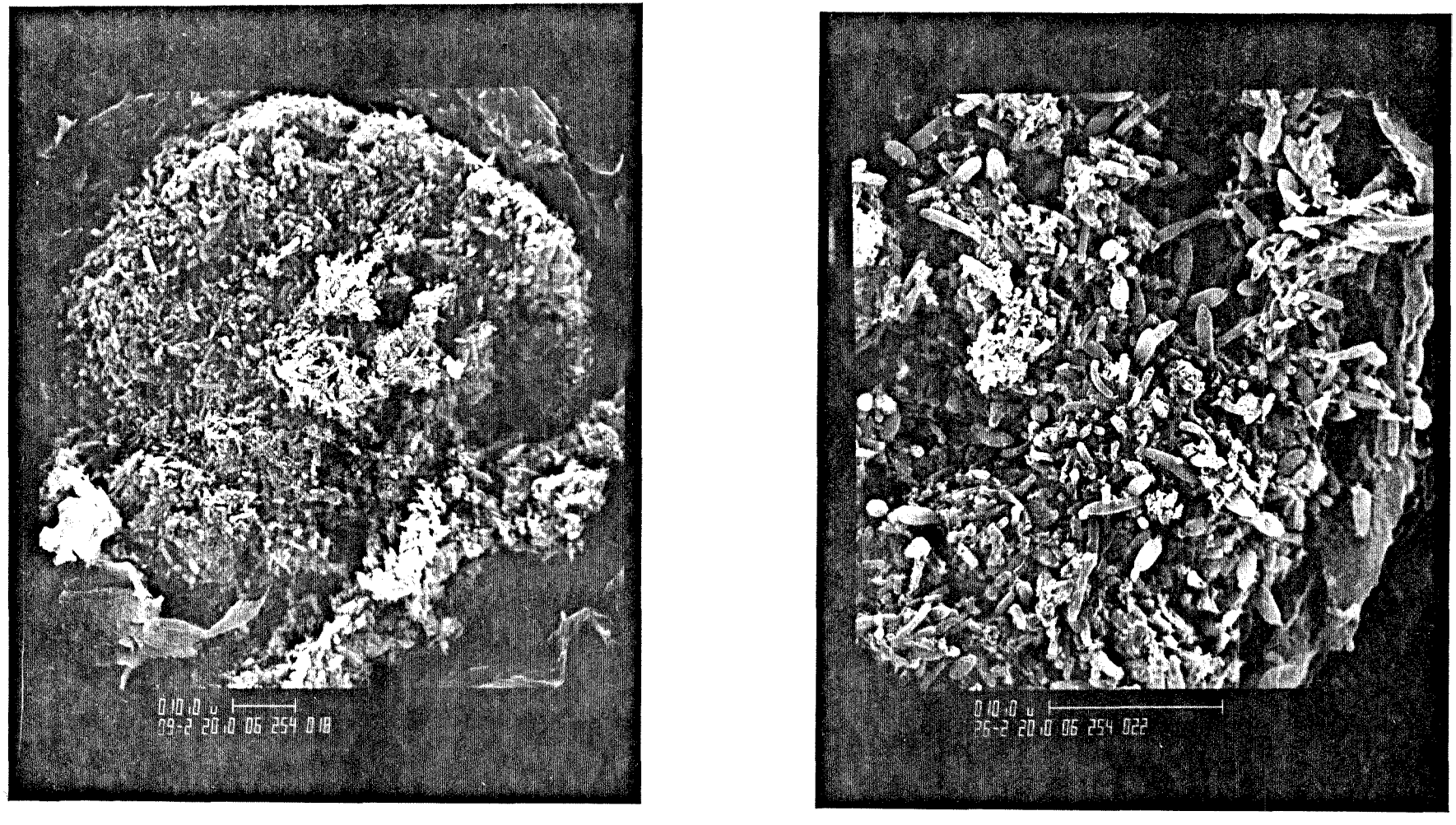

Figure 59. Scanning electron micrographs. The bar in the legend below each photograph shows the length scale in μm. **A (left), B (right)**: Run CI22, 54 hours of bioconversion.

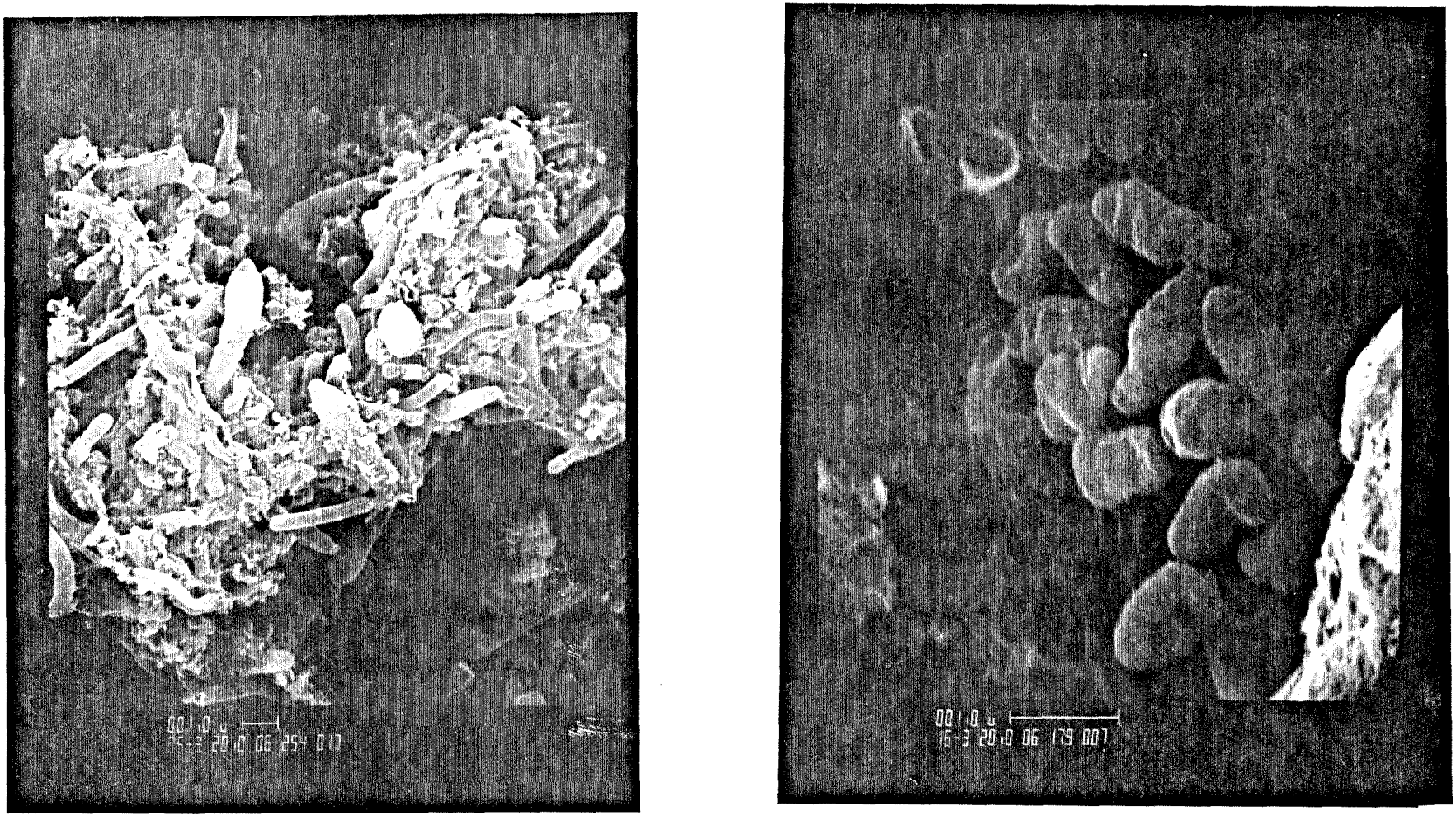

Figure 60. Scanning electron micrographs. The bar in the legend below each photograph shows the length scale in μm. **A (left)**: Run CI22 sample, 54 hours of bioconversion. **B (right)**: Run CI21 spores from a sample after 79 hours of bioconversion.

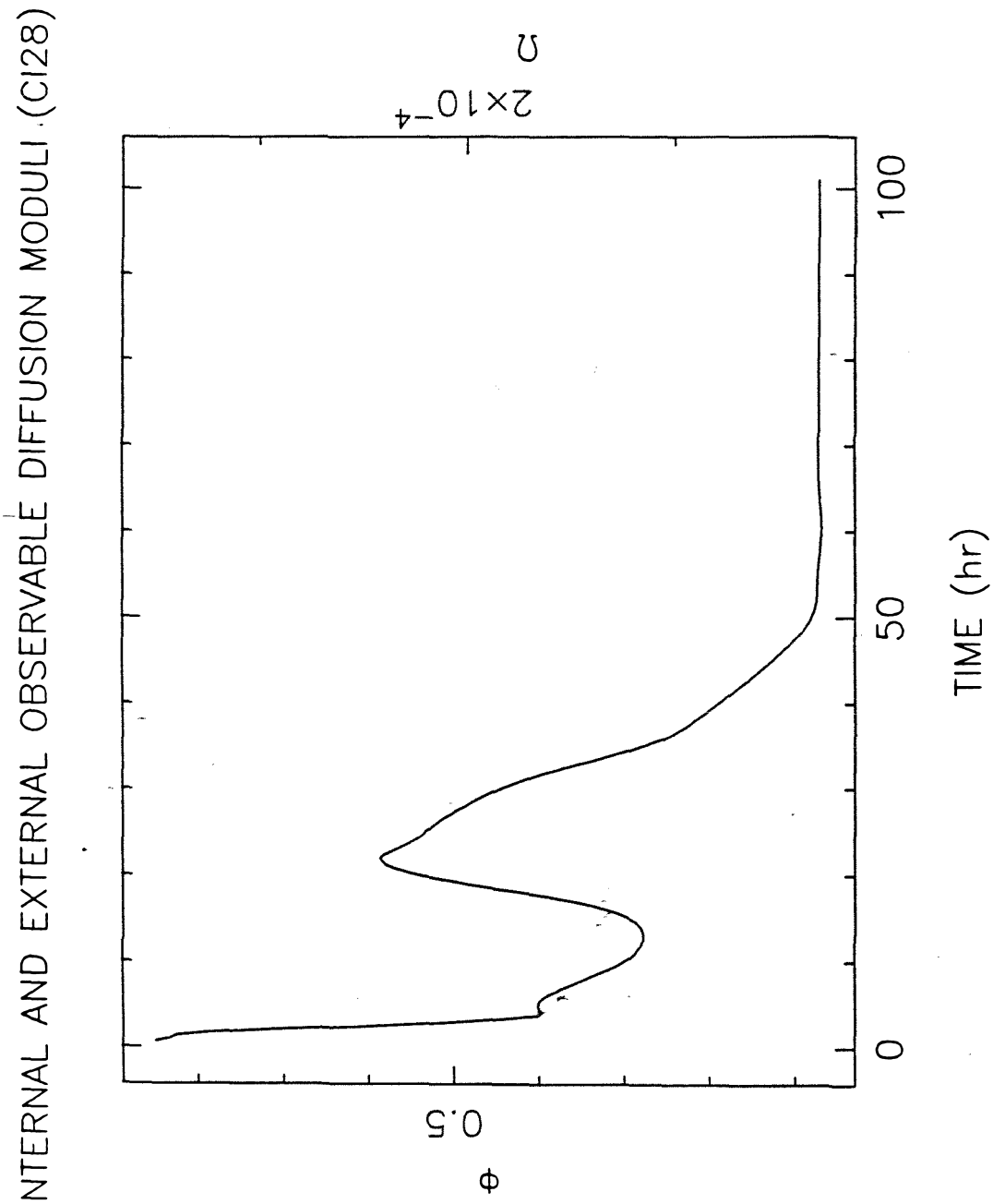

Figure 61. Internal and external diffusion moduli. Calculations based on run CI28.

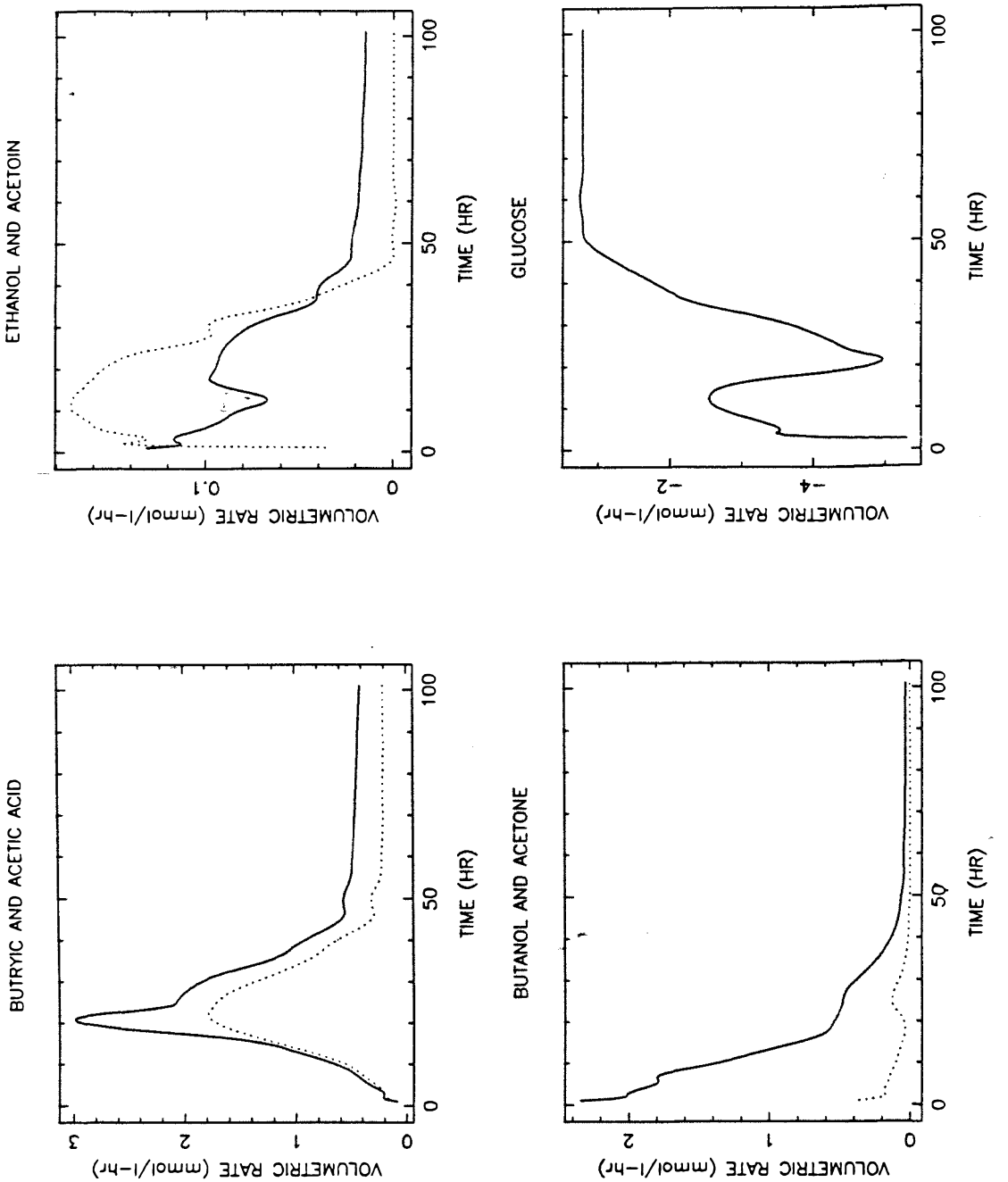

Figure 62. Volumetric rates of product formation for experiment CI28. **Upper left**: butyric acid (solid line) and acetic acid (dotted line). **Upper right**: ethanol (solid line) and acetoin (dotted line). **Lower left**: butanol (solid line) and acetone (dotted line). **Lower right**: glucose.

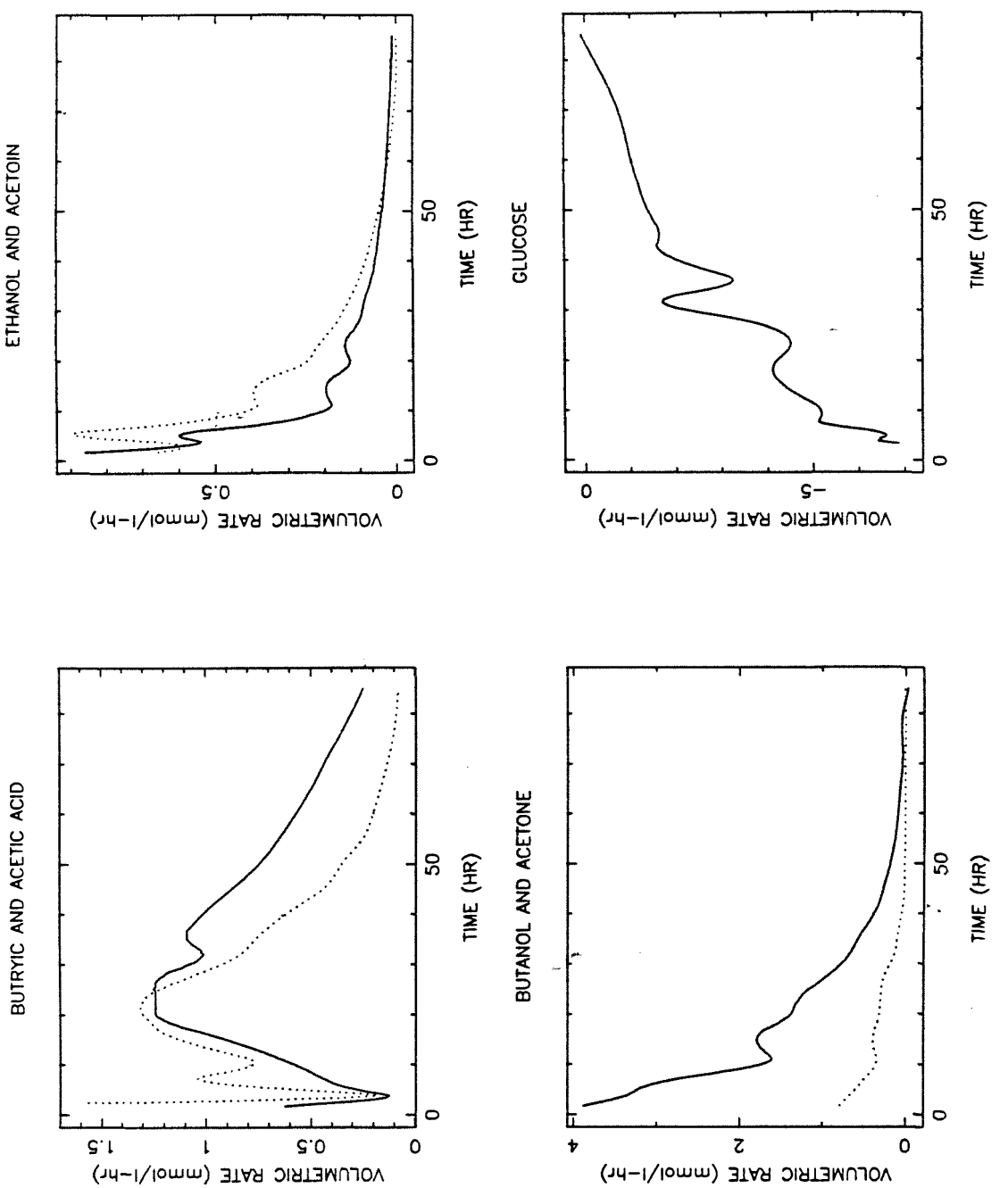

Figure 63. Volumetric rates of product formation for experiment CI30. **Upper left**: butyric acid (solid line) and acetic acid (dotted line). **Upper right**: ethanol (solid line) and acetoin (dotted line). **Lower left**: butanol (solid line) and acetone (dotted line). **Lower right**: glucose.

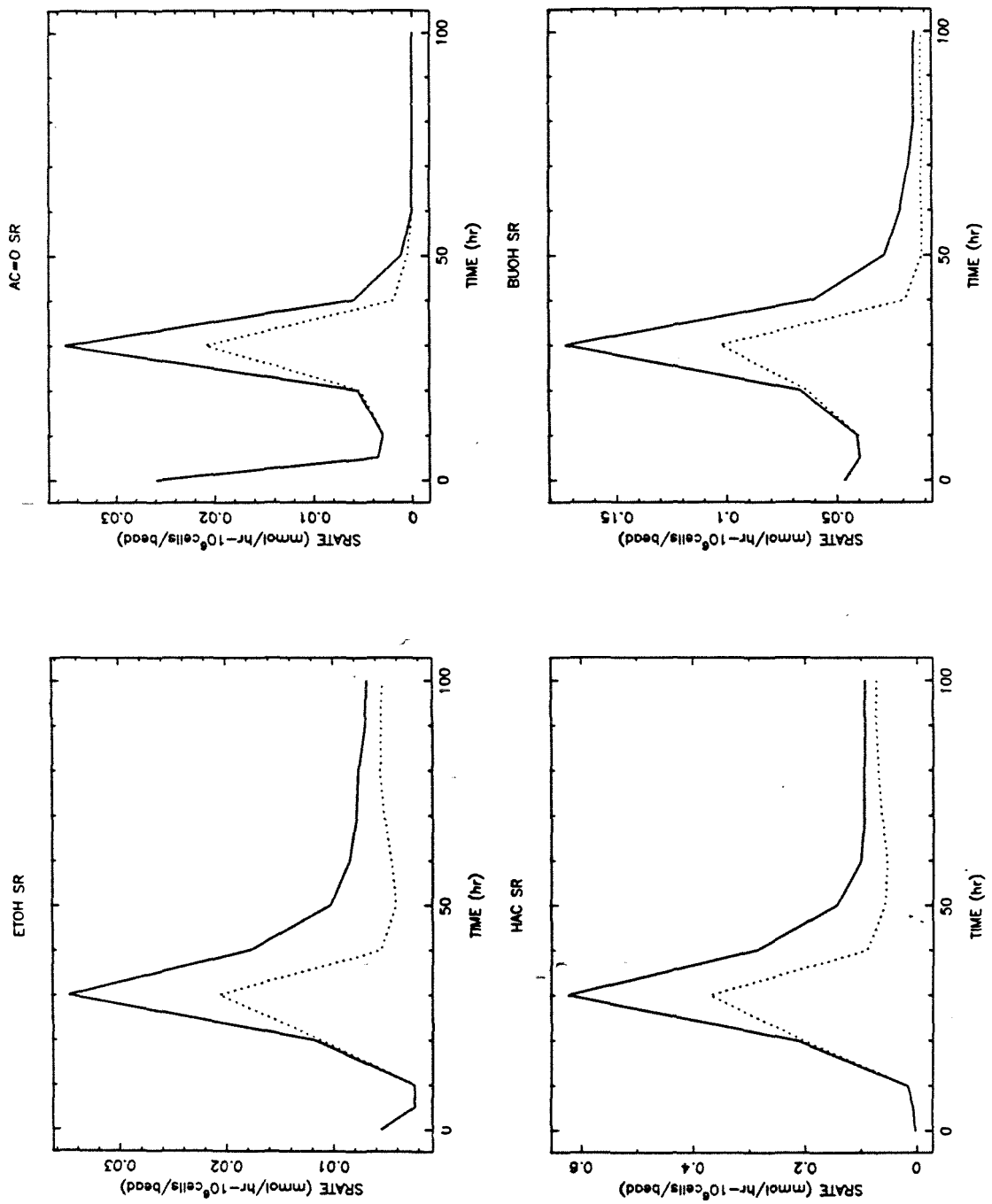

Figure 64. Run CI28 specific rates of product formation based on vegetative cell concentrations (solid lines) and vegetative plus clostridial cell concentrations (dotted lines).

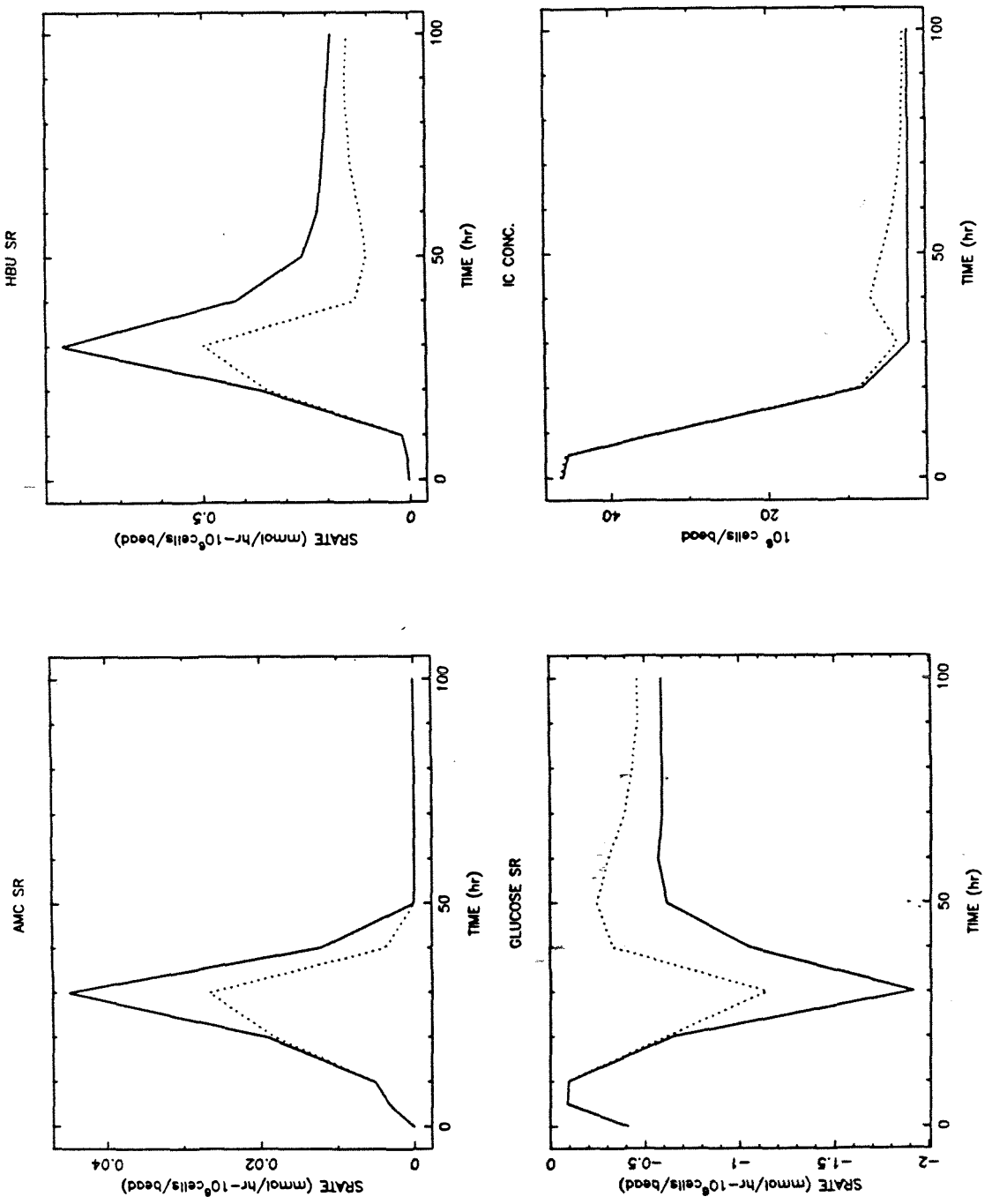

Figure 65. Run CI28 specific rates of product formation based on vegetative cell concentrations (solid lines) and vegetative plus clostridial cell concentrations (dotted lines).

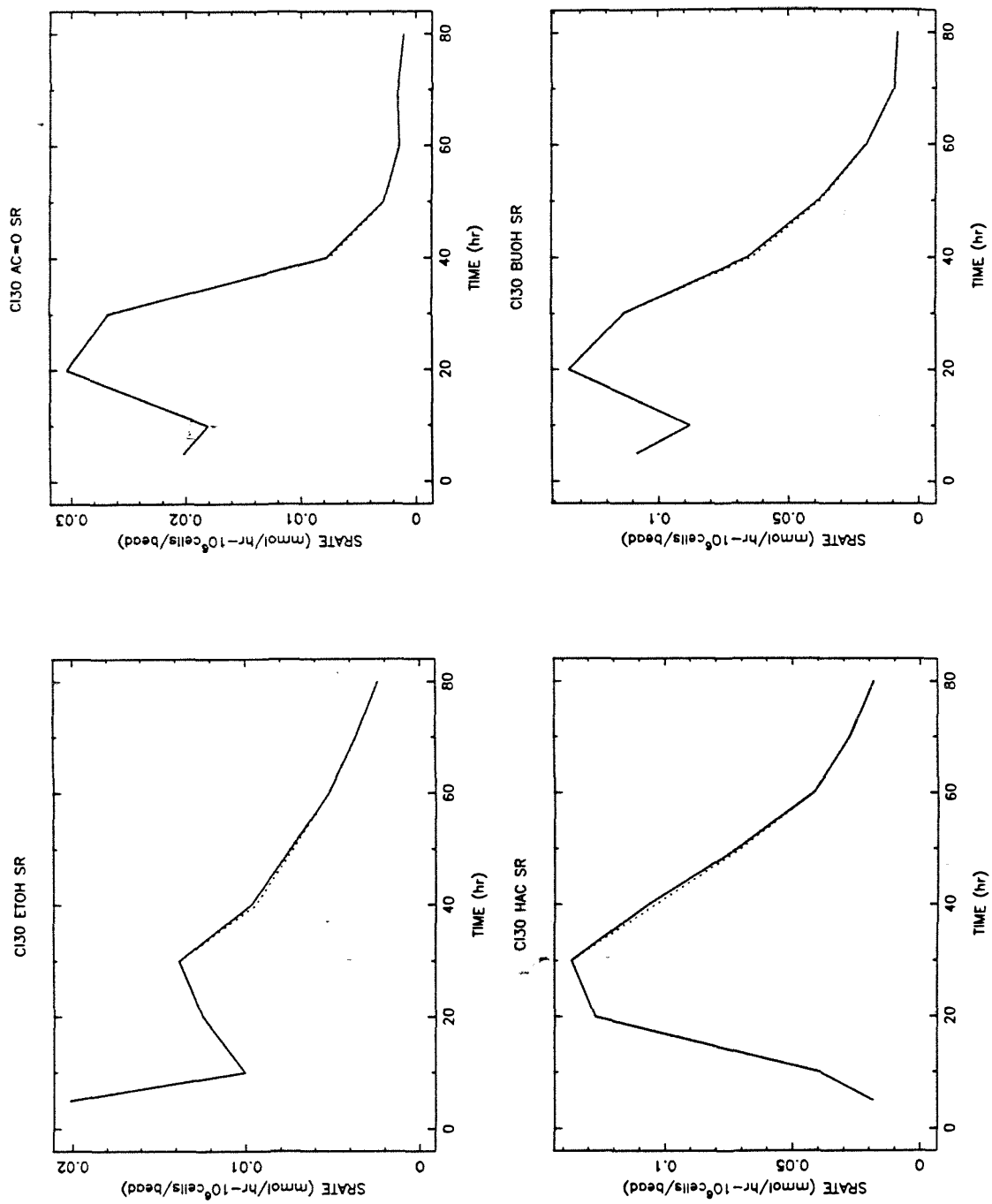

Figure 66. Run CI30 specific rates of product formation based on vegetative cell concentrations (solid lines) and vegetative plus clostridial cell concentrations (dotted lines).

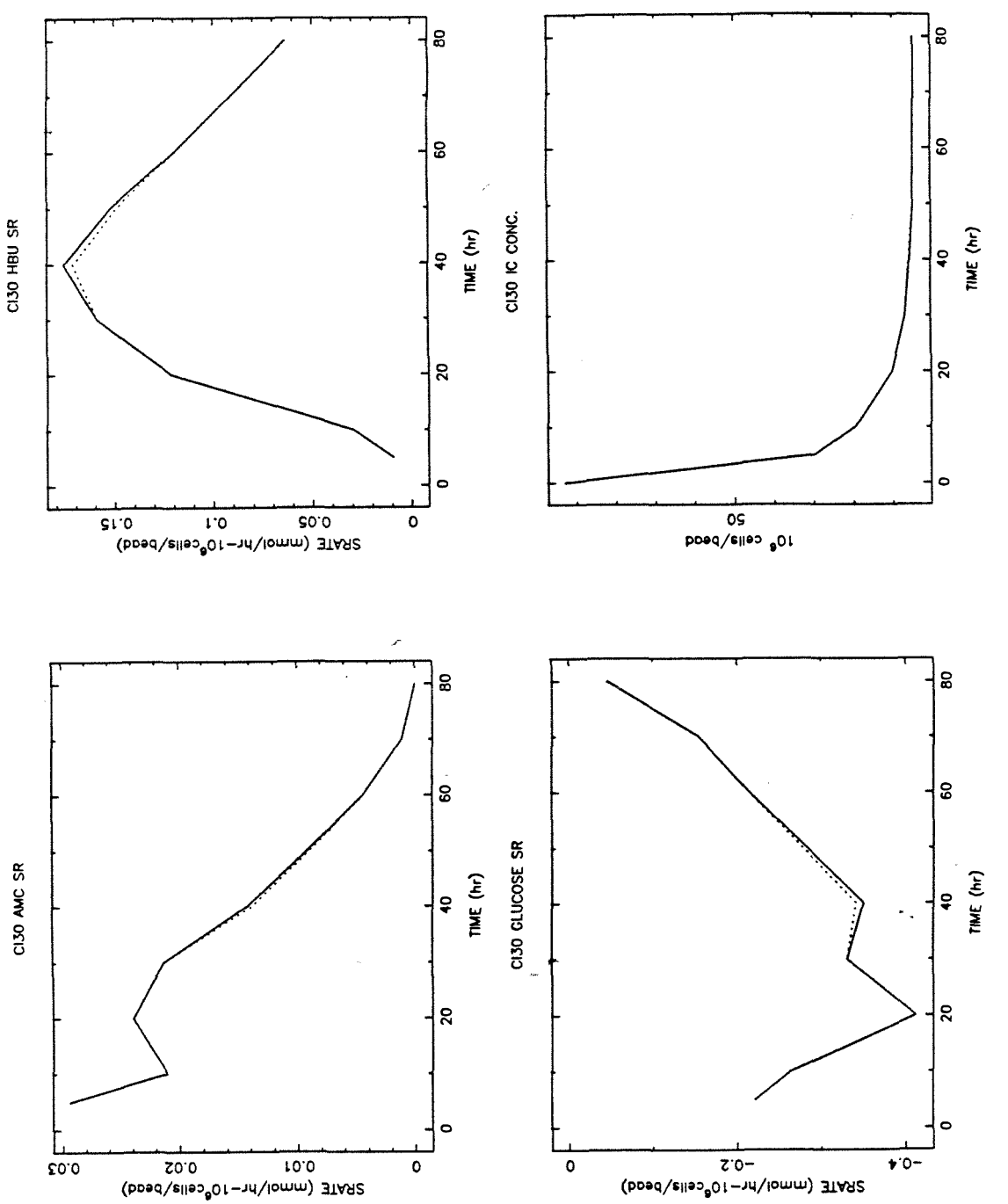

Figure 67. Run CI30 specific rates of product formation based on vegetative cell concentrations (solid lines) and vegetative plus clostridial cell concentrations (dotted lines).

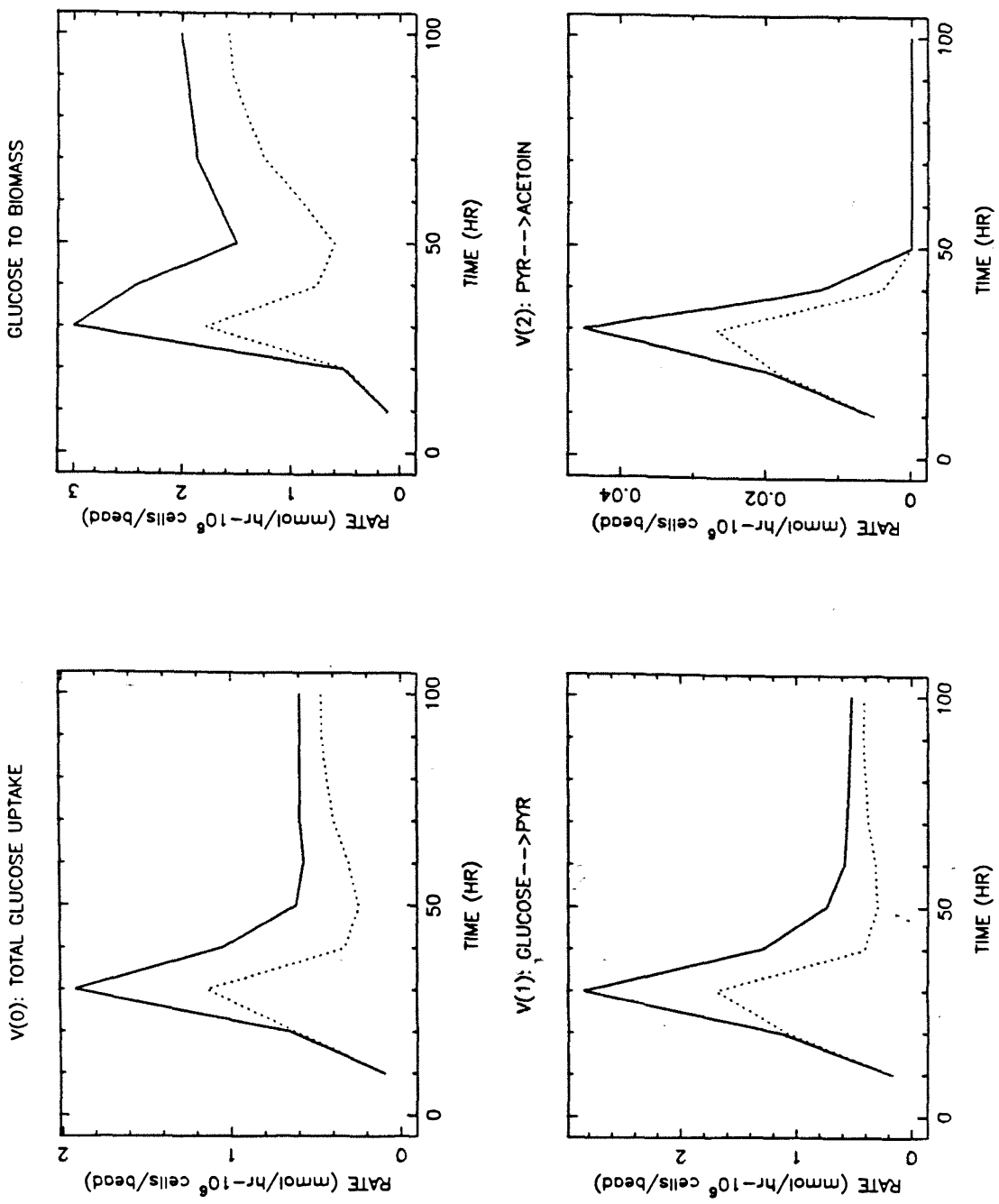

Figure 68. Run CI28 specific metabolic pathway branch rates based on vegetative cell concentrations (solid lines) and vegetative plus clostridial cell concentrations (dotted lines).

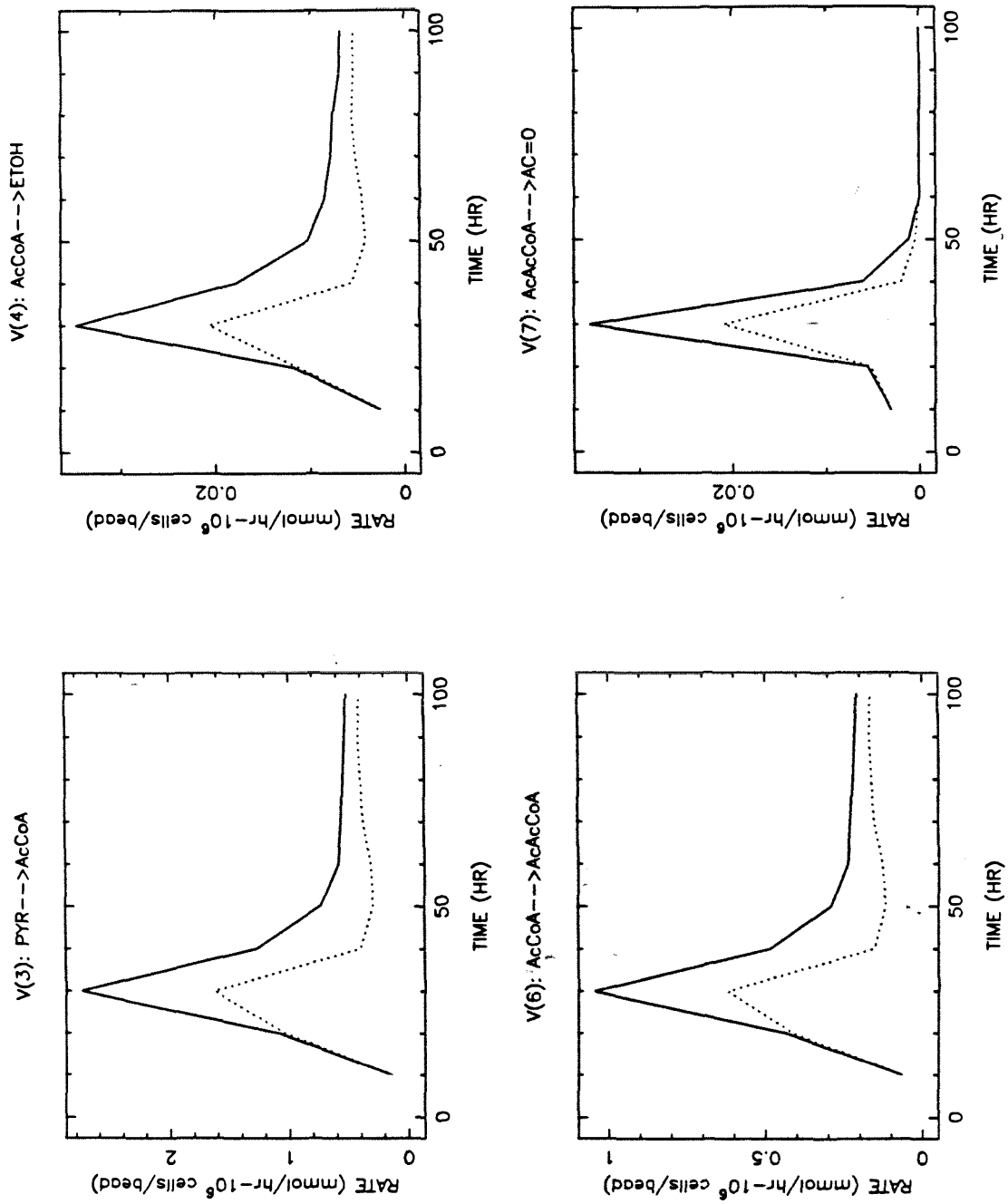

Figure 69. Run CI28 specific metabolic pathway branch rates based on vegetative cell concentrations (solid lines) and vegetative plus clostridial cell concentrations (dotted lines).

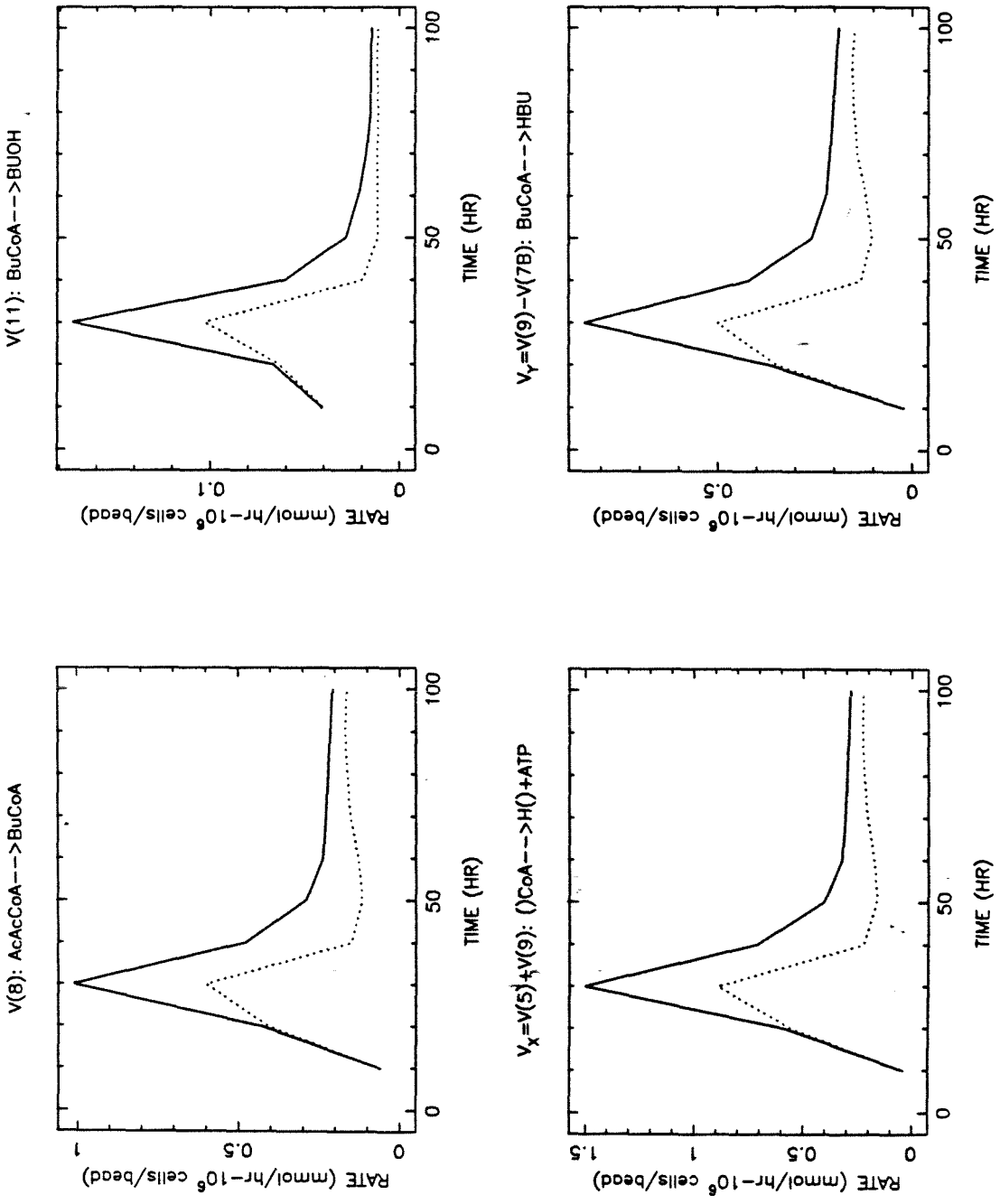

Figure 70. Run CI28 specific metabolic pathway branch rates based on vegetative cell concentrations (solid lines) and vegetative plus clostridial cell concentrations (dotted lines).

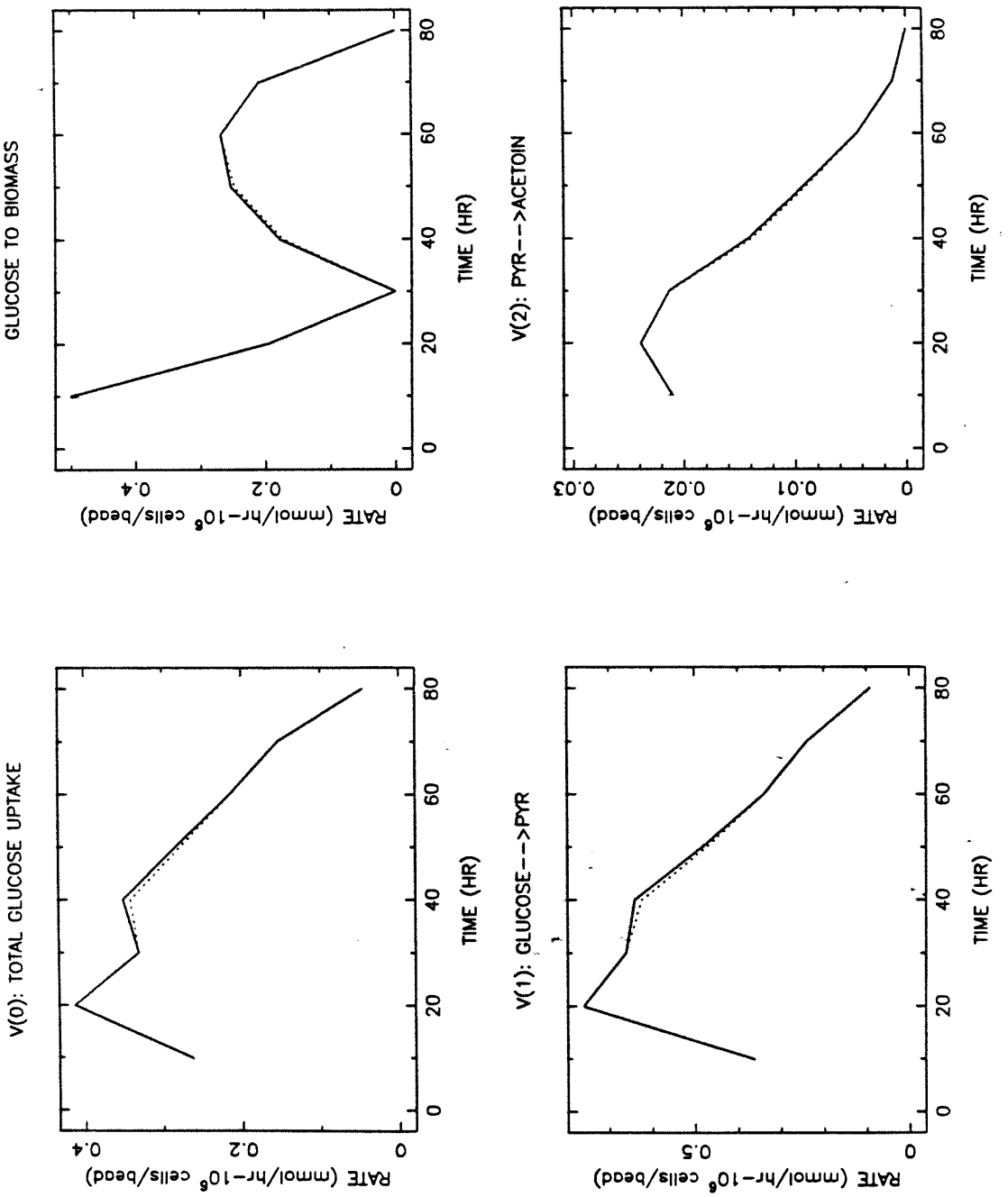

Figure 71. Run CI30 specific metabolic pathway branch rates based on vegetative cell concentrations (solid lines) and vegetative plus clostridial cell concentrations (dotted lines).

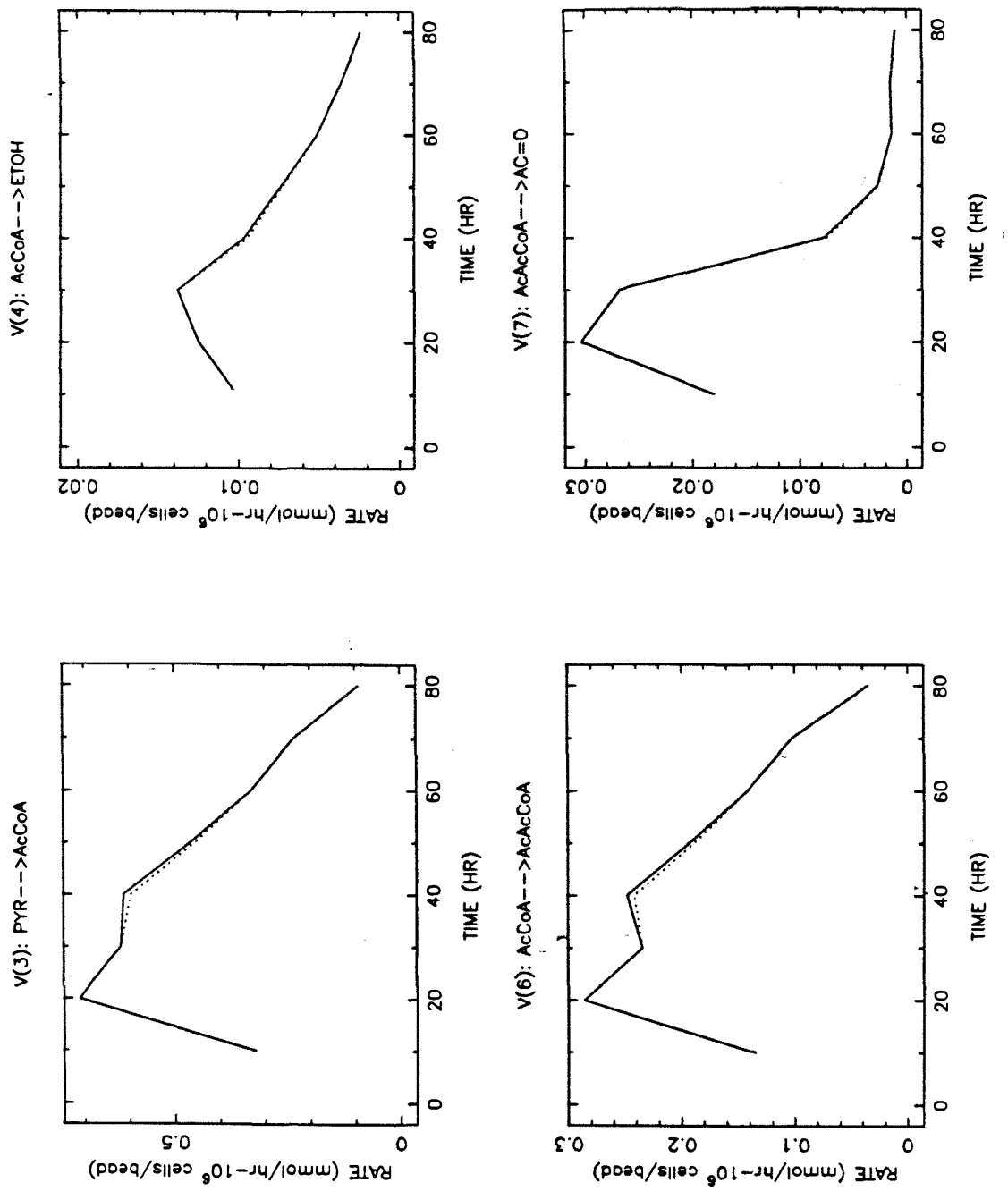

Figure 72. Run CI30 specific metabolic pathway branch rates based on vegetative cell concentrations (solid lines) and vegetative plus clostridial cell concentrations (dotted lines).

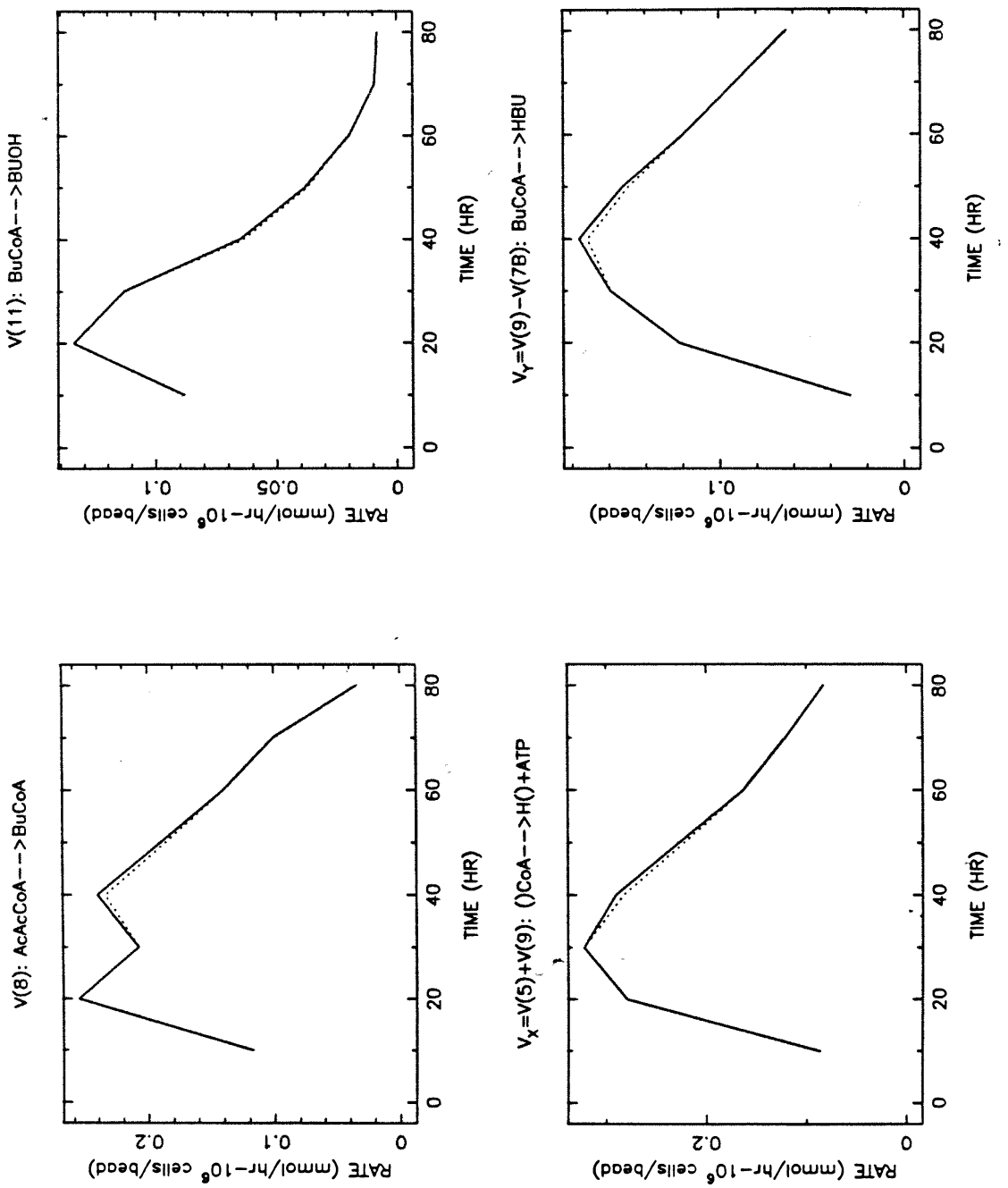

Figure 73. Run CI30 specific metabolic pathway branch rates based on vegetative cell concentrations (solid lines) and vegetative plus clostridial cell concentrations (dotted lines).

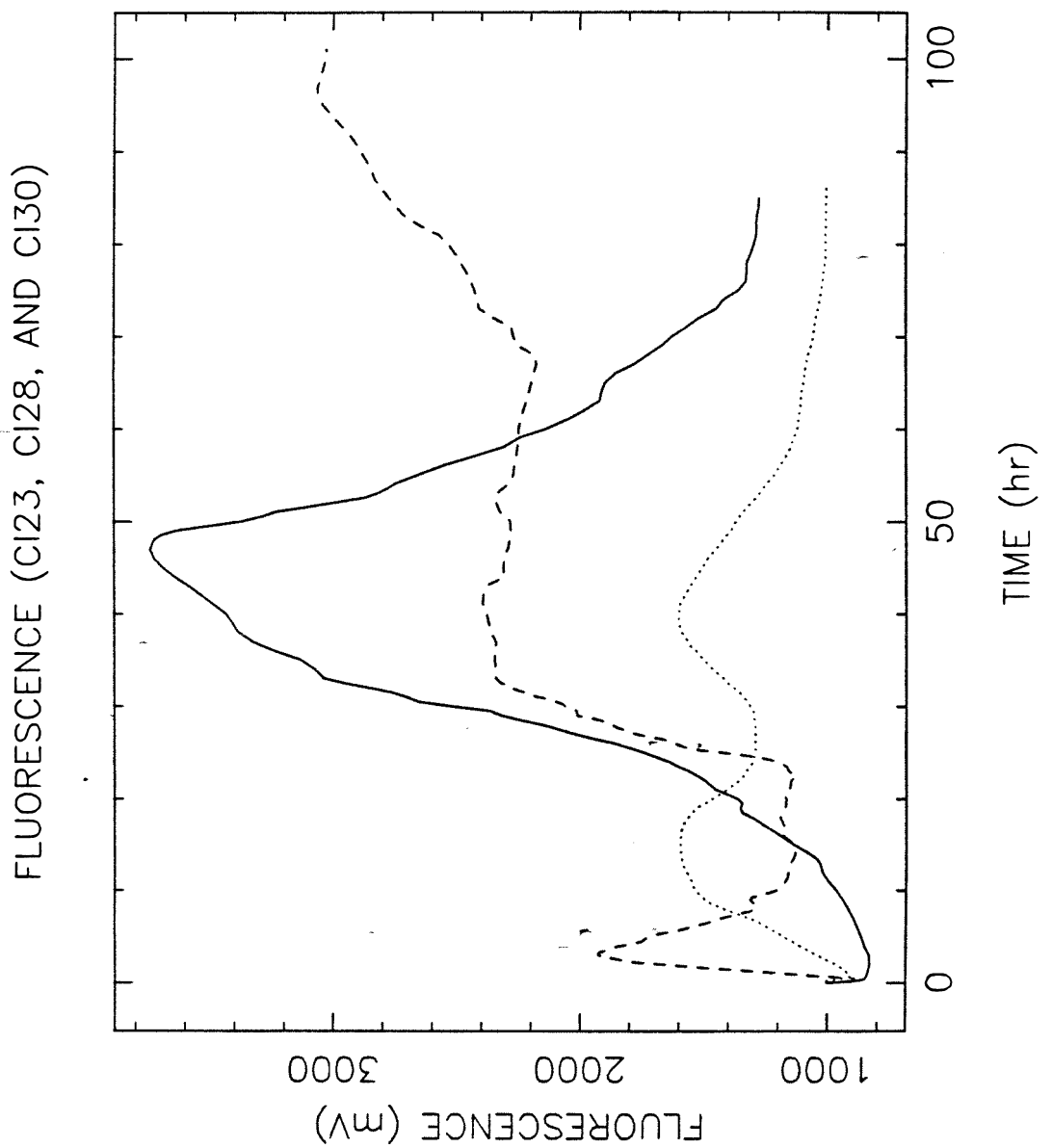

Figure 74. NAD(P)H-dependent culture fluorescence trajectories for CI30 (solid curve), CI28 (dashed curve), and CI23 (dotted curve).

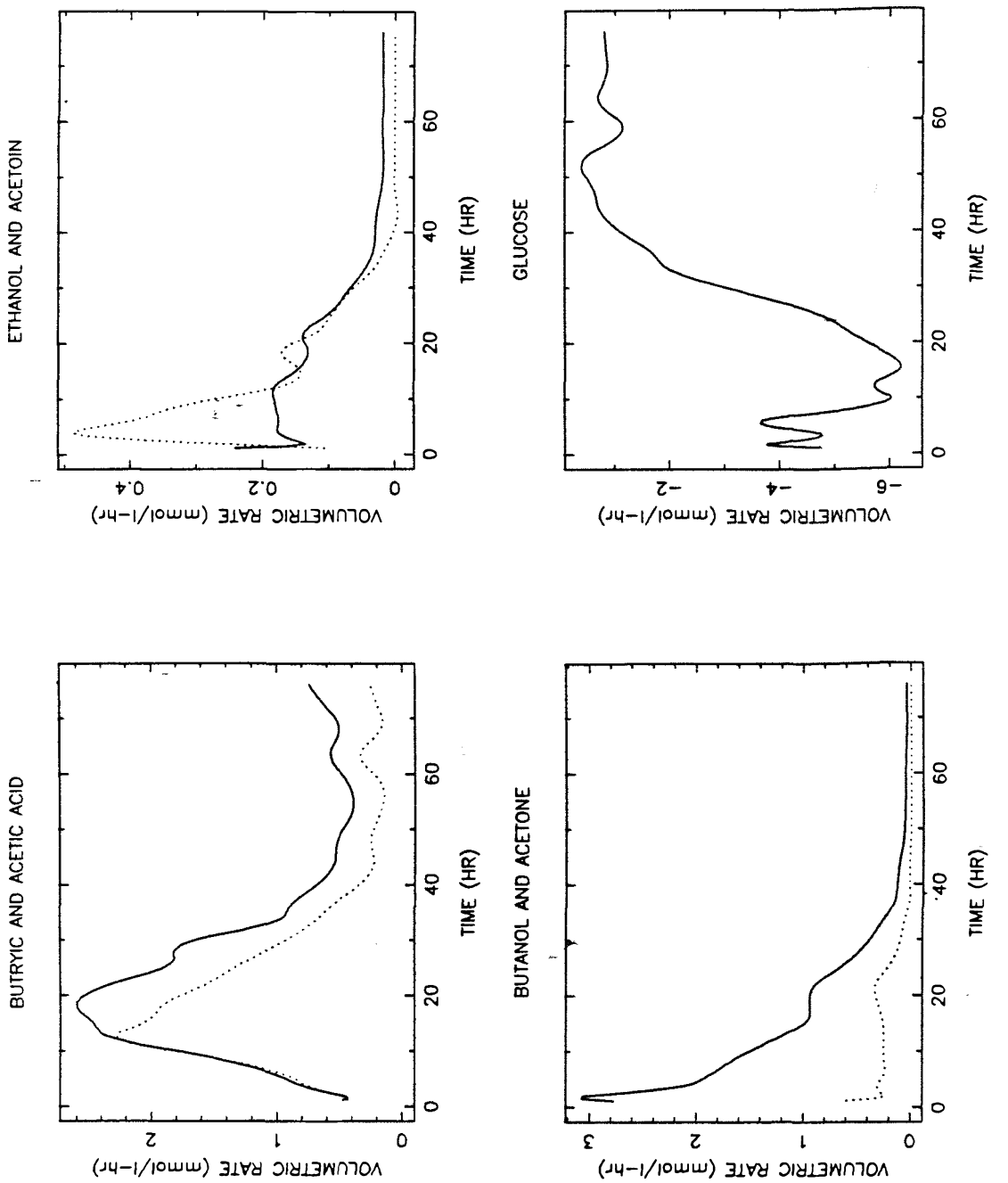

Figure 75. Volumetric rates of product formation for experiment CI18. **Upper left**: butyric acid (solid line) and acetic acid (dotted line). **Upper right**: ethanol (solid line) and acetoin (dotted line). **Lower left**: butanol (solid line) and acetone (dotted line). **Lower right**: glucose.

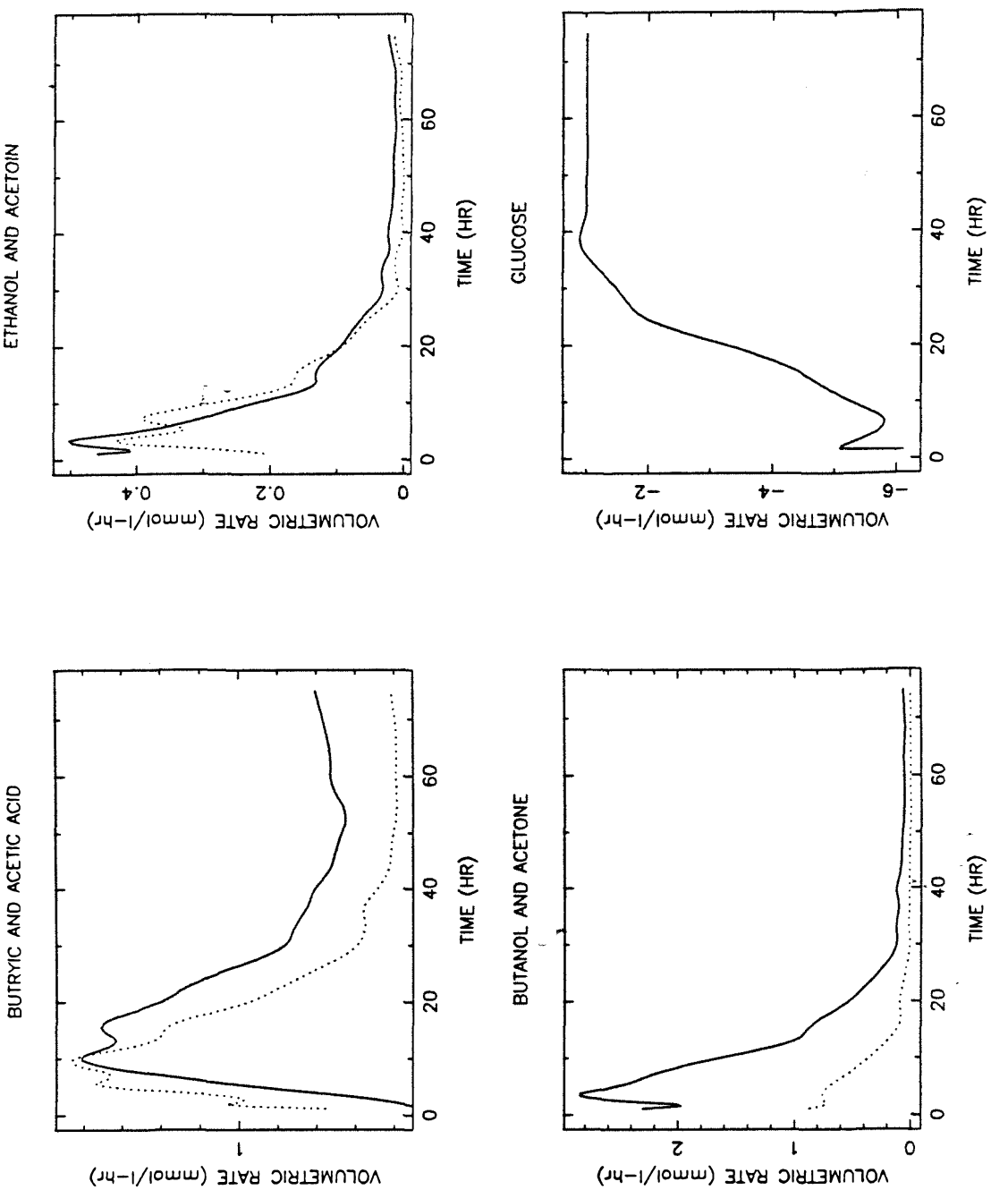

Figure 76. Volumetric rates of product formation for experiment CI15. **Upper left**: butyric acid (solid line) and acetic acid (dotted line). **Upper right**: ethanol (solid line) and acetoin (dotted line). **Lower left**: butanol (solid line) and acetone (dotted line). **Lower right**: glucose.

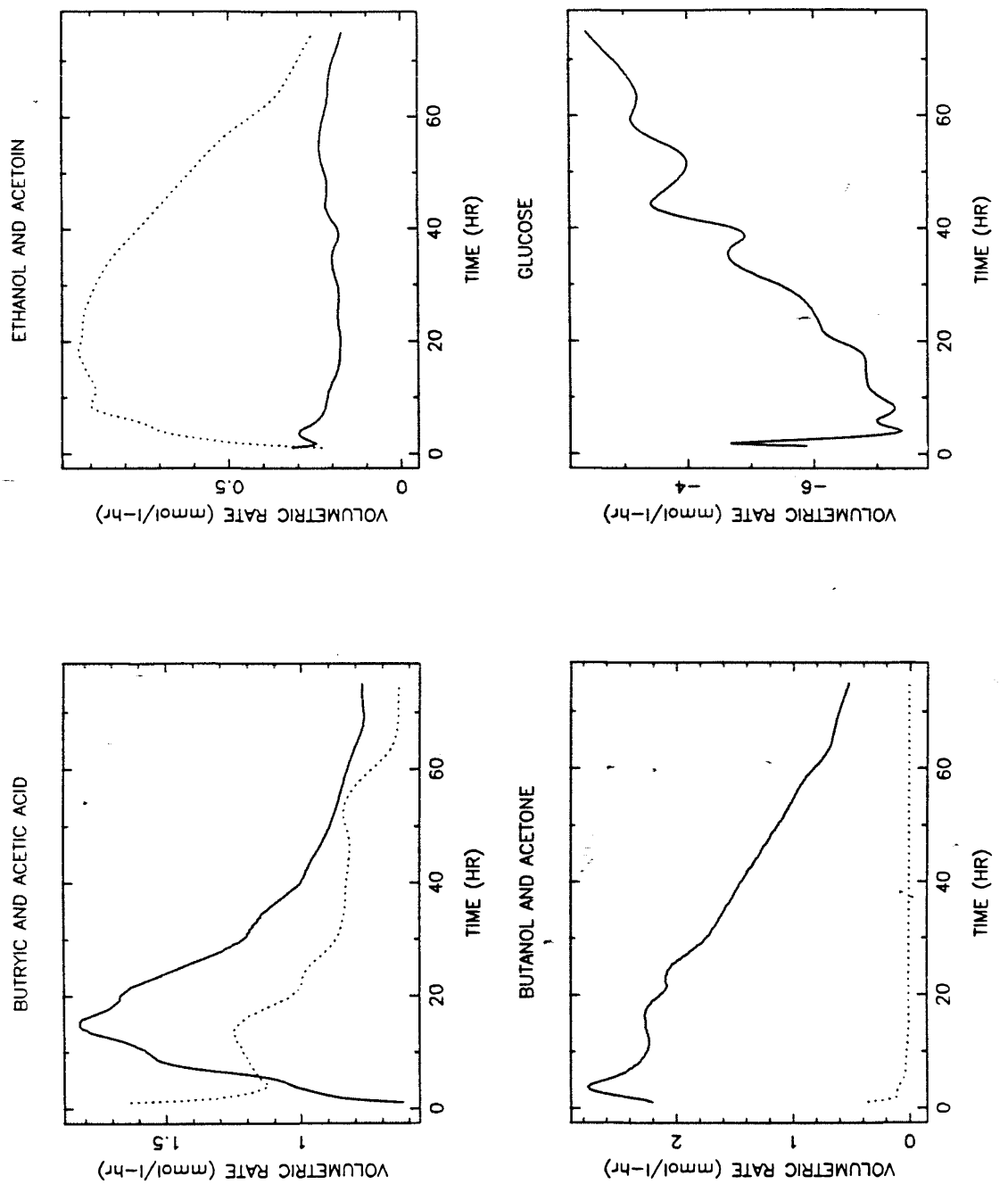

Figure 77. Volumetric rates of product formation for experiment CI19. **Upper left**: butyric acid (solid line) and acetic acid (dotted line). **Upper right**: ethanol (solid line) and acetoin (dotted line). **Lower left**: butanol (solid line) and acetone (dotted line). **Lower right**: glucose.

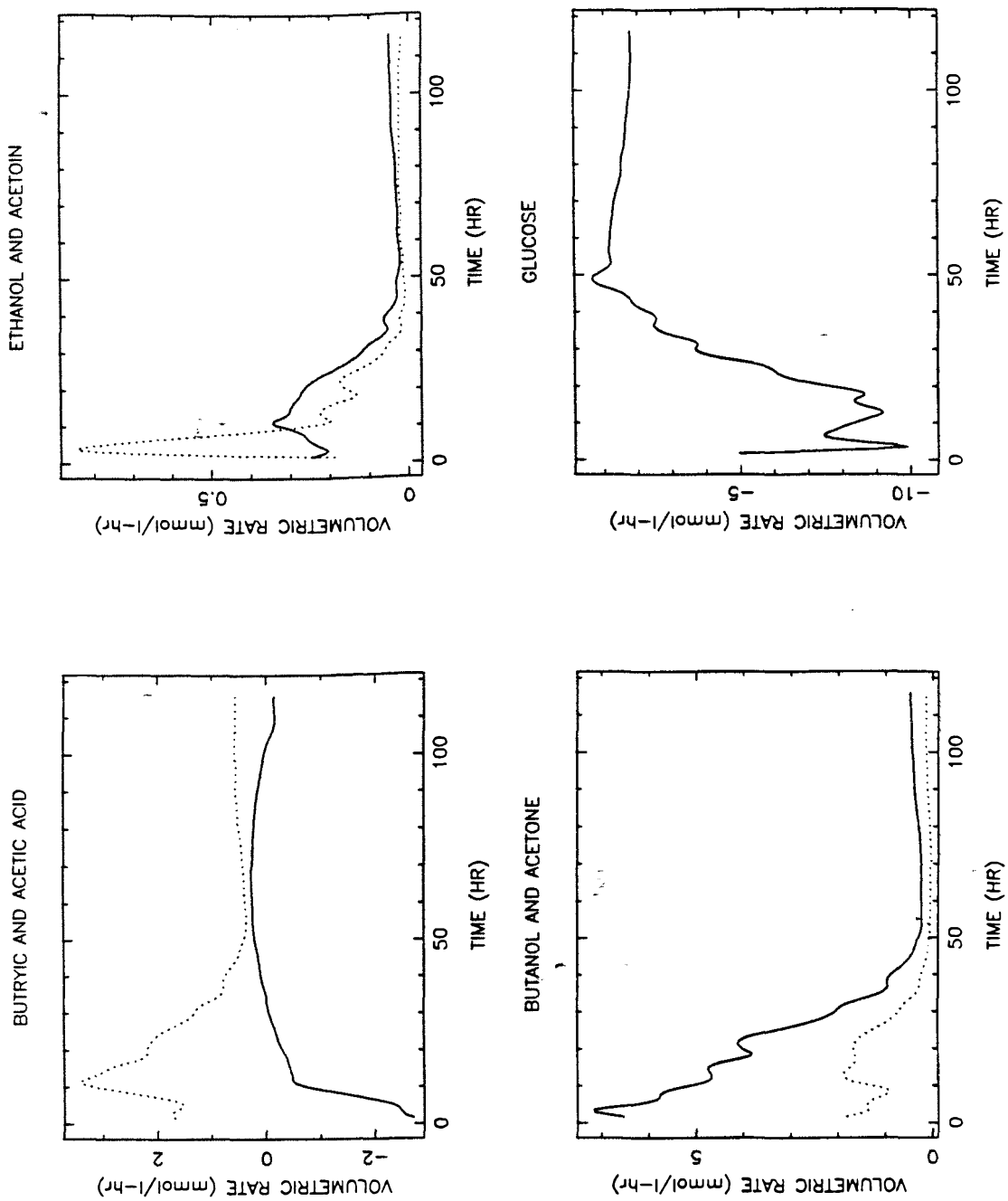

Figure 78. Volumetric rates of product formation for experiment CI17. **Upper left**: butyric acid (solid line) and acetic acid (dotted line). **Upper right**: ethanol (solid line) and acetoin (dotted line). **Lower left**: butanol (solid line) and acetone (dotted line). **Lower right**: glucose.

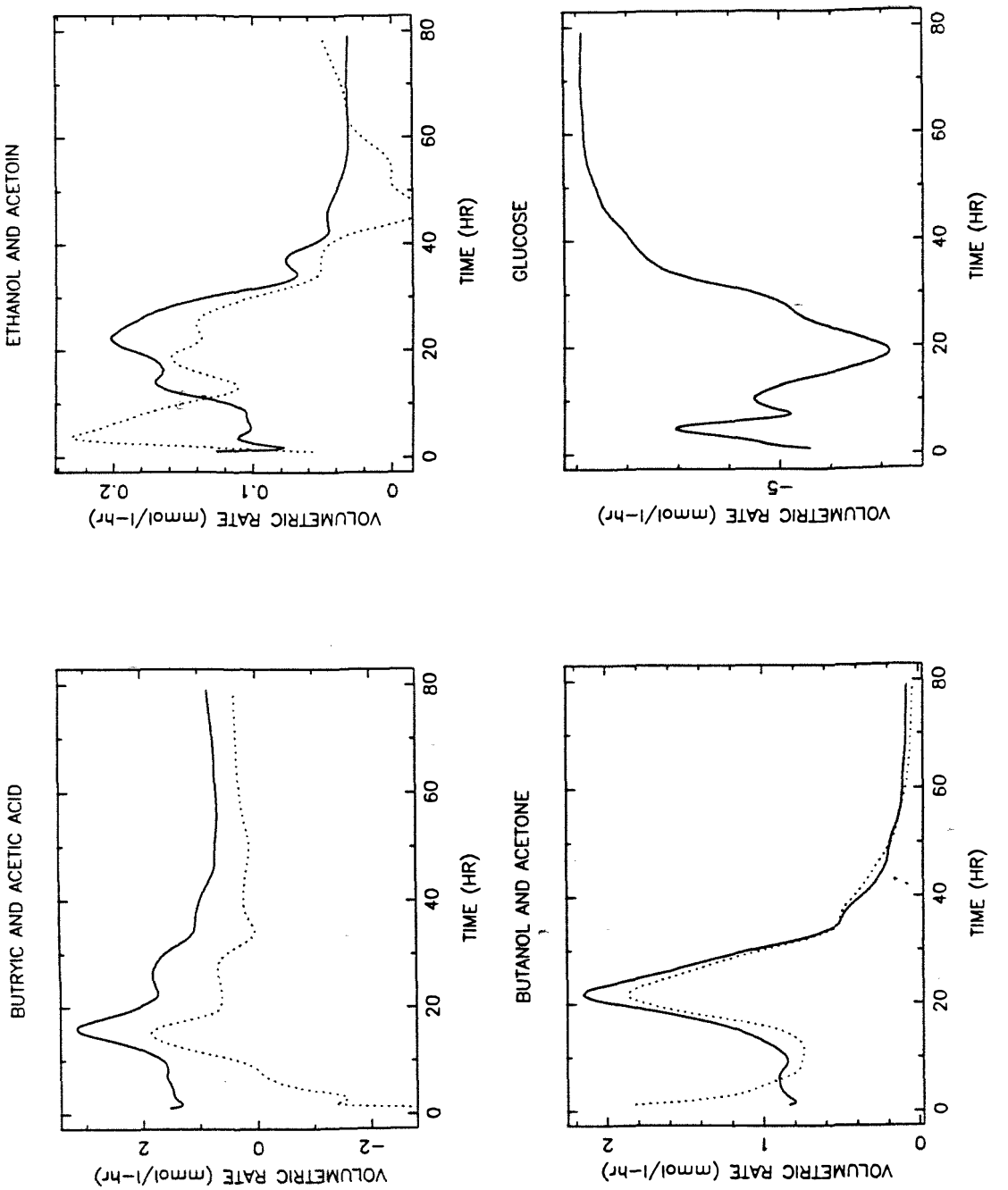

Figure 79. Volumetric rates of product formation for experiment CI21. **Upper left**: butyric acid (solid line) and acetic acid (dotted line). **Upper right**: ethanol (solid line) and acetoin (dotted line). **Lower left**: butanol (solid line) and acetone (dotted line). **Lower right**: glucose.

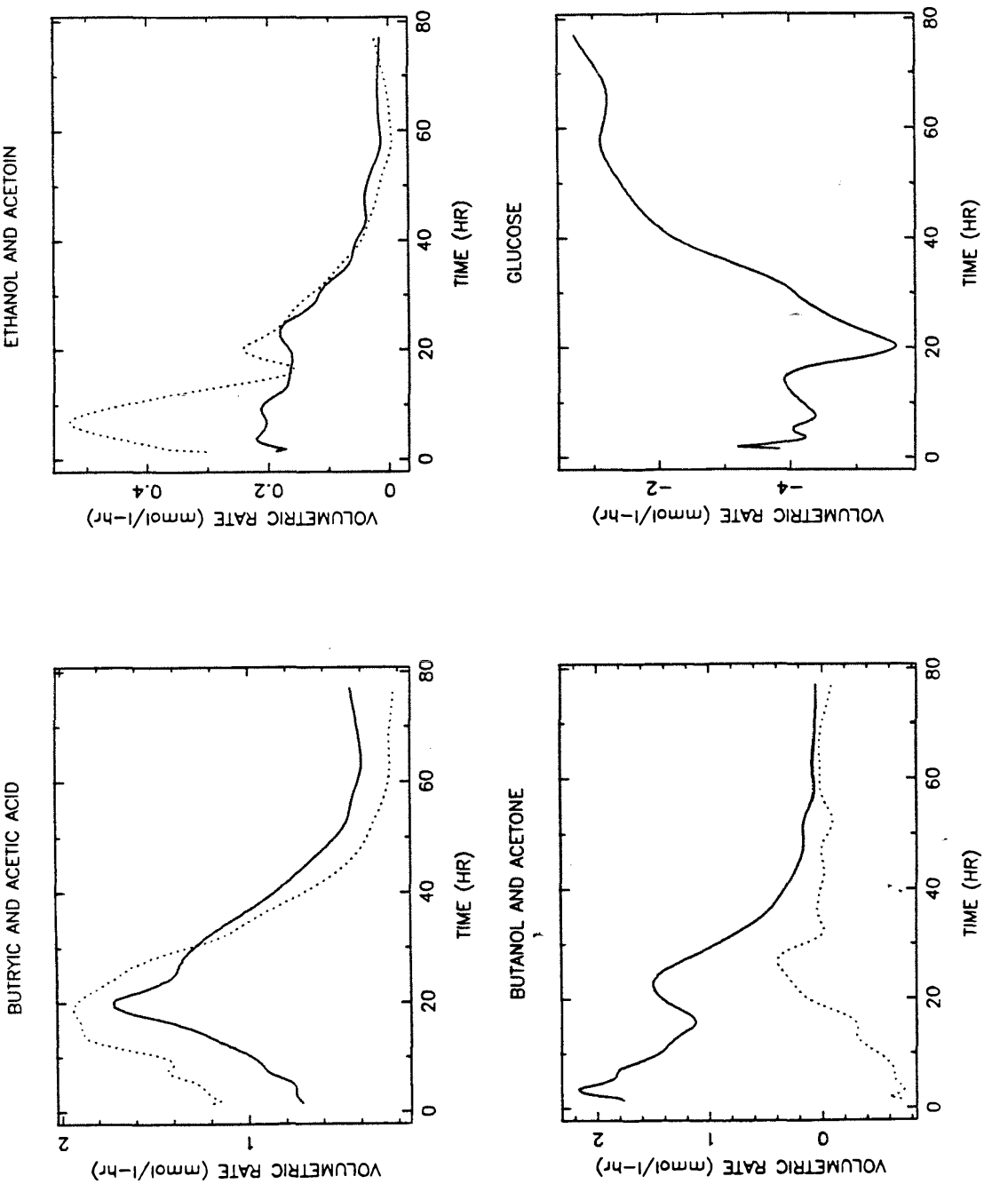

Figure 80. Volumetric rates of product formation for experiment CI22. **Upper left**: butyric acid (solid line) and acetic acid (dotted line). **Upper right**: ethanol (solid line) and acetoin (dotted line). **Lower left**: butanol (solid line) and acetone (dotted line). **Lower right**: glucose.

CHAPTER 6

ACTIVITY REGENERATION IN CONTINUOUS *CLOSTRIDIUM ACETOBUTYLICUM* BIOCONVERSIONS OF GLUCOSE

INTRODUCTION

The use of viable, but non-growing, cells in immobilized cell biocatalysts has several advantages over immobilized growing cells, including cell-free product streams and the potential for higher product:biomass ratios. However, because the non-growth state is usually achieved by nutrient limitation, loss of the desired conversion activity inevitably occurs. The cause(s) for this activity loss might include enzyme inactivation, cofactor leakage, or membrane damage; the experiments discussed in Chapter 5 indicated that cell lysis and sporulation accounted for rapid decreases in overall biocatalytic activity, while the effects of nitrogen starvation on macromolecular synthesis appeared responsible for deactivation on a longer time scale.

Many reports have indicated that the activity of nutrient-starved immobilized cells can be regenerated by exposure to growth medium [*e.g.*, 1–8]. In most cases, the nutrient medium contained undefined complex compounds such as yeast extract and peptone [*e.g.*, 3,4,5,6,7], but in a few, the effect of exposure to defined medium containing the missing nutrient (nitrogen) has been investigated [9,10,11].

The possible physiological mechanisms of activity regeneration by nutrient addition include enzyme synthesis, activating or relaxing inhibition of enzyme activity, and/or cell growth. Studies with polyacrylamide- or calcium alginate-entrapped *Arthrobacter simplex* cells indicated that the increase of steroid-Δ^1-dehydrogenase activity by exposure to peptone-glucose solutions was primarily due to cell growth, since the presence of benzylpenicillin or chloramphenicol (inhibiting cell wall synthesis and protein synthesis, respectively) prohibited regeneration [1,2,12,13]. Although these results were achieved on the basis of activity increases rather than on

the regeneration of lost activity, an investigation by Cheetham *et al.* showed that the presence of the same two antibiotics prevented the regeneration of isomaltulose-forming activity in deactivated immobilized *Erwinia rhapontici* cells [6].

Förberg *et al.* [5,14,15] developed a nutrient dosing technique for use with *Clostridium acetobutylicum* entrapped in calcium alginate or adsorbed to beechwood shavings. The feed to the continuous-flow reactor contained no nitrogen or vitamin sources, but was supplemented with complex nutrients for 15-minute periods at intervals ranging from 2 to 12 hours. By gradually increasing the nutrient dosing interval, butanol production was sustained and a lower fraction of feed glucose carbon appeared as biomass [5]. Unfortunately, the number and type of immobilized cells was not reported; microscopic examination of the calcium alginate beads indicated that some sporulation had occurred [5].

Inloes *et al.* studied the production of ethanol by immobilized *Saccharomyces cerevisiae* cells which were alternately fed complex nutrient medium and a nitrogen-free medium [10]. During the periods of nitrogen deficiency, ethanol productivity decreased, the amounts of acetaldehyde and glycerol produced relative to ethanol increased, the total protein content of the cells decreased, and the formation of large intracellular lipid droplets was observed. Exposure to the complex medium regenerated the ethanol-forming activity, but the level of activity achieved decreased with succeeding regeneration periods [10].

The majority of these regeneration studies have utilized complex nutrient compounds, and, with the exception of the latter investigation, little has been reported on the details of the regeneration process (*i.e.*, cell physiology and morphology). In this chapter, several experiments will be discussed that investigate product forma-

tion and immobilized cell concentration changes during alternating periods of bioconversion and regeneration. Regeneration was accomplished by supplying either nitrogen or growth vitamins plus nitrogen to calcium alginate-immobilized *Clostridium acetobutylicum* cells which had been starved for both types of nutrients. *In situ* NAD(P)H-dependent fluorescence monitoring and the use of an oligosporogenous mutant strain provided additional information on the events occurring during bioconversion and activity regeneration. Preliminary reports have appeared on one of these experiments [11,16]

MATERIALS AND METHODS

The culture media, immobilization procedure, experimental apparatus for batch and continuous phases, fluorescence measurement technique, and assay methods have been described in Chapter 3.

Experiments CI10, CI23, and CI28 utilized *C. acetobutylicum* ATCC 824, while experiment CI30 employed the oligosporogenous strain *C. acetobutylicum* ATCC 39236.

The regeneration experiments discussed in this chapter all began with the batch growth, rinsing, and continuous bioconversion procedures, materials, and methods outlined in Chapter 5. The bioconversion feed in these experiments was the same nitrogen- and vitamin-free medium used in the experiments discussed in Chapter 5 (10 g/L glucose for run CI10, 15 g/L for runs CI23, CI28, and CI30), while the feed during the regeneration phases consisted of the bioconversion feed plus NH_4Cl and (sometimes) vitamins. As before, all continuous-fermentation media

were filter-sterilized.

At various times during the experiments, a few drops of liquid sample were placed on FGM-agar petri plates and incubated aerobically at 30°C to check for facultative anaerobic contamination.

EXPERIMENTAL PROTOCOLS

1. Experiment CI10

Following a standard batch growth phase and nutrient rinsing, the immobilized cell reactor was fed bioconversion medium at a dilution rate of 0.22 hr^{-1} for 73 hours. The dilution rate was slowed to 0.04 hr^{-1} from 73 to 135 hours (still unsupplemented bioconversion feed), after which the feed was supplemented with 2 g/L butyric acid and the dilution rate was increased to 0.21 hr^{-1}, where it remained for the remainder of the run. At the 148.5 hour mark, the feed to the bioreactor was changed to a glucose medium containing 2 g/L butryric acid. The pH was maintained at 5.0 for the entire run.

2. Experiments CI23, CI28, and CI30

Experiments CI23 and CI28 utilized strain ATCC 824, while run CI30 used strain ATCC 39236. The pH was maintained at 4.5 for each of these experiments.

The changes in feed composition during each experiment are given in Table 5, and event schematics for these runs are presented in Figure 81 (the open areas are bioconversion intervals and the shaded ones are regeneration segments). In all of these runs, the change to regeneration conditions was done in a stepwise manner by

injecting a concentrated solution of nutrient(s) into the fermentor vessel; the level of nutrient(s) in the injection solution was calculated to bring the reactor liquid concentrations to that in the feed (at the moment of injection).

In experiments CI28 and CI30, the "vitamin mixture" (Table 5) contained (final concentrations) 1 mg/L *p*-aminobenzoic acid (PABA), 1 mg/L thiamine HCl, and 0.05 mg/L D-biotin. During the fourth regeneration period of experiment CI30, these vitamins were present in the feed medium at one-tenth these values.

In order to assess the effects of each of these vitamins on immobilized cell product-forming activity, pulses of each were injected into the fermentor so that the concentration of that vitamin in the system at the time of injection would be at the $\frac{1}{10}\times$ vitamin mix level. That is, PABA was injected at 250 hours (to a system concentration of 0.1 mg/L), thiamine HCl was injected at 270 hours (0.1 mg/L), and biotin was injected at 285 hours (0.005 mg/L).

RESULTS

A. Experiment CI10

The primary goal of this experiment, which used the sporogenous strain ATCC 824 and was carried out at pH 5, was to show the effects of activity regeneration by a complex nutrient compound (casamino acids). The time courses of product and glucose concentrations are presented in Figure 82; the level of butyric acid in the feed after 135 hours is also shown.

The first 73 hour period (unsupplemented feed, D=0.2 hr^{-1}) resembles the pH 5 bioconversion results given in Chapter 5 (the high initial ethanol levels were due

to incomplete rinsing of the ethanol-sterilized pH probe). The concentrations of all of the products increased slightly when the dilution rate was slowed by a factor of 5. When the dilution rate was increased and butyric acid added to the feed (135 hours), the concentrations of all of the products (except butyric acid) declined because of the lowered residence time. The addition of 1 g/L casamino acids to the butyrate-supplemented feed at 148.5 hours resulted in an immediate, rapid increase in acetic and butyric acid production and glucose consumption.

This was followed about 10 hours later by rapid increases in the concentrations of acetone, butanol, ethanol, and acetoin. The overall metabolic activity of the immobilized cells declined quickly about 5 hours after the feed was switched back to the butyric acid-supplemented bioconversion medium.

The profile of 590 nm absorbance during this run is also shown in Figure 82. Although the values of A_{590} increased after 73 hours, this was due to the increase in reactor residence time. The rapid increase in A_{590} to relatively high levels following the switch to casamino acid medium is due to both immobilized and suspended cell growth and illustrates one of the drawbacks to regeneration by rich nutrient feeding.

B. Experiment CI23

The time trajectories of glucose and product concentrations and 590 nm absorbance during experiment CI23 are shown in Figure 83. This experiment was operated at pH 4.5 and used *C. acetobutylicum* strain ATCC 824; the run consisted of bioconversion for 86 hours followed by regeneration on bioconversion medium supplemented with 0.8 g/L NH_4Cl. Although the levels of acetone and butanol during bioconversion were lower than in comparable pH 4.5 bioconversions (Chapter 5),

the overall patterns of product formation were typical of pH 4.5 bioconversions.

At the 86 hour mark, NH_4Cl was pulsed into the system and the feed changed to the regeneration medium. Figure 84 shows the concentration of nitrogen (as ammonia) in the effluent medium. It is apparent that the nitrogen was consumed by the immobilized cells at a high rate initially; after about 10 hours the concentration of ammonia in the bioreactor was nearly constant. A sharp increase in glucose consumption followed the step change in reactor nitrogen levels, and increases in the acetic and butyric acid concentrations began a few hours later. The concentrations of the acid products increased until they reached a plateau at levels near the maximum concentrations achieved during bioconversion. The concentrations of butanol, acetone, ethanol, and acetoin did not increase until 98 hours, six hours after the onset of renewed acid production activity. The concentrations of acetone and butanol were still increasing when the experiment was stopped.

In direct contrast to the increase in 590 nm absorbance as a result of casamino acid-caused activity regeneration, the increase in A_{590} during the NH_4Cl regeneration phase was relatively small. The 590 nm absorbance became nearly constant at about the same time that acid concentrations plateaued.

The trajectory of NAD(P)H-dependent fluorescence during this run is presented in Figure 85. The inset shows the levels of cell-free medium (background) fluorescence; clearly, these changes are very small when compared with those in the immobilized cell fluorescence profile. The part of the trajectory corresponding to the bioconversion phase was discussed in Chapter 5. Immediately following the addition of NH_4Cl, the fluorescence decreased briefly, then increased for about six hours. At the 92 hour mark, the immobilized cell fluorescence signal peaked and

then decreased for the duration of the experiment.

C. Experiment CI28

1. Substrate and Product Concentration Profiles

In this pH 4.5 experiment, calcium alginate immobilized ATCC 824 was exposed to three bioconversion phases and three regeneration phases (see Table 5 and Figure 81). The concentrations of the catabolic products and glucose are presented in Figures 86 and 87, and the nitrogen concentration profile is shown in Figure 88.

At the end of the first bioconversion phase, discussed in Chapter 5, the only products formed at appreciable levels were acetic and butyric acids. With the step change to nitrogen-supplemented regeneration medium (0.6 g/L NH_4Cl) at 101 hours, there was an immediate, rapid uptake of nitrogen and glucose, and the concentrations of acetic acid, butyric acid, acetoin, and ethanol began to increase. After a four to five hour lag, acetone and butanol concentrations also rose. There was also a relatively small increase in the 590 nm absorbance during this period.

Although the feed was not switched back to the bioconversion medium until 141 hours, and the bioreactor nitrogen content was not exhausted until *ca.* 160 hours, the concentrations of all of the products (except acetoin) peaked at about 138 hours and decreased through the next bioconversion phase. The acetoin concentration profile followed the same pattern, but reached its peak a few hours later. The 590 nm absorbance, however, increased during the early part of the second bioconversion phase before it peaked and decreased to very low values.

The response of the immobilized cell biocatalyst to the addition of ammonia in the second regeneration period was similar to that in the first regeneration phase,

except that the maximum concentration and the total amount of each product formed was significantly lower than those that occurred as a result of the previous nutrient feeding. Virtually no acetone or butanol was formed during this time.

The presence of both ammonia and the growth vitamins in the feed used during the final regeneration period stimulated high rates of acetic acid, acetoin, ethanol, and butyric acid within a few hours of the initial nutrient step change. The reactor concentrations of acetone and butanol did not begin to increase until the 310 hour mark, 20 hours after the start of the third regeneration period. The concentration profiles of Figures 86 and 87 show that the levels of the acid products began to decrease at this point. Lactic acid (L- and D- forms) was produced at a high rate during this regeneration period, although only small amounts of this compound had been produced during the preceding regeneration periods.

The profiles of nitrogen concentration during each of the three regeneration periods have similar patterns (Figure 88). The concentration decreased immediately after injection into the system, then increased for a short time before decreasing again (during the second regeneration phase, this second consumption period was very short). At some point, the concentration of nitrogen in the fermentor effluent began to increase until the feed was switched back to the nitrogen-free bioconversion medium. At this time, the amount of NH_4Cl in the system decreased rapidly due to both consumption and dilution.

2. Immobilized Cell Concentrations

The concentrations of each *C. acetobutylicum* morphological cell type in the alginate beads during experiment CI28 are shown in Figures 89 through 93. These

concentrations were estimated with the microscope-counting chamber method. Profiles are shown for vegetative cells (rod-shaped), pre-spore clostridial forms (phase-bright swollen cigar shapes), forespore-containing cells (club-shaped with a phase-bright end), mature spores (phase-bright ovoids), and germinating spores (phase-dark ovoids) [17].

As described in Chapter 5, the concentration of immobilized vegatative cells declined during the early hours of the first bioconversion phase because of extensive lysis, then decreased further when the majority of the remaining cells sporulated (Figure 89). Transient increases in the concentrations of the sporulation intermediate forms occurred (Figures 90 and 91) before the number of immobilized spores increased (Figure 92). Although the number of rod shapes counted increased during the middle of the first phase, this was not due to an increase in vegetative cell number, but rather to an artifact from inclusion of sporangia in the rod cell counts.

Although some germination occurred within the calcium alginate beads when the feed was changed at 101 hours to a regeneration medium containing NH_4Cl, the number of vegetative cells did not rise dramatically, as might be expected. Instead, there was a concomitant increase in the clostridial form population, followed by another large increase in the number of immobilized spores. Again, debris from sporulation (sporangia) and germination (exosporia) [18] was responsible for high counts of rod-shaped forms. During the second bioconversion phase, the number of mature spores increased, while the concentrations of all other cell types (except germinating spores) declined, until all populations plateaued by the 180 hour mark.

The start of the second regeneration phase (NH_4Cl medium) initiated an increase in the population of germinating spores, accompanied by a decrease in the

number of mature, phase-bright spores (Figure 93). Soon afterwards, the concentration of vegetative cells increased until the ammonia concentration fell to low levels during the third bioconversion phase. With the start of the third regeneration phase and the presence of NH_4Cl and growth vitamins in the medium, the numbers of germinating spores and vegetative cells increased rapidly. Although only very small numbers of clostridial and forespore forms were observed in bead samples from the 180 hour mark through the start of the last regeneration period, a rapid increase in the number of clostridial forms was noted in the bead sample from the end of the experiment, indicating the start of another sporulation cycle.

3. NAD(P)H-Dependent Culture Fluorescence

The time-dependent trajectory of the immobilized cell culture fluorescence is shown in Figure 94. Again, the changes in the cell-free medium background fluorescence are much smaller than changes in the immobilized cell fluorescence. The fluorescence signal during the first bioconversion phase (Chapter 5) rises to two early maxima before increasing steadily for all but the last four hours of this period. Although this behavior resembles that observed in experiment CI23 (Figure 85), there are differences in the time and duration of the first peak; also, no final increase is seen in the run CI23 fluorescence profile.

The response of the intracellular NAD(P)H-dependent fluorescence to the sudden presence of nitrogen in the medium (at 101 hours) is nearly identical to that of the cells in experiment CI23: a short rapid increase followed by a rapid, sustained decrease until the ammonia in the system was depleted early in the second bioconversion period (approximately 157 hours). After this time, the fluorescence profile

displays two maxima and the fluorescence signal had increased to a third when NH_4Cl was again injected into the system at the start of the second regeneration period. This behavior is similar to that of the first bioconversion phase.

The initial changes in the fluorescence profile at the start of the second regeneration phase are the same as those that occurred in the prior regeneration period—a brief increase succeeded by a longer decrease in the fluorescence intensity. However, the fluorescence signal reached a minimum after less than 10 hours of nitrogen exposure, and increased to two maxima before decreasing until the end of the second regeneration phase. During the final bioconversion period, the fluorescence intensity peaked once, and was decreasing when the NH_4Cl- and vitamin-supplemented feed was introduced to the system. Again, the fluorescence increased upon nitrogen addition, but the level remained constant for a few hours before it decreased to a minimum, and then rose for the remainder of the experiment.

All of these fluorescence changes are due to fluctuations in the intracellular NAD(P)H content of the immobilized cells. Correlations of the fluorescence changes with catabolic product formation, ammonia assimilation, and immobilized cell population changes during the experiment will be discussed shortly.

4. Other Measurements

The profile of excreted riboflavin concentration as a function of time during the experiment is shown in Figure 95. Concentration peaks occurred at the start of the first bioconversion phase and during the first regeneration period, but no other flavin fluorescence was noted until 10-15 hours after the start of the third regeneration period, when the concentration of riboflavin in the medium increased

rapidly to a high level. Riboflavin is a fluorescent yellow compound, and at levels above 1 μg/mL the fermentor liquid was noticeably yellow. Riboflavin excretion in *C. acetobutylicum* is related to iron limitation; this connection will be discussed later.

Several peaks are present in the 260 nm absorbance trajectory, presented in Figure 96. The initial maxima that occurred in the first bioconversion phase were discussed in the previous chapter. Other A_{260} profile peaks appear shortly after the start of the first regeneration period and towards the end of the second regeneration phase. A final large increase in the absorbance occurred near the end of the experiment, when the regeneration feed to the system contained NH_4Cl and vitamins. Absorbance at 260 nm measures primarily nucleic acids, and thus can be an indication of lysis or macromolecule degradation.

D. Experiment CI30

1. Substrate and Product Concentration Profiles

This experiment, conducted at pH 4.5, used the oligosporogenous *C. acetobutylicum* mutant strain ATCC 39236. The time-dependent product concentration, glucose concentration, and 590 nm absorbance (suspended cell) profiles are presented in Figures 97 and 98; the concentrations of nitrogen (as ammonia) during the run are shown in Figure 99. This experiment consisted of four bioconversion phases and five activity regeneration periods (Table 5 and Figure 81).

Since very little change was noticed during the first regeneration period (85–100 hours) with NH_4Cl-supplemented feed, a second regeneration phase was started (100–115 hours), utilizing a feed medium that contained both NH_4Cl (0.6 g/L) and

the vitamin mix described earlier (1 mg/L PABA, 1 mg/L thiamine, and 0.05 mg/L biotin). This medium was also used during the third regeneration phase (155–165 hours). The fourth regeneration period (195–205 hours) was conducted with a feed containing NH_4Cl and the vitamin mix, but the vitamins were used at one-tenth of the previous concentrations to try to determine the actual levels required by the immobilized cells. The fifth regeneration phase began at the 235 hour mark of the run and consisted of four subphases; a goal during this period was to investigate the effects of the individual components of the vitamin mixture. The feed during this final regeneration phase was always the NH_4Cl-supplemented medium. After the immobilized cells had been exposed to this feed for 15 hours, a pulse of PABA was injected; the final concentration in the system (immediately after injection) was 0.1 mg/L, the one-tenth vitamin mixture level. After four reactor residence times (20 hours), a pulse of thiamine HCl was introduced into the system (at a final concentration of 0.1 mg/L), and 15 hours later a pulse of biotin was added (0.005 mg/L). During the 315 to 318 hour period, the feed to the system was stopped inadvertently; this can be seen as a very slight perturbation in the concentration trajectories.

The behavior of the concentration profiles during the first bioconversion phase were discussed in Chapter 5. Although the overall activity during this time decreased less rapidly than during the bioconversion phase of run CI28, solvent-forming activity was still replaced by acid production.

A significant amount of nitrogen was consumed during the early hours of the first regeneration phase, but only very small changes occurred in the acetic acid, butyric acid, and glucose concentrations. Shortly after the vitamin mixture was

added to the feed, the acid product concentrations increased rapidly, as did the release of suspended cells. Maxima in the acids and suspended cell concentrations and a minimum in the glucose level occurred about five hours after the end of this second regeneration period. Small amounts of butanol and acetone were produced at this time, but the formation of these products was observed only during the second five hours of bioconversion phase number two. The levels of all of these products decreased during this second bioconversion period until all product concentrations were nearly zero, except those of acetic and butyric acids, which had plateaued at intermediate values.

As before, the change to nitrogen- and vitamin-supplemented feed at the start of the third regeneration phase (hour 155) initiated rapid increases in the concentration of acetic acid, butyric acid, and glucose, followed shortly by increased acetoin, ethanol, and suspended cell levels. All of these changes were reversed 5–10 hours after the end of nitrogen feeding, near the time that the ammonia levels reached zero. Only very small amounts of acetone and butanol were formed, beginning at the time that the acid concentrations peaked.

Virtually the same patterns occurred as a result of the fourth nitrogen/vitamin feeding (starting at hour 195), but less nitrogen was consumed (Figure 99), and the maximum A_{590} was lower during this regeneration phase than in the others.

The switch to NH_4Cl-containing feed at the start of the final regeneration phase (hour 235) initiated the typical rapid increases in acetic and butyric acid concentrations, and a decrease in the glucose level (Figure 100). Ethanol and acetoin concentrations also increased slightly during this time, but no significant release of suspended cells was observed. Shortly after the pulsewise addition of PABA (at

the 250 hour mark), the concentrations of butanol and acetone increased, and the amounts of the acid products in the system fell. Still, only a very low level of 590 nm absorbance was detected. The thiamine injection at 270 hours resulted in a slowing of the production of acetone, butanol, ethanol, and acetoin; the concentrations of the acids and glucose also leveled off during this interval. The injection of biotin at the 285 hour mark of the run caused an immediate increase in the acid product concentrations, in the level of 590 nm absorbance, and in the rate of glucose consumption. About 12 hours after the biotin pulse, the acid and A_{590} levels peaked, and the concentrations of butanol and ethanol increased rapidly. However, acetoin and acetone level fell during this alcohol production phase. Shortly after the 320 hour mark, the concentrations of ethanol and butanol also decreased, as did the rate of glucose consumption.

Lactic acid was not produced in this experiment until the end of the second regeneration period. In general, the times at which the lactic acid concentration increased and the relative levels reached as a result of each nitrogen feeding were similar to those of butanol. This indicates that lactic acid may be formed as a means of consuming intracellular reducing equivalents.

Except for the low concentration resulting from the initially high rate of nitrogen uptake, the ammonia levels in the bioreactor were nearly constant until the injection of biotin. At that time, the effluent nitrogen concentration began to decline, reaching a minimum about 10 hours later. The level of nitrogen in the system increased during the remainder of the experiment.

2. Immobilized Cell Concentrations

The concentration profiles for the different immobilized cell morphological types observed during this run are shown in Figures 101–104. No trajectory for forespore-containing cells is presented, because virtually none were observed.

A rapid decrease in the immobilized vegetative cell number occurred at the start of the first bioconversion phase of this experiment as in all of the others. The observation of a low frequency of sporulation during nitrogen and vitamin starvation indicates that this strain, ATCC 39236, is oligosporogenic.

The addition of NH_4Cl in the first regeneration phase had no effect on the various immobilized cell concentrations. However, the switch to vitamin-supplemented NH_4Cl feed at 100 hours caused some of the spores to germinate, and the level of vegetative rods increased until the end of the second regeneration phase. At this time, a few of the cells sprorulated, and a transient response in the population of immobilized clostridial forms was noted.

The same pattern of germination succeeded by an increased vegetative cell concentration during nitrogen and vitamin feeding, followed by infrequent sporulation when nitrogen levels fell during the next bioconversion period, was observed in the course of the following two regeneration/bioconversion cycles.

The step change in NH_4Cl concentration at the start of the fifth regeneration period apparently resulted in the initiation of both sporulation and germination events; this is possible because the cells can become committed to sporulation [19,20] or germination [21] but unable to complete the event because of a lack of exogenous nitrogen source [22,23]. The number of spores increased until the 290 hour mark, when the concentration of germinating cells increased. The size of the vegetative cell population also increased during this time, but the changes in number were

too large to be due to sporulation alone, and thus vegetative growth must have occurred. The addition of thiamine coincided with relatively high rates of cell growth, but very little increase in A_{590} occurred during this interval. Immobilized cell growth is often accompanied by the release of suspended cells. In contrast, the immobilized vegetative cell concentration did not increase appreciably following the injection of biotin, but the level of medium 590 nm absorbance did rise. An increase in the number of clostridial forms at the end of the experiment indicates the start of a new sporulation cycle in a few of the immobilized cells.

8. NAD(P)H-Dependent Culture Fluorescence

The immobilized cell fluorescence trajectory for experiment CI30 is presented in Figure 105. The changes in the cell-free medium background fluorescence (Figure 105 inset) are much smaller than those that were measured overall. The break in the profile during the second regeneration period (approximately 108 to 118 hours) corresponds to a period when the noise in the fluorescence signal due to high rates of gas generation made data smoothing impossible. The relative fluorescence levels before and after this break are not known; they have been placed as shown for convenience.

The fluorescence profile during the first bioconversion phase is marked by a single broad peak. The maximum in this peak occurs near the time of the second peak in the CI23 and CI28 peaks (Figures 85 and 94), but no connection could be established between these events (Chapter 5).

Nitrogen addition at the start of the first regeneration phase caused a rapid but brief increase in the fluorescence signal, followed by a small decrease to a

plateau. When the mixture of vitamins was added in the second regeneration period, the fluorescence intensity decreased, indicating a net consumption of intracellular NAD(P)H. The direction of the fluorescence profile change for the last part of this phase and the start of the second bioconversion period is not known, but since the fluorescence signal was decreasing both before and after the data break, it is likely that the signal was decreasing during this interval as well. The response of the immobilized cell fluorescence of run CI28 to nitrogen feeding was also a rapid decrease (Figure 94). Although the rate of decrease slowed, the fluorescence intensity continued to decline during the second bioconversion phase of this experiment. A similar pattern of rapid and slow fluorescence decrease is observed in the fluorescence profile during the third and fourth regeneration and bioconversion phase cycles, although the amount of the decrease was less each time. The point in each bioconversion phase at which the nitrogen concentration reaches zero (Figure 99) is marked by a sharp increase in the fluorescence intensity.

The fluorescence profile over the course of the final regeneration phase is shown in Figure 106. The switch to NH_4Cl-supplemented feed at the start of this period caused a decline in the fluorescence intensity, similar to the decreases observed during the other regeneration phases. However, the injection of PABA at the 250 hour mark caused the fluorescence signal to increase; this increase continued until several hours after the thiamine injection, after which the fluorescence level slowly decreased. The pulsewise addition of biotin, like that of thiamine, had no apparent direct effect on the intensity of the fluorescence signal. Approximately 8 hours after the biotin injection, the fluorescence profile drops rapidly to a plateau; this occurred at the same time that a large amount of nitrogen was consumed from the

medium. Finally, the signal decreased very rapidly for the remainder of the run (except during the time that the reactor feed was stopped).

4. Other Measurements

The time course of excreted riboflavin concentration is shown in Figure 107. A small peak in the riboflavin level occurred early in the first bioconversion phase, and larger concentration peaks were also measured during the first 5 to 10 hours of the other three bioconversion periods. Two maxima in the riboflavin profile occur during the final regeneration period, one about 5 hours after the thiamine injection (when the NAD(P)H-dependent fluorescence profile changes slope), and another at about the 308 hour mark of the run. The occurrence of these peaks corresponds well with the time and relative size of the maxima in the acetone and butanol concentration profiles.

The trajectory of liquid sample 250 absorbance during this experiment is shown in Figure 108. There are a number of absorbance profile peaks, indicating nucleic acid release from the immobilized cells due to lysis or excretion. The major A_{260} maxima occurred at the same time as the maxima in the excreted riboflavin concentration; this connection will be explored later.

ANALYSIS AND DISCUSSION

A. Rich Nutrient Feeding (Run CI14)

Although the strategy of exposing preparations of immobilized cells that have lost activity to complete nutrient media has been employed in many cases [*e.g.*,

1,5,6,7,10], the procedure and its effects on the immobilized microorganisms have not been analyzed in any detail. Longer term nutrient-dosing experiments in which the feed to the immobilized cell bioreactor alternately consisted of nutrient-deficient and nutrient-sufficient media have been reported [5,10,14,15], but the media used to regenerate the biocatalyst activity always contained complex undefined nutrient compounds such as yeast extract and/or peptone. Accurate assessment and control of activity regeneration require the use of defined regeneration conditions.

Experiment CI10 was performed to illustrate the effects of regeneration with complex nutrient medium. The metabolic activity of the immobilized cells increased sharply upon exposure to the casamino acid-supplemented medium. However, a comparison of the concentration profiles from this experiment (Figure 82) with the product levels during the first regeneration period of run CI28 (Figure 83) shows that, while nearly the same product concentrations were achieved, the release of suspended cells was much higher in the casamino acids feeding case (implying higher rates of cell growth). Thus, the conclusion of some researchers that activity regeneration is primarily due to new cell growth [2,6,12] may be a consequence of their use of these complex, undefined nutrient compounds.

B. Rates of Production and Consumption (Runs CI28 and CI30)

The volumetric rates of product formation and glucose consumption during the course of experiment CI28 (pH 4.5, ATCC 824) is shown in Figure 109; the profiles of the volumetric rates of nitrogen (ammonia) assimilation in this run are presented in Figure 110. The corresponding rate plots for experiment CI30 (pH 4.5, ATCC 39236) are shown in Figures 111 and 112. These rate trajectories were calculated

by using the concentration data of Figures 86–88 and 97–99 and the derivatives (with respect to time) of those data, obtained by cubic spline curve fitting, in the unsteady-state CSTR equation (Equation (24), Chapter 5).

After the first bioconversion phase of experiment CI28, in which the initially high acetone and butanol formation rates are succeeded by acid production, the rate profiles during the next two regeneration/bioconversion cycles show similar patterns of product formation. Each step change to nonzero levels of medium-supplied nitrogen results in a rapid increase and early peak in the profiles of acetic and butyric acid production, followed by lower rates of solvent formation. Although the rates of formation of all of the excreted catabolic products decrease during the early part of each ensuing bioconversion phase, the production rates of the acids reach low but steady values, while those of the solvents are essentially zero shortly after nitrogen depletion. The overall peak metabolic activity was clearly less during the second regeneration period, apparently as a result of more than 200 hours of vitamin starvation. When the vitamin combination was added to the regeneration medium at the end of this experiment, product formation rates increased rapidly; butanol production dominated after the 310 hour mark. Acetone formation rates were low during this final regeneration period, but relatively high rates of ethanol production were observed.

Although the regeneration periods in experiment CI30 were shorter and usually involved the addition of both vitamins and NH_4Cl, patterns similar to those just mentioned can be noted in the product formation rate profiles during the first bioconversion phase and the following three regeneration/bioconversion cycles. Another similaritiy between the two sets of rate trajectories is the occurrence of the

peak acetoin formation rate 5–10 hours after the time of the maximum rate of ethanol formation.

The profiles of the rates of ammonia assimilation, presented in Figures 110 and 112 for these two experiments, show interesting changes during each regeneration period. At the start of each nitrogen feeding phase, the rate of ammonia uptake was very high, but it decreased rapidly. After a few hours, the assimilation rate increased again, but to levels significantly below the initial rates. The uptake rate profile during the final regeneration period of experiment CI28 is an exception of this observation; the second increase in ammonia uptake rate reached higher levels because of the inclusion of vitamins in the medium after many hours of vitamin starvation. In run CI28, the nitrogen consumption rate increased to a maximum 10–20 hours after the step change in ammonia levels before decreasing during the remainder of the regeneration period. This feature did not occur in the rate profiles of CI30, probably because of the presence of the vitamins or to the shorter regeneration phases.

Some of the features of the nitrogen uptake rate trajectories can be explained in terms of the physiological mechanisms for ammonia assimilation (Figure 113). Ammonia from the medium can enter the cell either by the diffusion of the uncharged species or by the action of an energy-dependent ammonium ion translocase (AT-ase) [24,25,26]; since the pK_a of ammonia is 9.25, most transmembrane flux will utilize the translocase. The driving force for this facilitated diffusion system appears to be the membrane $\Delta\psi$, maintained by membrane-bound ATP-ase [25,26]. The existence of this transport system has been established in several *Clostridium* species [24,25,26,27].

Most bacteria possess two cytoplasmic ammonia uptake pathways [18,28,29,30] (Figure 113) which convert the ammonia to glutamate and glutamine for the synthesis of other nitrogenous compounds. One route involves L-glutamate dehydrogenase or L-alanine dehydrogenase for the reductive amination of either 2-oxoglutarate or pyruvate without the involvement of ATP [18]; both have been found in saccharolytic clostridia [24,27]. However, when ammonia concentrations become low (<1 mM [18]), the dehydrogenase enzyme is repressed and two new enzymes are synthesized: glutamine synthetase (GS) and glutamate synthase (GOGAT) [18,28,29,30]. Glutamine synthetase has a much higher affinity for ammonium ions than the dehydrogenases, as expressed by the 1000-fold difference in typical K_m values for these enzymes [30]. The synthesis and activity of GS may be regulated by several mechanisms in bacteria, including activity modulation by adenylation (indirectly inversely proportional to the energy charge) [28]. The glutamine synthetase of *C. acetobutylicum* P262 was recently cloned into *E. coli*; its activity did not appear to be regulated by adenylation in either the host or the donor [31].

From this discussion, it is apparent that the immobilized cells possessed an active high-affinity (GS/GOGAT) ammonia uptake system at the start of each regeneration phase. The addition of relatively high concentrations of NH_3 quickly saturated the GS system ($K_m \approx 10^{-4}$ M [30]), and the initially high assimilation dropped until glutamate or alanine dehydrogenase was derepressed or synthesized, at which time the rate of nitrogen consumption increased again. The subsequent decline in this rate after prolonged feeding of regeneration medium in run CI28 (Figure 110) may be due to decreased intracellular demand for ammonia.

C. Intermittent Bioconversion and Activity Regeneration

Before discussing the product formation aspects of these experiments with immobilized *C. acetobutylicum*, it is necessary to understand the conditions to which these cells have been exposed. Conditions of alternating nutrient excess and nutrient limitation are common in natural ecosystems, and thus many aspects of starvation have been studied [22,32,33,34,35], although relatively few investigations have involved anaerobes, and no reports of the starvation behavior of *Clostridium acetobutylicum* have been published. It is necessary to be cautious when applying conclusions based on one organism to another: while the response of most bacilli to nitrogen (or carbon) starvation is the initiation of the sporulation process, *C. acetobutylicum* is unable to sporulate in the absence of an exogenous nitrogen source [22,36]. Another example of different responses is the observation that nitrogen limitation in the presence of excess carbon source often leads to the production of intracellular reserve materials [29]; however, *C. acetobutylicum* does not synthesize granulose under conditions of low nitrogen concentrations [37].

While *C. acetobutylicum* is capable of sporulation when growth is limited, excess exogenous nitrogen, carbon, and energy supplies are required [22,36]. Although many of the immobilized cells in these experiments sporulated during the first bioconversion phase of each run, this was facilitated by the lysis of (and release of nitrogenous cytoplasmic compounds from) a significant proportion of the vegetative cell population. In each of the experiments many immobilized cells did not sporulate and were therefore exposed to nitrogen starvation conditions. Under conditions of nutrient limitation, evolutionary mechanisms for survival should allow an organism to grow at low environmental concentrations of the nutrient(s) in ques-

tions [34]. This would occur if the cell could assimilate the limiting nutrient and metabolize it at high rates to produce new cell material with a high efficiency [34]. The high-affinity ammonia uptake system is an example of this type of mechanism. In order to survive under the more strict condition of nutrient starvation, an organism must maintain cellular integrity and a low rate of energy production to satisfy the requirements for maintenance energy. (Maintenance energy is defined as the energy required for purposes other than the production of new cell material, *e.g.*, osmotic regulation and maintenance of intracellular pH [33]). When the cells are exposed again to nutrient-sufficient conditions, their ability to assimilate nutrients influences their "metabolic reactivity" [34]. In some cases, the reappearance of the growth-limiting nutrient can lead to "substrate-accelerated death" [38], but since this phenomenon can be prevented by the presence of magnesium ions, it most likely did not occur in these experiments.

Bacterial cells subjected to nutrient starvation often respond by metabolizing intracellular substrates. The concept of endogenous metabolism has been defined as the total of the metabolic reactions that occur when an organism is deprived of compounds that may serve as exogenous substrates [39]. Possible endogenous substrates include the free amino acid pool, protein, RNA, and storage compounds such as polysaccharides (granulose) and lipids (PHB) [DAW 39]. DNA does not appear to be degraded by bacteria under starvation conditions [33]. The degradation of macromolecules by starving bacteria has been reported for a number of different species [*e.g.*, 35,40,41,42]; in all of these cases, the RNA, protein, and free amino acid content of the cells decreased, with most of the net degradation occurring within the first 12 hours [41] or 2 days (for species with long-term survival abilities) [35,40,42].

RNA degradation does not diminish a cell's survival ability, since bacteria generally possess RNA in proportion to their growth rate. The products of RNA degradation are ribose and purine and pyrimidine bases, which may or may not be used by the cell; the excretion of the bases can be followed by measuring the 260 nm absorption [40].

Protein degradation occurs in all cells, regardless of the nutritional status of the cell. Certain proteins have much shorter half-lives than others, and these short-lived proteins typically appear to be enzymes at control points in various metabolic pathways [43]. Starvation conditions induce protein degradation rates several times higher than those normally observed, with the concomitant release of ammonia. It is interesting to note that protein degradation requires ATP energy, either directly or via an energized membrane [43].

The synthesis of granulose, the polyglucan storage compound formed by *C. acetobutylicum*, is carried out by two enzymes, ADPglucose pyrophosphorylase and granulose synthase [37,44,45], while its degradation is effected by α–1,4–polyglucan phosphorylase [44]. Fine allosteric control of granulose synthesis seems not to exist in this bacteria. However, enzymatic studies have indicated that a high adenylate energy charge promotes synthesis and that degradation is favored by a low energy charge [37,44,45]. Granulose was not synthesized under conditions of excess glucose and nitrogen limitation [36].

The special case of nitrogen limitation or starvation in the presence of excess exogenous carbon and energy source(s) seems to result in an increased adenylate energy charge in the starved cells [46,47]. The energy charge of *E. coli* increased from 0.74 to 0.87 when the ammonia in the medium was completely consumed (while

glucose was in excess) [46]. Since these nitrogen-limited cells have induced (or derepressed) the high-affinity glutamine synthetase/glutamate synthase ammonia uptake system (Figure 113), high levels of the substrates of this system (other than ammonia and glutamine) would allow for the most efficient assimilation of the limiting nutrient. Thus, ammonia-limited cells can be expected to generate high levels of ATP, NAD(P)H, glutamate, and 2-oxoglutarate [32,47].

Clostridium acetobutylicum has been reported to require two vitamins for growth, *p*-aminobenzoic acid and D-biotin [33]. In addition, many investigators supplement the growth medium with thiamine HCl, and this compound was included in the vitamin mixture added to the feed during some regeneration periods. While a number of studies have reported on the optimization of the concentrations of compounds in synthetic growth media for *C. acetobutylicum* [49,50,51,52], little attention has been paid to the effects of variations in vitamin concentrations. At any rate, these investigations have all utilized growing suspended cells; the effect of the omission of these vitamins from a synthetic, defined medium would result in the non-growth of the culture inoculum.

The general functions of these three vitamins are fairly well known. Biotin functions in the enzymatic transfer of carbon dioxide, as in the fatty acid biosynthetic carboxylation of acetyl-CoA to form malonyl-CoA [53,54,55]. Thiamine occurs in cells as the coenzyme thiamine pyrophosphate (TPP), which is involved in four types of reactions: decarboxylation, oxidative decarboxylation, α-ketol formation, and transketolation [53,55,56]. At least two important catabolic enzymes of *C. acetobutylicum* require TPP as a prosthetic group: pyruvate-ferredoxin oxidoreductase (for the reductive decarboxylation of pyruvate to acetyl-CoA) and α-acetolactate

synthase (one of two enzymes converting pyruvate to acetoin) [30]. The third of these vitamins, *p*-aminobenzoic acid (PABA), is a precursor in the formation of folic acid; the coenzyme form is tetrahydrofolic acid. Tetrahydrofolate serves as a carrier of hydroxymethyl, formyl, and methyl groups, and it is active in the synthesis of purines and pyrimidines [53,54,55,57]. Although PABA is required for the synthesis of folic acid, it is not necessarily true that folic acid can substitute for the PABA requirement [53]; Lampen and Peterson found that PABA was required for growth but that folic acid had no effect on *C. acetobutylicum* [48]. Reports have also been published on the enhancement of error-free DNA repair in *E. coli* by PABA [58,59].

It should be possible to rationalize the patterns of product formation in these immobilized *C. acetobutylicum* experiments by applying a knowledge of the different environments to which the cells were exposed. Throughout the experiments, solvent product (acetone and butanol) formation that was present at the start of a bioconversion phase always declined rapidly. The products formed during most of each bioconversion phase were acetic and butyric acids. This can now be understood as the response of the cell to the need for high-efficiency ATP production to fulfill a number of requirements for ATP, including (1) the priming of the high affinity GS/GOGAT ammonia uptake system, (2) the degradation of proteins, and (3) maintenance metabolism (*e.g.*, preserving membrane gradients). Examination of the ATP production in the catabolic pathways of *C. acetobutylicum* (Figure 15, Chapter 4) shows that the ATP yield per mol of glucose fermented is higher for acid product formation (because of the acyl kinase reactions) than for the formation of acetone and butanol, and thus acidogenesis occurs during nitrogen starvation. This conclusion would seem to be at odds with the results of some reports on suspended

cell fermentations, in which nitrogen-limited cultures were observed to produce primarily solvents because they were not ATP-limited [60]. However, those conclusions were based on results with growing, suspended cells which were limited but not starved for nitrogen; the advantage to those cells in consuming acetic and butyric acids for solvent formation is in the removal of the membrane gradient-uncoupling effects of those weak acids [61,62,63]. In addition, many of these suspended cell investigations utilized yeast extract as the nitrogen source [*e.g.*, 60]; the physiological mechanisms for the transport and assimilation of organic nitrogen sources are not well understood and most likely have different ATP (or adenylate energy charge) requirements than the GS/GOGAT ammonia uptake system [29]. In the experiments discussed in this chapter, the cells were immobilized, were growing slowly or not at all, were often starved for ammonia, and were not exposed to concentrations of the weak acids that could be damaging to the membrane ΔpH.

The high adenylate energy charge in the starved cells also affects the overall metabolic rate. Glucose transport in *C. acetobutylicum* occurs by a phosphoenolpyruvate-energized phosphotransferase system (PTS) [64], which yields cytoplasmic glucose-6-phosphate. This compound is then converted by the enzymes of the Embden-Meyerhof-Parnas (EMP) pathway to pyruvate; from this point, the different catabolic pathway branches (Figure 15, Chapter 4) allow the formation of the various end products. The activities of two important enzymes of the EMP pathway, phosphofructokinase and pyruvate kinase, are inhibited by high energy charges [65]. Since phosphoenolpyruvate is formed in a reaction that occurs later in the EMP pathway than phosphofructokinase, a high energy charge effectively slows the transport of glucose (by a phosphotransferase system) as well. Although the

effects of ATP and the energy charge on the other catabolic enzymes of *C. acetobutylicum* are not known, those effects are much less important than the influence of the energy charge on the carbon flux through the EMP pathway. Thus, an additional effect of nitrogen starvation is the slowing of glucose metabolism with the resultant low rates of acetic and butyric acid formation.

When the nitrogen-starved, low-activity, acid-forming cells experienced a step change in exogenous ammonia concentration at the start of a regeneration period, they responded by assimilating nitrogen at a very high rate (until the high affinity system is saturated) and by sharply increasing their rates of glucose consumption and acid production. This rapid increase in acid product formation was caused by the sudden derepression of glucose metabolism through the EMP pathway (because of the lowered energy charge). The sudden increase in the carbon flux through pyruvate led to the rapid inflation of the rates of the pathway branches for which enzymes were already induced—those leading to the formation of acetic and butyric acids. Since the rates of production of ethanol and acetoin increased soon after the metabolic activity regeneration, a reasonable hypothesis is that the enzymes in those pathways were more readily induced, synthesized, or derepressed than the enzymes leading to acetone and butanol formation. Alternatively, the induction or derepression of the acetoin and ethanol enzymes may be less tightly controlled than those for acetone and butanol synthesis.

The rates of formation of acetone and butanol began to increase about 10 hours after the start of most regeneration phases. Since the formation of solvent products provides less ATP energy to the cell (per mol of glucose metabolized) than acidogenesis, there must be advantages to the *C. acetobutylicum* cell in utilizing

these pathways in addition to, or instead of, the acid-forming reactions. Three different effects are thought to promote the use of solvent-forming pathways: (1) detoxification of the cell's environment by removal of the membrane pH gradient-uncoupling weak acids; (2) the release of reducing equivalents, since the acidogenic pathways provide a net production of NAD(P)H and the solventogenic reactions consume NAD(P)H (this argument neglects the action of hydrogenase); and (3), the need for a lower rate of ATP production. As was discussed in Chapter 4, hydrogenase normally acts to release or supply reducing equivalents. Only under special conditions, such as the inactivation of hydrogenase by CO [66,67], would the second effect be a factor in the induction of solvent formation. In addition, the fluorescence trajectories of experiments CI23, CI28, and CI30 (Figures 85, 94, and 105) illustrate that the NAD(P)H content of the cells was decreasing **before** solvent formation. Although the concentrations of acetic and butyric acids in the bioreactor at the time of solvent formation were not as high as those noted near the start of solventogenesis in the pH 4.5 suspended cell batch fermentation of Chapter 4 (15–20 mM total acids *vs.* 80–100 mM), the sudden increase in the rate of formation and the addition of a slight diffusion barrier (in the form of the alginate gel) may have caused the acid concentration in the microenvironment of the cell to be substantially higher than that in the surrounding medium.

Furthermore, the real effect of the toxicity of the weak acids is the value of the intracellular pH, which may be different in the immobilized cells than in suspended cells. Using ^{31}P nuclear magnetic resonance spectroscopy (NMR), Galazzo *et al.* found that the pH_i of calcium alginate-immobilized yeast cells was 0.2 pH units lower than that of comparable suspended cells [68]. If a similar phenomenon occurred

in immobilized *C. acetobutylicum* , then the threshold level of weak acids needed to lower the pH_i to solvent enzyme-inducing levels would be lower than noted in suspended cell cultivations. The third possible effector of the induction of solvent production is related to the differences in ATP formation efficiencies between the two sets of reactions. Although the number of immobilized vegetative cells increased during the shorter regeneration periods of experiments CI28 and CI30 (Figures 89 and 101), the rate of increase was slow, and some of the increase was due to germinating spores instead of vegetative cell growth. Thus, the rate of consumption of ATP was probably lower than the rate of its production, and so the enzymes for solvent formation were induced or derepressed.

The duration of solvent production occurring as a result of regeneration varied from run to run, and depended on both the length of the regeneration period and the differentiation activity of the cells. In experiment CI28, the volumetric solvent rate during the first regeneration phase (Figure 109) began to decrease before the nitrogen feed was exchanged to the bioconversion feed. However, Figure 89 indicates that the total vegetative cell number had begun to decline by this time because of the sporulation of a significant fraction of the vegetative cell population. This is reflected in the rates of Figure 109, which are based on the total biocatalytic activity of the immobilized cells and are not on a per-cell basis.

This type of volumetric rate modulation did not occur in the oligosporogenous strain used in experiment CI30. The peaks in the acetone and butanol formation rate profiles (Figure 111) caused by the first three (10 or 15 hour) regeneration phases began just as the regeneration phase ended and the bioreactor feed was switched to the nitrogen-free bioconversion medium. In this case, solvent production

ended because nitrogen starvation conditions were reestablished along with the need for high-efficiency ATP production.

The maximum rates of product formation and glucose consumption also changed during each of the two experiments (CI28 and CI30) with multiple bioconversion/regeneration cycles. In run CI28, only very small amounts of acetone and butanol were formed during the second regeneration phase, but this is a result of the lower rate of acid production at that time. Apparently, the ability of the cells to synthesize the RNA and protein needed for rapid metabolism had been compromised by the more than 200 hours of vitamin starvation. Although the actual quantitiy of each vitamin required by the cells was undoubtedly very small, and the lysis of some of the cells made additional amounts available near the start of the first bioconversion phase, the long period of activity in the absence of an exogenous vitamin supply resulted in vitamin deficiency. The validity of this hypothesis is shown by the response of the immobilized cells in the third regeneration phase, when the feed contained the vitamins in addition to ammonia. The volumetric rates of product formation and glucose consumption increased dramatically as a result of the addition of vitamins to the feed. The population of immobilized vegetative cells also increased sharply during this period, but not to the same degree as the change in butanol formation rate.

In experiment CI30, the cells of ATCC 39236 responded sluggishly and to a small extent to the addtition of NH_4Cl at the start of the first regeneration phase. The reasons for this are not known, although this strain may have a higher vitamin requirement than strain ATCC 824. The response to vitamin addition at the 100 hour mark was more rapid and much larger in magnitude than the addition of

ammonia alone, as can be seen in the concentration profiles of the products, glucose, and nitrogen (Figures 97–99). The inclusion of vitamins in the feed also resulted in significant levels of suspended cell release and in some immobilized vegetative cell growth. The maximum product formation rates initiated by the second regeneration phase were slightly lower than those of the first, primarily because the length of ammonia and vitamin feeding was lower (30 and 15 hours, respectively, reduced to 10 hours for both nutrients). Peak volumetric rates resulting from the third regeneration period were somewhat higher than those of the second, but this was due to the higher immobilized vegetative cell concentration later in the run.

The changing environmental nutrient concentrations affected the morphological processes in the immobilized cells as well as the patterns of product formation. Although the events of sporulation and solvent production are closely related in suspended cell batch cultivations, the two events do not appear to be coupled in these experiments.

The regeneration of product-forming activity in experiments CI23, CI28, and CI30 was accompanied by some increases in the immobilized vegetative cell concentration, but the synthesis of new cells was not the primary cause for the observed activity increases, as has been concluded by other researchers [2,6]. For example, the butyric acid rate of formation increased fivefold during the first regeneration phase of run CI28, while the immobilized vegetative cell population doubled; furthermore, the increase in vegetative cell number was a result of both spore germination and vegetative cell growth. Similar observations may be made for the regeneration of activity during the other nutrient feeding phases. Even when the addition of vitamins during the third regeneration period of run CI28 cause a fivefold increase in

the number of immobilized rods (again, with a substantial contribution from the germination of spores), the volumetric rate of butyric acid increased from 0.2 to 5.2 $mM \cdot hr^{-1}$, and that of butanol rose to 9 $mM \cdot hr^{-1}$ from levels less than 0.1 $mM \cdot hr^{-1}$ (Figure 111).

The fluorescence trajectories during experiments CI23, CI28, and CI30 all show fairly complex behavior (Figures 85, 94, and 105). While the changes in the measured fluorescence intensity are due to variations in the intracellular NAD(P)H content of the immobilized cells, it has not been possible to rationalize each change in terms of specific metabolic events. This is due in part to the undetermined effect of changes in the concentration of immobilized vegetative cells, clostridial forms, spores, and germinating spores on the attenuation of the fluorescence signal, and also to a lack of knowledge about the extent of NAD(P)H consumption in reactions not shown in Figure 15, especially in sporulation and germinating cell types. However, some of the features in each fluorescence profile can be attributed to the changes in product formation rates and ammonia uptake mechanisms, since there are differences in the NAD(P)H yields (or requirements) between the acid- and solvent-producing pathways and between the GS/GOGAT and the dehydrogenase ammonia assimiliation pathways (for glutamine synthesis).

One such feature found in the fluorescence profiles of all three experiments is the increase in fluorescence intensity that occurs shortly after the addition of NH_4Cl to the bioreactor. In many cases this increase was preceded by a brief, sharp decrease in the fluorescence signal (*e.g.*, Figure 85). These changes were due to the involvement of NAD(P)H in the uptake of ammonia (Figure 113); the rapid decrease corresponded to the immediate uptake of nitrogen by the high affinity GS/GOGAT

system. Saturation of glutamine synthetase occurred rapidly, and the NAD(P)H consumption rate due to ammonia slowed. Since the rate of glucose consumption and acid formation had begun to increase at this point in a regeneration phase, the net rate of NAD(P)H generation increased, and thus the fluorescence intensity increased. The time at which the fluorescence profile is a maximum (following one of these increases) corresponds well with the start of the secondary increase in ammonia assimilation rate. At this time, the dehydrogenase (glutamate or alanine) pathway is used, with the concomitant consumption of NAD(P)H. Similarly, an increase (though often brief) in the fluorescence trajectories occurs near the time that the level of ammonia in the system reaches zero. This can be understood as a sudden drop in the rate of NAD(P)H consumption, leading to a time of net NAD(P)H production.

The basis for the general observation of fluorescence signal (NAD(P)H concentration) decrease during nitrogen assimilation and a relatively constant signal (concentration) level during the bioconversion phases is not entirely clear. While ammonia uptake consumes NAD(P)H , it seems unlikely that intracellular NAD(P)H changes of the magnitude observed in these experiments could be caused by this reaction alone. A more reasonable hypothesis is that the fluorescence decreased because NAD(P)H was consumed at a high rate in biosynthetic reactions.

Finally, it should be noted that the fluorescence profile during the last (vitamin and ammonia) regeneration period of run CI28 (Figure 94) closely resembles the specific fluorescence trajectory of the pH 4.5 suspended cell batch fermentation in Chapter 4 (Figure 23). Since the product formation patterns (acid production followed by acid consumption for solvent formation) are the same in both cases,

and the immobilized cell fluorescence seems to be relatively insensitive to cell concentration, this agreement serves to verify the observations made in both cases.

As was discussed in Chapter 5, riboflavin oversynthesis and excretion occur as a result of the synthesis of FMN-based flavodoxin during periods of iron limitation (<1 μM iron) [69,70]. In these experiments, feed iron concentrations were lowered to *ca.* 1.6 μM due to inadvertent iron(III) phosphate precipitation before medium filtration. Flavodoxin is capable of substituting for ferredoxin in all of the ferredoxin-mediated redox reactions (catalyzed by pyruvate:ferredoxin oxidoreductase, NADH:ferredoxin oxidoreductase, and hydrogenase) [71,72]; although flavodoxin is less efficient than ferredoxin in these reactions, a large amount of the FMN-based protein is synthesized (up to 2% of the total cell protein) [73]. Although some key enzymes in the *C. acetobutylicum* metabolic pathway are iron proteins (*e.g.*, hydrogenase and acetoacetate decarboxylase), the metabolic activity of the immobilized cells did not seem to be drastically altered by this limitation. The monitoring of excreted riboflavin fluorescence can be used as an indicator of periods of relatively rapid cell growth, when the demand for iron exceeds the 1.6 μM supply. A comparison of the immobilized vegetative cell and riboflavin concentration profiles shows that these two events were related.

The level of 260 nm absorbance in the medium (after corrections for the contributions of riboflavin, acetoin, and acetone) is a measure of the excretion of nucleic acis from the immobilized cells. While this excretion is often due to the degradation of RNA by starving cells [33], the occurrence of all of the A_{260} peaks during periods of nitrogen feeding indicates that RNA degradation did not contribute to the measured A_{260} in these experiments. Instead, the peaks correspond to peri-

ods of sporulation and/or germination within the calcium alginate gel [21]. It is interesting to note that the fluctuations in the cell-free medium background fluorescence (shown in the insets of Figures 85, 94, and 105) follow essentially the same trajectory as the A_{260} of the same experiment.

During the final regeneration phase of experiment CI30, the effects of each of the vitamins used in the vitamin mixture were investigated by pulsing them individually into the bioreactor system with NH_4Cl-supplemented medium as the system feed. At least three residence times passed before the injection of the next vitamin (four residence times after the PABA injection), and in this time the concentration of the vitamin was reduced to a maximum of 5% (2% for PABA) of its initial concentration; however, the actual concentration was probably much lower because of assimilation by the immobilized bacteria. The cells retain these vitamins for long periods of time, so the observed effects were essentially cumulative.

Figures 100 and 106 show the concentration profiles and fluorescence trajectory during this regeneration period. While obvious changes occurred in these quantities, and in the concentrations of immobilized vegetative cells and effluent ammonia, not all are related to the presence of a specific vitamin. For example, the pattern of vegetative cell increase between 270 and 290 hours was most likely due to the presence of nitrogen for 35 hours instead of the 10 or 15 hour regeneration periods used earlier. However, some changes seemed to be directly connected to the appearance of a specific vitamin. Although the addition of NH_4Cl (alone) at the start of this period (235 hours) resulted in a significant increase in the rate of acid production, the preceding regeneration period (NH_4Cl and vitamins) had ended only 30 hours earlier and so the cells may have contained enough of the necessary vitamins to

respond to the switch to nitrogen-containing feed. The injection of PABA at 250 hours resulted in very large increases in the rates of ethanol and butanol formation, with only a small increase in the immobilized vegetative cell population. In addition, the NAD(P)H-dependent fluorescence intensity increased shortly after the biotin was pulsed into the system; this trend continued for about 25 hours. Thiamine had very little effect on the rates of product formation or the fluorescence intensity. Although the volumetric formation rates were essentially constant for the 15 hours following the addition of thiamine, the rapid increase in the concentration of immobilized vegetative cells (not due to the presence of thiamine) indicates that the specific rates of product formation decreased. The injection of biotin into the bioreactor (at 285 hours) caused an immediate increase in the rates of ammonia assimilation and acid formation. Approximately ten hours after the biotin addition, the rates of nitrogen uptake and acid production peaked, and the volumetric rates of ethanol and butanol increased sharply. The fluorescence intensity was constant from this time until the 300 hour mark, when it declined rapidly.

CONCLUSIONS

Although the regeneration of immobilized cell bioconversion activity by the addition of complex, undefined organic nutrient compounds has led other researchers to conclude that the major cause of the observed increase in (volumetric) activity was the growth of new cells, three experiments discussed in this chapter have shown that activity regeneration under more carefully defined conditions can result in large increases in product formation rates without significant cell growth. The patterns

of product formation during the experiments were due to the nutritional state of the immobilized cells as they were exposed to alternating conditions of nitrogen starvation and surplus. Decreasing levels of exogenous nitrogen induced the high affinity ammonia uptake system, causing the adenylate energy charge of the cells to increase; this in turn resulted in the repression of glucose carbon flow through the EMP pathway and the use of the acid-forming catabolic reactions for the more efficient production of ATP. While nutrient limitation or starvation can be used to control the growth of immobilized cells, the effects of the limitation need to be well understood for the design of an optimal feeding scheme.

In situ NAD(P)H-dependent fluorescence measurements indicated that intracellular NAD(P)H levels changed significantly throughout each experiment. In most cases, the beginning of nitrogen feeding and the exhaustion of the medium ammonia could be detected with the fluorescence probe. Measurements of the 260 nm absorbance of the bioreactor effluent correlated with sporulation and germination events and could be readily adapted for on-line monitoring of these events.

LITERATURE CITED

1. Larsson, P.O., S. Ohlson, and K. Mosbach, "New approach to Steroid Conversion Using Activated Immobilised Microorganisms," *Nature*, **263**, 796–797 (1976).

2. Ohlson, S., P.-O. Larsson, and K. Mosbach, "Steroid Transformation by Living Cells Immobilized in Calcium Alginate," *Eur. J. Appl. Microbiol. Biotechnol.*, **7**, 103–110 (1979).

3. Szwajcer, E., P. Brodelius, and K. Mosbach, "Production of α-Keto acids: 2. Immobilized Whole Cells of *Providencia* sp. PCM 1298 Containing L-Amino Acid Oxidase," *Enz. Microb. Tech.*, **4**, 409–413 (1982).

4. Lee, T.H., J.C. Ahn, and D.D.Y. Ryu, "Performance of an Immobilized Yeast Reactor System for Ethanol Production," *Enz. Microb. Tech.*, **5**, 41–45 (1983).

5. Förberg, C., S.-O. Enfors, and L. Häggstrom, "Control of Immobilized, Non-Growing Cells for Continuous Production of Metabolites," *Eur. J. Appl. Microbiol. Biotechnol.*, **17**, 143–147 (1983).

6. Cheetham, P.S.J., C. Garrett, and J. Clark, "Isomaltulose Production Using Immobilized Cells," *Biotech. Bioeng.*, **27**, 471–481 (1985).

7. Kloosterman IV, J., and M.D. Lilly, "Maintenance and Operational Stability of Immobilized *Arthrobacter simplex* for the Δ^1-Dehydrogenation of Steriods," *Enz. Microb. Tech.*, **7**, 377–382 (1985).

8. Klein, J. and F. Wagner, "Different Strategies to Optimize the Production Phase of Immobilized Cells," *Ann. N.Y. Acad. Sci.*, **501**, 306–316 (1987).

9. Briffaud, J. and M. Engasser, "Citric Acid Production from Glucose. II. Growth and Excretion Kinetics in a Trickle-Flow Fermentor," *Biotech. Bioeng.*, **21**, 2093–2111 (1979).

10. Inloes, D.S., A.S. Michaels, C.R. Robertson, and A. Matin, "Ethanol Production by Nitrogen-Deficient Yeast Cells Immobilized in a Hollow-Fiber Membrane Bioreactor," *Appl. Microbiol. Biotechnol.*, **23**, 85–91 (1985).

11. Reardon, K.F., T. Scheper, and J.E. Bailey, "*In situ* Fluorescence Monitoring of Immobilized *Clostridium acetobutylicum*," *Biotech. Lett.*, **8**, 817–822 (1986).

12. Larsson, P.O., S. Ohlson, and K. Mosbach, "Steroid Conversion Using Immobilized Living Microorganisms," *Enzyme Eng.*, **4**, 317–322 (1978).

13. Ohlson, S., P.O. Larsson, and K. Mosbach, "Steroid Transformation by Activated Living Immobilized *Arthrobacter simplex* Cells," *Biotech. Bioeng.*, **10**, 1267–84 (1978).

14. Förberg and L. Häggström, "Adsorbed Cell Systems Controlled by the Nutrient Dosing Technique," 3rd European Congress on Biotechnology, vol II, Munich, 10–14 September 1984, Verlag-Chemie, p. II-115–II-120.

15. Förberg, C. and L. Häggström, "Control of Cell Adhesion and Activity During Continuous Production of Acetone and Butanol with Adsorbed Cells," *Enz. Microb. Tech.*, **7**, 230–234 (1985).

16. Reardon, K.F., T.-H. Scheper, and J.E. Bailey, "Einsatz eines Fluoreszenzsensors zur Messung der NAD(P)H-Abhängigen Kulturfluoreszenz Immobilisierter Zellsysteme," *Chem.-Ing.-Tech.*, **59**, 600-601 (1987).

17. Gould, G.W., in *The Bacterial Spore*, G.W. Gould and A. Hurst (eds.), Academic Press, New York, 1969, pp. 397–444.

18. Schlegel, H.G., *General Microbiology*, 6^{th} Ed., Cambridge University Press, New York, 1986, pp. 254–255.

19. Fitz-James, P. and E. Young, "Morphology of Sporulation," in *The Bacterial*

Spore, G.W. Gould and A. Hurst (eds.), Academic Press, New York, 1969, pp. 39–72.

20. Rose, A.H., *Chemical Microbiology—An Introduction to Microbiol Physiology*, 3rd Ed., Butterworths, London, 1976, pp.397–414.

21. Setlow, P., "Biochemistry of Bacterial Forespore Development and Spore Germination," in *Sporulation and Germination*, H.S. Levinson, A.L. Sonenshein, and D.J. Tipper (eds.), Amer. Soc. Microbiol., Washington, 1981, pp. 13–25.

22. Woods, D.R. and D.T. Jones, "Physiological Responses of *Bacteroides* and *Clostridium* Strains to Environmental Stress Factors," *Adv. Microbial Physiol.*, **28**, 1–64 (1986).

23. Long, S., D.T. Jones, and D.R. Woods, "Initiation of Solvent Production, Clostridial Stage and Endospore Formation in *Clostridium acetobutylicum* P262," *Appl. Microbiol. Biotechnol.*, **20**, 256–261 (1984).

24. Kleiner, D., "Regulation of Ammonium Uptake and Metabolism by Nitrogen Fixing Bacteria. II. *Clostridium pasteurianum*," *Arch. Microbiol.*, **120**, 263–270 (1979).

25. Kleiner, D. and E. Fitzke, "Some Properties of a New Electrogenic Transport System: The Ammonium (Methylammonium) Carrier From *Clostridium pasteurianum*," *Biochim. Biophys. Acta*, **641**, 138–147 (1981).

26. Kleiner, D., "Bacterial Ammonium Transport," *FEMS Microbiol. Rev.*, **32**, 87–100 (1985).

27. Bogdahn, M. and D. Kleiner, "N_2 Fixation and NH_4^+ Assimilation in the Thermophilic Anaerobes *Clostridium thermosaccharolyticum* and *Clostridium thermoautotrophicum*," *Arch. Microbiol.*, **144**, 102–104 (1986).

28. Tyler, B., "Regulation of the Assimilation of Nitrogen Compounds," *Ann. Rev. Biochem.*, **47**, 1127–1162 (1978).

29. Harder, W. and L. Dijkhuizen, "Physiological Responses to Nutrient Limitation," *Ann. Rev. Microbiol.*, **37**, 1–23 (1983).

30. Gottschalk, G., "Bacterial Fermentations," in *Bacterial Metabolism*, 2^{nd} Ed., G. Gottschalk (ed.), Springer-Verlag, New York, 1985, p. 208–282.

31. Usdan, K.P., H. Zappe, D.T. Jones, and D.R. Woods, "Cloning, Expression, and Purification of Glutamine Synthetase from *Clostridium acetobutylicum*," *Appl. Env. Microbol.*, **52**, 413–419 (1986).

32. Neijssel, O. and D.W. Tempest, "The Physiology of Metabolite Overproduction," *Symp. Soc. Gen. Microbiol.*, **29**, 53–82 (1979).

33. Dawes, E.A., "Endogenous Metabolism and the Survival of Starved Prokaryotes," *Symp. Soc. Gen. Microbiol.*, **26**, 19–53 (1976).

34. Harder, W., L. Dijkhuizen, and H. Veldkamp, "Environmental Regulation of Microbial Metabolism," *Symp. Soc. Gen. Microbiol.*, **36**, 51–95 (1984).

35. Boyaval, P. E. Boyaval, and M.J. Desmazeaud, "Survival of *Brevibacterium linens* During Nutrient Starvation and Intracellular Changes," *Arch. Microbiol.*, **141**, 128–132 (1985).

36. Long, S., D.T. Jones, and D.R. Woods, "The Relationship Between Sporulation and Solvent Production in *Clostridium acetobutylicum* P262," *Biotech. Lett.*, **6**, 529–534 (1984).

37. Reysenbach, A.L., N. Ravenscroft, S. Long, D.T. Jones, and D.R. Woods, "Characterization, Biosynthesis, and Regulation of Granulose in *Clostridium acetobutylicum*," *Appl. Env. Microbiol.*, **52**, 185–190 (1986).

38. J.R. Postgate and J.R. Hunter, "Accelerated Death of *Aerobacter aerogenes* Starved in the Presence of Growth-Limiting Substrates," *J. Gen. Microbiol.*, **34**, 459–473 (1964).

39. Dawes, E.A. and D.W. Ribbons, "Some Aspects of Endogenous Metabolism of Bacteria," *Bact. Rev.*, **28**, 126–149 (1964).

40. Boylen, C.W. and J.C. Ensign, "Intracellular Substrates for Endogenous Metabolism During Long-Term Starvation of Rod and Spherical Cells of *Arthrobacter crystallopoietes*," *J. Bacteriol.*, **103**, 578–587 (1970).

41. Montague, M.D. and E.A. Dawes, "The Survival of *Peptococcus prevotii* in Relation to the Adenylate Energy Charge," *J. Gen. Microbiol.*, **80**, 291–299 (1974).

42. Scherer, C.G. and C.W. Boylen, "Macromolecular Synthesis and Degradation in *Arthrobacter* During Periods of Nutrient Deprivation," *J. Bacteriol.*, **132**, 584–589 (1977).

43. Goldberg, A.L. and A.C. St. John, "Intracellular Protein Degradation in Mammalian and Bacterial Cells: Part 2," *Annu. Rev. Biochem.*, **45**, 747–803 (1976).

44. Robson, R.L. and J.G. Morris, "Mobilization of Granulose in *Clostridium pasteurianum*: Purification and Properties of Granulose Phosphorylase," *Biochem. J.*, **144**, 513–517 (1974).

45. Robson, R.L., R.M. Robson, and J.G. Morris, "The Biosynthesis of Granulose by *Clostridium pasteurianum*," *Biochem. J.*, **144**, 503–512 (1974).

46. Dietzler, D.N., C.J. Lais, and M.P. Leckie, "Simultaneous Increases of the Adenylate Energy Charge and the Rate of Glycogen Synthesis in Nitrogen-Starved *Escherichia coli* W 4597(K)," *Arch. Biochem. Biophys.*, **160**, 14–25

(1974).

47. Hueting, S. and D.W. Tempest, "Influence of the Glucose Input Concentration on the Kinetics of Metabolite Production by *Klebsiella aerogenes* NCTC 418: Growing in Chemostat Culture in Potassium- or Ammonia-Limited Environments," *Arch. Microbiol.*, **123**, 189–194 (1979).

48. Lampen, J.D. and W.H. Peterson, "Growth Factor Requirements of Clostridia," *Arch. Biochem.*, **2**, 443–449 (1943).

49. Monot, F., J.-R. Martin, H. Petitdemange, and R. Gay, "Acetone and Butanol Production by *Clostridium acetobutylicum* in a Synthetic Medium," *Appl. Env. Microbiol.*, **44**, 1318–1324 (1982).

50. Soni, B.K., P. Soucaille, and G. Goma, "Continuous Acetone-Butanol Fermentation: A Global Approach for the Improvement in the Solvent Productivity in Synthetic Medium," *Appl. Microbiol. Biotechnol.*, **25**, 317–321 (1987).

51. M^{c}Neil, B. and B. Kristiansen, "The Effect of Medium Composition on the Acetone-Butanol Fermentation in Continuous Culture," *Biotech. Bioeng.*, **29**, 383–387 (1987).

52. Yerushalmi, L. and B. Volesky, "Culture Conditions for Growth and Solvent Biosynthesis by a Modified *Clostridium acetobutylicum*," *Appl. Microbiol. Biotechnol.*, **25**, 513–520 (1987).

53. Koser, S.A., *Vitamin Requirements of Bacteria and Yeasts*, Charles C. Thomas, Springfield (Ill.), 1968, pp. 39–181.

54. *The Vitamins. Chemsitry, Physiology, Pathology, Methods*, vol. II, 2nd Ed., W.H. Sebrell, Jr. and R.S. Harris (eds.), Academic Press, New York, 1968, pp. 261–336.

55. Lehninger, A.L., *Biochemistry*, 2nd Ed., Worth Publishers, New York, 1975, pp. 335–359.

56. Dagley, S. and D.E. Nicholson, *An Introduction to Metabolic Pathways*, Wiley, New York, 1970, pp. 93–108.

57. Doelle, H.W., "Enzymes, Coenzymes, and Bacterial Growth Kinetics," in *Bacterial Metabolism*, 2nd Ed., Academic Press, 1975, pp. 39–83.

58. Vasil'eva, S.V., L.S. Davnichenko, and I.A. Rapoport, "Intensification by p-Aminobenzoic Acid of DNA Repair Processes in *Escherichia coli* K-12," *Soviet Genetics*, **18**, 381–391 (1982).

59. Vasil'eva, S.V., T.E. Gorb, and I.A. Rapoport, "The Vitamin p-Aminobenzoic Acid Prevents the Development of SOS Functions in *tif-1* Mutants of *Escherichia coli* at a Restrictive Temperature," *Soviet Genetics*, **19**, 1952–1957 (1984).

60. Roos, J.W., J.K. McLaughlin, and E.T. Papoutsakis, "The Effect of pH on Nitrogen Supply, Cell Lysis, and Solvent Production in Fermentations of *Clostridium acetobutylicum*," *Biotech. Bioeng.*, **27**, 681–694 (1985).

61. Huang, L., L.N. Gibbons, and C.W. Forsberg, "Transmembrane pH Gradient and Membrane Potential in *Clostridium acetobutylicum* During Growth under Acetogenic and Solventogenic Conditions," *Appl. Env. Microbiol.*, **50**, 1043–1047 (1985).

62. Gottwald, M. and G. Gottschalk, "The Internal pH of *Clostridium acetobutylicum* and its Effect on the Shift from Acid to Solvent Formation," *Arch. Microbiol.*, **143**, 42–46 (1985).

63. Terracciano, J.S. and E.R. Kashket, "Intracellular Conditions Required for

Initiation of Solvent Production by *Clostridium acetobutylicum*," *Appl. Env. Microbiol.*, **52**, 86–91 (1986).

64. Dills, S.S., A. Apperson, M.R. Schmidt, and M.H. Saier, Jr., "Carbohydrate Transport in Bacteria," *Microbiol. Rev.*, **44**, 385–418 (1980).

65. Bailey, J.E. and D.F. Ollis, *Biochemical Engineering Fundamentals*, 2nd Ed., McGraw-Hill, New York, 1986, pp. 269–273.

66. Datta, R. and J.G. Zeikus, "Modulation of Acetone-Butanol-Ethanol Fermentation by Carbon Monoxide and Organic Acids," *Appl. Env. Microbiol.*, **49**, 522–529 (1985).

67. Meyer, C.L., J.W. Roos, and E.T. Papoutsakis, "Carbon Monoxide Gasing Leads to Alcohol Production and Butyrate Uptake Without Acetone Formation in Continuous Cultures of *Clostridium acetobutylicum*," *Appl. Microbiol. Biotechnol.*, **24**, 159–167 (1986).

68. Galazzo, J.L., J.V. Shanks, and J.E. Bailey, "Comparison of Suspended and Immobilized Yeast Metabolism Using ^{31}P Nuclear Magnetic Resonance Spectroscopy," *Biotech. Techniques*, **1**, 1–6 (1987).

69. Demain, A.L., "Riboflavin Oversynthesis," *Ann. Rev. Microbiol.*, **26**, 369–388 (1972).

70. Schönheit, P., A. Brandis, and R.K. Thauer, "Ferredoxin Degradation in Growing *Clostridium pasteurianum* During Periods of Iron Deprivation," *Arch. Microbiol.*, **120**, 73–76 (1979).

71. Knight, Jr., E., and R.W.F. Hardy, "Isolation and Characteristics of Flavodoxin from Nitrogen-Fixing *Clostridium pasteurianum*," *J. Biol. Chem.*, **241**, 2752–2756 (1966).

72. Knight, Jr., E. and R.W.F. Hardy, "Flavodoxin. Chemical and Biological Properties," *J. Biol. Chem.*, **242**, 1370–1374 (1967).

73. Ragsdale, S.W. and L.G. Ljungdahl, "Characterization of Ferredoxin, Flavodoxin, and Rubredoxin from *Clostridium formicoaceticum* Grown in Media with High and Low Iron Contents," *J. Bacteriol.*, **157**, 1–6 (1984).

EXPERIMENT CI23

TIME INTERVAL	FEED
0-86	Bioconversion
86-126	Regeneration (0.8 g/L NH_4Cl)

EXPERIMENT CI28

TIME INTERVAL	FEED
0-101	Bioconversion
101-141	Regeneration (0.6 g/L NH_4Cl)
141-221	Bioconversion
221-261	Regeneration (0.6 g/L NH_4Cl)
261-291	Bioconversion
291-331	Regeneration (0.6 g/L NH_4Cl, vitamin mixture)

EXPERIMENT CI30

TIME INTERVAL	FEED
0-85	Bioconversion
85-100	Regeneration (0.6 g/L NH_4Cl)
100-115	Regeneration (0.6 g/L NH_4Cl, vitamin mixture)
115-155	Bioconversion
155-165	Regeneration (0.6 g/L NH_4Cl, vitamin mixture)
165-195	Bioconversion
195-205	Regeneration (0.6 g/L NH_4Cl, $1/10^{th}$ vitamin mixture)
205-235	Bioconversion
235-250	Regeneration (0.6 g/L NH_4Cl)
250-270	Regeneration (0.6 g/L NH_4Cl, PABA at 250)
270-285	Regeneration (0.6 g/L NH_4Cl, thiamine at 270)
285-335.5	Regeneration (0.6 g/L NH_4Cl, biotin at 285)

Table 5. Experimental Schedules.

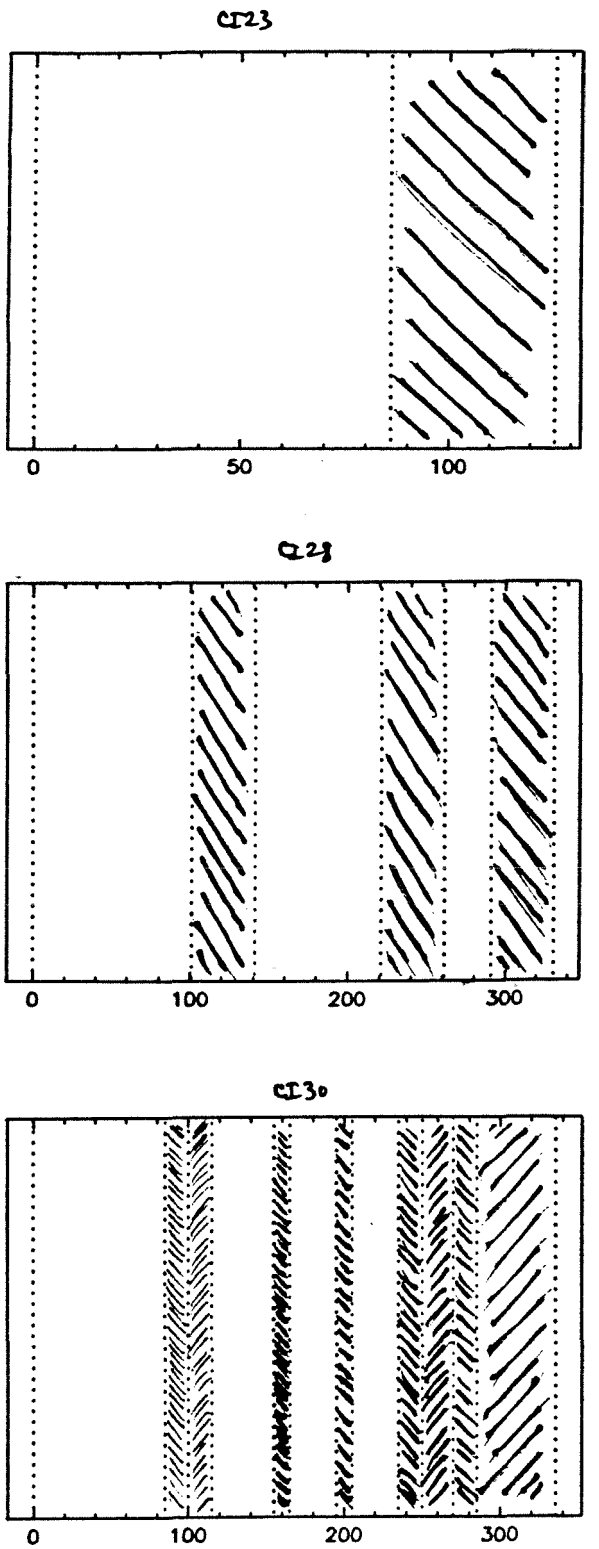

Figure 81. Event schematics for experiments CI23, CI28, and CI30. The shaded areas represent the regeneration periods.

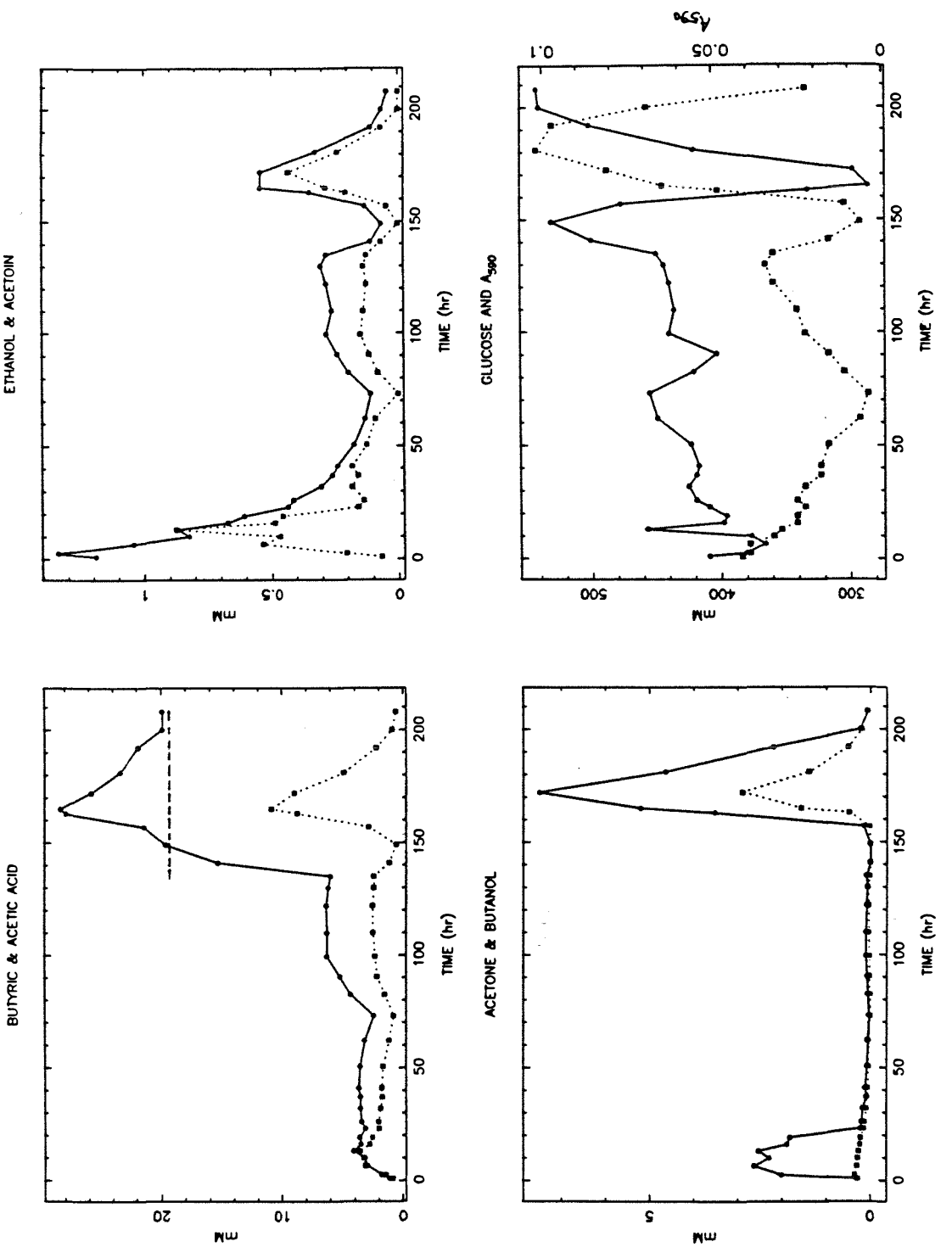

Figure 82. Concentration profiles for experiment CI10. **Upper left**: Butyric acid (solid line) and acetic acid (dotted line). **Upper right**: Ethanol (solid line) and acetoin (dotted line). **Lower left**: Butanol (solid line) and acetone (dotted line). **Lower right**: Glucose (solid line) and A590 (dotted line, right-hand scale). The level of butyric acid in the feed after 135 hours is indicated by the dashed line.

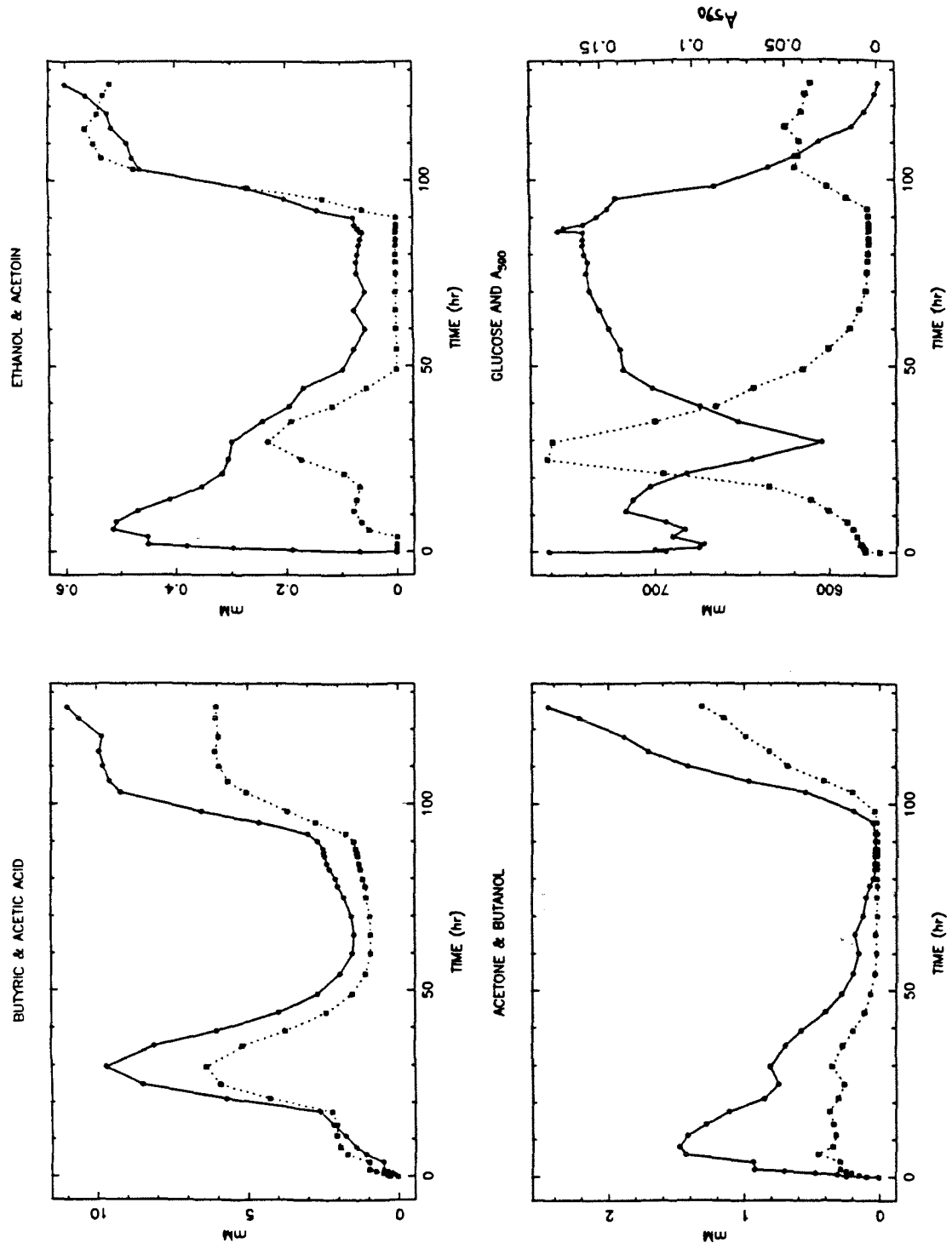

Figure 83. Concentration profiles for experiment CI23. **Upper left**: Butyric acid (solid line) and acetic acid (dotted line). **Upper right**: Ethanol (solid line) and acetoin (dotted line). **Lower left**: Butanol (solid line) and acetone (dotted line). **Lower right**: Glucose (solid line) and A590 (dotted line, right-hand scale).

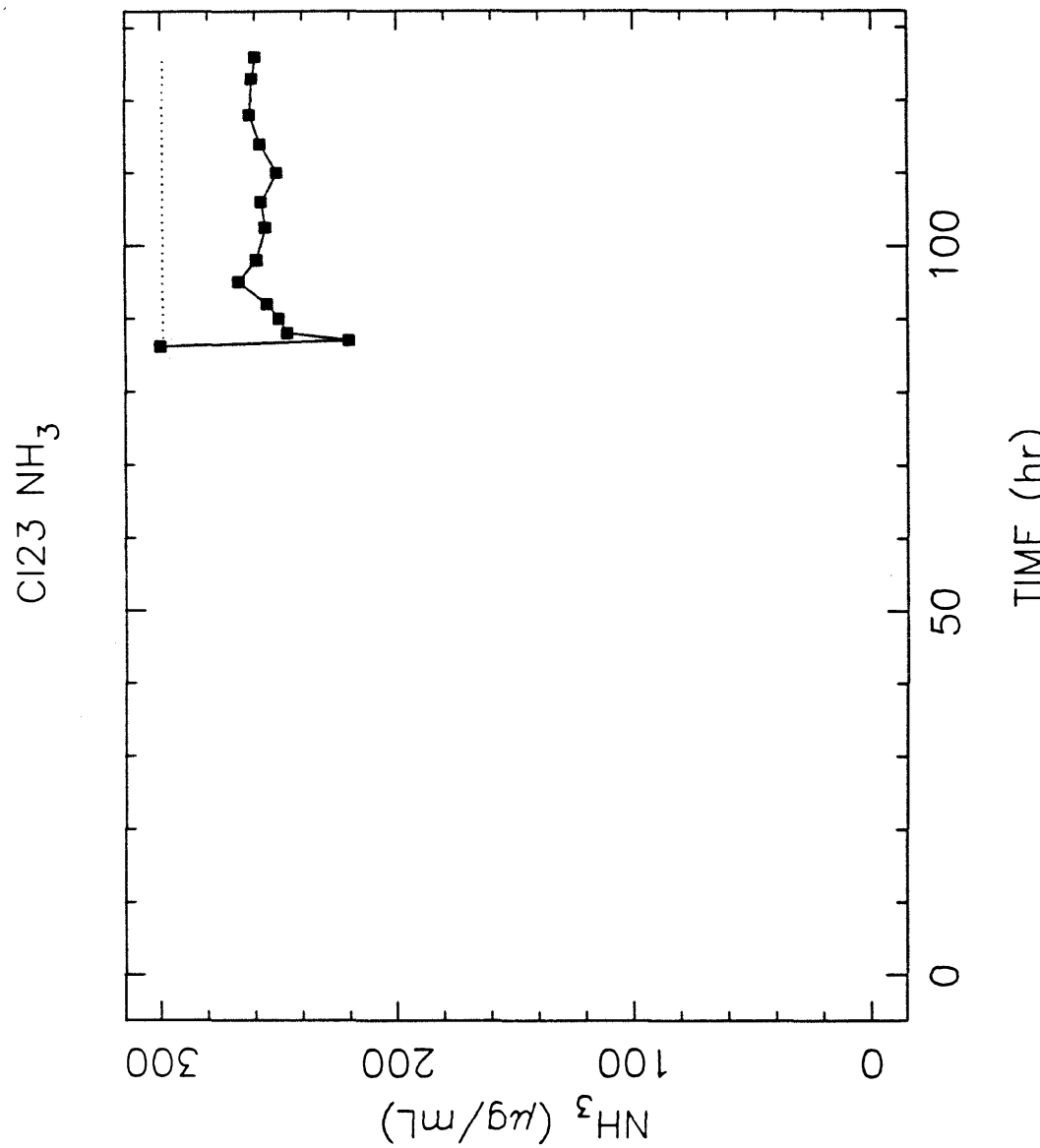

Figure 84. Ammonia concentrations in the fermentor during run CI23. The feed level is indicated by the dotted line.

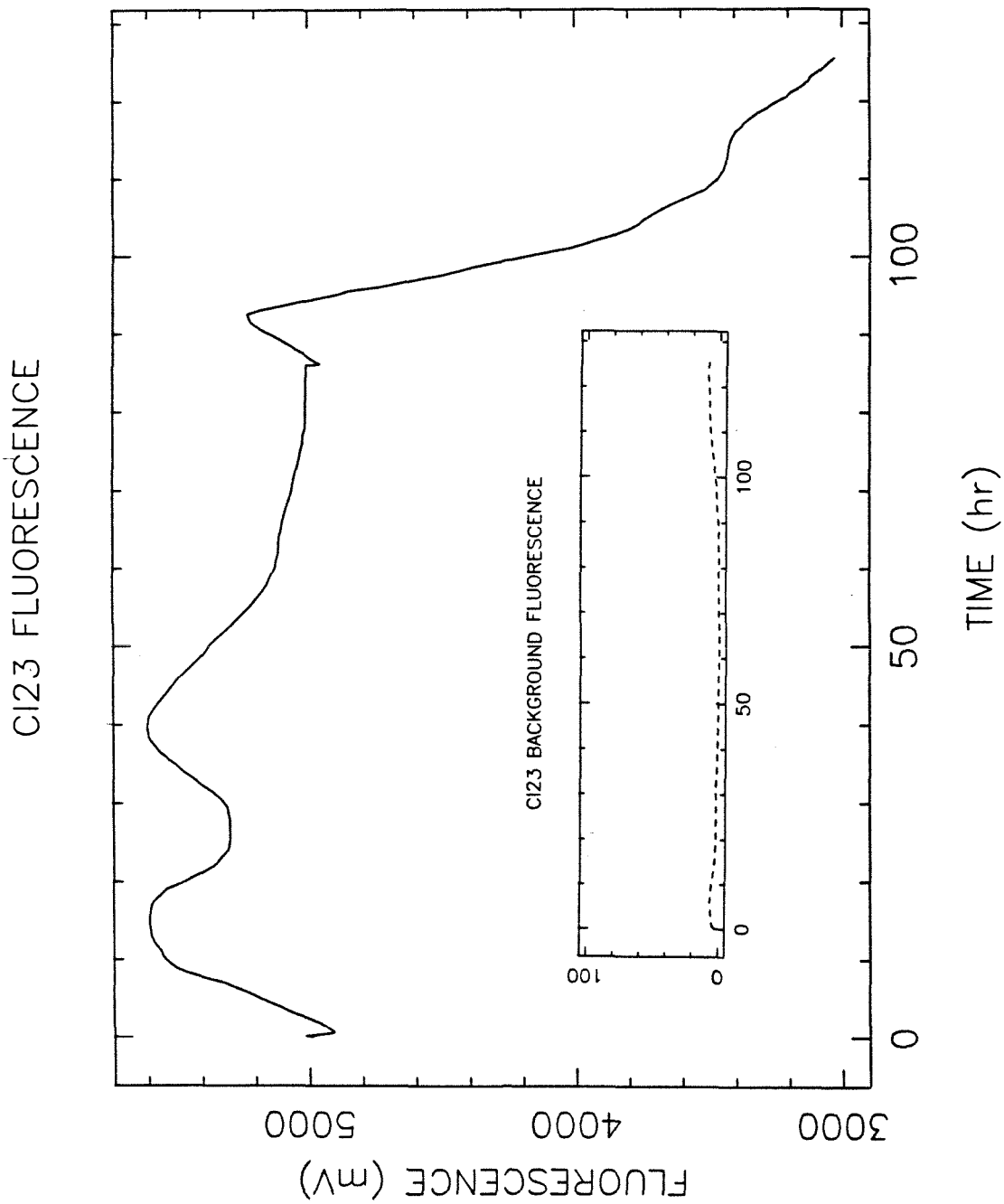

Figure 85. NAD(P)H-Dependent fluorescence during experiment CI23.

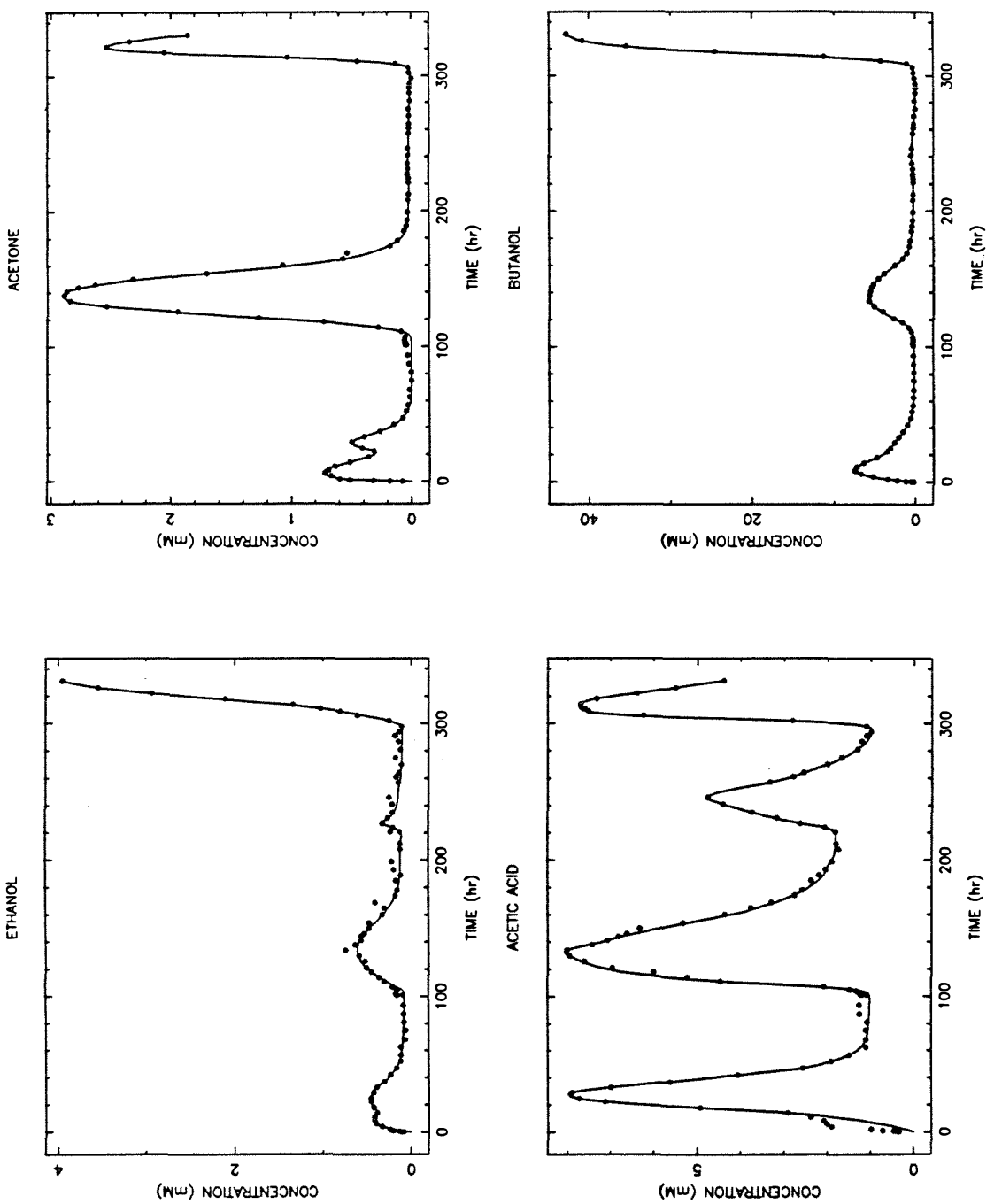

Figure 86. Experiment CI28 concentration profiles. Ethanol, acetone, acetic acid, and butanol.

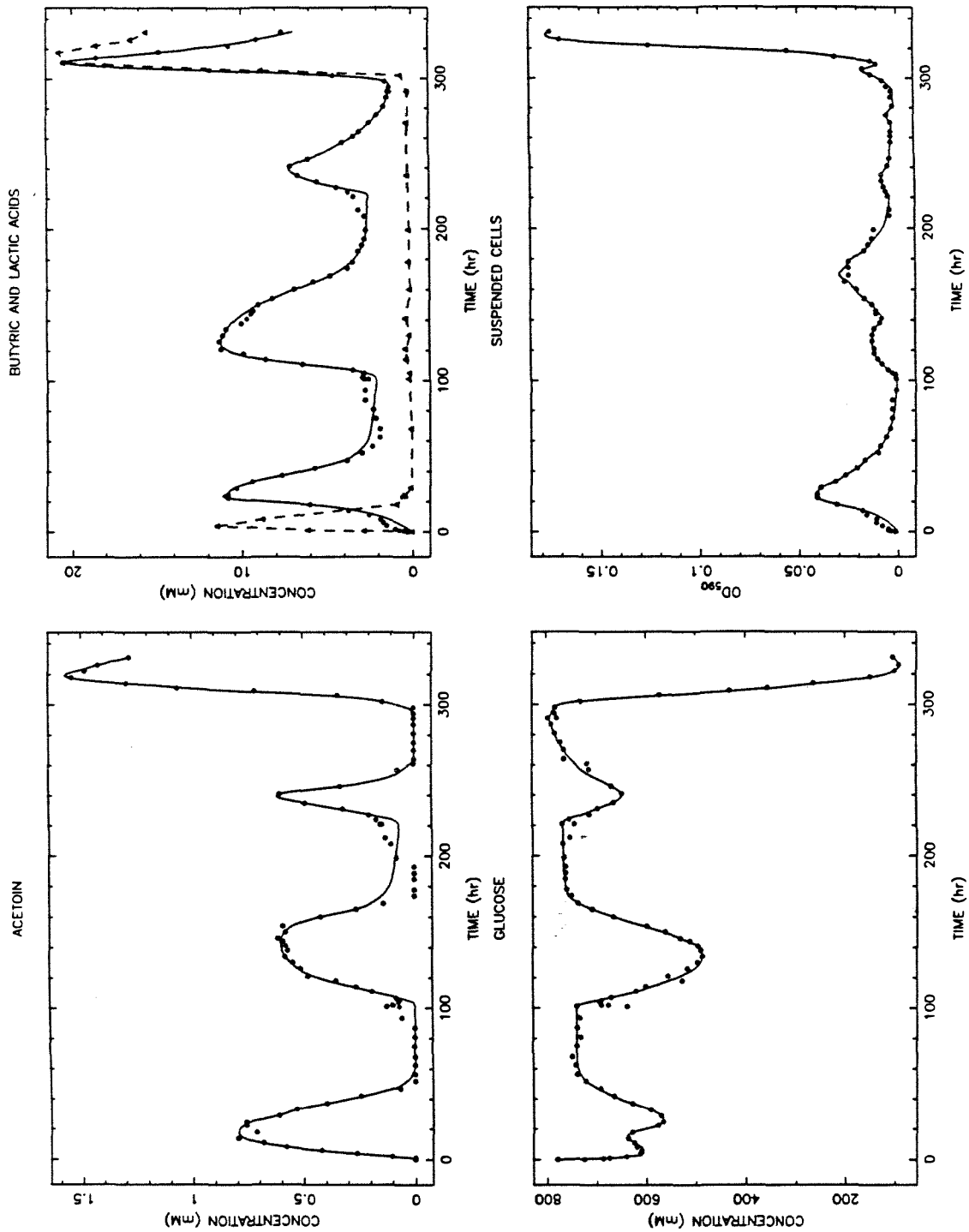

Figure 87. Experiment CI28 concentration profiles. Acetoin, butyric acid, total lactic acid, glucose, and suspended cells.

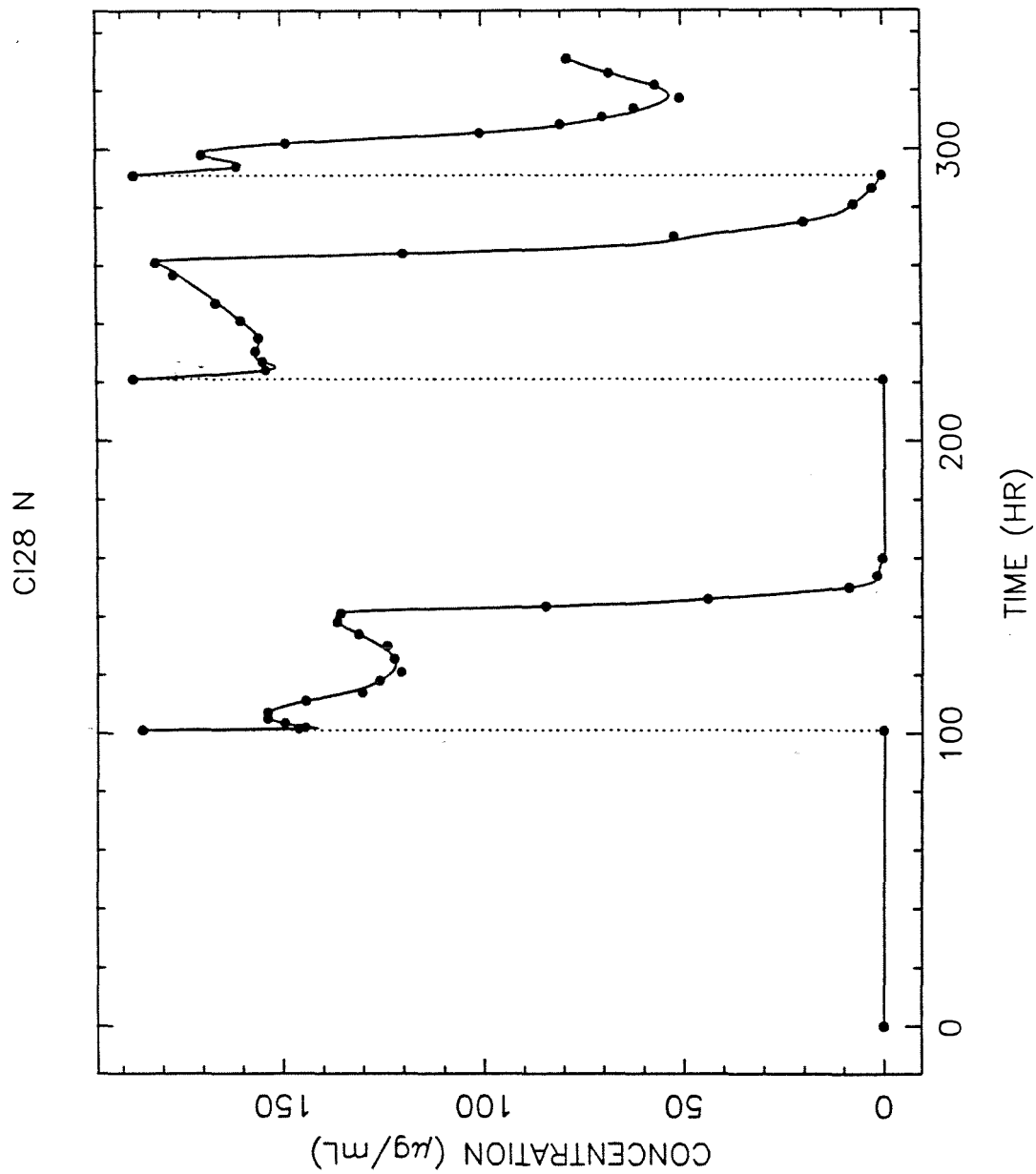

Figure 88. Experiment CI28 ammonia concentration profile.

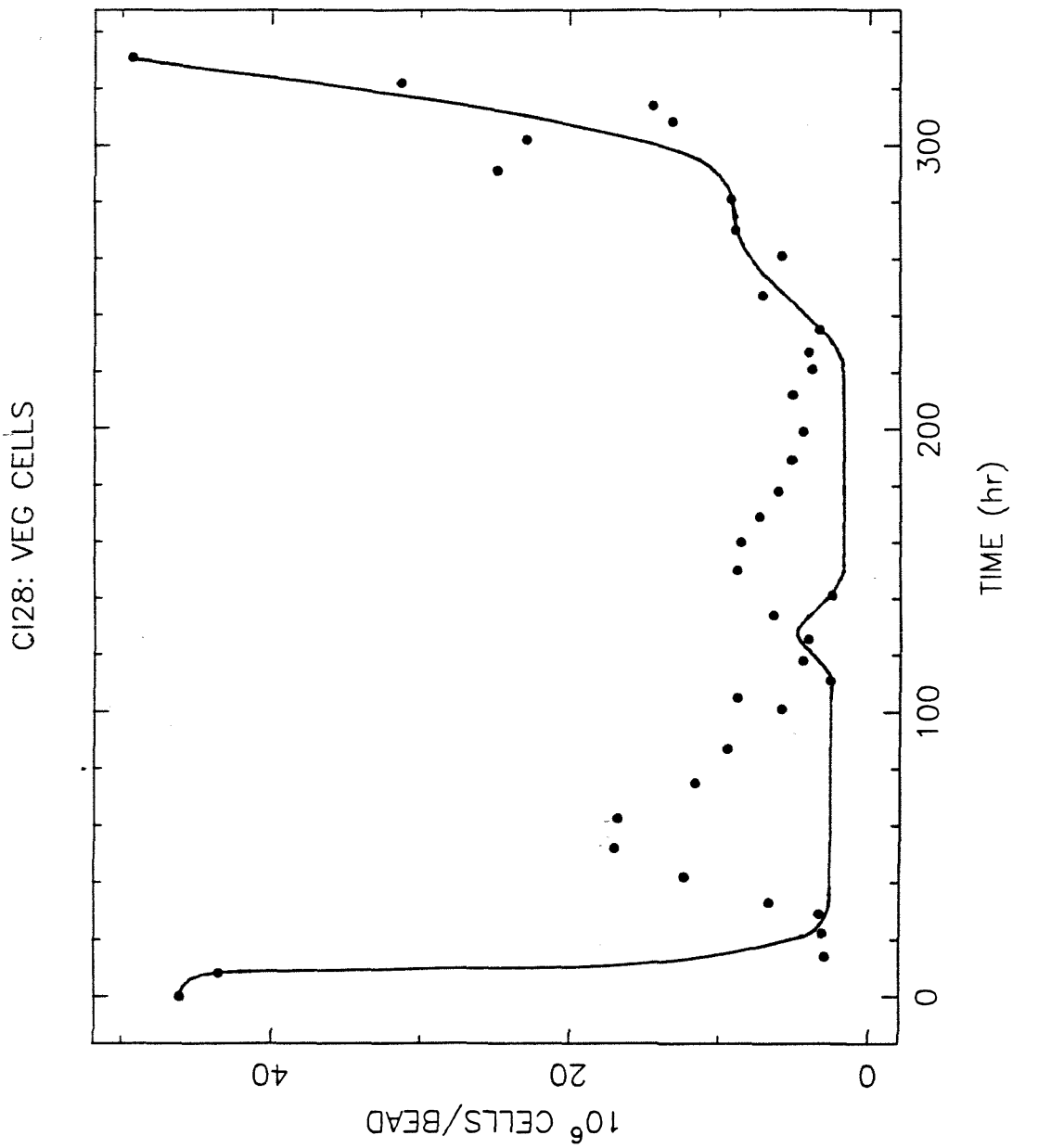

Figure 89. Immobilized vegetative cell concentrations during experiment CI28.

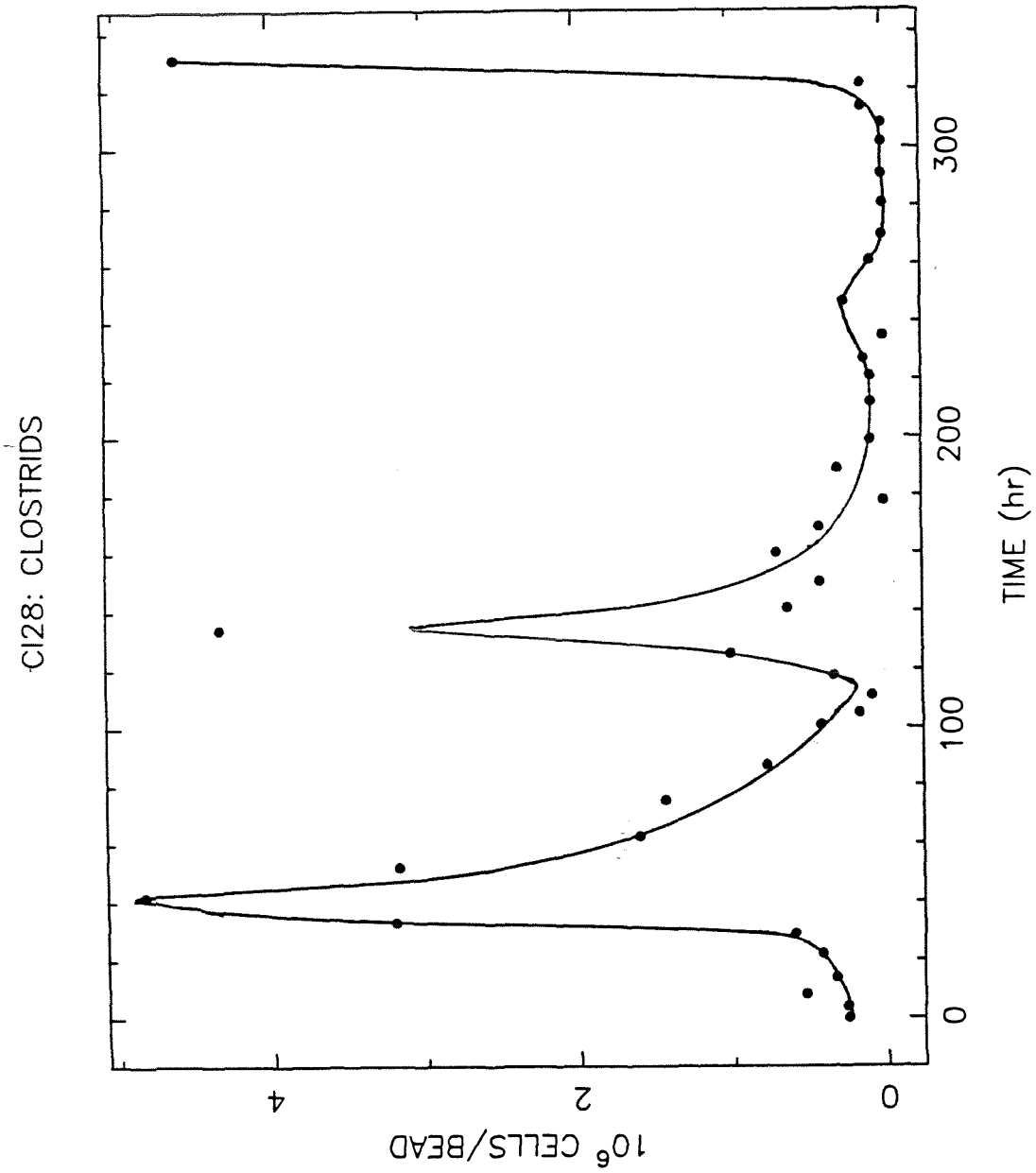

Figure 90. Immobilized clostridial form concentrations during experiment CI28.

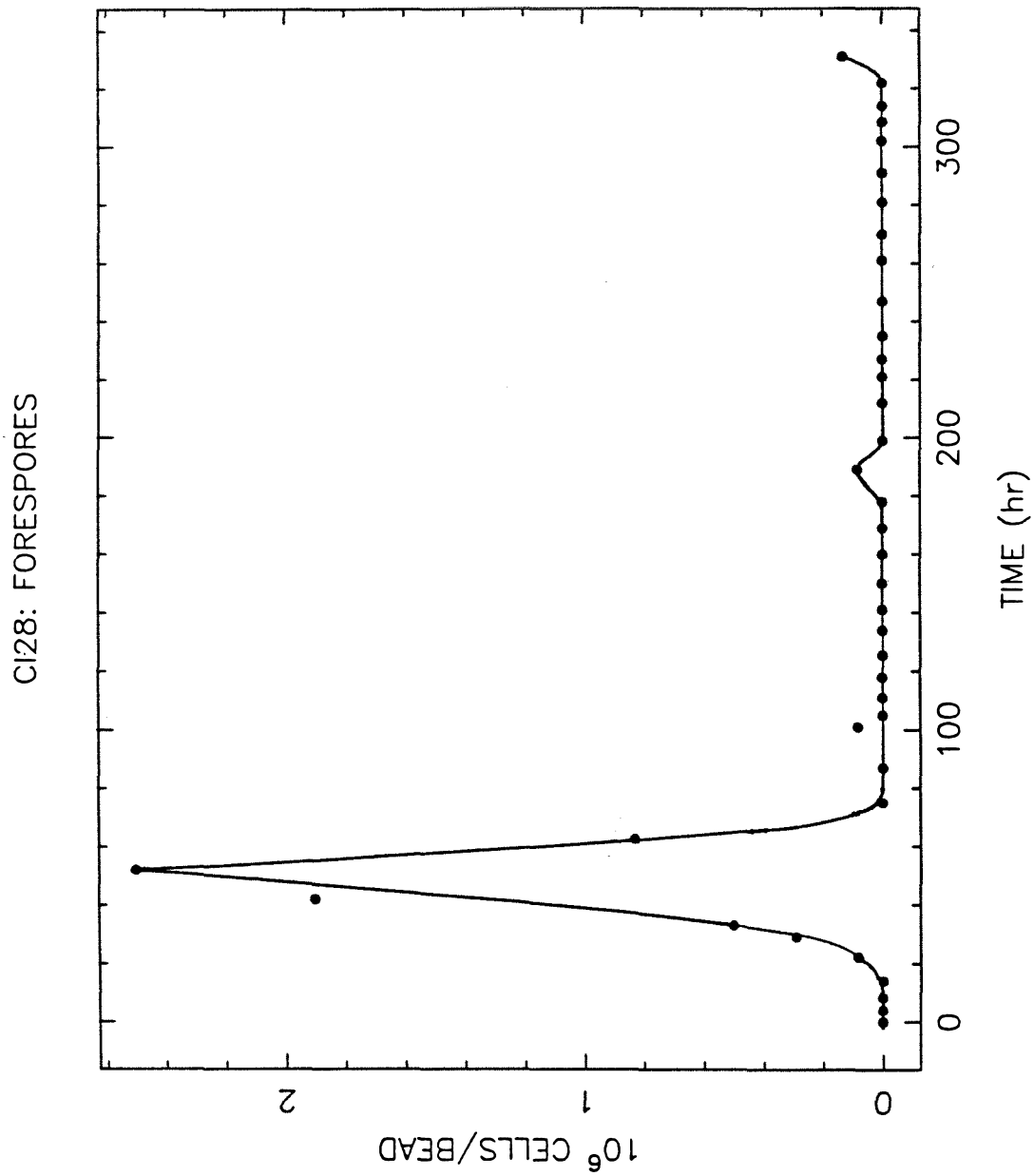

Figure 91. Immobilized forespore-containing cell concentrations during experiment CI28.

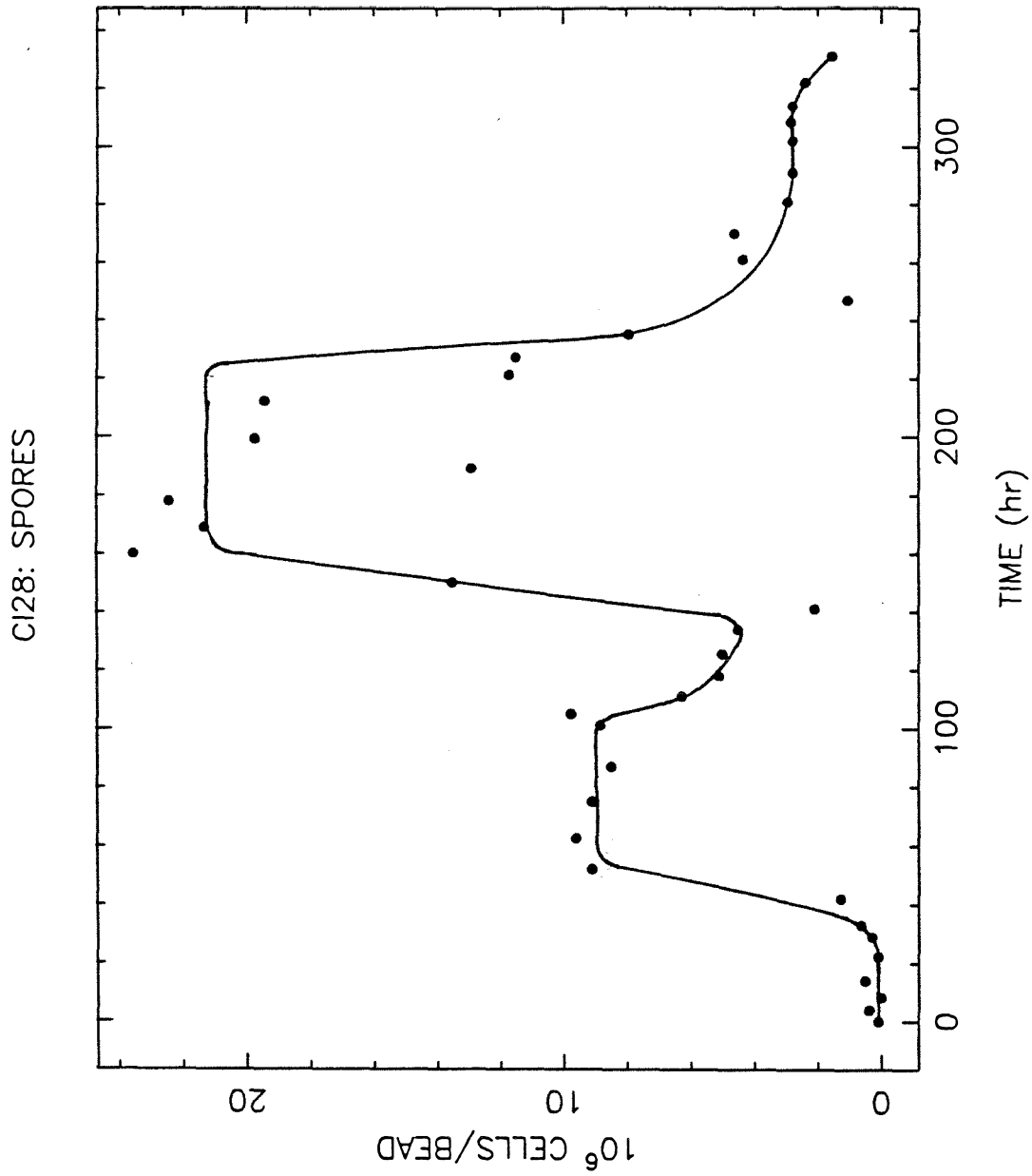

Figure 92. Immobilized spore concentrations during experiment CI28.

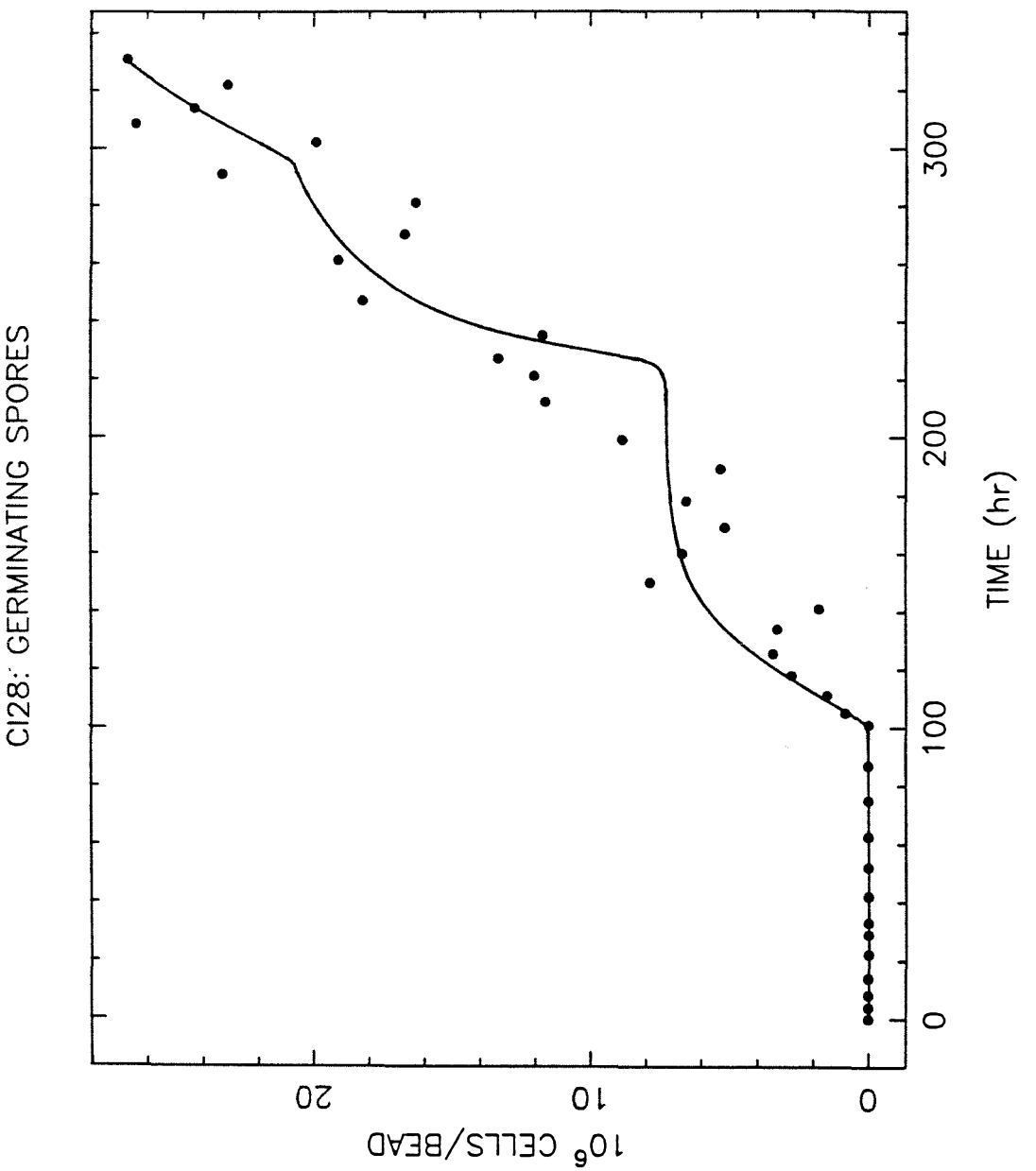

Figure 93. Immobilized germinating spore concentrations during experiment CI28.

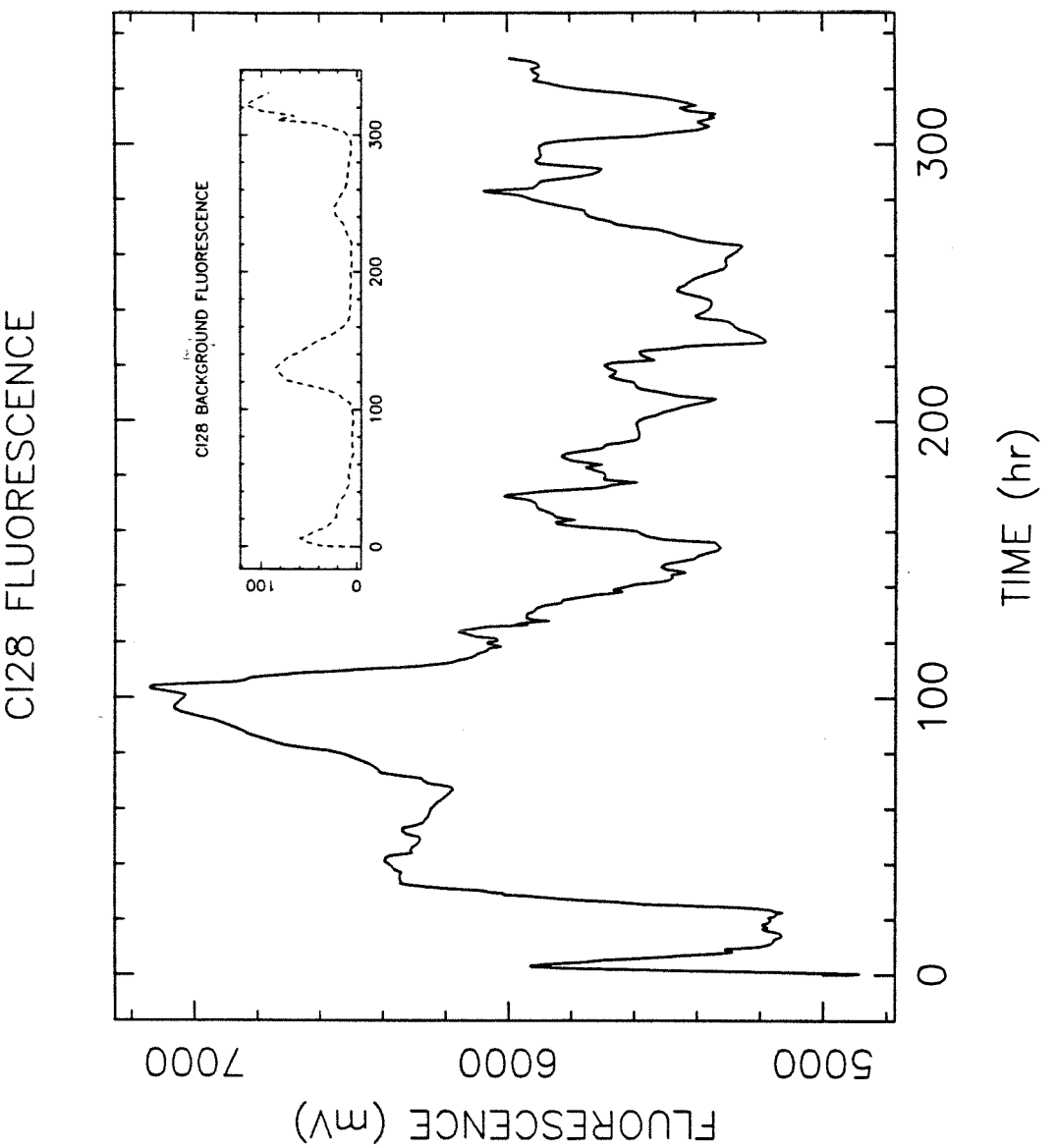

Figure 94. NAD(P)H-dependent fluorescence during experiment CI28.

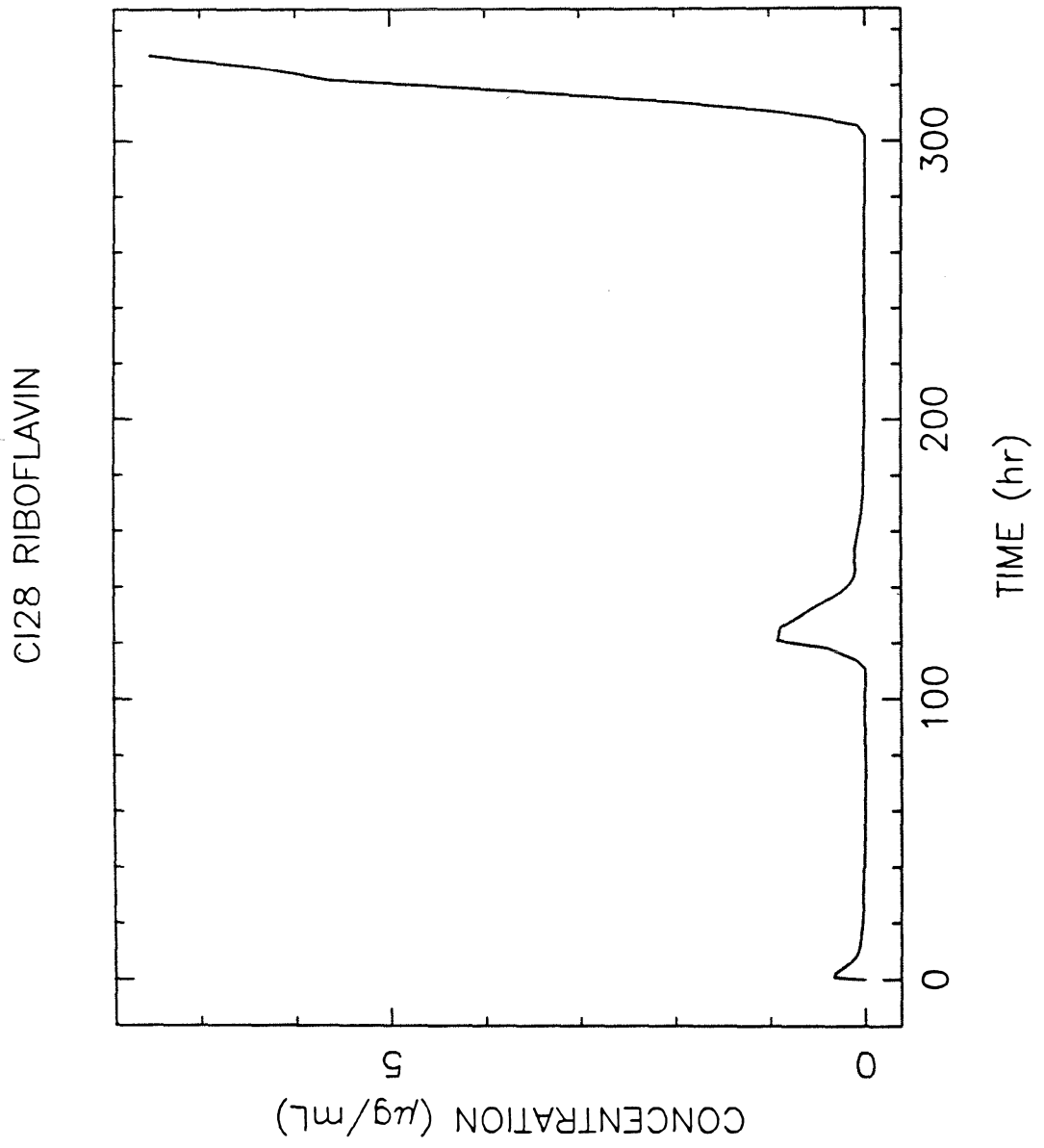

Figure 95. Concentrations of riboflavin during experiment CI28.

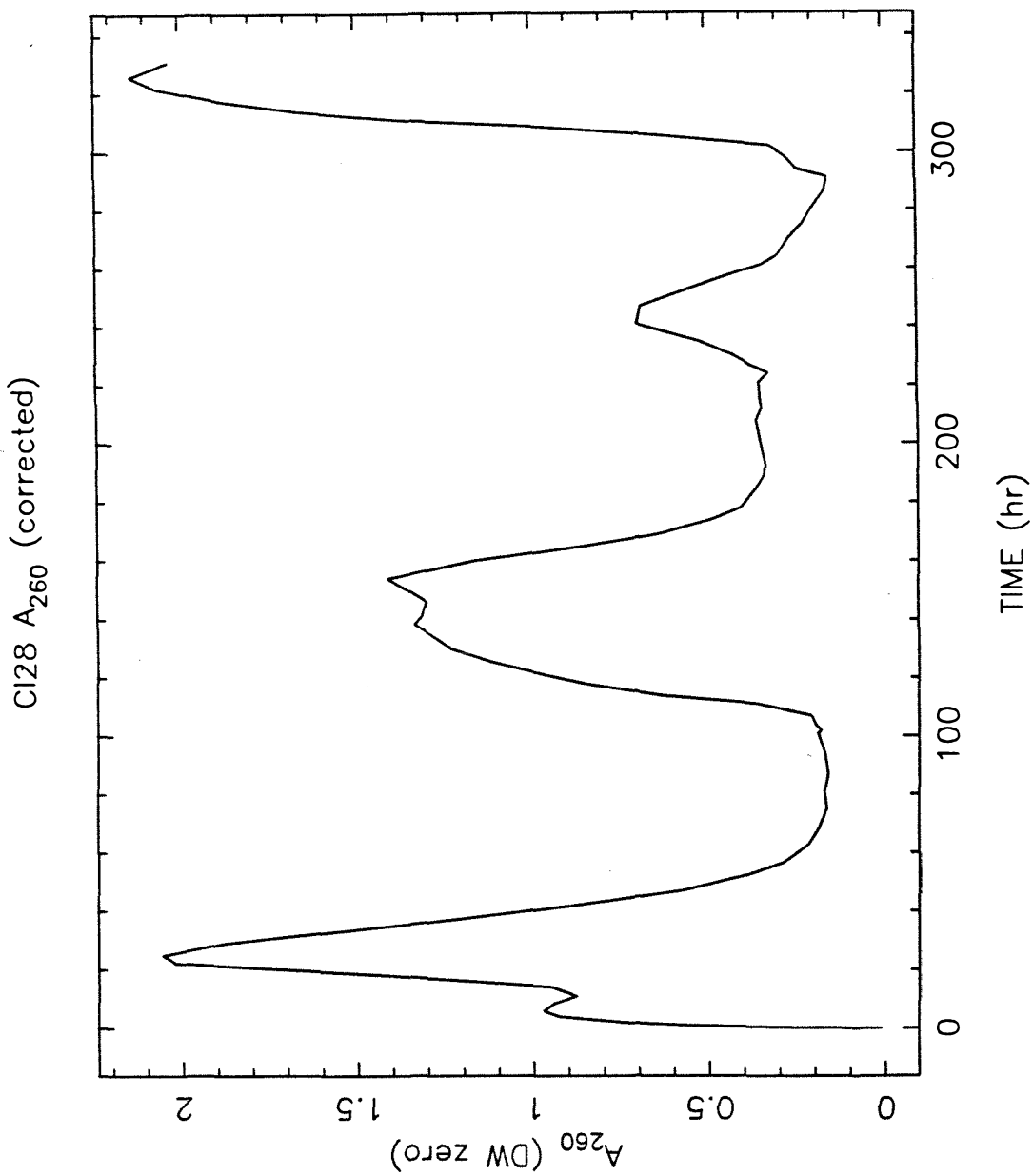

Figure 96. Levels of 260 nm absorbance during experiment CI28.

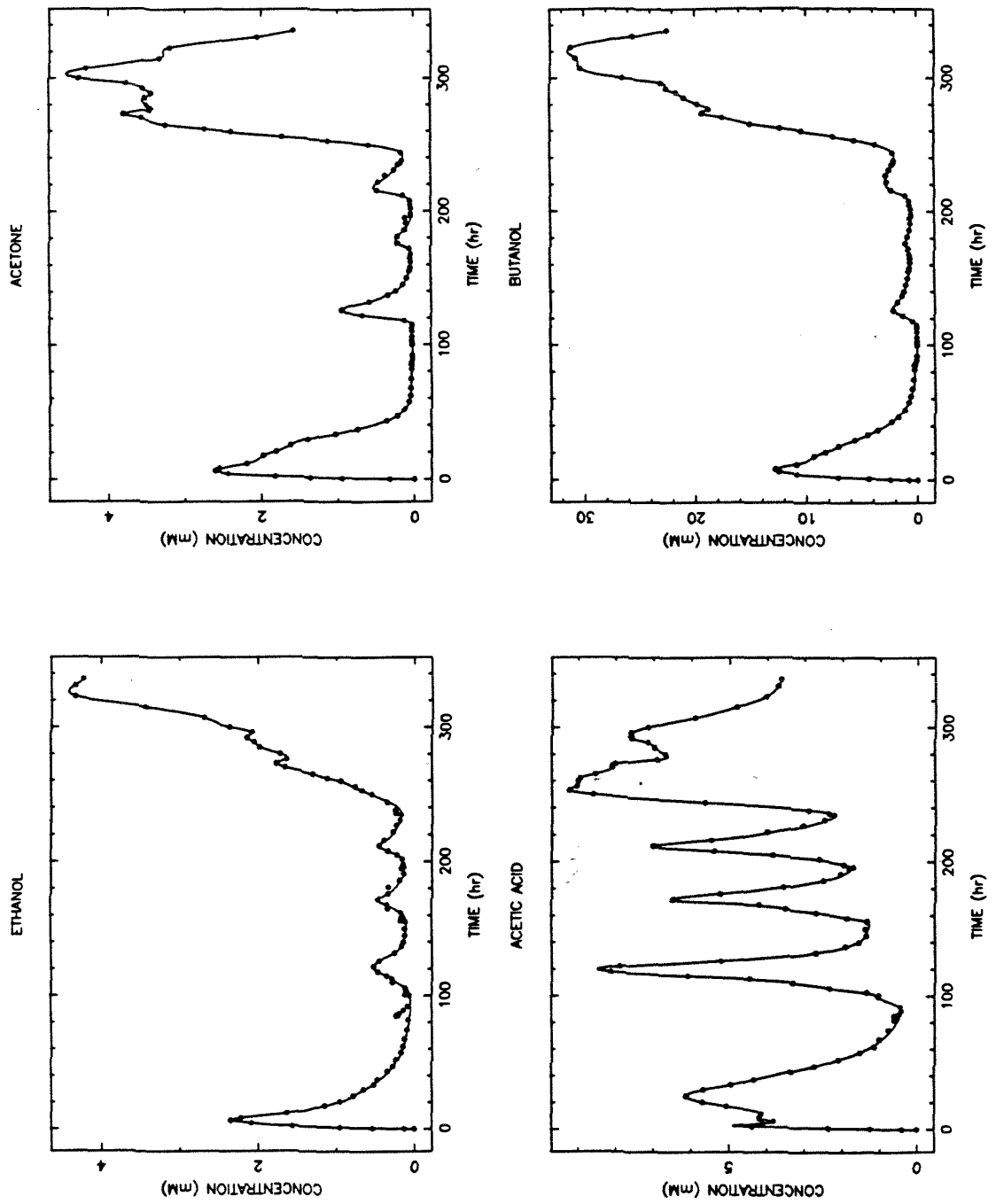

Figure 97. Experiment CI30 concentration profiles. Ethanol, acetone, acetic acid, *and butanol.*

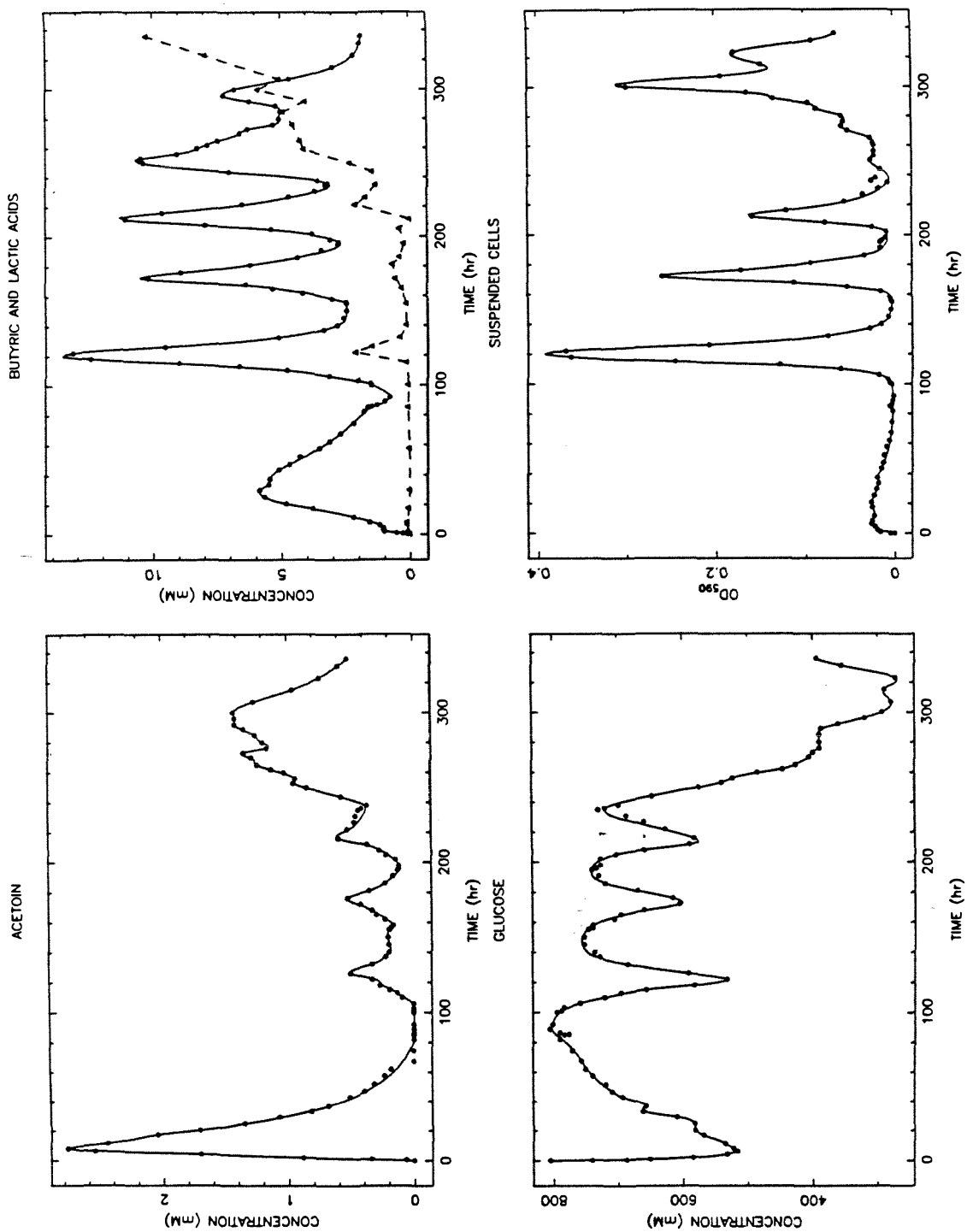

Figure 98. Experiment CI30 concentration profiles. Acetoin, butyric acid, total lactic acid, glucose, and suspended cells.

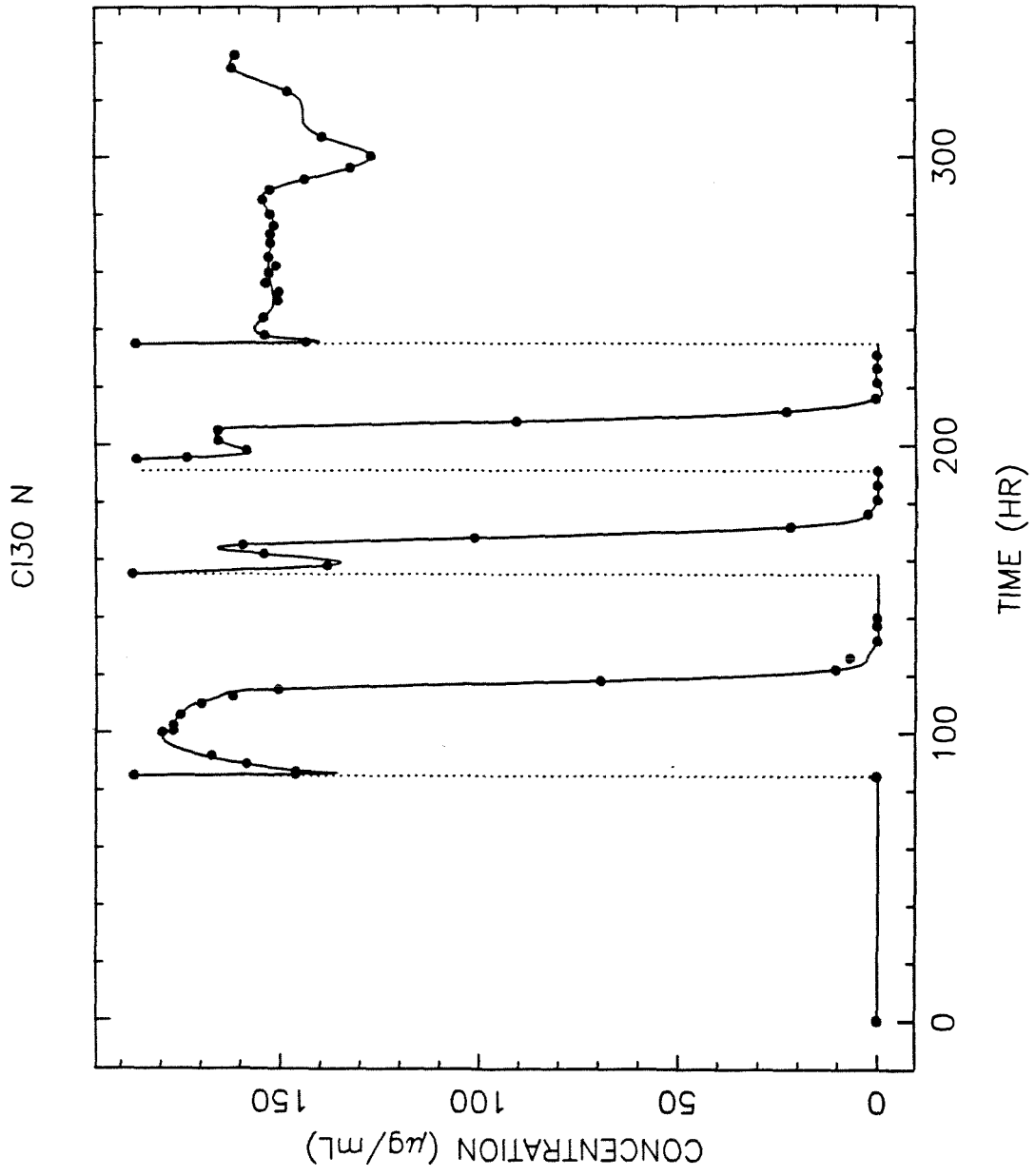

Figure 99. Experiment CI30 ammonia concentration profiles.

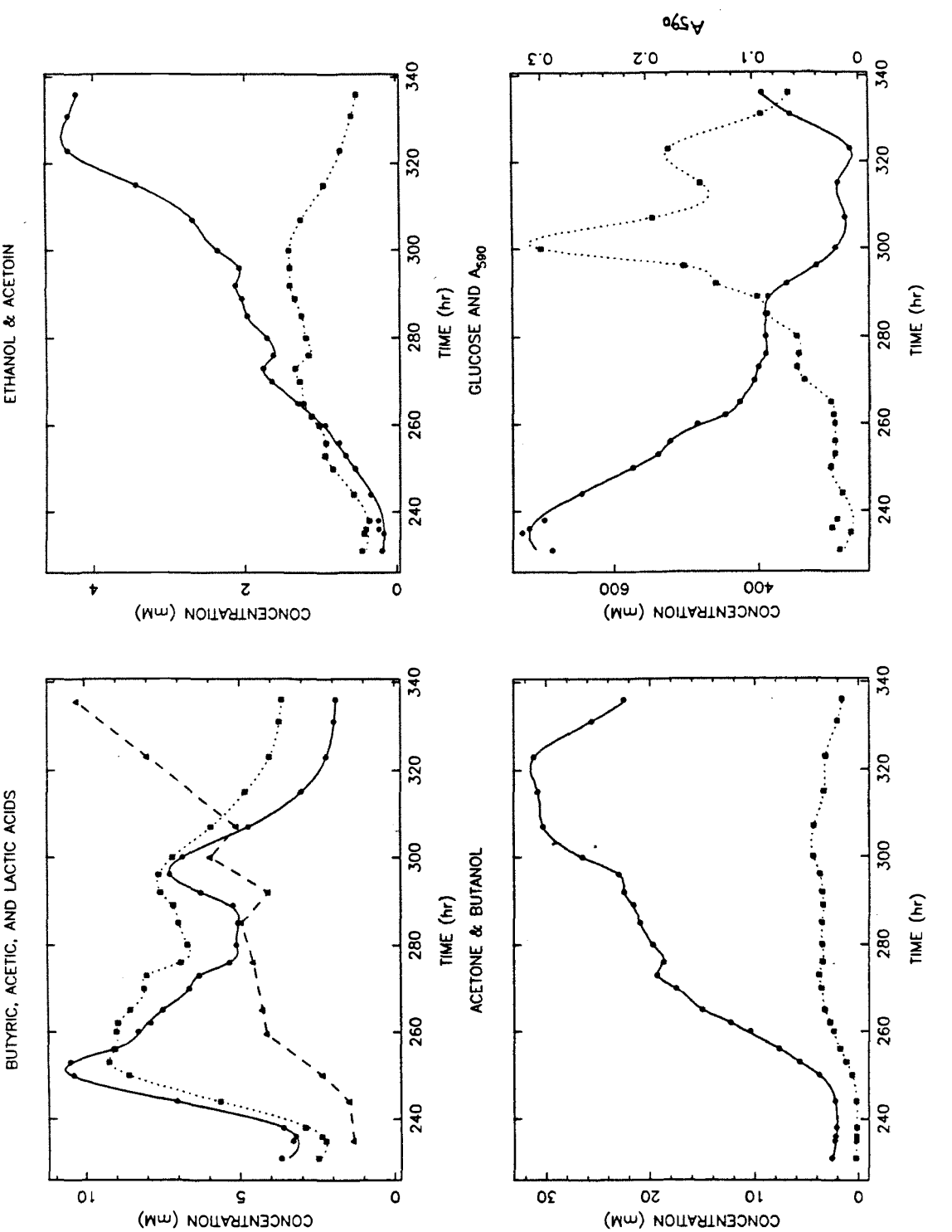

Figure 100. Concentration profiles during the final regeneration phase of experiment CI30. **Upper left**: butyric acid (solid line), acetic acid (dotted line), and total lactic acid (dashed line). **Upper right**: ethanol (solid line) and acetoin (dotted line). **Lower left**: butanol (solid line) and acetone (dotted line). **Lower right**: glucose (solid line) and A590 (dotted line).

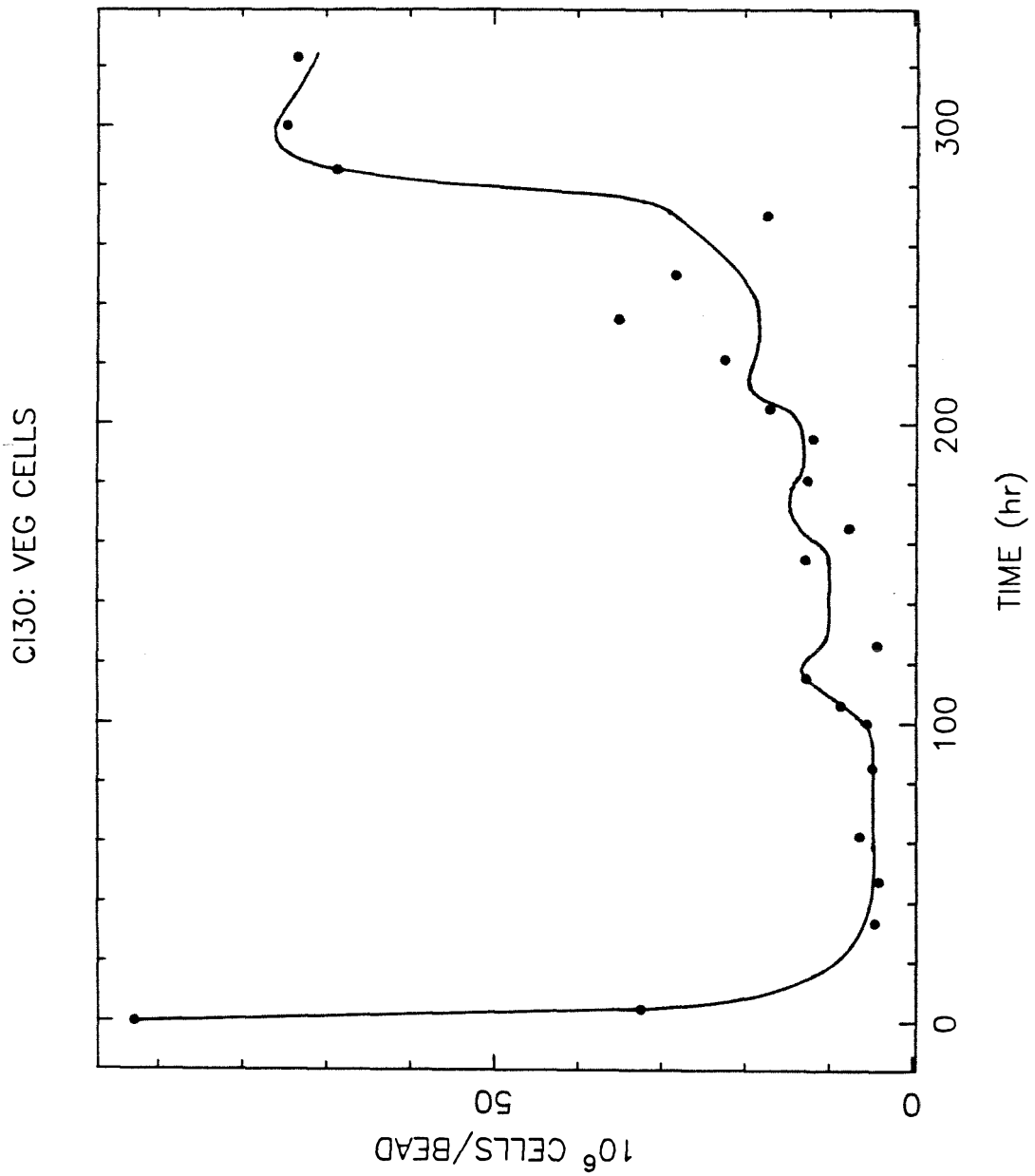

Figure 101. Immobilized vegetative cell concentrations during experiment CI30.

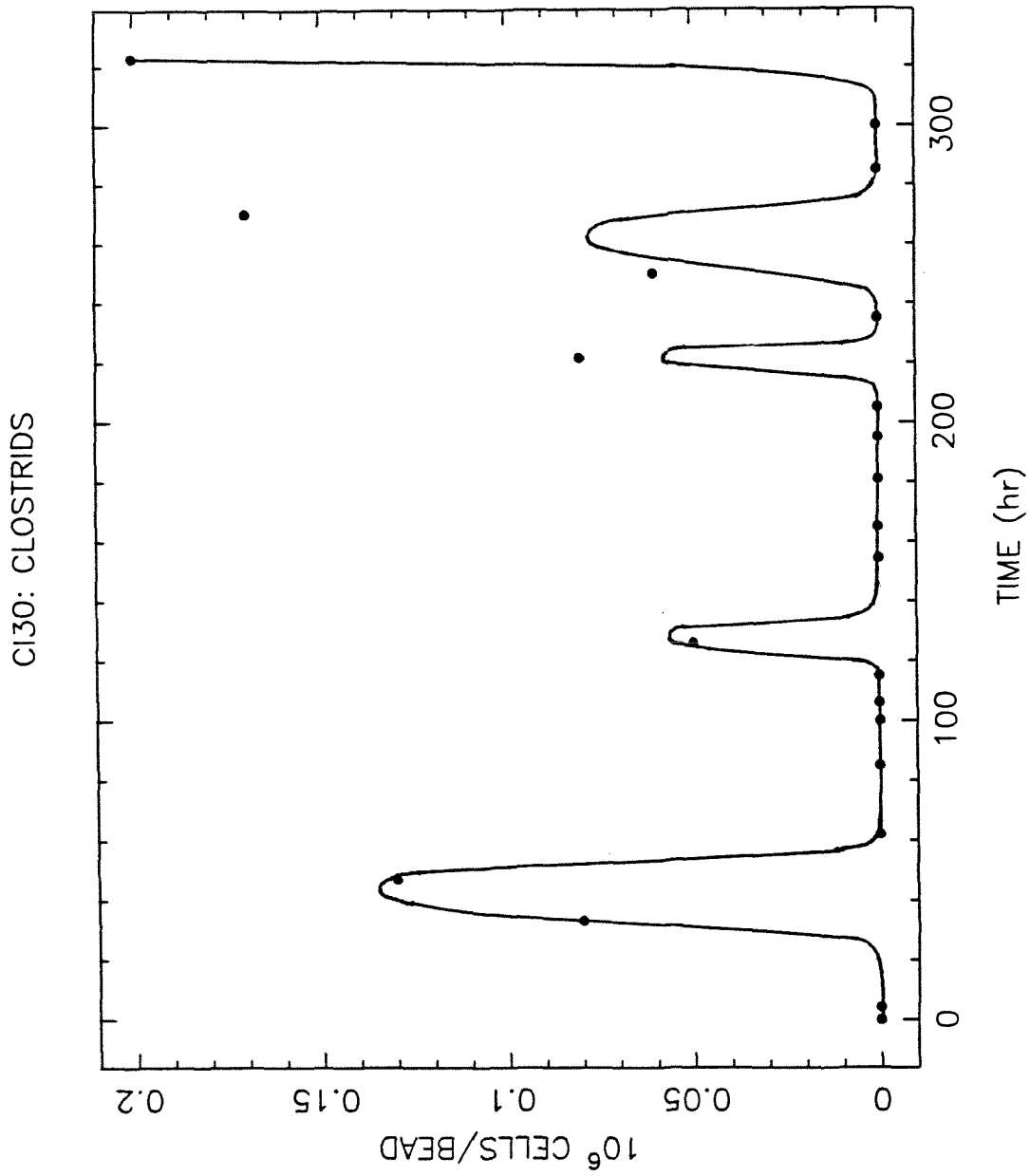

Figure 102. Immobilized clostridial form concentrations during experiment CI30.

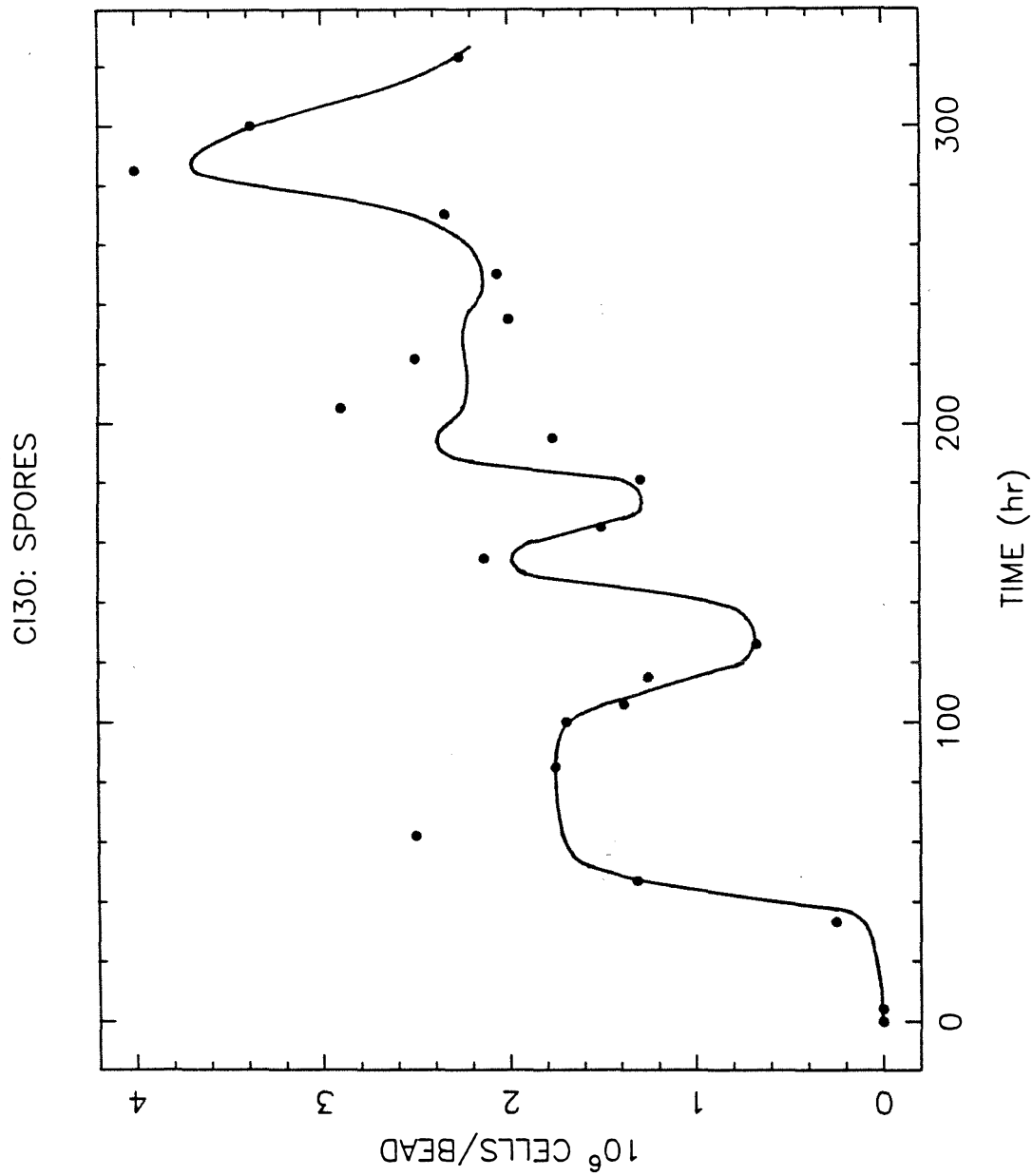

Figure 103. Immobilized spore concentrations during experiment CI30.

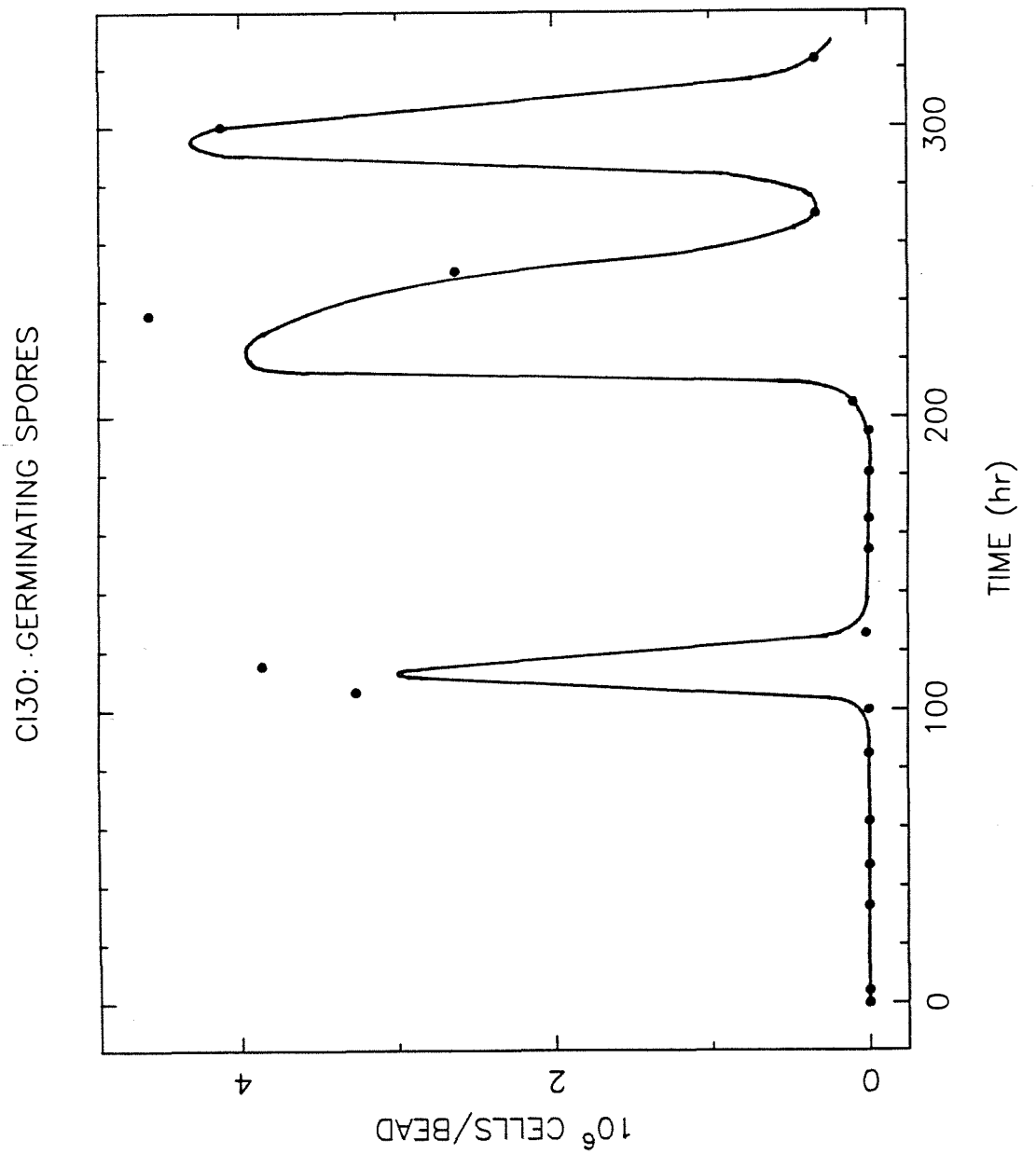

Figure 104. Immobilized germinating spore concentrations during experiment CI30.

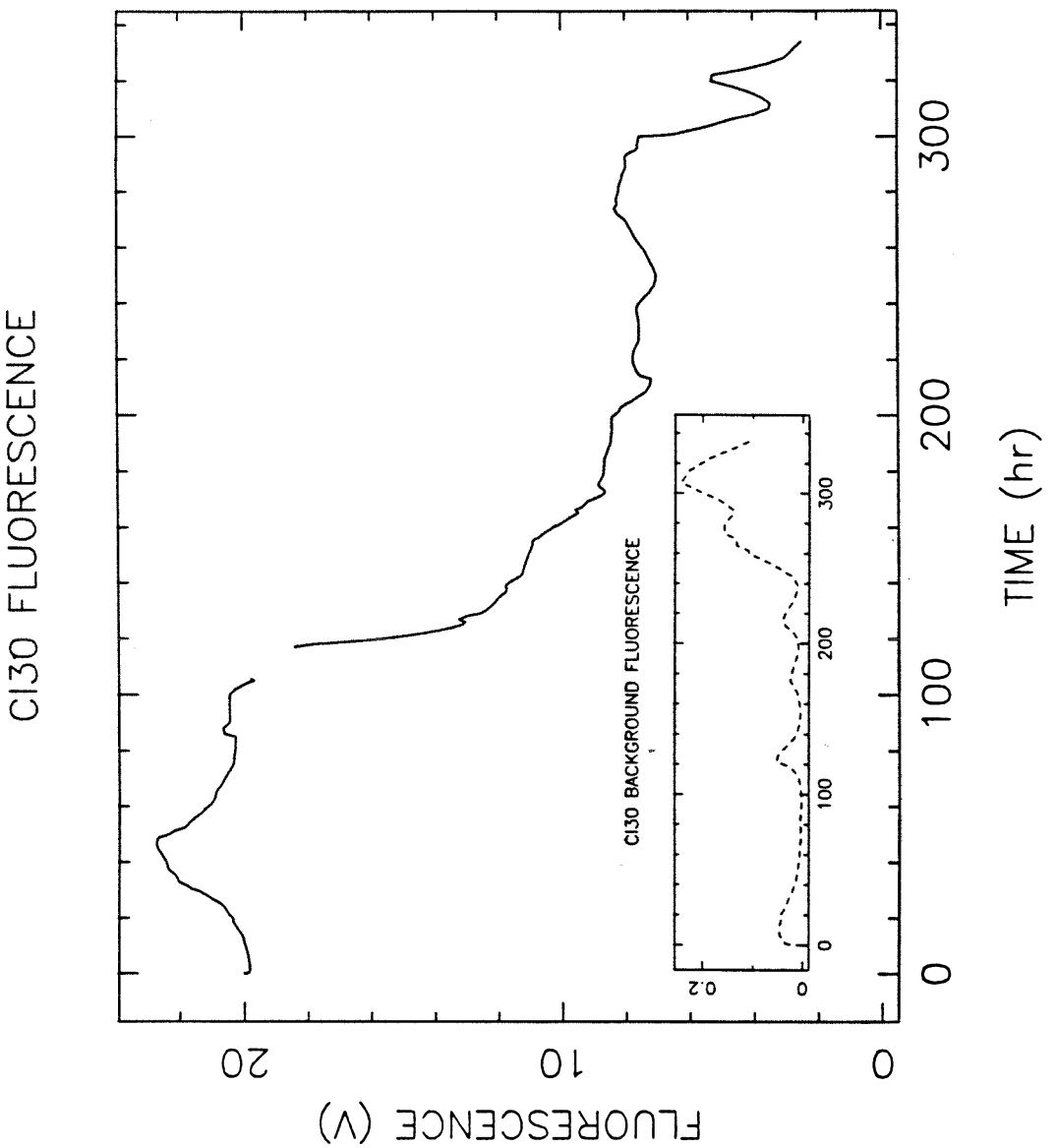

Figure 105. NAD(P)H-dependent fluorescence during experiment CI30.

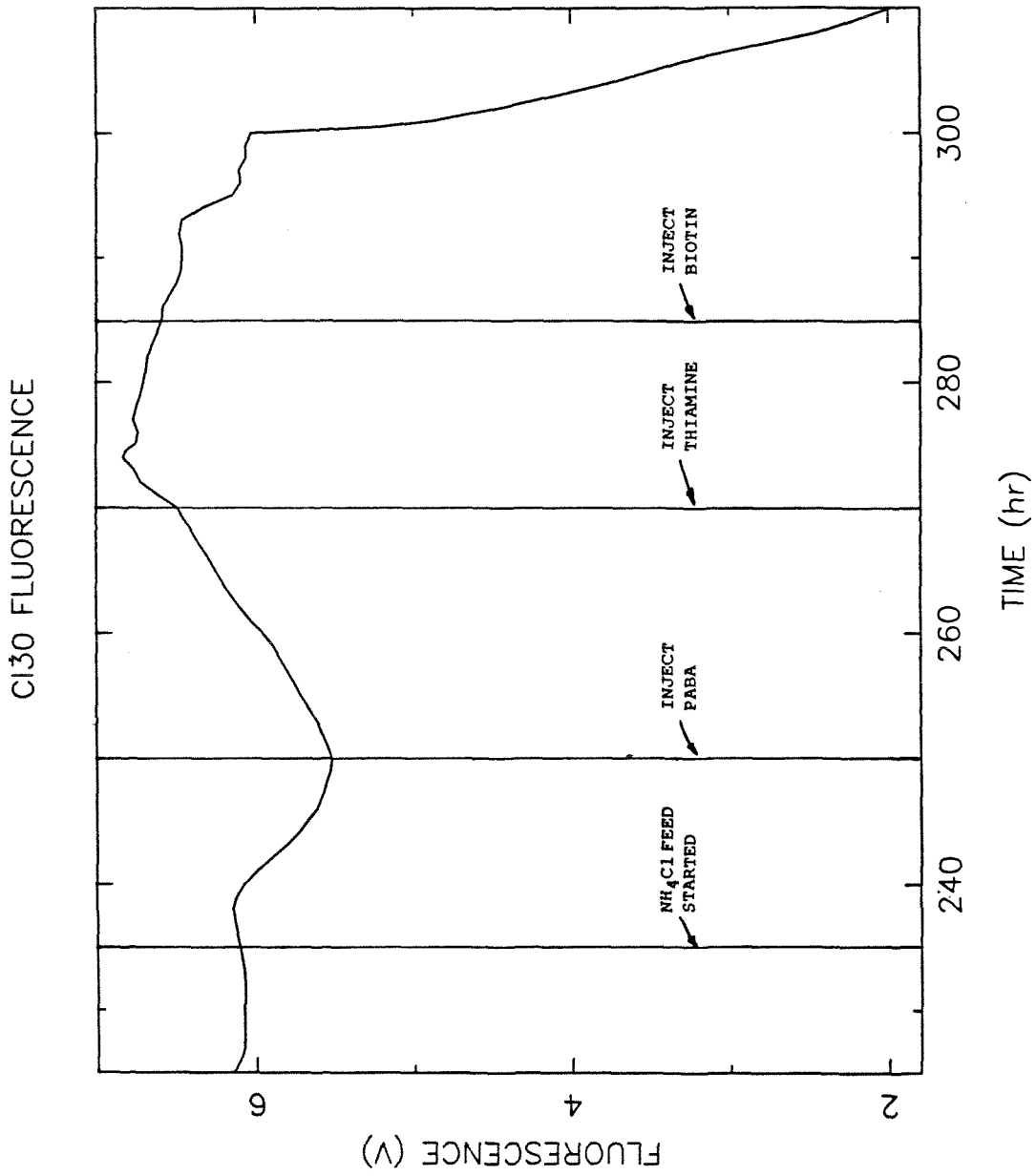

Figure 106. NAD(P)H-dependent fluorescence during the final regeneration period of experiment CI30.

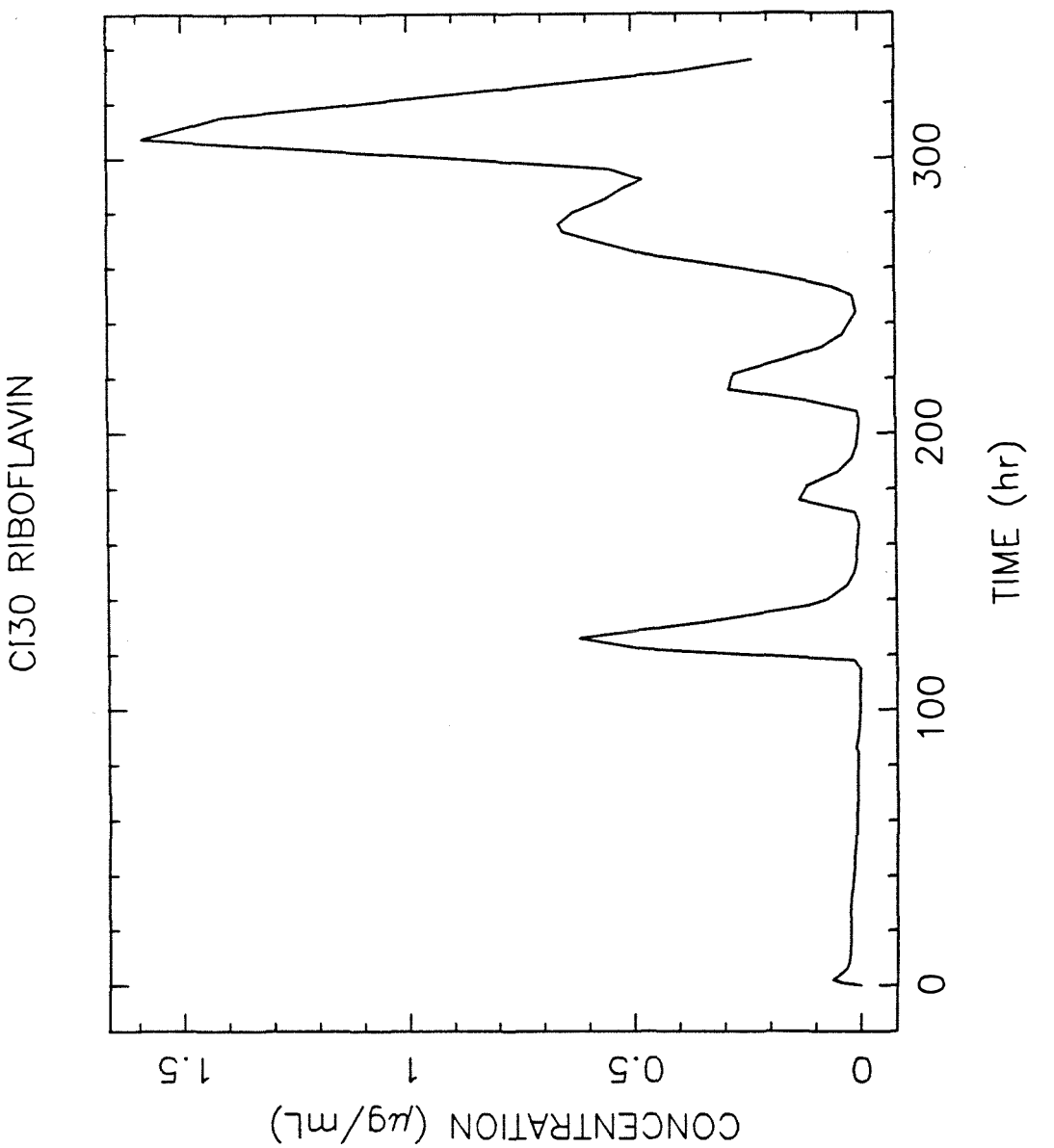

Figure 107. Concentrations of riboflavin during experiment CI30.

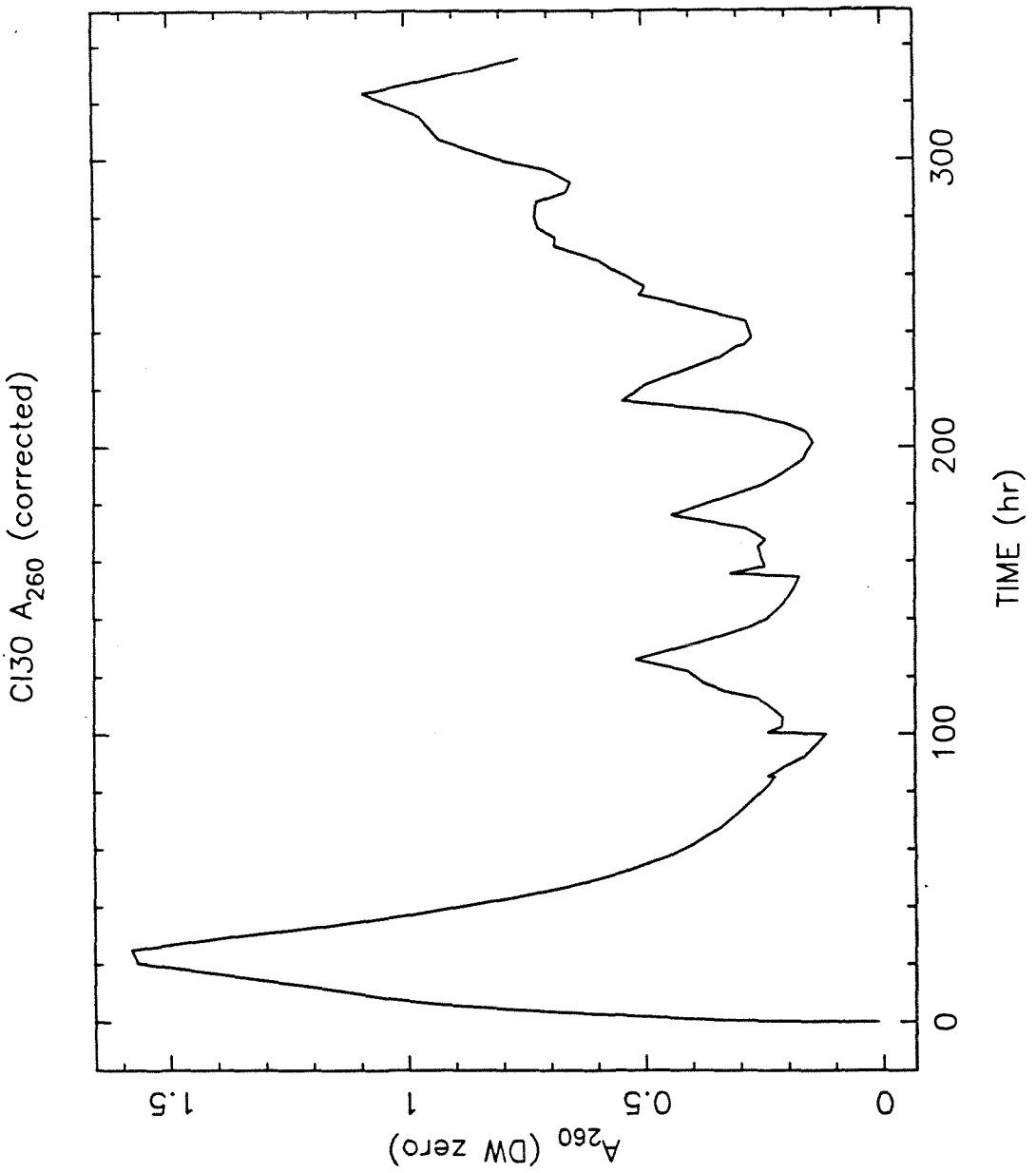

Figure 108. Levels of 260 nm absorbance during experiment CI30.

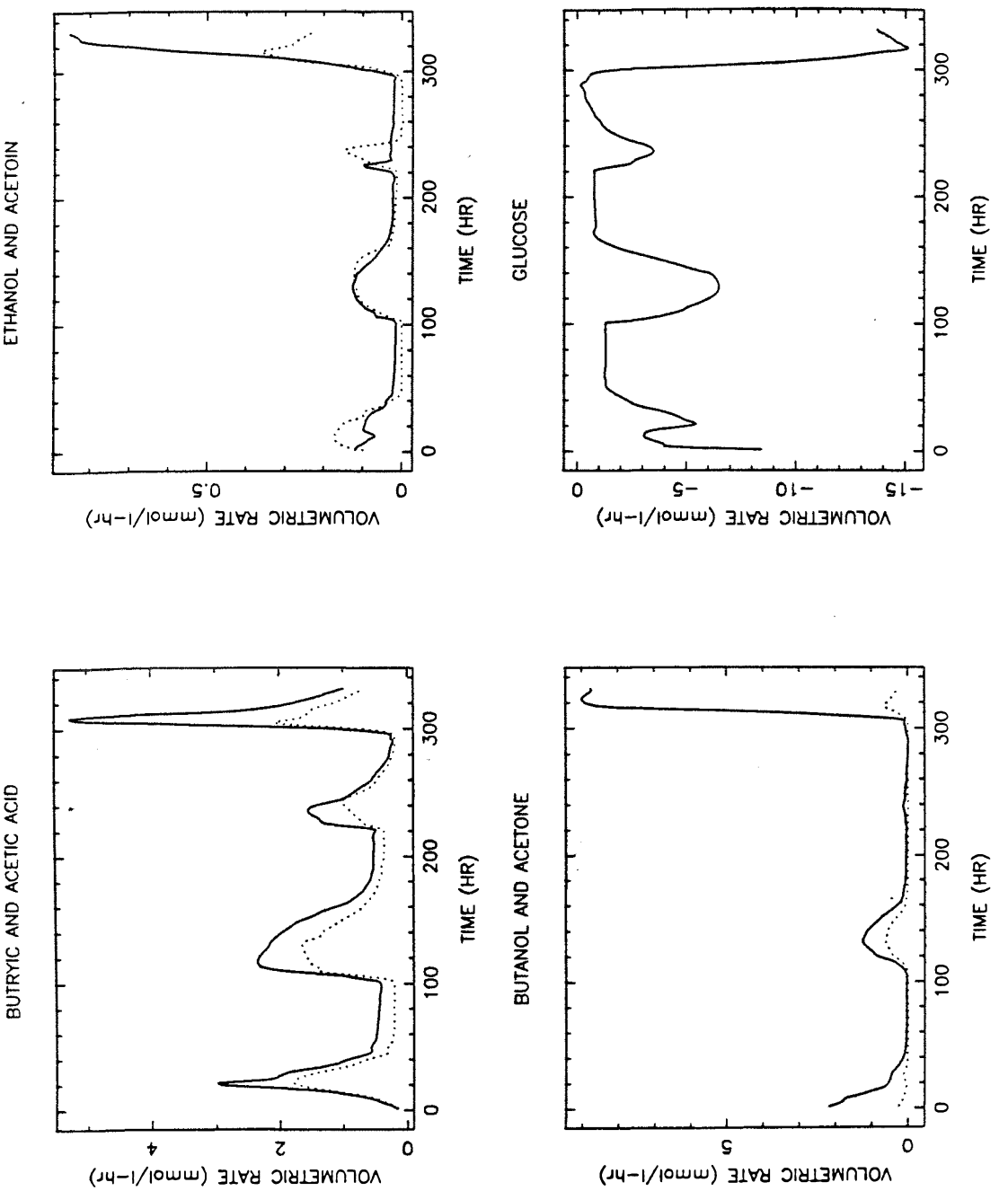

Figure 109. Volumetric rates of product formation during experiment CI28. **Upper left**: butyric acid (solid line) and acetic acid (dotted line). **Upper right**: ethanol (solid line) and acetoin (dotted line). **Lower left**: butanol (solid line) and acetone (dotted line). **Lower right**: glucose.

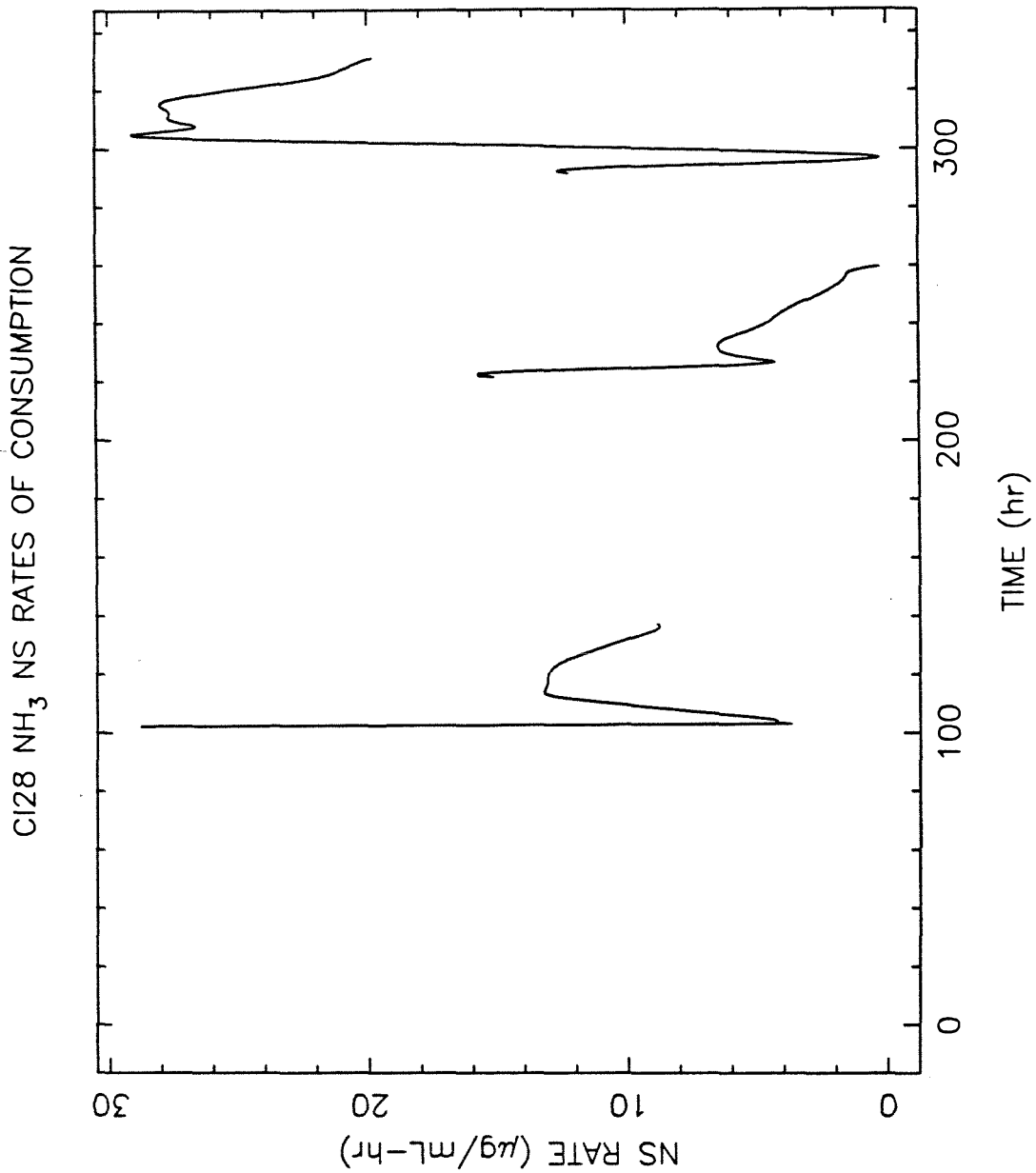

Figure 110. Volumetric rates of ammonia assimilation during experiment CI28.

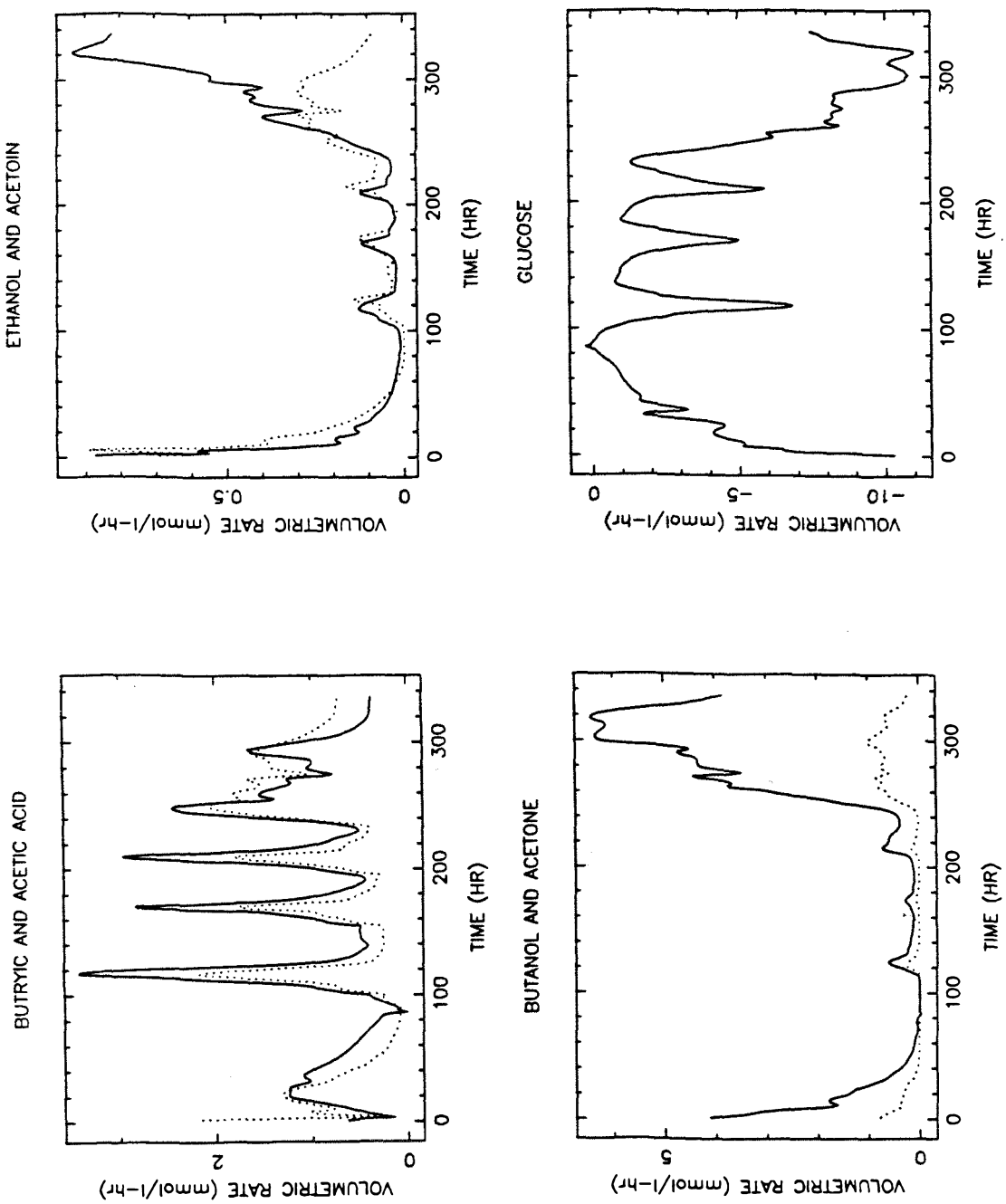

Figure 111. Volumetric rates of product formation during experiment CI30. **Upper left**: butyric acid (solid line) and acetic acid (dotted line). **Upper right**: ethanol (solid line) and acetoin (dotted line). **Lower left**: butanol (solid line) and acetone (dotted line). **Lower right**: glucose.

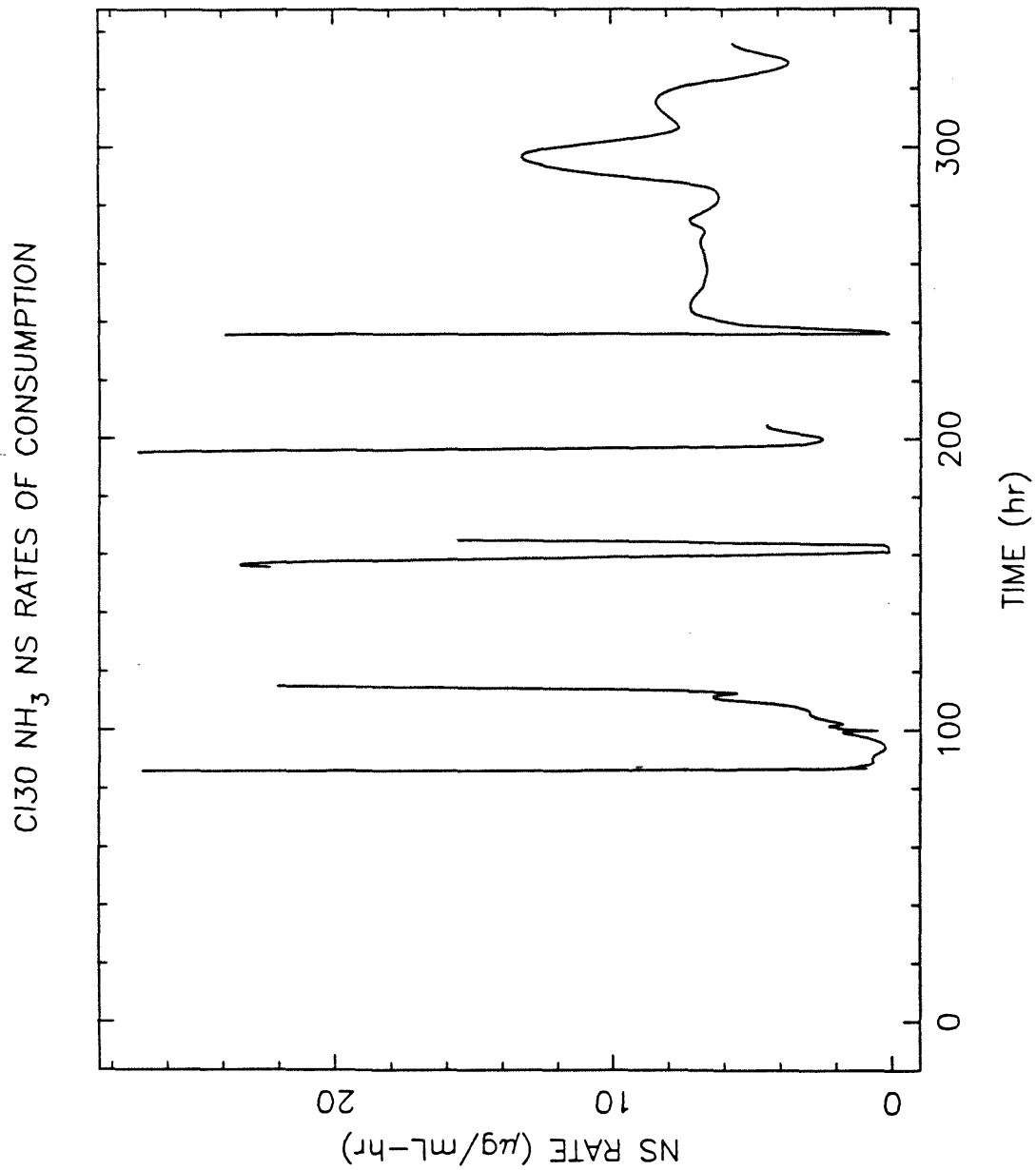

Figure 112. Volumetric rates of ammonia assimilation during experiment CI30.

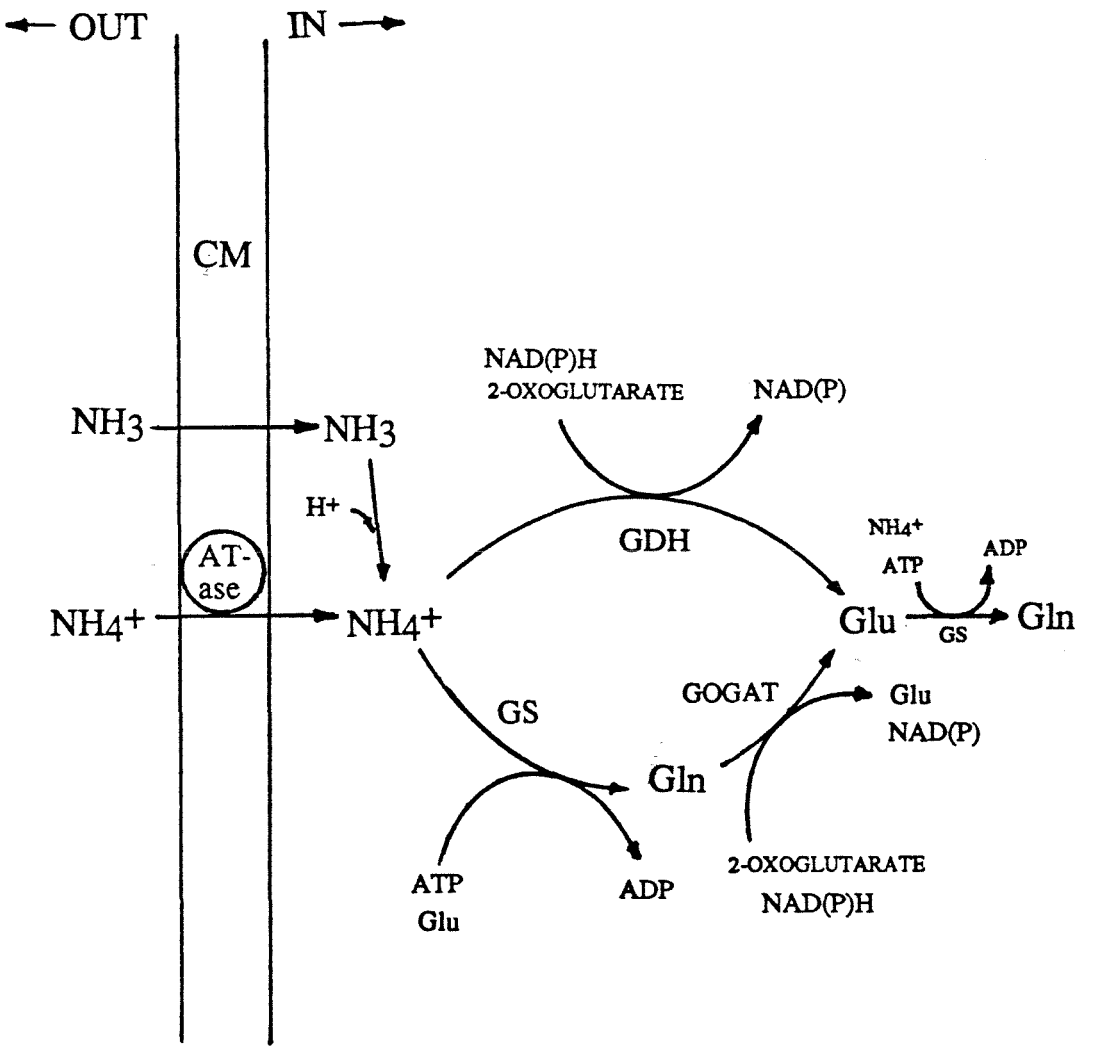

Figure 113. Ammonia assimilation pathways. Abbreviations: CM, cytoplasmic membrane; AT-ase, ammonium ion translocatase; GDH, glutamate (or alanine) dehydrogenase; GS, glutamine synthetase; GOGAT, glutamate synthase; Gln, glutamine; and Glu, glutamate.

CHAPTER 7

CONCLUSIONS

Some specific conclusions have been presented at the end of each of the three preceding chapters, but other, more general comments may be made on the basis of this work as a whole.

First, the initial loss of activity due to widespread immobilized cell lysis observed in these experiments seems to be a result of rinsing followed by exposure to the nitrogen-free medium; this may indicate that glucose is acting to induce substrate-accelerated death, or it may be another response of the cells to sudden environmental shifts. In future experiments, growth on defined full nutrient medium suceeded by a gradual shift to nitrogen-free conditions would be preferred for the retention of high initial cell number. For optimal butanol productivity during a bioconversion phase with an ATCC 824 biocatalyst, two sets of operating conditions seem promising. If the feed is to contain no nitrogen source, then a pH 6 process gives relatively high yields because both sporulation and acetone formation are inhibited. On the other hand, the addition of ammonia (but not the growth vitamins) allowed high, long term production of butanol. The effects of very low ammonia concentrations and pH on the longevity of activity in this system should be investigated.

Since the product selectivity and the overall rate of metabolic activity in this system was shown to be closely related to the energy charge in the immobilized cells, the optimal regeneration strategy must take the effects of the high-affinity ammonia assimilation system into account. The best procedure for nitrogen feeding would thus consist of relatively short (5–10 hour) periods of nitrogen or nitrogen plus vitamin feeding, followed by approximately 10 hour phases during which the feed to the system contained no nitrogen source. Since the rate of solvent formation

decreased as soon as the ammonia in the reactor was exhausted, the abrupt change in the NAD(P)H-dependent fluorescence signal that occurs at this time could be used as a signal for the start of a new nutrient-feeding cycle.

The addition of weak acid metabolites enhanced solvent production, both by providing the immediate precursor to a solvent product and by acting to uncouple the cell membrane pH gradient. However, this strategy did not improve the butanol-to-acetone ratio, because the uptake of the acids was coupled to the formation of acetone. This obstacle might be avoided by raising the process pH from 4.5 to 6 so that the acetoacetate decarboxylase is less active, or by the addition of a non-metabolizable ΔpH uncoupler.

The advent of recombinant DNA technology has made it possible to isolate or design mutant strains of bacteria with many new characteristics. While only a few investigations have been reported on cloning and genetic mapping in *C. acetobutylicum*, recent advances with this organism indicate that opportunities will soon exist to construct mutants of this strain with certain desired properties. The results of the experiments presented in this work indicate several potentially interesting possibilities for new strain design. A number of sporulation mutants have been isolated, including the strain used in experiment CI30, ATCC 39236. The requirement for long-term activity in immobilized cell bioconversions will necessitate the use of asporogenous strains. However, more potential exists in the use of *C. acetobutylicum* strains with mutations in metabolic pathway enzymes. When this type of metabolic engineering becomes available for this organism, useful improvements might be made either by deleting the hydrogenase gene or by moving the gene from the chromosomal DNA to a plasmid, where its transcription could be

controlled. Loss of hydrogenase activity would force the transfer of reducing equivalents to NAD, and the resulting high NADH:NAD ratio would increase solvent production. However, because solvent production alone does not produce enough ATP for cell growth, the cells would best be used in an immobilized form. Another desirable mutant would be one that was deficient in glutamine synthetase, so that the demand for high energy charge would not be induced under low ammonia conditions. For the purposes of controlled-nutrient bioconversion processes, ammonia assimilation by glutamine or alanine dehydrogenase would be sufficient.

The results from this work show that the use of nitrogen starvation to control growth in immobilized cell systems can lead to somewhat unexpected changes in the metabolism and product-forming activities of the immobilized cells. In addition, environmental parameters such as pH and the presence of some intermediate metabolites in the feed can affect the product specificity greatly. The consequences of these environmental pertubations must be investigated with the cells in or on the chosen support, partly because different supports may affect the cell behavior differently, but primarily because the environmental conditions experienced by immobilized cells are often unlike those in a suspended cell cultivation. Although these effects naturally vary from organism to organism, this work shows that knowledge of the metabolism and the underlying physiological responses of the cell to environmental changes can be used to understand and predict cell behavior.